

Alma Mater Studiorum - Università di Bologna

DOTTORATO DI RICERCA IN

FISICA

Ciclo 34

**Settore Concorsuale:** 02/A2 - FISICA TEORICA DELLE INTERAZIONI FONDAMENTALI

**Settore Scientifico Disciplinare:** FIS/02 - FISICA TEORICA, MODELLI E METODI MATEMATICI

EFFECTIVE FIELD THEORIES AND THEIR PHENOMENOLOGICAL  
APPLICATIONS

**Presentata da:** Luca Pagani

**Coordinatore Dottorato**

Michele Cicoli

**Supervisore**

Fabio Maltoni

**Esame finale anno 2022**



*“First of all, the beauty that he sees  
is available to other people and to me [...].  
At the same time, I see much more  
about the flower than he sees.  
I could imagine the cells in there, the complicated actions inside [...],  
there is also beauty at smaller dimensions”.*

Richard P. Feynman





## Abstract

Effective field theories (EFTs) are ubiquitous in theoretical physics and in particular in field theory descriptions of quantum systems probed at energies much lower than one or few characterizing scales. More recently, EFTs have gained a prominent role in the study of fundamental interactions and in particular in the parametrisation of new physics beyond the Standard Model, which would occur at scales  $\Lambda$ , much larger than the electroweak scale. In this thesis, EFTs are employed to study three different physics cases. First, we consider light-by-light scattering as a possible probe of new physics. At low energies it can be described by dimension-8 operators, leading to the well-known Euler-Heisenberg Lagrangian. We consider the explicit dependence of matching coefficients on type of particle running in the loop, confirming the sensitiveness to the spin, mass, and interactions of possibly new particles. Second, we consider EFTs to describe Dark Matter (DM) interactions with SM particles. We consider a phenomenologically motivated case, i.e., a new fermion state that couples to the Hypercharge through a form factor and has no interactions with photons and the  $Z$  boson. Results from direct, indirect and collider searches for DM are used to constrain the parameter space of the model. Third, we consider EFTs that describe axion-like particles (ALPs), whose phenomenology is inspired by the Peccei-Quinn solution to strong CP problem. ALPs generically couple to ordinary matter through dimension-5 operators. In our case study, we investigate the rather unique phenomenological implications of ALPs with enhanced couplings to the top quark.



# Contents

<b>Introduction</b>	<b>1</b>
<b>1 The Standard Model</b>	<b>5</b>
1.1 Fundamental Principles . . . . .	5
1.2 Gauge Theories . . . . .	8
1.2.1 The Abelian Case: QED . . . . .	8
1.2.2 The non-Abelian Case: QCD . . . . .	13
1.3 Electroweak Theory . . . . .	18
1.4 Physics Beyond the Standard Model . . . . .	23
<b>2 Effective Field Theories</b>	<b>25</b>
2.1 Introduction to EFTs . . . . .	25
2.2 EFT Lagrangian . . . . .	26
2.2.1 Power Counting . . . . .	28
2.2.2 Tree-Level Matching . . . . .	29
2.2.3 Loops . . . . .	32
2.2.4 Matching . . . . .	33
2.2.5 Fields Redefinition and Equations of Motion . . . . .	36
2.3 Decoupling of Heavy States . . . . .	38
2.4 Standard Model Effective Field Theory . . . . .	40
2.4.1 SMEFT Corrections to SM . . . . .	41
<b>3 Light-by-light Scattering</b>	<b>45</b>
3.1 The Euler-Heisenber Lagrangian . . . . .	45
3.2 The Effective Lagrangian . . . . .	46
3.2.1 Cross-Section . . . . .	49
3.3 Spinor QED . . . . .	50
3.3.1 Amplitude Evaluation . . . . .	51
3.4 Scalar QED . . . . .	54
3.5 Vector QED . . . . .	55
3.6 Conclusions and Outlook . . . . .	56
<b>4 Dark Matter</b>	<b>59</b>
4.1 The $\Lambda$ -CDM model . . . . .	59
4.2 Indirect Evidences of Dark Matter . . . . .	63
4.3 Effective Field Theory Approach . . . . .	65

4.4	Comparing EFTs: Hypercharge vs Electromagnetic . . . . .	67
4.4.1	Electromagnetic Form Factors Beyond their Limits . . . . .	67
4.5	Collider Searches of Dark Matter . . . . .	71
4.5.1	Electromagnetic EFT in Vector Boson Fusion . . . . .	72
4.5.2	The Latest on the Mono-jet Signature . . . . .	76
4.6	DM Phenomenology in hypercharge EFT . . . . .	79
4.6.1	Dark Matter Production . . . . .	80
4.6.2	Direct Searches . . . . .	84
4.6.3	Indirect Searches . . . . .	87
4.7	Conclusions and Outlooks . . . . .	93
<b>5</b>	<b>Axion-like Particles</b> . . . . .	<b>97</b>
5.1	The Strong CP Problem . . . . .	97
5.1.1	Axions and Axion-like Particles . . . . .	98
5.2	Effective Field Theory of ALP . . . . .	99
5.2.1	Phase Redefinition of SM Fields . . . . .	100
5.2.2	Comparing Effective Field Theories . . . . .	102
5.3	Top-philic Axions-like Particles . . . . .	106
5.3.1	Renormalization of ALP theory . . . . .	106
5.4	NLO amplitude of $\bar{q}q \rightarrow \bar{t}t$ . . . . .	109
5.4.1	Scalar Axion-like Particles . . . . .	110
5.4.2	Massless Limit . . . . .	111
5.5	Yukawa Potential in the non-Relativistic Limit . . . . .	111
5.6	Conclusions and Outlook . . . . .	116
	<b>Conclusions</b> . . . . .	<b>119</b>
<b>A</b>	<b>Appendix</b> . . . . .	<b>123</b>
A.1	Pauli Matrices . . . . .	123
A.2	Dirac Matrices . . . . .	124
A.2.1	Dirac Matrices in D-dimensions . . . . .	124
A.3	Gell-Mann Matrices . . . . .	126
A.4	Embedding Particles in Fields . . . . .	127
A.4.1	The Scalar Field . . . . .	128
A.4.2	The Vector Field . . . . .	128
A.4.3	The Spinor Field . . . . .	131
A.5	Light-by-light Formulas . . . . .	134
A.6	Dark Matter Table . . . . .	138
A.7	ALPs Computations . . . . .	139
A.7.1	Explicit Calculation of Phase Redefinition . . . . .	139
A.7.2	Derivatives in Pseudo-Scalar Potential . . . . .	142
A.8	Passarino Veltman Scalar Integrals . . . . .	144





# Introduction

The twentieth century has been a period of great discoveries in physics. In a time span of about 80 years, the understanding of Nature has rapidly accelerated, from classical mechanics and electromagnetism to general relativity, quantum mechanics, and the rise of quantum field theory as the framework to study fundamental interactions. Among the most glaring successes of quantum field theory, the electroweak theory has achieved an overwhelming experimental confirmation, to some extent even unexpected, to the point of being renamed, along with Quantum Chromodynamics, the *Standard Model* (SM) of elementary particles. In order to explore phenomena described by the Standard Model, it is necessary to carry out research at extremely high energies. For this purpose, particle accelerators were built, the last and more energetic of which, is the LHC at CERN in Geneva, which achieved worldwide visibility in 2012 with the discovery of the Higgs boson, the last missing ingredient of the SM, theorized about 50 years earlier.

Despite the successes of SM and, naturally, of those scientists who contributed to its conception, nowadays we know that it is not a complete theory of fundamental interactions. Not only does gravity lack a quantum description yet, thus escaping classification within SM, but also several other observations, such as neutrino masses and baryonic asymmetry, cannot be predicted while others do not find a description at all, such as Dark Matter and Dark Energy.

Search for physics beyond the Standard Model, therefore still attracts a considerable attention, and many high-energy physicists, either theorists or experimentalists, are involved in activities meant at establishing in the laboratory clear evidence of new phenomena. These searches have been traditionally performed with some specific models in mind, one leading example being supersymmetry, and then working out all phenomenological consequences top-down. However, the lack of a clear indication on what model of new physics might be lurking at high scales, leaves so much freedom that it is difficult to identify clear model independent signatures. In this endeavor, more and more interest has grown around the idea of proceeding bottom-up and considering effective field theory descriptions of UV complete theories, extending the Standard Model with either a few light states and/or just by adding higher-dimensional operators.

The work collected in this thesis fits exactly into this context, leveraging on the use of effective field theories to attack some specific problems in particle physics. In the first chapter, the Standard Model is introduced and its critical issues highlighted. Chapter 2 is devoted to the description of effective field theories, presenting the most salient features of the method. The remaining chapters represent the original part

of the work, and illustrate three different applications of the effective field theories. In particular, in chapter 3, EFTs are used to study light-by-light scattering, while in chapter 4 we consider it in several models describing dark matter, assuming that it is composed by at least one stable flavor. Finally, in chapter 5, EFT is used to study the interactions of a new pseudo-scalar particle, an axion-like particle, which could not only resolve some of the fundamental issues of the Standard Model, i.e., the strong CP problem, but could also provide an ideal candidate for dark matter.







The Standard Model<sup>1</sup> of particle physics (SM) is the theory used to describe Nature at subatomic scales. It depicts a world ruled by electromagnetic and nuclear forces, since gravity appears to be relevant only at the macroscopic level. The Standard Model also provides a complete pattern to classify all particles discovered by experiments until today.

The first steps towards SM can be traced back to the late 1920s, with quantum electrodynamics; research, however, continued over a time span of about fifty years, during which the initial theories were abandoned and then restored several times. The current formulation was only achieved in the mid-1970s, after the experimental proof of quark model for strong interactions and the implementation of Higgs mechanism to explain particle masses.

An increasing number of experiments have been conducted to stress test the SM, which gained credibility as more empirical confirmations came through. The Standard Model reached a widespread acknowledgement in 2012 with the discovery of Higgs boson at CERN, in Geneva. Although the Standard Model has demonstrated great accuracy in foreseeing experimental outcomes, it leaves some phenomena unexplained and fails to be a complete theory of fundamental interactions.

This chapter retraces the present state-of-the-art of the Standard Model without claiming to be a complete description of it, for which we refer to well-known books such as *Peskin & Schroeder* [3] or *Schwartz* [4]. However, we will dwell on some features of SM that will prove useful in the following chapters.

## 1.1 Fundamental Principles

The Standard Model is a relativistic quantum field theory based on gauge invariance that aims to describe fundamental interactions in flat Minkowski space-time<sup>2</sup>. On one hand, the request for a relativistic theory is fulfilled by covariant formulation, that automatically embeds Einstein's *Relativity Principle*, introducing the symmetries of *Poincaré group*, a non-Abelian Lie group of ten generators. Noether's

---

<sup>1</sup>The name "Standard Model" was first coined by A. Pais and S. Treiman in 1975 for the Electroweak theory with four quarks.

<sup>2</sup>The flat Minkowski space-time is a four-dimensional manifold arising from the combination of the three-dimensional Euclidean space and the time coordinate. The chosen signature for its metric is the widely-adopted in particle physics, i.e.,  $(+, -, -, -)$ . Vectors in Minkowski space are denoted by italic type, while bold symbol merely indicates spatial components.

theorem makes the rest: ten conservation laws arise, one for each generator, including energy and momentum conservation – besides conservation of total angular momentum and center of mass velocity. On the other hand, unitarity is necessary to deal with a quantum theory that yearns to be predictable. The convergence point is accounted by the irreducible unitary representations of Poincaré group, called *fields*, that appears to be infinite-dimensional.

According to Wigner’s classification, each irreducible unitary representation is characterised by the mass and the spin, the latter is an integer number for bosons and a half-integer number for fermions. In addition, at the accelerators, such as the Large Hadron Collider (LHC) in Geneva, physicists track composed and elementary particles, therefore reducible representations are understood as composed objects, being irreducible representations associated with fundamental particles. A brief overhaul of how particles are embedded in fields is given in Appendix A.4.

In classical field theory as well as in its quantum counterpart, every law describing the behavior of a physical system can be derived from the fundamental action principle. The action  $\mathcal{S}$  is nothing but a dimensionless real quantity related to the Lagrangian density  $\mathcal{L}(x)$ , or merely Lagrangian for brevity, by the equation:

$$\mathcal{S} = \int d^4x \mathcal{L}(x).$$

The Lagrangian must be Lorentz invariant and transforms covariantly under translations to ensure the principles of Special Relativity, therefore in absence of background fields it can not explicitly depend on the space-time coordinates, otherwise translation invariance would be violated. In other words, Lagrangian is a function of the fields and their first partial derivatives only:

$$\mathcal{L}(x) = \mathcal{L}(\phi(x), \partial_\mu \phi(x), \psi(x), \partial_\mu \psi(x), \dots),$$

where dots indicate that we can introduce every other field, up to its first derivative, we need to describe the physical system under consideration. The constraint on derivative order greatly reduces the number of allowed operators and is dictated by causality: a third order differential equation in time acting on fields will lead to solutions where causality is violated, indeed the uniqueness of the related Cauchy problem is fulfilled by a system of second order derivative in time, at most. The Abraham-Lorentz equation of electrodynamics is a well-known example of third order differential equation where a-causal effects arise, such as pre-acceleration of charged particles, even before they have been hit by radiation. Another constraint comes from dimensional analysis: the Lagrangian must have the dimension of  $[\text{length}]^{-4}$  as well as any combination of fields that aspires to appear in it.

While in classical field theory, the space-time evolution of a system follows the Euler-Lagrangian equations of motion (EOMs) obtained by Hamilton’s principle of stationary action, in quantum field theory the physics of a system is understood in terms of the path integral which enables the direct calculation of scattering amplitudes – the latter being the generalisation of the former. The original suggestion of the path integral is due to P. M. Dirac in 1933 but it was successfully elaborated by R. P. Feynman in the 1940s. The simple idea behind it can be figured out recalling the *superposition principle* of quantum mechanics: the amplitude of a process that can take place in multiple ways is given by the coherent sum of the probability

associated to each path, moreover if such a process occurs as a succession of steps, one has to multiply the probability of each step. This probability can be written as a pure phase that in non-relativistic limit is equal to the classical action since only one path is allowed, i.e., the classical path. In quantum field theory (QFT), the path integral for a real scalar field evolving from the configuration  $\phi_i(\mathbf{x})$  at  $t = 0$  to  $\phi_f(\mathbf{x})$  at  $t = T$ , reads:

$$\langle \phi_f(\mathbf{x}) | e^{-iHT} | \phi_i(\mathbf{x}) \rangle = \int D\phi \exp \left[ i \int d^4x \mathcal{L} \right],$$

where  $H$  is the Hamiltonian function, i.e., the time evolution operator, while  $\int D\phi$  is the sum over all configurations.

The wide use of path integral in QFT is due to its link with correlation functions, indeed for a certain ground state  $|\Omega\rangle$ , the  $n$ -point correlation function can be written as:

$$\langle \Omega | T \{ \phi(x_1) \dots \phi(x_n) \} | \Omega \rangle = \frac{\int D\phi \phi(x_1) \dots \phi(x_n) \exp \left[ i \int d^4x \mathcal{L} \right]}{\int D\phi \exp \left[ i \int d^4x \mathcal{L} \right]},$$

where  $T$  is the time-ordering operator. Taking advantage of this equation, the Feynman rules of the theory can be derived directly. In fact, for the two-points correlation function the computation of the right-hand side of this equation returns the Feynman propagator. Once the Feynman rules of a specific theory have been obtained, they can be assembled to draw any desired diagram that connects the initial and final configurations of fields.

Scattering amplitude is a physical quantity that plays a fundamental role in particle physics experiments; the general relation linking Feynman diagrams, or alternatively correlation functions, to scattering amplitude was obtained by H. Lehman, K. Symanzik and W. Zimmermann, and is nowadays known as LSZ reduction formula. In terms of Feynman diagrams, it states that only connected diagrams with amputated external lines<sup>3</sup> enter in the computation of  $S$ -matrix elements, moreover each external field with a non-null spin value involves a multiplication for a polarization spinor or vector. The reduction formula can also be applied when the fundamental particles of a theory are unknown; for example, as long as we are not interested in the nucleons substructure, we can treat them as elementary particles by introducing the corresponding fields in the Lagrangian and calculating the  $S$ -matrix elements in perturbation theory. This general technique, called *effective field theory* (EFT), is very useful and represent the main content of this thesis.

The computation of Feynman diagrams often leads to ultraviolet divergences, however there is a class of QFTs where these divergences can be systematically removed. This feature, named *renormalizability*, ensures that divergences never show up in observable quantities and enables the use of measured parameters to make predictions of further experiments. Practically, it results as a constraint for the Lagrangian: in front of interaction operators only dimensionless constants can appear, likewise the electric charge  $e$ .

In the 1970s, the picture that was emerging from experiments was about a matter composed by a set of fermions, *leptons* and *quarks*, mainly interacting by

---

<sup>3</sup>Disconnected Feynman diagrams should be disregarded as they do not carry the singularity structure, while the multiplication of external lines by a factor  $p^2 + m^2$  together with the on-shell limit  $p^2 \rightarrow -m^2$ , automatically amputates all external lines.

the exchange of boson particles. Three fundamental forces have been identified: electromagnetic, strong and weak interactions. The *electromagnetic interaction* couples charged fermions, the *strong interaction* is responsible for atomic nuclei formation and quarks interaction, while the *weak interaction* is accountable for beta decay.

The great success of *Quantum Electrodynamics* (QED) as a description for electromagnetic interactions persuaded physicists that strong and weak interactions could be explained with similar theories. QED is an Abelian gauge theory in which the interaction between charged particles simply arises from the request of Lagrangian invariance under the local  $U(1)$  transformation. The natural extension of QED is provided by non-Abelian gauge theories, also termed Yang-Mills theories, based on the  $SU(N)$  gauge groups. The story of these theories was troubled. They were first developed in 1954 but suddenly abandoned since experiments suggested the presence of massive bosons for weak interactions, that could not be predicted by these theories. One decade later, the idea of spontaneous symmetry breaking (SSB) restored Yang-Mills theories: the Higgs mechanism, i.e., the SSB of gauge symmetries, enables weak bosons to acquire mass; it also suggests the presence of a new particle, named Higgs boson, detected at CERN in 2012.

The present formulation of SM is based on gauge theories, in particular the combined  $SU(3)_c \times SU(2)_L \times U(1)_Y$  gauge group is that of the SM. The indices  $c$ ,  $L$  and  $Y$  denote the charges that belong to each group: the color, the left-handed weak isospin and the hypercharge, respectively. Nowadays, SM consists in two sectors: the *Quantum Chromodynamics* (QCD), based on  $SU(3)_c$ , that provides a theoretical description for strong forces, and the *Electroweak* (EW) theory, related to  $SU(2)_L \times U(1)_Y$ , that provides a unified model for electromagnetic and weak interactions.

## 1.2 Gauge Theories

The Standard Model is based on the key concept of gauge theories. An early indication that gauge theories could have a physical application was given by Maxwell equations, which in terms of scalar and vector potentials show gauge invariance. Subsequently, the success of QED in predicting electromagnetic phenomena definitively paved the way for these theories.

### 1.2.1 The Abelian Case: QED

The simplest example of a gauge theory is provided by the Abelian case related to the local group  $U(1)$ , that furnishes the theoretical framework to build QED.

Quantum Electrodynamics can explain almost all the observed electromagnetic phenomena. Not only can QED – as a quantum theory – explain events happening at a femtometer scale, but also at a macroscopic one, since it embeds Maxwell equations. At the same time, QED represents the first complete quantum field theory and its birth dates back to the publication of *Quantum theory of emission and absorption of radiation*, by Dirac in 1927 [2]. Dirac described the quantized electromagnetic field as an ensemble of harmonic oscillators and introduced the idea of creation and annihilation operators of particles. In the following years, many

physicists contributed to the development of an elegant formulation for the theory. Even though they initially believed that QED would enable every calculation of processes involving photons and charged particles, they soon realized that from higher-order computations some infinities were emerging, thus making calculations meaningless and even casting doubts on the internal consistency of the theory. At first, the problem was overcome by H. Bethe in 1947 who, while traveling on a train, back from the famous Shelter Island conference, computed the line shift of hydrogen atom as measured by Lamb and Rutherford. Bethe's idea of relating infinities to the mass and charge corrections represents the foundations of the modern renormalization procedure that ensures finite results at any order in perturbation series. Due to its large success in predicting experimental outcomes, QED has served as basic template for all subsequent quantum field theories.

The starting point to build QED is provided by Dirac Lagrangian for a massive fermion

$$\mathcal{L} = \bar{\psi} (i\cancel{\partial} - m) \psi,$$

whose derivation is shown in Appendix A.4.3. Dirac Lagrangian is symmetric under the global  $U(1)$  transformation, that acts on the fermion field as  $\psi(x) \rightarrow e^{i\alpha} \psi(x)$ . In quantum mechanics, changes in phase of the wave function must be unobservable thus the symmetry under a unitary transformation is demanded to express the conservation of probability.

Nevertheless, the Dirac Lagrangian describes a free fermion field, while the aim of QED is to build a theoretical framework for interacting particles since charged particles interact among them and with photons. Furthermore, classical electromagnetism suggests that gauge theories are suitable for describing an interacting theory because Maxwell equations are blind to the addition of a gradient to the four-vector potential, i.e., they are symmetric under a gauge transformation. In addition, Maxwell equations are expected to rise as equations of motion from the appropriate QED Lagrangian.

The simple way to get a gauge – or local – transformation from the global unitary  $U(1)$  is just to make the phase dependent on the space-time, such that  $\alpha \rightarrow \alpha(x)$ . The *gauge transformation* of Dirac field is:

$$\psi(x) \rightarrow e^{i\alpha(x)} \psi(x) \equiv U(x) \psi(x). \quad (1.1)$$

The Dirac Lagrangian, however, does not remain unchanged under a local transformation since the derivative operator does not transform homogeneously with the field. The symmetric property is restored once the extra term, generated by deriving the phase, is absorbed by the suitable derivation operator. The latter, named gauge covariant derivative,  $D_\mu$ , must transform under the local  $U(1)$  homogeneously with the field

$$D_\mu \psi(x) \rightarrow U(x) D_\mu \psi(x). \quad (1.2)$$

The simplest choice for such gauge covariant derivative is dictated by minimal coupling:

$$D_\mu \equiv \partial_\mu + ieA_\mu,$$

where the constant  $e$ , i.e., the classical electric charge, represents the strength of the interaction between the photon and the charged fermion, whose charge is indeed

*e.* Moreover, a new gauge vector field,  $A_\mu(x)$ , is introduced, that accordingly to equation (1.2) transforms as

$$A_\mu(x) \rightarrow A_\mu(x) - \frac{1}{e} \partial_\mu \alpha(x).$$

The QED Lagrangian is nothing but Dirac Lagrangian with the minimal substitution, namely  $\partial \rightarrow D$ , plus the kinetic term for the new gauge vector boson, derived in Appendix A.4.2. In absence of external sources, the QED Lagrangian for a single fermion flavor is

$$\mathcal{L}_{QED} = \bar{\psi} (i\not{D} - m) \psi - \frac{1}{4} F_{\mu\nu} F^{\mu\nu}, \quad (1.3)$$

where  $F_{\mu\nu} = \partial_\mu A_\nu - \partial_\nu A_\mu = -\frac{i}{e} [D_\mu, D_\nu]$  is the field strength tensor. One can notice that a mass term for gauge vector field would break local symmetry. In other words, requiring an invariant Lagrangian under the local  $U(1)$  automatically fixes at zero the mass of  $A_\mu(x)$ . The gauge vector field is understood as the photon field since its equations of motion are, as expected, the inhomogeneous Maxwell equations:

$$\partial_\mu F^{\mu\nu} = e \bar{\psi} \gamma^\nu \psi,$$

while the EOM for Dirac field is the well-known Dirac equation:

$$(i\not{D} - m) \psi = 0.$$

Since QED Lagrangian is symmetric under a gauge transformation of fields, consequently, a conserved current arises via Noether theorem

$$\partial_\mu j^\mu = 0,$$

which is nothing but the continuity equation with  $j^\mu = \bar{\psi} \gamma^\mu \psi$ . The related conserved charge is:

$$Q = \int d^3x \psi^\dagger \psi = \int d^3x \rho,$$

where  $\rho$  is the electric charge density.

Since gauge theories are equivalent to constrained Hamiltonian systems, the derivation of their Feynman rules is not straightforward. Specifically, the propagator of the photon field cannot be obtained from the kinetic as it appears in equation (1.3). At first, we have to rearrange the kinetic term as

$$-\frac{1}{4} F_{\mu\nu} F^{\mu\nu} \rightarrow \frac{1}{2} A^\mu (g_{\mu\nu} \partial^2 - \partial_\mu \partial_\nu) A^\nu, \quad (1.4)$$

which is not an equality since total derivatives were suppressed. The term in the brackets, being singular, does not admit an inverse operator, i.e., its determinant is null, thereby the photon propagator cannot be defined. The motivation for that still lies in gauge symmetry, indeed the same operator appears in Maxwell equations, which can be recast as  $(g_{\mu\nu} \partial^2 - \partial_\mu \partial_\nu) A^\nu = e j_\mu$ . Maxwell equations show that a specified vector current  $j^\nu(x)$  does not uniquely define the field  $A^\nu(x)$ . The



technique to solve this issue was identified by L. D. Faddeev and A. S. Popov and consists in the introduction of the a gauge fixing term

$$\mathcal{L}_{gf} = \frac{1}{2\xi} A^\mu \partial_\mu \partial_\nu A^\nu, \quad (1.5)$$

where  $\xi$  is a free parameter. Adding together equations (1.4) and (1.5), the complete Lagrangian for the photon field reads:

$$\mathcal{L}_\xi = \frac{1}{2} A^\mu (g_{\mu\nu} \partial^2 - (1 - \xi^{-1}) \partial_\mu \partial_\nu) A^\nu,$$

where the operator inside the brackets now admits an inverse, leading to the definition of the photon propagator  $i\Pi_{\mu\nu}$ , that, in the so-called  $R_\xi$ -gauge, is:

$$i\Pi_{\mu\nu} = \frac{-i}{p^2 + i\varepsilon} \left( g_{\mu\nu} - (1 - \xi) \frac{p_\mu p_\nu}{p^2} \right). \quad (1.6)$$

Remarkably, all observables in QED are independent from the parameter  $\xi$ , whose value can be arbitrarily chosen to simplify computations; indeed, selecting a specific value of  $\xi$ , we are *fixing* the gauge.

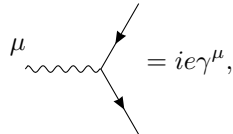
The Faddeev and Popov's method is not the only known solving strategy to fix the issue, the same result can be achieved by introducing an auxiliary field<sup>4</sup>, however it is the widely adopted since it appears to be particularly useful in non-Abelian gauge theories.

The other Feynman rules for QED directly follow from the Lagrangian. The internal lines, or propagators, including again the photon in Feynman gauge ( $\xi = 1$ ), are

$$\begin{aligned} \mu \text{ --- } \text{wavy} \text{ --- } \nu &= \frac{-i g_{\mu\nu}}{p^2 + i\varepsilon}, \\ \text{--- } \text{arrow} \text{ ---} &= \frac{i(\not{p} + m)}{p^2 - m^2 + i\varepsilon}, \end{aligned}$$

while external lines give the polarization vectors for the boson field, with  $\epsilon_\mu(p)$  for an incoming and  $\epsilon_\mu^*(p)$  for an outgoing photon, and spinors for the fermion fields, with  $u^s(p)$  ( $\bar{v}^s(p)$ ) and  $\bar{u}^s(p)$  ( $v^s(p)$ ) for an incoming and outgoing particle (antiparticle), respectively. External lines are forced by LSZ formula to be on-shell, thus they satisfy the equations of motion.

The interaction vertex of QED is



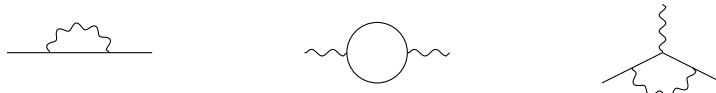
$$= ie\gamma^\mu,$$

---

<sup>4</sup>The equation (1.5) can be obtained by introducing the auxiliary scalar field,  $B(x)$ , whose Lagrangian is  $\mathcal{L}_{gf} = \xi B^2/2 + A^\mu \partial_\mu B$ . Since the equation of motion for the scalar field is  $\partial_\mu A^\mu = \xi B$ , the Lagrangian of the auxiliary field can be written, up to a total derivative, as equation (1.5), where the auxiliary field does not even appear.

which does not depend on the momenta of the interacting particles. Two extra rules should be added: a -1 factor for the interchange of external identical fermions that is related to Wick's contraction, and a -1 factor for each fermion loop, as it involves a trace operation over spinor indices, reflecting the anti-commuting nature of spinors.

Feynman rules lead to a direct computation of observables, for both tree-level and higher-orders diagrams. In four dimensions, QED is, in fact, a renormalizable theory as it brings a finite number of ultraviolet divergences related to the electron self-energy, the vacuum polarization and the correction to vertex interaction, whose diagrams are



Whenever another diagram shows up a divergence, that means it contains as components one, or more, of previous diagrams. Thus, renormalization procedure aims to remove just the primary divergences by absorbing them into unobservable Lagrangian parameters.

Despite QED predicts experimental outcomes with great accuracy, it cannot be the ultimate theory of electromagnetic interactions. From the vacuum polarization diagram, the effective fine structure constant is:

$$\alpha_{eff}(-p^2) = \alpha_R \left[ 1 + 0.00077 \ln \left( \frac{-p^2}{m_e^2} \right) \right],$$

where  $\alpha_R = e_R^2/(4\pi)$ , while  $p$  is the momentum of the external photon and  $m_e$  the mass of the electron running in the loop. The correction term introduces a weak dependence on photon momentum, expressed by the logarithmic function in the previous equation. The positive sign of logarithm entails an increasing behavior in energy for the fine structure constant, even though only high-precision experiments are sensitive to it, due to the numerically tiny magnitude of its coefficient. Nevertheless, one can wonder what is the energy scale at which the correction becomes comparable to the leading term, i.e.,  $0.00077 \ln(-p^2) \sim 1$ . The result is an extremely high-energy level,  $Q^2 = -p^2 \sim 10^{286}$  eV, far away from the maximum energies accessible at Large Hadron Collider (LHC), around  $10^{13}$  eV. At such high scale, the perturbation theory breaks down as higher-order diagrams become larger than lower ones, identifying the so-called *Landau Pole* for QED. Thus, QED allows to make predictions at relatively large distances, since at short scales the perturbation theory for electromagnetism becomes meaningless.

Within the framework of the SM, QED is included alongside to the theory of weak interactions, in the Electroweak theory, which is associated to the gauge group  $U(1)_Y \times SU(2)_L$ , where  $Y$  and  $L$  denote the hypercharge<sup>5</sup> and the left-handed weak isospin, respectively. This unified model describes the weak and the electromagnetic forces as two different aspects of the same interaction, merging them at the energy scales above 246 GeV.

<sup>5</sup>Landau pole persists in  $U(1)_Y$  gauge group.

### 1.2.2 The non-Abelian Case: QCD

The straight extension for Abelian case is provided by Yang-Mills theory, that is non-Abelian gauge theory associated to the local symmetry group  $SU(N)$ . Quantum Chromodynamics serves as a concrete example to explain non-Abelian gauge theory since it is associated to the local  $SU(3)$ .

Quantum Chromodynamics is the theory that describes strong interactions. The elementary fermions affected by strong force are named quarks, while gluons are the force-carriers. On the contrary of photon, gluons are themselves affected by strong interaction since they are charged under  $SU(3)$ . The charge of  $SU(3)$  is called color charge, even though the analogy with real colors is limited to the number 3: a single quark of a specific flavor can appear in three different states of color as three is the number of basic colors in the additive RGB-model.

In the 1950s, the number of new particles considerably picked up due to the invention of the bubble chamber, however physicists were convinced that not all of these new states were fundamental. New particles, later called hadrons and mesons, were classified in many different frameworks for the purpose of understand the connections between them, however, pieces began to fall into place, only in 1963 thanks to Gell-Mann and Zweig, who hypothesized the existence of three new fundamental fermion flavors, i.e., the quarks. The two physicists introduced three quark flavors, called *up*, *down* and *strange*, whom in different combinations form mesons and hadrons. In 1968, performing deep inelastic scattering processes, at SLAC, was gather the first evidence of proton as a composed particle.

The need for introducing a new gauge freedom, i.e., the color charge, became quite evident when physicists tried to explain the  $\Delta^{++}$  baryon with quark theory, indeed such a state is understood to be composed of three quarks up, which due to Pauli exclusion principle cannot have the same quantum numbers in a bound state.

The mathematical framework for QCD was built in the early 1970s, again by Gell-Mann and others, that employed the non-Abelian field theory developed in 1954 by Chen Ning Yang and Robert Mills, to explain an interaction where also the mediator takes part in it by radiating further force carriers.

Nevertheless, experiments were not able to identify single quarks, thus discharging the theory. The discovery that asymptotic freedom and color confinement are directly embedded in non-Abelian gauge theory gave back credibility to QCD. First experimental evidences of gluons were obtained at PETRA in 1979, while the number of quark flavors was increased in the following years, up to six, with the discoveries of *charm* (1974), *bottom* (1977) and *top* (1995) quarks.

Quantum Chromodynamics appears to be well-defined once the appropriate gauge group and fermion representation under a selected group have been defined. Since color charge was introduced just to restore Fermi-Dirac statistics for quarks, but does not bring any fundamental physical role, it was identified as the quantum number for the gauge group. Based on this assumption, the choice for  $SU(3)$  appeared straightforward, and further experiments provided support to it, for instance, eight states of gluon were identified as predicted by  $SU(3)$ <sup>6</sup>.

The derivation of Quantum Chromodynamics Lagrangian starts with Dirac Lagrangian, likewise in QED. For a single flavor of quark  $\psi(x)$  that can appear in three

---

<sup>6</sup>The dimension of the adjoint representation for  $SU(N)$  to which vector bosons belong is  $N^2 - 1$ .

different states of color, Dirac Lagrangian reads

$$\mathcal{L} = \sum_i^3 \bar{\psi}_i (i\cancel{\partial} - m) \psi_i,$$

where  $i$  is the color index. This Lagrangian is invariant under the global  $SU(3)$  transformation of the field

$$\psi_i(x) \rightarrow (e^{i\omega^a T^a})_{ij} \psi_j(x)$$

where  $\omega_a$ , with  $a = \{1, \dots, 8\}$ , are the group parameters and  $T^a$  are  $3 \times 3$  Hermitian matrices, that span the 3-dimensional representation of the  $SU(3)$  Lie algebra, i.e., they are the generators of the fundamental representation of  $SU(3)$ . In particular,  $T^a$  are half of the Gell-Mann matrices, usually labeled as  $\lambda^a$ , see Appendix A.3.

Similarly to the Abelian case, even in the non-Abelian one the global transformation describes a non-interacting theory; once again, the coupling arises from the demand for invariance of Lagrangian under a local transformation. Using a less pedantic notation that drops out spinor color indices

$$\psi(x) \rightarrow U(x) \psi(x) = (e^{i\omega^a(x) T^a}) \psi(x), \quad (1.7)$$

where  $\psi(x)$  stands for a column of three Dirac spinors. Looking for a derivative operator that transforms homogeneously with the field

$$D_\mu \psi(x) \rightarrow U(x) D_\mu \psi(x),$$

we can introduce a new field through the minimal coupling

$$D_\mu = \partial_\mu - ig_s A_\mu(x) \equiv \partial_\mu - ig_s A_\mu^a(x) T^a,$$

where the constant  $g_s$  represents the strength of the coupling. The gauge bosons  $A_\mu(x)$  is a vector of eight real potentials. Its transformation under  $SU(3)$  is:

$$A_\mu(x) \rightarrow U(x) A_\mu(x) U^\dagger(x) - \frac{i}{g_s} [\partial_\mu U(x)] U^\dagger(x), \quad (1.8)$$

that in terms of components is

$$A_\mu^a(x) \rightarrow A_\mu^a(x) + \frac{1}{g_s} \partial_\mu \omega^a(x) - f^{abc} \omega^b(x) A_\mu^c(x).$$

Since we have introduced a new field in the Lagrangian, we require a kinetic term to describe its dynamics. According to the Abelian case, we can build the tensor field strength by using the covariant derivative:

$$G_{\mu\nu}(x) = G_{\mu\nu}^a(x) T^a \equiv \frac{i}{g_s} [D_\mu, D_\nu] = \partial_\mu A_\nu(x) - \partial_\nu A_\mu(x) - ig_s [A_\mu(x), A_\nu(x)],$$

which, due to the presence of the very last term, does not fulfill the commutative property. Each component of the tensor field strength is:

$$G_{\mu\nu}^a(x) = \partial_\mu A_\nu^a(x) - \partial_\nu A_\mu^a(x) + g_s f^{abc} A_\mu^b(x) A_\nu^c(x).$$

Its transformation law is completely fixed by that of covariant derivative, which in turn is set by equation (1.7) and is  $D_\mu \rightarrow U(x) D_\mu U^\dagger(x)$ . Then the transformation law for  $G_{\mu\nu}$  reads

$$G_{\mu\nu}(x) \rightarrow U(x) G_{\mu\nu}(x) U^\dagger(x),$$

in other words, the tensor field strength transforms accordingly to the adjoint representation of gauge group. The kinetic term of the gauge potentials is equivalent to that found for the photon, since even in non-Abelian case is the square of the tensor field strength, i.e.,  $G_{\mu\nu} G^{\mu\nu}$ .

The Lagrangian of Quantum Chromodynamics<sup>7</sup> for a single quark flavor, making explicit color indices, is

$$\mathcal{L}_{QCD} = \sum_{i,j=1}^3 \bar{\psi}_i [(i\not{\partial} - m) \delta_{ij} + g_s A^a T_{ij}^a] \psi_j - \frac{1}{4} G_{\mu\nu}^a G^{a\mu\nu}. \quad (1.9)$$

This theory just depends upon two parameters, namely the mass of the fermion and the coupling constant. Since QCD Lagrangian is symmetric under the local transformations of the fields, identified by equation (1.7) and equation (1.8), a conserved vector of currents<sup>8</sup> arises due to Noether theorem

$$J^{\mu a}(x) \equiv -\bar{\psi}_i(x) \gamma^\mu T_{ij}^a \psi_j(x) + f^{abc} A_\nu^b(x) G^{c\mu\nu}(x),$$

which satisfies  $\partial_\mu J^{\mu a} = 0$ , for each value of  $a$ . Nevertheless, the vector of currents, i.e.,  $J^\mu(x)$ , is not gauge invariant, hence it does not have any physical meaning and no charge can be associated to it, according to Weinberg-Witten theorem<sup>9</sup>. In fact, in QCD as in any non-Abelian gauge theory, gauge fields are related to matter fields in a non-linear way and the characteristic current of charged particles does not even exist. Only the fermionic part of the previous current, defined as

$$j^{\mu a}(x) \equiv -\bar{\psi}_i(x) \gamma^\mu T_{ij}^a \psi_j(x),$$

proves to be gauge invariant. It satisfies the continuity equation  $\nabla_\mu^{ab} j^{\mu b} = 0$ , where  $\nabla_\mu^{ab} \equiv \partial_\mu \delta^{ab} + g f^{abc} A_\mu^c$ , is the adjoint covariant derivative.

The EOM for the matter field is again the Dirac equation for each single state of color, while that for gauge fields are:

$$\nabla_\mu^{ab} G^{\mu\nu b} = j^{\nu a}.$$

---

<sup>7</sup>In the Standard Model a mass term for fermion is forbidden due to the chiral gauge symmetry  $SU(2)_L$ ; fermions are indeed introduced massless, but their mass arise from the interaction with Higgs boson. In the massless limit, QCD satisfies the global chiral symmetry  $SU(N)_L \times SU(N)_R$ , where left-handed and right-handed chiral components of  $N$  flavors of quark can be independently rotated among themselves. The symmetry is spontaneously broken by the vacuum expectation value of the bilinear operator  $\bar{q}_L q_R$  that being different from zero, acts as an effective mass for quark. The residual symmetry is  $SU(N)$ , that identically rotates the two chiral components. Due to Goldstone theorem, one should expect to find  $N^2 - 1$  massless states. Nonetheless, QCD does not embed massless matter particles, but it contains a relatively light pseudoscalar triplet: the pions. These mesons are the pseudo Nambu-Goldstone bosons since the symmetry is explicitly broken by quark masses, explaining the relatively small mass of pions compared to that of other mesons with similar quark content.

<sup>8</sup>In non-Abelian gauge theories there are  $N^2 - 1$  conserved currents, one for each symmetry direction  $\omega^a$ , thus in QCD the vector of currents has eight components.

<sup>9</sup>The Weinberg-Witten theorem states that a non-Abelian theory involving massless 1-spin bosons does not admit any conserved current that is gauge invariant.

All Feynman rules of QCD follow from the Lagrangian with the exception of the gluon propagator, that, as the photon propagator, requires a special attention in order to be defined. The Faddeev and Popov trick can be used again to identify the gluon propagator; however, in the non-Abelian case is necessary to add not only a gauge-fixing term – equivalent to equation (1.5) – but also a ghosts Lagrangian

$$\mathcal{L}_{gf} = \frac{1}{2\xi} A^{a\mu} \partial_\mu \partial_\nu A^{a\nu} + \bar{c}^a (-\partial^2 \delta^{ac} - g \partial^\mu f^{abc} A_\mu^b) c^c, \quad (1.10)$$

where  $c(x)$  and  $\bar{c}(x)$  are the ghost and anti-ghost fields, respectively. The ghost part of  $\mathcal{L}_{gf}$  is simply given by a kinetic term, plus the interaction between ghosts and gluons. Note that for each gauge field exists one associated ghost<sup>10</sup>. The Faddeev and Popov ghosts are an artifact due to the insistence on describing Nature with gauge theories. In fact, the path integral formulation of a gauge theory is ambiguous and singular since we are overcounting the field configurations corresponding to the same physical state. Nevertheless, Faddeev and Popov method fix this issue, but the price to be paid is the appearance of ghosts. These fields might be included in higher orders of perturbation series and then in Feynman diagrams, although as virtual states. Ghosts are not physical particles since they violate the spin-statistics theorem, indeed they are anti-commuting complex scalars. In loops diagrams, where a gauge field can go off-shell and acquiring non-physical degrees of freedom, the ghost acts by counterbalancing this effect, thus the fermionic rule of -1 factor in loops must hold for ghosts.

The Faddeev and Popov ghosts do not appear in all gauges, indeed in the so-called Dirac compatible gauges they are unnecessary. A Dirac-type gauge is a proper functional of canonical variables, in other words it cannot include Lagrange multipliers associated to primary constraints. The standard choices for gauge, namely the Lorenz gauge ( $\partial_\mu A^\mu = 0$ ), but even the temporal gauge ( $A_0 = 0$ ), do not belong to Dirac-type, on the contrary, axial ( $A_3 = 0$ ) and Coulomb gauge ( $\nabla \cdot \mathbf{A} = 0$ ) do. The equation (1.10) clarifies why ghosts are not required in QED: in Abelian theories the structure constants are null, leading to a ghost Lagrangian with just the kinetic term.

The Lagrangian resulting from the sum of QCD and the gauge fixing terms, namely equations (1.9) and (1.10), does no longer satisfy the gauge invariance, it, however, fulfills a global symmetry, called BRST. The total Lagrangian is invariant under the transformation

$$\begin{aligned} A_\mu^a(x) &\rightarrow A_\mu^a(x) + \frac{1}{g} \theta D_\mu c^a(x), \\ \psi(x) &\rightarrow \psi(x) + i g \theta c^a T^a \psi(x), \\ c^a(x) &\rightarrow c^a(x) - \frac{1}{2} \theta f^{abc} c^b c^c, \\ \bar{c}^a(x) &\rightarrow \bar{c}^a(x) - \frac{1}{g} \theta \frac{1}{\xi} \partial^\mu A_\mu^a(x), \end{aligned}$$

where  $\theta$  is a Grassmann number. In BRST,  $\theta c(x)$  plays the same role as  $\alpha(x)$  in a

---

<sup>10</sup>The gauge field and its ghost have a very close connection. In a theory with spontaneous symmetry breaking, if the gauge field becomes massive through Higgs mechanism, then its ghost acquires an equal value of mass.

gauge transformation, then we can state that the former is a generalization of the latter. Moreover, BRST still holds despite the gauge fixing term.

The BRST operator, which is accountable for the transformation of fields, is a nilpotent operator that commutes with the Hamiltonian. In charge of that, it divides the eigenstates of  $\mathcal{H}$  into three subgroups; two of them, including forward and backward polarizations of gauge bosons as well as ghost and anti-ghost, are non-physical, while the third subgroup is that of physical states, in fact longitudinal polarizations of the gluons belongs to it.

A paramount implication of BRST symmetry is the renormalization of non-Abelian gauge theories. In fact, not only BRST is preserved in loop since it is an exact symmetry of the Lagrangian, but the most general BRST-invariant Lagrangian also appears to have all the required parameters in order to absorb the infinities.

The gauge fixing term for QCD leads to the definition of the Feynman propagator for the gluon field in the  $R_\xi$ -gauge, that is:

$$i\Pi_{\mu\nu}^{ab} = \frac{-i\delta^{ab}}{p^2 + i\varepsilon} \left( g_{\mu\nu} - (1 - \xi) \frac{p_\mu p_\nu}{p^2} \right).$$

The Feynman propagators for QCD, including the gluon propagator in Feynman gauge, are:

$$\begin{aligned} \mu, a \text{ --- } \text{wavy} \text{ --- } \nu, b &= \frac{-ig_{\mu\nu} \delta^{ab}}{p^2 + i\varepsilon}, \\ i \text{ --- } \text{arrow} \text{ --- } j &= \frac{i(\not{p} + m) \delta_{ij}}{p^2 - m^2 + i\varepsilon}, \\ a \text{ --- } \text{dotted} \text{ --- } b &= \frac{i\delta^{ab}}{p^2 + i\varepsilon}, \end{aligned}$$

while the interaction vertices between gauge fields only, are

$$\begin{aligned} \begin{array}{c} p_2, \nu, b \\ \text{wavy} \\ p_1, \mu, a \\ \text{wavy} \\ p_3, \rho, c \end{array} &= -g_s f^{abc} [g^{\mu\nu}(p_1 - p_2)^\rho + g^{\nu\rho}(p_2 - p_3)^\mu + g^{\rho\mu}(p_3 - p_1)^\nu], \\ \begin{array}{c} \mu, a \quad \nu, b \\ \text{wavy} \quad \text{wavy} \\ \text{wavy} \quad \text{wavy} \\ \sigma, d \quad \rho, c \end{array} &= -ig_s^2 \left[ f^{abe} f^{cde} (g^{\mu\rho} g^{\nu\sigma} - g^{\mu\sigma} g^{\nu\rho}) + f^{ace} f^{bde} (g^{\mu\nu} g^{\rho\sigma} - g^{\mu\sigma} g^{\nu\rho}) \right. \\ &\quad \left. + f^{ade} f^{bce} (g^{\mu\nu} g^{\rho\sigma} - g^{\mu\rho} g^{\nu\sigma}) \right], \end{aligned}$$

while those between gluon and matter, including the non-physical ghosts, are

$$\begin{array}{cc}
 \begin{array}{c} i \\ \nearrow \\ \mu, a \\ \text{~~~~~} \\ \searrow \\ j \end{array} & = ig_s \gamma^\mu T_{ij}^a, & \begin{array}{c} b \\ \text{~~~~~} \\ \mu, a \\ \text{~~~~~} \\ \text{~~~~~} \\ c, p \end{array} & = -g_s f^{abc} p^\mu.
 \end{array}$$

The computation of next to leading order Feynman diagrams in QCD could lead to divergent results. However, like QED, even Quantum Chromodynamics is a renormalizable theory since it embeds a finite number of primary divergences, related to the radiative correction of the two and three-point correlation functions, that can be absorbed in unobservable Lagrangian parameters<sup>11</sup>. The renormalization of QCD gauge coupling introduces a scale dependence with opposite behavior to that identified in QED. In fact, Quantum Chromodynamics becomes non-perturbative at energies below one GeV, where  $\alpha_s = g_s^2/(4\pi) \approx 0.4$ , while at high energy is well-defined. This property, known as asymptotic freedom, also leads to quark confinement: quarks cannot be observed as free particles since the potential between colored states grows linearly with the separation until the energy involved is enough to create a new couple of quarks.

Not only the property of asymptotic freedom has been shown to be a common feature of the whole set of non-Abelian gauge theories, but also a prerogative of it since among renormalizable theories in four dimensions is exclusive to this set. If on one side, the running constant in QED is interpreted as the production of virtual electron-positron pairs by a background electromagnetic field, causing a screening effect of the bare charge, on the other side, in QCD the asymptotic freedom introduces an additional effect of anti-screening. The two effects, on balance, do not have the same magnitude, with the anti-screening that is almost twelve times greater than screening. The overall impact is a decreasing value of the coupling constants at high-energy scales.

At the energy scale below one GeV, where the perturbation theory breaks down, the adopted technique for Quantum Chromodynamics computations is the Lattice QCD, introduced by K. Wilson, where the space-time is discretized in a grid of points. Perturbative QCD is recovered when the lattice is taken infinitely large and its points infinitesimally close to each other.

### 1.3 Electroweak Theory

The electroweak (EW) theory provides a unified description of weak and electromagnetic interactions. The gauge group of EW theory is the local  $SU(2)_L \times SU(1)_Y$ . However, a non-Abelian gauge theory alone fails in describing experimental observations, since short-range nature of the interaction requires massive force-carriers. A further ingredient is needed for bosons to gain mass: spontaneous symmetry breaking.

<sup>11</sup>In QED the number of required counter-terms is three, while QCD needs eight counter-terms to be renormalized.



The electroweak theory achieved its present formulation after more than forty years of research and efforts by several physicists. The starting point is Fermi theory of weak interaction, outlined by the Italian Nobel physicists in 1933. Subsequently, Feynman and Gell-Mann implemented the theory giving rise to the famous V-A theory [5], that, however, is a non renormalizable theory of dimension-6 operators (see chapter 2). Despite its moderate success in describing experimental observations, the theory proved unfruitful at sufficiently high energies. Furthermore, in 1956 Wu observed parity and charge violations in weak interaction, a fact that led to the search for a unified framework for weak and electromagnetic interactions.

In 1961 Glashow proposed a model based on the gauge group  $SU(2) \times SU(1)$ , he predicted two neutral vectors, the massless photon and the massive  $Z$ ; however, at that time spontaneous broken symmetry was not known yet, and the breaking was enforced by the explicit addition of mass terms for vector boson and for leptons [6]. Moreover, Glashow's theory was not renormalizable. In the mid-1960s, Salam and Ward made a similar attempt, obtaining a theory with four bosons, three massive and one massless [7]; nonetheless, their theory suffered from the same problem as that of Glashow: the symmetry had to be broken by hand.

The breakthrough came in 1967, when Weinberg integrated the spontaneous symmetry breaking research of Englert [8], Higgs [9] and others into the model of electroweak interactions [10]. Finally, in 1971 't Hooft showed that gauge theories with spontaneous symmetry breaking are renormalizable [11].

The model of electroweak interactions theorized the existence of  $W$  and  $Z$  bosons and predicted their mass values even before they were experimentally identified. The collaborations UA1 and UA2, at CERN, confirmed the existence of these particles only in the early 1980s, while the Higgs boson had to wait until 2012, when it was tracked by the ATLAS and CMS experiments, once again at CERN.

The EW theory is based on the key concept of spontaneous symmetry breaking, which is caused by the non-vanishing vacuum expectation value of a scalar field, that at low energy shatters the gauge group of the theory leaving just a residual symmetry that is the electromagnetic  $U(1)_{EM}$ , discussed in section 1.2.1

$$SU(2)_L \times U(1)_Y \rightarrow U(1)_{EM}. \quad (1.11)$$

At high energy, where the symmetry is unbroken, the gauge structure of the group is given by the combination of  $SU(2)_L$ , which has similar properties to those discussed in previous section for  $SU(3)^{12}$ , and  $U(1)_Y$  that is equivalent to the phase change of QED, but with a different charge, named the hypercharge  $Y$ . Thus EW includes four gauge bosons, named  $W_{\mu\nu}^i$  and  $B_{\mu\nu}$ . The former is similar to the gluon field strength tensor  $G_{\mu\nu}^a$ , while the latter to the electromagnetic field strength tensor  $F_{\mu\nu}$ . In EW theory the gauge group is broken by the vacuum expectation value ( $vev$ ) of a complex  $SU(2)_L$  doublet  $H$ , named Higgs doublet, with hypercharge 1/2. The electroweak Lagrangian for gauge bosons and Higgs doublet is:

$$\mathcal{L}_{EW} = -\frac{1}{4}W_{\mu\nu}^i W^{i\mu\nu} - \frac{1}{4}B_{\mu\nu} B^{\mu\nu} + (D_\mu H)^\dagger (D^\mu H) + \mu^2 H^\dagger H - \lambda(H^\dagger H)^2. \quad (1.12)$$

The covariant derivative, that couples the gauge fields to Higgs doublet, is

$$D_\mu = \partial_\mu - igW_\mu^a \tau^a - \frac{1}{2}ig' B_\mu, \quad (1.13)$$

---

<sup>12</sup>The group generators in  $SU(2)$  are half of Pauli matrices, while the completely antisymmetric structure constants are  $\epsilon^{ijk}$ .

where  $g$  and  $g'$  are the  $SU(2)_L$  and  $U(1)_Y$  coupling constants, respectively. The factor  $1/2$ , in front of  $B_{\mu\nu}$  comes from the fact that Higgs doublet has hypercharge  $Y = 1/2$ .

The potential  $V(H) = -\mu^2 H^\dagger H + \lambda(H^\dagger H)^2$  induces a non null  $vev$  to the Higgs doublet, that is  $v = \mu\lambda^{-1/2}$ . Furthermore, it allows to write the field  $H$  as:

$$H = e^{2i\frac{\pi^i\tau^i}{v}} \begin{pmatrix} 0 \\ \frac{v+h}{\sqrt{2}} \end{pmatrix}, \quad (1.14)$$

where  $\pi^i$  are the massless Goldstone bosons, which are responsible for the mass of the weak vector bosons. The real scalar fields  $h$  is the renowned Higgs bosons.

Expanding the EW Lagrangian by equations (1.13) and (1.14) and assuming the unitary gauge for the latter so that  $\pi^i = 0$ ; for the kinetic terms we get

$$\mathcal{L}_{gauge} = -\frac{1}{2} (\partial_\mu W_\nu^+ - \partial_\nu W_\mu^+) (\partial_\mu W_\nu^- - \partial_\nu W_\mu^-) - \frac{1}{4} F_{\mu\nu} F^{\mu\nu} - \frac{1}{4} Z_{\mu\nu} Z^{\mu\nu},$$

where the fields has been defined as

$$\begin{aligned} Z_\mu &\equiv \cos\theta_w W_\mu^3 - \sin\theta_w B_\mu, \\ A_\mu &\equiv \sin\theta_w W_\mu^3 + \cos\theta_w B_\mu, \\ W^\pm &\equiv \frac{1}{\sqrt{2}} (W_\mu^1 \mp iW_\mu^2), \end{aligned}$$

with the weak angle that is

$$\tan\theta_w \equiv \frac{g'}{g}. \quad (1.15)$$

Moreover, some massive terms arises

$$\mathcal{L}_{masses} = \frac{1}{2} m_Z^2 Z_\mu Z^\mu + m_W^2 W_\mu^+ W^{-\mu} - \frac{1}{2} m_h^2 h^2,$$

while the field  $A_\mu$  remains massless. Moreover, one can notice that the masses of weak bosons are related to the parameters of the theory

$$\begin{aligned} m_W &= \frac{gv}{2}, \\ m_Z &= \frac{m_W}{\cos\theta_w}, \\ m_h &= \sqrt{2\lambda}v^2. \end{aligned}$$

These equations introduce a hierarchy in the masses of weak bosons, since  $m_Z$  must be greater than  $m_W$ . Moreover, rewriting the covariant derivative in terms of the mass eigenstate, it becomes

$$D_\mu = \partial_\mu - \frac{ig}{\sqrt{2}} (W_\mu^+ \tau^+ + W_\mu^- \tau^-) - \frac{ig}{\cos\theta_w} (\tau^3 - \sin^2\theta_w Q) Z_\mu - ieQ A_\mu, \quad (1.16)$$

where  $\tau^\pm = (\tau^1 \pm i\tau^2)$ ,  $Q = T^3 + Y$  and  $g = e/\sin\theta_w$ . Even if the free parameters of the electroweak theory are  $g$ ,  $g'$ ,  $\mu$  and  $\lambda$ , from the experimental point of view it is more straightforward to make use of

$$\begin{aligned} m_Z &= 91.19 \text{ GeV}, & m_W &= 80.38 \text{ GeV}, \\ m_h &= 125 \text{ GeV}, & G_F &= 1.166 \times 10^{-5} \text{ GeV}^{-2}, \end{aligned}$$

where the Fermi constant is related to the  $vev$  via  $v = (\sqrt{2}G_F)^{-1/2} = 246$  GeV. As we will see in chapter 2, the value of  $G_F$  can be obtained from muon decay.

The complete expansion of the EW Lagrangian shows that several interactions are allowed among gauge bosons and between gauge and Higgs field. The propagator of  $Z$  and  $W$  is the Proca propagator for massive gauge bosons, while the Higgs boson has the typical propagator of a scalar field.

The covariant derivative, in equation (1.16), also determines the coupling of gauge fields with fermions. Nevertheless, experimental evidences show that  $W$  boson only couple to left-handed fermion (and right handed anti-fermion), thus we have to treat  $\psi_L$  and  $\psi_R$  separately, see appendix A.4.3. Left-handed leptons and left-handed quarks transform under the fundamental representation of  $SU(2)_L$ <sup>13</sup>, thus they are arranged in doublets. The Standard Model includes three generation of leptons and three generation of quarks, namely

$$\ell^i = \begin{pmatrix} \nu_e \\ e^- \end{pmatrix}_L, \begin{pmatrix} \nu_\mu \\ \mu^- \end{pmatrix}_L, \begin{pmatrix} \nu_\tau \\ \tau^- \end{pmatrix}_L, \quad q^i = \begin{pmatrix} u \\ d \end{pmatrix}_L, \begin{pmatrix} c \\ s \end{pmatrix}_L, \begin{pmatrix} t \\ b \end{pmatrix}_L, \quad (1.17)$$

where  $i = \{1, 2, 3\}$ . On the contrary, right-handed fermions does not transform under  $SU(2)_L$ , i.e., they form the singlets

$$e_R^i = \{e_R, \mu_R, \tau_R\}, \quad u_R^i = \{u_R, c_R, t_R\}, \quad d_R^i = \{d_R, s_R, b_R\}, \quad (1.18)$$

where right-handed neutrinos have not been included for reasons we will explain shortly. Since all fermions couple to hypercharge gauge bosons, but with different hypercharge, we distinguish between  $Q_L$  and  $Q_R$ . The fermion Lagrangian is:

$$\mathcal{L} = \sum_{\psi_L} i\bar{\psi}_L(\not{\partial} - igW^a\tau^a - ig'Y_L\mathcal{B})\psi_L + \sum_{\psi_R} i\bar{\psi}_R(\not{\partial} - ig'Y_R)\psi_R, \quad (1.19)$$

where  $\psi_L = l, q$  and  $\psi_R = e_R, u_R, d_R$ . Notice that, no mass term has been introduced, in fact, an explicit term like  $\psi_L\psi_R$  violates the  $SU(2)_L$  invariance. Fermions are introduced as massless in electroweak theory, but the Yukawa-like interaction with Higgs doublet will be responsible for their mass after the EW symmetry breaking. A distinction between quarks and leptons is necessary. Starting with the former

$$\mathcal{L}_{Yuk} = -Y_{ij}^d\bar{q}_iH^\dagger d_{Rj} - Y_{ij}^u\bar{q}_i\tilde{H}u_{Rj} + \text{h.c.}, \quad (1.20)$$

where  $i$  and  $j$  run over the three generations and the dual Higgs doublet  $\tilde{H}$  has hypercharge  $-1/2$ . After the EW symmetry breaking all the mass terms become

$$\mathcal{L}_{Yuk, quark} = -\frac{v}{\sqrt{2}}(\bar{d}_LY_d d_R + \bar{u}_LY_u u_R) + \text{h.c.}.$$

The Yukawa matrices in this expression can be diagonalized

$$Y_d Y_d^\dagger = U_d M_d^2 U_d^\dagger, \quad Y_u Y_u^\dagger = U_u M_u^2 U_u^\dagger,$$

where the matrices  $U_i$  are unitary while the matrix  $(Y_i Y_i^\dagger)$  is Hermitian and thus has real eigenvalues. Additionally, in a general way we can write:

$$Y_d = U_d M_d K_d^\dagger, \quad Y_u = U_u M_u K_u^\dagger, \quad (1.21)$$

<sup>13</sup>Now, the meaning of subscript  $L$  is clear.

where  $K_i$  are others unitary matrices. The Yukawa couplings become

$$\mathcal{L}_{Yuk, quark} = -\frac{1}{\sqrt{2}} \left( \bar{d}_L U_d M_d K_d^\dagger d_R + \bar{u}_L U_u M_u K_u^\dagger u_R \right) + \text{h.c.}, \quad (1.22)$$

where the freedom of changing phase can be used in order to remove the matrices  $U$  and  $K$  from the Yukawa term. Rotating the left-handed quark as  $d_L \rightarrow U_d d_L$  and the right-handed as  $d_R \rightarrow K_d d_R$  – the same holds for up-type quarks – each term in equation (1.22) becomes diagonal

$$\mathcal{L}_{mass, quark} = -m_\psi \left( \bar{\psi}_L \psi_R + \bar{\psi}_R \psi_L \right), \quad (1.23)$$

where  $\psi = u, d$ . The coefficients  $m_\psi$  are the diagonal elements of the matrices  $vM_\psi/\sqrt{2}$ .

The rotation affects also the kinetics and the interactions terms; in particular, in the so-called flavor basis, defined by equations (1.17) and (1.18), the interaction with  $W^\pm$  boson is diagonal, see equation (1.19), while in the mass bases, where the quarks acquired a mass, the interaction is no longer diagonal

$$\mathcal{L}_{mass, int} = \frac{e}{\sqrt{2} \sin \theta_s} \left( W_\mu^+ \bar{u}_L^i \gamma^\mu V_{ij} d_L^j + W_\mu^- \bar{d}_L^i \gamma^\mu V_{ij}^\dagger u_L^j \right), \quad (1.24)$$

where  $V = U_u^\dagger U_d$  is a unitary matrix known as Cabibbo-Kobayashi-Maskawa (CKM) matrix. This matrix counts for all the mixing effects of weak interactions in the mass basis. Although CKM is a complex  $3 \times 3$  matrix, it is characterized by just four<sup>14</sup> real parameters: 3 angles  $\theta_i$  and one complex phase  $\delta_{CP}$ , that accounts for CP-violation in charged-current interactions. On the contrary, the neutral current is unaffected by this rotation and therefore is CP-conserving. Given that the angles  $\theta_i$  are quite small, CKM matrix results almost diagonal, therefore flavor and mass basis are nearly overlapping<sup>15</sup>. Additionally, in EW theory CKM matrix is unitarity by construction, but assuming, for instance, the existence of a fourth generation of quarks, it loses this feature, therefore, we can understand how accurate the present theoretical description is by experimentally testing CKM unitarity. Finally, we have to introduce a Yukawa-like interaction between Higgs doublet and leptons. Similar to up-type quark, for charged leptons, we have

$$\mathcal{L}_{Yuk, fermion} = -Y_{ij}^e \bar{\ell} H e_R + \text{h.c.}, \quad (1.25)$$

that will generate a mass term like that in equation (1.23), with  $m_e$  that are the diagonal elements of  $vM_e/\sqrt{2}$ . On the contrary, neutral leptons are massless in Electroweak theory, indeed the second term of equation (1.19) is simply missing for right-handed neutrinos since they are neutral and the lack of  $\nu_R$  does not allow to introduce a Yukawa-like mass term. Nonetheless, neutrino oscillations, theoretically predicted by Pontecorvo in 1957 and observed by Super-Kamiokande in 2015, can be only explained by massive neutrinos. Including a mass term for neutrinos, an equivalent mixing to that discussed for quarks, arises for leptons, with the analogous to CKM matrix that is known as Pontecorvo-Maki-Nakagawa-Sakata (PMNS)

<sup>14</sup>A general  $3 \times 3$  complex matrices has 18 parameters, however unitarity halves them. Moreover, each quark field can be redefined up to a phase, fixing further 5 parameters.

<sup>15</sup>Flavor and mass bases would be equivalent if CKM were diagonal.

Sector	Fields	$SU(3)_c$	$SU(2)_L$	$U(1)_Y$	$Q_{EM}$
Fermion	$(u, d)_L$	3	2	1/6	$(2/3, -1/3)$
	$u_R$	3	1	2/3	2/3
	$d_R$	3	1	-1/3	-1/3
	$(\nu_e, e)_L$	1	2	-1/2	$(0, -1)$
	$e_R$	1	1	-1	-1
Gauge	$G^a$	8	-	-	0
	$W^\pm$	-	$\tau^1 \pm i\tau^2$	-	$\pm 1$
	$Z$	-	$\tau^3$	Y	0
	$A$	-	$\tau^3$	Y	0
Higgs	H	1	2	1/2	0

Table 1.1: The Standard Model fields with their gauge quantum numbers and the electric charge.. The fermion sector is repeated over 3 generations.

matrix. A compelling theory for massive neutrinos has not been identified yet, some attempts, based on effective field theory include, not without any problems, a dimension-5 mass term for neutrinos, which breaks lepton and baryon numbers.

The matter content and gauge mediators of the Standard Model are collected in table 1.1, according to their Lorentz transformation properties and quantum numbers under the three gauge groups of the theory

## 1.4 Physics Beyond the Standard Model

The Standard Model is, undoubtedly, the most successful theoretical framework for describing Nature. It provides a pattern to outlines all the composed particles observed in Nature or produced at the accelerators, in term of a few<sup>16</sup> elementary particles that interacts among them with the electroweak and strong interactions. Despite this, SM leaves some phenomena unexplained and fails to be a complete theory of fundamental interactions. In fact, several problems do not find any explanation within the SM; to name a few:

- Neutrino masses: right-handed neutrinos are not included in the SM, therefore is not possible to build – after electroweak symmetry breaking – a Yukawa-like term for neutrino masses. On the contrary, neutrino oscillations pointed out that they are light but massive particles.
- Dark Matter: assuming that the  $\Lambda$ -CDM model correctly describes our Universe and taking into account only its matter content, a measly 20% of the whole matter can be explained by the SM. Experimental observations, such as rotational curves of hydrogen clusters around galaxies, Cosmic Microwave Background and galaxies merging, show that a large amount of stable and electrically neutral matter is located inside galaxies.
- Strong CP problem: the  $SU(3)_c$  sector of the SM Lagrangian does not take into account the CP violation term  $\theta G^{\mu\nu} \tilde{G}_{\mu\nu}$ , while it is allowed by gauge

<sup>16</sup>Here we refer to flavors.

invariance. In fact, CP violations have never been observed in experiments involving strong interactions, moreover the measurement of the neutron's electric dipole moment enables us to state that the coefficient of such a term is very small,  $\theta \leq 10^{-10}$ .

- Baryon asymmetry: in the Universe only one kind of matter is widely present – what we refer to as matter – while anti-matter is almost absent. Nevertheless, matter and antimatter are produced together, therefore a large amount of anti-matter is missing. The explanation of this phenomenon requires a large amount of CP violation. The  $SU(2)_L$  sector of the SM Lagrangian includes such term – the complex phase of CKM matrix – but its magnitude is not enough to explain observations.
- Gravity: SM describes Nature in a space-time with a flat metric, therefore gravity is not included. In order to unify SM with gravity, a quantum theory of the latter is needed, but so far, all the efforts have been inconclusive.
- Hierarchy problem: SM requires the manual insertion of some basic parameters<sup>17</sup> (such as coupling constants and masses, measured by the experiments), which are far apart in terms of magnitude. For example, the strength of strong interaction compared to gravity is about  $10^{41}$  times greater and the theory does not provide any clues to explain that.

Experimental observations, as well as theoretical hints, seem to converge on the conclusion that SM is a low-energy approximation of a more fundamental theory. In the next chapter we will present a compelling method, i.e., the effective field theories, that can be employed to overcome these open problems.

---

<sup>17</sup>The free parameters of the Standard Model are 18: 1 strong coupling constant, 4 EW parameters, 9 Yukawa couplings and 4 mixing parameters of quark.

# CHAPTER 2 | Effective Field Theories

In this chapter we will introduce the key concept of effective field theories. At first, we will dwell on the need for EFTs in the search for new physics, then we will explain how to build an effective Lagrangian and, giving a few examples, clarify how to perform the matching procedure with the full theory. We will also discuss next to leading order EFTs focusing in particular on decoupling of heavy states. In the final part a basic introduction to SMEFT is given.

The main references for this chapter are [12, 13, 14, 15, 16, 17], while for SMEFT [12, 18, 23].

## 2.1 Introduction to EFTs

Universe, superclusters, galaxies, solar systems, planets, continents, countries, cities, human beings, apparatus, body tissues, molecules, atoms, subatomic particles and strings (maybe): Nature comes to us in different scales. It is a matter of fact that we can investigate and make predictions on a specific scale by considering one relevant scale at a time, without caring or even knowing the theory that rules at smaller size. Engineers are able to build skyscrapers like Burj Khalifa<sup>1</sup> without any knowledge on QED or quantum gravity; on the contrary, a thorough understanding of the laws of classical mechanics, specifically, gravity, fluid dynamics and theory of elasticity is necessary to prevent the structure from collapsing. The needed parameters, such as compressive strength of materials, are measured at macroscopic scale; engineers do not ask high-energy physicists to measure steel density from collision at LHC. In some way, we can assert that effective field theories are the path we have always followed to discover even more fundamental laws of Nature and any theory formulated so far is undoubtedly an EFT, since it is nothing more than an approximation of an underlying theory, which, in turn, will – probably – be an effective field theory.

In this thesis, we will only focus on EFTs that are quantum field theories and which admit a Lagrangian description, thus a regularization and renormalization scheme are necessary to deal with predictive theories. Likewise QED, that requires two input parameters, namely the charge and the mass of the electron, EFTs allow us to compute measurable quantities only when the free parameters are fixed. Since

---

<sup>1</sup>With a total height of 829.8 meters, Burj Khalifa, sometimes called Burj Dubai because of its location, is the tallest structure and building in the world.

an EFT is an approximation for an underlying *full theory*, it automatically embeds a finite error, which is tracked in the power counting parameter, denoted by  $\delta$ . If the EFT Lagrangian is an expansion in  $\delta$  up to some order  $n$ , then the error will be of order  $\delta^{n+1}$ . It is clear that we can arbitrarily reduce the error by increasing  $n$  to a sufficiently large number and then including higher-order corrections in the Lagrangian.

According to [17], we can split EFTs in two sets:

- *type I*: EFTs of which we know the underlying theory,
- *type II*: EFTs of which we ignore the underlying theory.

EFTs of *type I* may, at first glance, represent a nonsense since one might wonder why we are using an approximate theory if the underlying theory is available; however, in the same way we add velocities much lower than the speed of light with Galilean composition without disturbing special relativity, the EFTs of *type I* provide the required level of accuracy with simplified computations. Some examples are the Heavy Quark Effective Theory (HQET), the Four Fermi theory for weak interactions, the non-relativistic quantum field theories, such as NRQED or NRQCD, Heuler-Eisenberg theory of low-energy QED, and even QED itself; the latter together with QCD represents the effective field theory for the Standard Model below the energy-scale of  $m_W$  and  $m_Z$ .

Some examples of EFTs of *type II* are the Standard Model, described in the previous chapter, the General Relativity and the Cosmological model, called  $\Lambda$ -CDM that we will introduce in chapter 4, but even all the EFTs that we build to implement SM and GR.

## 2.2 EFT Lagrangian

The action  $\mathcal{S}$ , being a scalar, fixes the engineering dimension of the Lagrangian. In a  $D$ -dimensional space we have

$$[\mathcal{S}] = [M]^0 \equiv 0, \quad [\mathcal{L}] = [M]^D \equiv D, \quad [d^D x] = [M]^{-D} \equiv -D.$$

In general, the Lagrangian is given by the sum of local, gauge and Lorentz invariant operators

$$\mathcal{L}(x) = \sum_i c_i \mathcal{O}_i(x), \quad (2.1)$$

whose engineering dimension is  $[\mathcal{O}] = d$ , while the coefficients  $c_i$  have  $[c] = D - d$ . The fields that appear in the operators are the usual scalar, fermion and vector fields. Their engineering dimensions, determined by the corresponding kinetic terms, are

$$[\phi] = \frac{D-2}{2}, \quad [\psi] = \frac{D-1}{2}, \quad [A_\mu] = \frac{D-2}{2}, \quad [g] = \frac{4-D}{2},$$

where the dimension of the coupling constant is obtained from the covariant derivative, that is  $D_\mu = \partial_\mu - igA_\mu$ , thus  $[D_\mu] = 1$ .

Based on their dimension  $d$ , the operators are classified in three ensembles, called *relevant* operators for  $d < D$ , *marginal* operators for  $d = D$  and *irrelevant* operators



for  $d > D$ . The claim for renormalization is equivalent to discarding operators whose coefficients have negative mass dimensions, i.e., irrelevant operators. In terms of the Lagrangian, this is a strong constraint, namely  $d \leq D$ . Making explicit the dimensions of operators and their coefficients, equation (2.1) becomes

$$\mathcal{L} = \sum_{i, d=0}^D c_i^{(D-d)} \mathcal{O}_i^{(d)}.$$

In the usual four-dimensional space-time, the dimensions of the fields and the coupling constant are

$$[\phi] = [A_\mu] = 1, \quad [\psi] = \frac{3}{2}, \quad [g] = 0,$$

thus in this space-time the allowed gauge and Lorentz invariant operators are those with  $d \leq 4$ , namely

$$\begin{aligned} d = 0 &: 1 \\ d = 1 &: \phi \\ d = 2 &: \phi^2 \\ d = 3 &: \phi^3, \bar{\psi}\psi \\ d = 4 &: \phi^4, \phi\bar{\psi}\psi, D\phi D\phi, \bar{\psi}D\psi, FF, \tilde{F}F. \end{aligned}$$

On the contrary, in EFT the validity limits of the theory are ‘*a priori*’ established, therefore the constraint of being renormalizable at all orders in the perturbation series is not required. Renormalization, strictly speaking<sup>2</sup>, guarantees that the theory is valid at arbitrarily short scales. Nevertheless, this assumption leads to a twofold problem: theoretically because we are assuming that the theory is exact at all scales and experimentally because is impossible to reach arbitrarily short distances.

Discarding renormalization, the Lagrangian will admit also higher-dimensional operators, that are, however, multiplied by coefficients of negative mass power. The coefficients  $c_i$ , are often written as the product between dimensionless constant and a negative power of the energy scale  $\Lambda$  that represents the validity limit above which the effective theory is meaningless, namely  $c_i = C_i/\Lambda$ . Moreover, this convention on coefficients allows us to easily recognize operator of decreasing significance. Then the most general Lagrangian of an EFT is:

$$\mathcal{L}_{EFT} = \sum_{i, d \geq 0} \frac{C_i}{\Lambda^{d-D}} \mathcal{O}_i^{(d)} = \mathcal{L}_{d \leq D} + \sum_{d > D} \frac{\mathcal{L}_d}{\Lambda^{d-D}}, \quad (2.2)$$

which in four-dimensional space-time becomes

$$\mathcal{L}_{EFT} = \mathcal{L}_4 + \frac{\mathcal{L}_5}{\Lambda} + \frac{\mathcal{L}_6}{\Lambda^2} + \dots,$$

---

<sup>2</sup>Here nomenclature is a bit confusing, indeed “renormalizable” means that the theory embeds a finite number of amplitudes that superficially diverge. However, as we will see in the following of this chapter, we can perform the renormalization procedure at fixed order for an EFT, that on the contrary, belongs to the set of non-renormalizable theories.

where the sum is over infinite terms which, however, will produce even smaller contributions to observables as the dimension increase. Hence, only a few terms are needed to reproduce the experimental outcomes of a fixed level of accuracy. This explains why non-renormalizable theories are as good as renormalizable ones: by truncating an infinite series of operators, we are selecting a finite number of parameters to make predictions, which is what happens when dealing with renormalizable theories. It is important to emphasize that, in theoretical computations as well as in experimental measurements, the relevant quantity is the product  $c_i \Lambda^{D-d}$  and not  $c_i$  and  $\Lambda^{D-d}$  taken individually.

### 2.2.1 Power Counting

Once the Lagrangian has been defined, we can figure out how an operator contributes to physical observables like the amplitudes. Assuming that in a  $D$ -dimensional space the amplitude  $\mathcal{M}$  is dimensionless for a certain momentum scale  $p$ , then if a single operator of dimension  $d$  competes to the tree-level amplitude, we have

$$\mathcal{M} \sim \left( \frac{1}{\Lambda^{d-D}} \right) \left( \frac{1}{p^{D-d}} \right) = \left( \frac{p}{\Lambda} \right)^{d-D}.$$

From dimensional analysis the power of  $\Lambda$  is fixed by the dimension of the operator, see equation (2.2), while kinematic factors, such as external momenta, determine the power of  $p$ . Higher-dimensional operators, still at tree-level, give

$$\mathcal{M} \sim \left( \frac{p}{\Lambda} \right)^n, \quad n = \sum_i (d_i - D). \quad (2.3)$$

where  $i$  runs over all required operators. Equation (2.3) is known as *EFT power counting formula* and furnishes the information about the suppression of a given diagram. In four-dimensional space, it reduces to

$$n = \sum_i (d - 4).$$

A remarkable aspect of equation (2.3) must be highlighted since it represents the key-point to understand the difference between a renormalizable theory and an EFT: let us consider the four-dimensional space where a diagram is given by two insertions of dimension-5 operators, or a double insertion of the same operator, from  $\mathcal{L}_5$ . The contribution to the amplitude is proportional to  $(p/\Lambda)^2$ , which is equivalent to a single insertion of dimension-6 operator, from  $\mathcal{L}_6$ . Moreover, if such a diagram with insertion of dimension-5 operators presents a loop, then we expected it to be divergent, hence a counter-term is necessary to renormalize it. In this case, the renormalization term is a dimension 6-operator, indeed for  $\mathcal{L}_{d \geq D}$  we can generate arbitrarily high-dimensional operators by multiple insertions of lower-dimensional operators, but still with  $d - D > 0$ . On the contrary, starting with the operators that appears in  $\mathcal{L}_{d \leq D}$ , we cannot generate higher-dimensional operators since we do not need counter-terms of operators of negative mass-dimensions, thus we are, in such a case, restricted to the set of operators whose dimension is  $d - D \leq 0$ , i.e., the same size of those already included in the Lagrangian. From this point of view, renormalizable theories are a subset of EFT, where the limit  $\Lambda \rightarrow \infty$

has been performed, which means that we can compute amplitudes of arbitrary accuracy, since there are no  $p/\Lambda$  corrections. In EFT, including the whole series of operators with  $d \geq D$ , an infinite number of higher-dimension counter-term would be required, however, such a series is, in practice, truncated and only a finite number of counter-terms is necessary to perform the renormalization procedure.

### The Blue Sky

The blue color of sky was explained by J. W. S. Rayleigh, who demonstrated that the light intensity of low-energy radiation scattered by atoms from the atmosphere is proportional to the fourth inverse power of light wavelength. Blue light, being the one with the smallest wavelength, scatters the most. The derivation of Rayleigh scattering formula is rather complicated and long; however, we can achieve the same result more directly by power counting in EFT.

Assuming that a photon is going to scatter with an atom from the atmosphere and that its energy  $E_\gamma$  is much smaller than the excitation energy  $E_a$  of the atom, which in turn is much smaller than the inverse size of the atom and its mass, namely

$$E_\gamma \ll E_a \ll a_0^{-1} \ll M_a,$$

then we can ignore the atom recoil and consider the interaction as an elastic scattering. The Lagrangian for the EFT will include all the allowed operators that describe an elastic interaction between the photon and the atom, and that, at the same time, respect the symmetries of Nature, namely Lorentz and gauge symmetries. Moreover, the atom is electrically neutral, a condition that combined with gauge invariance, does not allow for a direct interaction with  $A_\mu$ . The only available object for describing the photon is the tensor field strength, thus given that the atom is a fermion  $\Psi$ , the lowest-order operator is of dimension-7 and it is

$$\mathcal{L}_{int} = a_0^3 \Psi^\dagger (c_E \mathbf{E}^2 + c_B \mathbf{B}^2) \Psi. \quad (2.4)$$

A term proportional to  $\mathbf{E} \cdot \mathbf{B}$  is forbidden by parity conservation. This interaction Lagrangian leads to the scattering amplitude  $\mathcal{M} \sim a_0^3 E_\gamma^2$  since the electric and magnetic fields are gradients of the vector potential, therefore each factor  $\mathbf{E}$  or  $\mathbf{B}$  produces a factor  $E_\gamma$ . The cross section is

$$\sigma_{\gamma-atom} \propto a_0^6 E_\gamma^4, \quad (2.5)$$

thus blue light, having twice the frequency, will scatter 16 times stronger than red light, in agreement with Rayleigh formula.

### 2.2.2 Tree-Level Matching

Before going further, we present some examples of matching at tree level between the the full theory and its low-energy EFT, which will clarify what has been discussed so far.

#### Yukawa Toy Model

Assume that a massless fermion exists in Nature and that a certain experimental apparatus, working at energy scale  $E_l$ , has traced the interaction of four of these

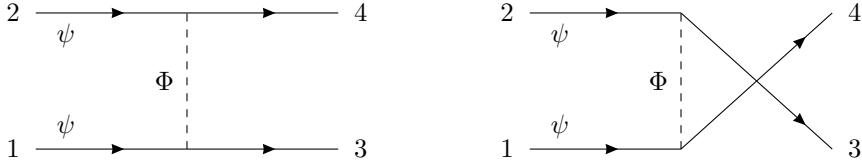


Figure 2.1: Tree-level Feynman diagrams proportional to  $\lambda^2$  that contribute to  $\psi\psi \rightarrow \psi\psi$  scattering.

fermions. A high-energy physicist will describe the process with the Lagrangian:

$$\mathcal{L}_{EFT} = i\bar{\psi}\not{\partial}\psi + \frac{C}{2}(\bar{\psi}\psi)^2,$$

where  $C$  is the coupling constant. Computing the Feynman diagram of the process he finds

$$\equiv i\mathcal{M}_{EFT} = \bar{u}(p_3)u(p_1)\bar{u}(p_4)u(p_2) (iC) - \{3 \leftrightarrow 4\}. \quad (2.6)$$

Now, imagine that, with the increasing of technology, a new energy threshold  $E_h$ , with  $E_l \ll E_h$  can be achieved in experiments. Repeating the collision of four fermions, experimental physicists discover that the interaction is mediated by an heavy scalar  $\Phi$  of mass  $M$ , such that  $E_l \ll M \ll E_h$ . Then assuming a Yukawa-like coupling, the new theory reads

$$\mathcal{L}_F = i\bar{\psi}\not{\partial}\psi + \frac{1}{2}\partial_\mu\Phi\partial^\mu\Phi - \frac{1}{2}M^2\Phi^2 - \lambda\Phi\bar{\psi}\psi.$$

At leading order, the scattering process  $\psi\psi \rightarrow \psi\psi$  in the new theory is obtained by computing the Feynman diagrams represented in figure 2.1. The amplitude is:

$$i\mathcal{M}_F = \bar{u}(p_3)u(p_1)\bar{u}(p_4)u(p_2)(-i\lambda)^2 \frac{i}{(p_1 - p_3)^2 - M^2} - \{3 \leftrightarrow 4\}, \quad (2.7)$$

However, before the discovery of the heavy mediator, the Lagrangian  $\mathcal{L}_{EFT}$  well described observations, just as the Lagrangian  $\mathcal{L}_F$  does after the increasing of energy threshold. Thus, the new “full theory” must reproduce, in the low-energy limit the result of equation (2.6). Performing the limit  $(p_1 - p_3)^2 \ll M^2$ , the amplitude of the full theory becomes

$$i\mathcal{M}_{F,low} = \bar{u}(p_3)u(p_1)\bar{u}(p_4)u(p_2) \frac{i\lambda^2}{M^2} - \{3 \leftrightarrow 4\}. \quad (2.8)$$

The matching procedure requires that equations (2.8) and (2.6) must describe the same physics

$$\mathcal{M}_{F,low} - \mathcal{M}_{EFT} = 0, \quad \text{implies} \quad C = \frac{\lambda^2}{M^2}. \quad (2.9)$$

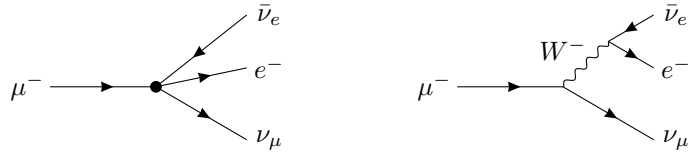


Figure 2.2: Muon decay,  $\mu^- \rightarrow \bar{\nu}_e e^- \nu_\mu$  at tree-level. On the left in Fermi theory, on the right in electroweak theory.

The matching procedure just described is simple and straight, however, it also holds in more complex cases, for instance in tuning the low-energy electroweak theory with the four-fermion Fermi interaction.

### Fermi Theory

Nowadays, Fermi theory belongs to what we call EFT of *type I*, since its underlying theory is available. However, when E. Fermi tried to describe  $\beta$ -decay, the  $W$  boson had not been discovered yet. Taking as an example the muon decay,  $\mu^- \rightarrow \nu_\mu e^- \bar{\nu}_e$ , in Fermi theory the interaction is described by the Lagrangian

$$\mathcal{L}_{Fermi} = -\frac{G_F}{\sqrt{2}} [\bar{\nu}_\mu \gamma^\rho (1 - \gamma_5) \mu] [\bar{e} \gamma_\rho (1 - \gamma_5) \nu_e],$$

where  $G_F = 1.166 \times 10^{-5} \text{ GeV}^{-2}$  is the Fermi constant. The Feynman diagram for muon decay in Fermi theory is represented in figure 2.2, on the left. The amplitude of the process is

$$i\mathcal{M}_{Fermi} = -\frac{iG_F}{\sqrt{2}} \bar{\nu}_\mu \gamma^\rho (1 - \gamma_5) \mu \bar{e} \gamma_\rho (1 - \gamma_5) \nu_e. \quad (2.10)$$

Within the SM, muon decay is understood by considering an intermediate virtual state of  $W$  boson, see the right diagram in figure 2.2. The mediator  $W^-$  couples to the weak charged current as

$$j_W^\mu = \frac{g}{2\sqrt{2}} \bar{\nu}_\ell \gamma^\mu (1 - \gamma_5) \ell.$$

In Feynman-'t Hooft gauge, the amplitude of the process is

$$i\mathcal{M}_{EW} = \left( \frac{-ig}{2\sqrt{2}} \right)^2 (\bar{\nu}_\mu \gamma^\rho (1 - \gamma_5) \mu) \left( \frac{-ig_{\rho\sigma}}{p^2 - m_W^2} \right) (\bar{e} \gamma^\sigma (1 - \gamma_5) \nu_e)$$

which in the low energy limit, defined by  $p \ll m_W^2$ , becomes

$$i\mathcal{M}_{EW,low} = \left( \frac{-ig}{2\sqrt{2}} \right)^2 (\bar{\nu}_\mu \gamma^\rho (1 - \gamma_5) \mu) \frac{ig_{\rho\sigma}}{m_W^2} (\bar{e} \gamma^\sigma (1 - \gamma_5) \nu_e) \quad (2.11)$$

The amplitude obtained with Fermi theory, in equation (2.10), must be equal to that computed in low-energy electroweak, hence

$$\frac{G_F}{\sqrt{2}} \equiv \frac{g^2}{8m_W^2} = \frac{1}{2v^2}, \quad (2.12)$$

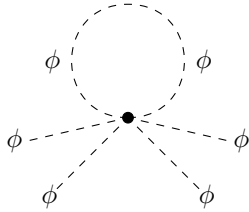


Figure 2.3: One-loop contribution of  $\mathcal{L}_6$  to  $\phi\phi$  scattering.

with  $v \sim 246$  GeV, that is the  $vev$  of the Higgs. Thus, at energies well below the mass of  $W$  boson, Fermi theory can be employed to describe weak interaction. In particular, in the region where  $W$  is no longer a degree of freedom – it has been integrated out of Lagrangian – the effects of an exchange of this particle are absorbed into the four-fermion operator.

### 2.2.3 Loops

EFTs not only simplify the derivation of tree-level amplitudes, but also prove to be useful in performing loop calculations. First of all, it must be emphasized that equation (2.3) holds even for loop diagrams. This is anything but straight, in EFT the computation of loop diagrams represents a conceptual problem since the integration domain is extended to the whole phase space, including the breaks down regions of EFT.

For simplicity, we consider the Lagrangian for a massive scalar field, that up to dimension-8 is:

$$\mathcal{L} = \mathcal{L}_{d \leq 4} + \frac{C_6}{\Lambda^2} \frac{\phi^6}{6!} + \frac{C_8}{\Lambda^4} \frac{\phi^4 (\partial_\mu \phi)^2}{8!},$$

where  $\mathcal{L}_6$  operator contributes to  $\phi\phi$  scattering with the diagram represented in figure 2.3. The amplitude of the process is:

$$i\mathcal{M}_6 = -\frac{iC_6}{2\Lambda^2} \int \frac{d^4 l}{(2\pi)^4} \frac{1}{l^2 - m_\phi^2},$$

however, the validity region of this EFT is defined by  $l < \Lambda$ , thus the introduction of a cut-off momentum  $\Lambda_l$ , with  $\Lambda_l < \Lambda$ , seems the most reasonable choice. Additionally, for  $m_\phi \ll \Lambda_l$ , we have

$$i\mathcal{M}_6 \approx -\frac{iC_6}{\Lambda^2} \frac{\Lambda_l^2}{16\pi^2},$$

which diverges with the square of the cut-off momentum since the integral was quadratically divergent. Computing in the same way the contribution of dimension-8 operator, we get

$$i\mathcal{M}_8 = -\frac{iC_8}{\Lambda^4} \int \frac{d^4 l}{(2\pi)^4} \frac{l^2}{l^2 - m_\phi^2} \approx -\frac{iC_8}{\Lambda^4} \frac{\Lambda_l^4}{16\pi^2},$$

which diverges with the fourth power of the cut-off momentum. When  $\Lambda_l \approx \Lambda$ , the theory is no longer predictive since both contributions are of order  $O(1)$ , thus the

power counting formula is lost. Moreover, being  $\Lambda_l$  an artificial scale without any connection to physical world, it cannot appear in observables, therefore the cut-off regularization does not seem to be the right tool for loop computations in EFTs. In order to retain the EFT power counting, the regularization scheme cannot introduce any contribution that depends on  $\Lambda_l$ , thus dimensional regularization seems to be the suitable one, given also the feature of preserving gauge invariance.

Dimensional regularization is implemented via the integration master formula

$$\mu^{2\epsilon} \int \frac{d^D l}{(2\pi)^D} \frac{(l^2)^a}{(l^2 - A)^b} = \frac{i\mu^{2\epsilon} (-1)^{a-b} A^{a-b+\frac{D}{2}}}{(4\pi)^{\frac{D}{2}}} \frac{\Gamma(a + \frac{D}{2}) \Gamma(b - a - \frac{D}{2})}{\Gamma(\frac{D}{2}) \Gamma(b)}, \quad (2.13)$$

where  $A$  does not depend on loop momentum and  $\Gamma(x)$  is the Euler Gamma function. Since  $D = 4 - 2\epsilon$ , the expansion of Gamma around  $\epsilon$  is give by:

$$\Gamma(\epsilon) = \frac{1}{\epsilon} - \gamma_E + \mathcal{O}(\epsilon), \quad (2.14)$$

where  $\gamma_E = 0.577$  is the Euler-Mascheroni constant.

If we consider again the the two contribution of  $\mathcal{L}_6$  and  $\mathcal{L}_8$ , in dimensional regularisation we have:

$$\begin{aligned} \mu^{2\epsilon} \int \frac{d^D l}{(2\pi)^D} \frac{1}{l^2 - m_\phi^2} &= \frac{im_\phi^2}{16\pi^2} \left[ \frac{1}{\epsilon} + \log\left(\frac{\tilde{\mu}^2}{m_\phi^2}\right) + 1 + \mathcal{O}(\epsilon) \right], \\ \mu^{2\epsilon} \int \frac{d^D l}{(2\pi)^D} \frac{l^2}{l^2 - m_\phi^2} &= \frac{im_\phi^4}{16\pi^2} \left[ \frac{1}{\epsilon} + \log\left(\frac{\tilde{\mu}^2}{m_\phi^2}\right) + 1 + \mathcal{O}(\epsilon) \right]. \end{aligned} \quad (2.15)$$

where  $\tilde{\mu}^2 \equiv 4\pi e^{-\gamma_E} \mu^2$ . These integrals depend on  $m_\phi$ , which defines an infrared (IR) scale, while all the UV divergences are embedded in  $1/\epsilon$ , that we expected to cancel by adding the counter-terms. Moreover,  $\tilde{\mu}$  appears only in the argument of the logarithm, and since there are no power of this parameter in previous equation, the only source of  $\tilde{\mu}$  is the parameter  $\mu^{2\epsilon}$  in front of the integrals. One remarkable property of dimensional regularization is that scaleless integral vanishes, indeed in the limit  $m_\phi \rightarrow 0$ , equation (2.13), returns a null result.

In EFTs, the choice for dimensional regularization was made because it complies with the power counting formula. Consider a loop diagram with the insertions of effective operators that lead to vertices of order  $1/\Lambda^a$ ,  $1/\Lambda^b$  and others, then the amplitude will be dependent on  $\Lambda$  as

$$\mathcal{M} \propto \frac{1}{\Lambda^{a+b+\dots}}, \quad (2.16)$$

indeed, as we have seen from equation (2.15), the only scales that can appear in the numerator come from the poles of Feynman propagators, which are much smaller than the cut-off scale.

## 2.2.4 Matching

For a better understanding of this point, we can perform an explicit matching procedure between an EFT and its full underlying theory. Imagine that in the

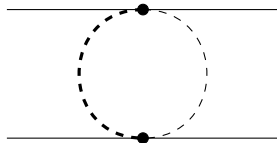


Figure 2.4: One loop Feynman diagram for the full theory where two light fields (external solid lines) interact by exchanging a heavy (thick dotted line) and a light (thin dashed line) scalar fields.

theory discussed above, two scalar fields with different masses are involved in a loop diagram as represented in figure 2.4. In the full theory the integral describing the diagram is

$$I_F = g^2 \mu^{2\epsilon} \int \frac{d^D l}{(2\pi)^D} \frac{1}{(l^2 - M^2)(l^2 - m^2)}, \quad (2.17)$$

with  $m \ll M$ , where  $M$  represents the UV scale, while  $m$  the IR scale. This integral depends on both energy scales since they appear in the denominator of the scalar propagators. Using Feynman parameters and the master formula (2.13), we get:

$$I_F = \frac{ig^2}{16\pi^2} \left[ \frac{1}{\epsilon} + \log\left(\frac{\tilde{\mu}^2}{M^2}\right) + \frac{m^2}{M^2 - m^2} \log\left(\frac{m^2}{M^2}\right) + 1 \right], \quad (2.18)$$

here the dependence on the IR and UV scales is expressed by the argument of the logarithms: the first depends only upon the UV scale, while the second one on both of them.

On the contrary, in the low-energy EFT the heavy particle does not show up, therefore we have to integrate it out by expanding the propagator of the heavy particle as:

$$\frac{1}{l^2 - M^2} = -\frac{1}{M^2} \left( 1 + \frac{l^2}{M^2} + \frac{l^4}{M^4} + \dots \right),$$

and substituting in equation (2.17). This procedure removes the UV scale from the theory, therefore we will end up with a low-energy EFT, where the loop integral reads

$$\begin{aligned} I_{EFT} &= -\frac{g^2 \mu^{2\epsilon}}{M^2} \int \frac{d^D l}{(2\pi)^D} \frac{1}{l^2 - m^2} \left( 1 + \frac{l^2}{M^2} + \frac{l^4}{M^4} + \dots \right) \\ &= \frac{ig^2 m^2}{16\pi^2 (M^2 - m^2)} \left( -\frac{1}{\epsilon} - \log\left(\frac{\tilde{\mu}^2}{m^2}\right) - 1 \right). \end{aligned} \quad (2.19)$$

Note that, as expected, the argument of the logarithm does not present the UV scale. This result must be compared with equation (2.18), obtained within the full theory. It is clear that the two results are different, in particular the coefficients of the divergent terms do not match. In fact, the full theory and the EFT are two independent theories that we can regulate with different schemes, thus the divergent terms will be fixed by different counter-terms. As if that were not enough, we can also choose different values for the gauge-fixing parameters. As said before, the EFT is only tuned with the full theory in order to reproduce the same matrix element, while being a completely independent theory.



Assuming that divergent terms have been fixed in both theories by making use of the  $\overline{\text{MS}}$ -scheme, then we can compute the matching integral named  $I_M$

$$\begin{aligned}
I_M &= I_F - I_{EFT} \\
&= \frac{ig^2}{16\pi^2} \left[ \log\left(\frac{\tilde{\mu}^2}{M^2}\right) + 1 + \frac{m^2}{M^2} \left( \log\left(\frac{\tilde{\mu}^2}{M^2}\right) + 1 \right) + \dots \right] \\
&= \frac{ig^2}{16\pi^2} \left[ \log\left(\frac{\tilde{\mu}^2}{M^2}\right) + 1 \right] \sum_{n=0}^{\infty} \left(\frac{m^2}{M^2}\right)^n,
\end{aligned} \tag{2.20}$$

from which it emerges that the logarithm inside square brackets, that is analytic in the IR scale, represents a correction to operators of order  $M^{-2n}$ . What is remarkable is that we can read the result from a completely different point of view by writing the full underlying theory, which embeds both the UV and IR scales, as the sum of two one-scales theories, i.e.,  $I_F = I_M + I_{EFT}$ . If on one hand the IR scale affects the EFT theory, as highlighted by equation (2.19); on the other hand, the matching integral, in equation (2.20), depends only on the UV scale. Hence, by using the parameter  $\tilde{\mu}$ , we can write

$$\underbrace{\log\left(\frac{m^2}{M^2}\right)}_{\text{full theory}} = \underbrace{\log\left(\frac{\tilde{\mu}^2}{M^2}\right)}_{\text{matching}} - \underbrace{\log\left(\frac{\tilde{\mu}^2}{m^2}\right)}_{\text{EFT}}. \tag{2.21}$$

The separation of the two energy-scales leads to easier computations, since integrals with multi-scales require a more attention and techniques compared to single-scale ones.

In this derivation we have obtained the matching integral as a result, but we may wonder whether there is another way to obtain the  $I_M$  integral. Both the integrals  $I_F$  and  $I_{EFT}$  contain non-analytic terms in the IR scale, while their difference, i.e., the integral  $I_M$ , is analytic in this scale. Thus, we can remove the IR scale both in the full theory and in EFT, by expanding them in  $m \ll l$ , hence

$$\begin{aligned}
I_F^{(IR)} &= g^2 \mu^{2\epsilon} \int \frac{d^D l}{(2\pi)^D} \frac{1}{l^2 - M^2} \left( \frac{1}{l^2} + \frac{m^2}{l^4} + \dots \right), \\
I_{EFT}^{(IR)} &= g^2 \mu^{2\epsilon} \int \frac{d^D l}{(2\pi)^D} \left( \frac{1}{l^2} + \frac{m^2}{l^4} + \dots \right) \left( -\frac{1}{M^2} - \frac{l^2}{M^4} + \dots \right).
\end{aligned} \tag{2.22}$$

Now, as expected, the denominators do not depend on  $m$  anymore. Note that, in dimensional regularization the non-analytic terms in  $m$  are proportional to

$$\frac{m^\epsilon}{\epsilon} = \frac{1}{\epsilon} [m^\epsilon + \epsilon m^{\epsilon-1} + \dots],$$

where we first expanded in the IR scale  $m$  and then respect to the parameter  $\epsilon$ . In the limit  $m \rightarrow 0$ , it returns a null contribution.

We can obtain the same outcome starting from  $I_{EFT}^{(IR)}$ , in equation (2.22), which is composed by scaleless terms, since two expansion took place; therefore, its contribution is null. This result is completely general.

On the contrary, the integral in  $I_F^{(IR)}$  still depends on a specific scale, i.e., the UV scale, and its integration will produce the same result of equation (2.20), since  $I_M = I_F^{(IR)} - I_{EFT}^{(IR)}$ , with  $I_{EFT}^{(IR)} = 0$ .

In order to perform a general derivation, it is sufficient to split the UV and IR divergences of a scaleless integral

$$\int \frac{d^D l}{(2\pi)^D} \frac{1}{k^4} = \frac{i}{16\pi^2} \left( \frac{1}{\epsilon_{UV}} - \frac{1}{\epsilon_{IR}} \right) = 0. \quad (2.23)$$

Moreover, the integrals that appear in the full theory and in the EFT after the expansion in the IR scale, can always be written as

$$I_F^{(IR)}(m) = \sum_n m^n I_F^{(n)} = \sum_n m^n \left( \frac{A^{(n)}}{\epsilon_{UV}} + \frac{B^{(n)}}{\epsilon_{IR}} + C^{(n)} \right),$$

$$I_{EFT}^{(IR)}(m) = \sum_n m^n I_{EFT}^{(n)} = \sum_n m^n \left( -\frac{B^{(n)}}{\epsilon_{UV}} + \frac{B^{(n)}}{\epsilon_{IR}} \right),$$

where  $A^n$ ,  $B^n$  are the UV and IR divergent integrals respectively, while  $C^n$  is the finite part. Adopting once again the  $\overline{\text{MS}}$ -scheme to remove the UV divergences, we get

$$I_M^{(n)} = \left[ I_F^{(n)} - I_{F,ct}^{(n)} \right] - \left[ I_{EFT}^{(n)} - I_{EFT,ct}^{(n)} \right] = C^{(n)}.$$

where  $I_{c.t.}$  are the counter-terms. The last equation states that to obtain the matching condition we simply have to expand the integral of the full theory in the IR scale and keep only the finite part of it.

## 2.2.5 Fields Redefinition and Equations of Motion

Four-dimensional operators, as well as lower-dimensional ones, are common in quantum field theory and we are used to deal with them; on the contrary, we cannot state the same for higher-dimensional operators. First of all, for a given dimension we have to identify a basis which can only contain local operators that are also gauge and Lorentz invariant. Usually, we have to handle redundant terms that have to be eliminated. If on one side, a redefinition of fields does not prove efficient in this task; on the other side, by making use of equation of motions (EOMs) we can fulfill the assignment directly. In fact, operator proportional to EOMs can be deleted, since they do not affect the  $S$ -matrix. We can prove this statement by recalling that EOMs are a special case of redefinition of fields.

First of all, we recall that the redefinition of fields has no physical implications: assuming that a certain theory depends on the scalar field  $\phi$ , then the map

$$\phi(x) \rightarrow f[\phi(x)].$$

will affect the correlation functions, but will leave the observables, such as  $S$ -matrix, unmodified. This is true as long as  $\langle p|f[\phi]|0\rangle \neq 0$ , where  $|p\rangle$  is the one-particle state created by the field  $\phi$ , since the LSZ reduction formula, which connects correlation functions to  $S$ -matrix elements, still holds and identifies the poles corresponding to the external physical states in scattering amplitudes.

From their side, equations of motion are a special case of redefinition of fields. They can be written in a compact manner as

$$E[\phi] \equiv \frac{\delta \mathcal{S}[\phi]}{\delta \phi}.$$

If we deal with an operator of  $\phi$ , which is proportional to the EOMs, it can be recast as

$$\mathcal{O}[\phi] = f[\phi] E[\phi] = f[\phi] \frac{\delta \mathcal{S}[\phi]}{\delta \phi}.$$

Thus, operating the redefinition of the scalar field

$$\phi \rightarrow \phi + \epsilon f[\phi],$$

where  $\epsilon \ll 1$ , the Lagrangian turns to

$$\mathcal{L}[\phi] \rightarrow \mathcal{L}[\phi] + \epsilon f[\phi] \frac{\delta \mathcal{S}[\phi]}{\delta \phi} + O(\epsilon^2) = \mathcal{L}[\phi] + \epsilon \mathcal{O}[\phi] + O(\epsilon^2),$$

proving that an operator proportional to the EOMs can always be removed from the Lagrangian since it disappears when we perform a specific redefinition of the fields.

A concrete example of this procedure can be shown within the scalar theory. Up to dimension-4 the Lagrangian for a massive scalar particle is

$$\mathcal{L} = \frac{1}{2} \partial_\mu \phi \partial^\mu \phi - \frac{1}{2} m^2 \phi^2 - \frac{1}{4!} \lambda \phi^4,$$

whose EOMs are

$$(\partial^2 + m^2)\phi + \frac{1}{3!} \phi^3 = 0.$$

Now suppose that we want to include some dimension-6 operators to build a new EFT Lagrangian. Among other, these operators might be  $\phi^6$ ,  $\phi^3 \partial^2 \phi$  and  $(\partial^2 \phi)^2$ . Nevertheless, EOMs shows that only one of them is independent

$$\begin{aligned} (\partial^2 \phi)^2 &\sim \phi^6, \\ \phi^3 (\partial^2 \phi)^2 &\sim \phi^6, \end{aligned}$$

where  $\sim$  stands for equivalence between operators. Thus, there is no need to include the operators  $\phi^3 \partial^2 \phi$  and  $(\partial^2 \phi)^2$  in the Lagrangian. In an equivalent manner, we can remove the redundant operators by making use of field redefinition. Let us imagine that we have already removed the operator  $(\partial^2 \phi)^2$ , then the Lagrangian for the effective field theory of dimension six is

$$\mathcal{L}_{EFT} = \frac{1}{2} \partial_\mu \phi \partial^\mu \phi - \frac{1}{2} m^2 \phi^2 - \frac{1}{4!} \lambda \phi^4 - \frac{C_1}{\Lambda^2} \phi^3 \partial^2 \phi - \frac{C_2}{\Lambda^2} \phi^6 + O(1/\Lambda^4).$$

Under the field redefinition

$$\phi \rightarrow \phi - \frac{C_1}{\Lambda^2} \phi^3, \tag{2.24}$$

the Lagrangian becomes

$$\mathcal{L}_{EFT} = \frac{1}{2} \partial_\mu \phi \partial^\mu \phi - \frac{1}{2} m^2 \phi^2 - \left( \frac{\lambda}{4!} - \frac{C_1 m^2}{\Lambda^2} \right) \phi^4 - \left( \frac{C_1 \lambda}{3! \Lambda^2} - \frac{C_2}{\Lambda^2} \right) \phi^6 + O(1/\Lambda^4).$$

which, as expected, contains just one operator of dimension six.

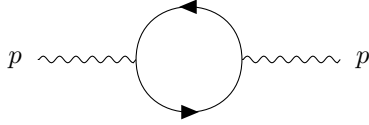


Figure 2.5: The leading order diagram for the vacuum polarization of the photon.

Generally speaking, the EFT Lagrangian might contain redundant operators that can be eliminated by EOMs or redefinition of fields. On one hand, the superfluous operators  $\mathcal{O}_i$  mix among themselves when we renormalize the theory

$$\mu \frac{d}{d\mu} \mathcal{O}_i = \beta_{ij} \mathcal{O}_j,$$

where  $\beta_{ij}$  can be gauge-dependent, but the operators  $\mathcal{O}_i$  are not observable quantities. On the other hand, for non-EOMs operators  $\mathcal{K}_i$ , the anomalous dimension is

$$\mu \frac{d}{d\mu} \mathcal{K}_i = \gamma_{ij} \mathcal{K}_j + \beta_{ij} \mathcal{O}_j. \quad (2.25)$$

The operators  $\mathcal{K}_i$  contribute to  $S$ -matrix, thus  $\gamma_{ij}$  is gauge independent. Under the evolution of  $\mu$ , the operators  $\mathcal{K}_i$  can mix with EOMs-operators, but this is not a problem since  $\mathcal{O}_i$  are, as said, unobservable.

## 2.3 Decoupling of Heavy States

Usually, at low-energy scale the heavy states do not contribute. Consider, for instance, the one-loop  $\beta$ -function of QCD

$$\beta(g_s) = -\frac{g_s^3}{(4\pi)^2} \left( 11 - \frac{2}{3} n_f \right),$$

where  $n_f$  is the number of quark flavors. At the energy level well below the quark top mass, we do not expect that this particle contributes to the  $\beta$ -function; in other words, we assume that the heavy state decouples at low energy.

The decoupling of heavy particles can be understood considering the one-loop  $\beta$ -function of QED, which comes from the vacuum polarization diagrams, in figure 2.5. In dimensional regularization we have

$$i\Pi(p^2) \equiv \frac{ie^2}{2\pi^2} \left[ \frac{1}{6\epsilon} - \int_0^1 dx x(1-x) \log \left( \frac{m^2 - p^2 x(1-x)}{\tilde{\mu}^2} \right) \right], \quad (2.26)$$

where  $m$  is the mass of the particle running in the loop and  $p$  the momentum of the external photon.

### Momentum-Subtraction Scheme

Adopting a mass-dependent renormalization procedure, such as the space subtraction scheme where the renormalized vacuum polarization function is given by the

difference between  $\Pi(p^2) - \Pi(\mu_M^2)$ , we get

$$\Pi_m(p^2, m^2, \mu_M^2) = -\frac{e^2}{2\pi^2} \left[ \int_0^1 dx x(1-x) \log \left( \frac{m^2 - p^2 x(1-x)}{m^2 + \mu_M^2 x(1-x)} \right) \right]. \quad (2.27)$$

We can compute the contribution to the  $\beta$ -function for a generic fermion running in the loop by acting on this function with the operator  $(e/2)\mu_M d/d\mu_M$ , hence

$$\beta_m(e) = \frac{e^3}{2\pi^2} \int_0^1 dx x(1-x) \frac{\mu_M^2 x(1-x)}{m^2 + \mu_M^2 x(1-x)}.$$

Two opposite situation can occur: if we consider a particle lighter than the scale  $\mu_M$ , such as the electron, for which we have  $m_e \ll \mu_M$ , then previous equation becomes

$$\beta(e) \approx \frac{e^3}{2\pi^2} \int_0^1 dx x(1-x) = \frac{e^3}{12\pi^2} \quad (2.28)$$

while for an heavy fermion  $\mu_M \ll M$ , thus

$$\beta(e^2) \approx \frac{e^3}{2\pi^2} \int_0^1 dx x(1-x) \frac{\mu_M^2 x(1-x)}{M^2} = \frac{e^3 \mu_M^2}{60\pi^2 M^2} \rightarrow 0.$$

thus, as anticipated, in momentum-subtraction scheme the heavy particles decouple.

### Minimal-Subtraction Scheme

Now, we repeat the computation, but in a mass-independent scheme, such as the  $\overline{\text{MS}}$ -scheme. In this case, the renormalized vacuum polarization function can be obtained from equation (2.26) by removing its divergent term

$$\Pi_{\overline{\text{MS}}}(p^2, m^2, \tilde{\mu}^2) = -\frac{e^2}{2\pi} \int_0^1 dx x(1-x) \log \left( \frac{m^2 - p^2 x(1-x)}{\tilde{\mu}^2} \right). \quad (2.29)$$

As we did before, to get the  $\beta$ -function, we must act with the operator  $(e/2)\mu_M d/d\mu_M$  on the vacuum polarization function. For light state, we recover the same result of the mass-dependent scheme, indeed equation (2.28) is independent both from the mass of the fermion and from the parameter  $\tilde{\mu}$ . Nevertheless, for heavy particles we find a non-vanishing contribution, thus heavy states do not decouple.

In the  $\overline{\text{MS}}$ -scheme, an additional problem comes out, indeed evaluating equation (2.29) for a particle with low-momentum

$$\Pi_{\overline{\text{MS}}}(0, m^2, \tilde{\mu}^2) = -\frac{e^2}{2\pi} \int_0^1 dx x(1-x) \log \left( \frac{m^2}{\tilde{\mu}^2} \right),$$

which is divergent in the limit of heavy particles  $\tilde{\mu} \ll m$ , causing the breakdown of the perturbation theory.

The problems of non-decoupling and theory break down are strictly related and they can be solved by integrating out heavy states. In fact, the contribution of heavy particles is embedded in higher-dimensional operators, which are suppressed by the inverse powers of their mass. At Lagrangian level

$$\mathcal{L}^{(n_i+1)} \rightarrow \mathcal{L}^{(n_i)},$$

which states that we are moving from a theory with  $n_l$  light particles and one heavy states to a theory with just  $n_l$  light particles. The two theories must generate the same  $S$ -matrix for the scattering of a light-particle scattering in low-energy regime. In the  $\overline{\text{MS}}$ -scheme, we can integrate out the heavy-states by computing the vacuum polarization function for  $p^2 \ll m^2$

$$\begin{aligned}\Pi_{\overline{\text{MS}}}(p^2, m^2, \tilde{\mu}^2) &= -\frac{e^2}{2\pi} \int_0^1 dx x(1-x) \left[ \log\left(\frac{m^2}{\tilde{\mu}^2}\right) + \log\left(1 - \frac{p^2 x(1-x)}{\tilde{\mu}^2}\right) \right] \\ &= -\frac{1}{6} \log\left(\frac{m^2}{\tilde{\mu}^2}\right) + \frac{p^2}{30m^2} + O\left(\frac{p^4}{m^4}\right).\end{aligned}$$

In order to get this result, QED Lagrangian was adjusted by integrating out heavy-states, which is equivalent to the shift of the gauge coupling constant

$$\frac{1}{e_l^2(\tilde{\mu})} = \frac{1}{e_h^2(\tilde{\mu})} - \frac{1}{12} \log\left(\frac{m^2}{\tilde{\mu}^2}\right),$$

where  $e_l(\tilde{\mu})$  and  $e_h(\tilde{\mu})$  are low-energy and high-energy gauge couplings. The shift is responsible for the first term in equation (2.3), while the second term comes from a dimension-6 operator of the EFT Lagrangian, namely

$$\mathcal{L} = \frac{e^2}{240\pi^2 m^2} \partial_\rho F_{\mu\nu} \partial^\rho F^{\mu\nu}.$$

## 2.4 Standard Model Effective Field Theory

We conclude this chapter on effective field theories by presenting the Standard Model effective field theory (SMEFT), which represents a viable proposal to look for new physics. SMEFT enables for higher-dimensional operators, while the allowed fields are those of the SM. On the contrary, our research is focused on the search for new fields that interacts with the SM particles through high-order operators, while SM is left untouched; see chapter 4 and 5. This does not detract from the fact that SMEFT is both a compelling theory and a fundamental example of EFT.

SMEFT comes from the assumption that SM itself is an effective field theory which approximates a more fundamental theory of elementary interactions. From this point of view, what we have done so far is describing the Nature with the Lagrangian

$$\mathcal{L}_{SM} = \mathcal{L}_{d \leq 4},$$

that turned out to accurately foresee experimental outcomes. Nevertheless, it is expected that as the energy of the accelerators increases, more discrepancies will be found between theory and experimental data.

The SMEFT Lagrangian is

$$\mathcal{L}_{SMEFT} = \mathcal{L}_{SM} + \frac{\mathcal{L}_5}{\Lambda} + \frac{\mathcal{L}_6}{\Lambda^2} + \dots,$$

where  $\Lambda$  is the energy scale of new physics at which SMEFT breaks down. Since SMEFT allows for the SM fields only – in addition, before the EW symmetry breaking – we have to build higher-dimensional operators that respect Lorentz and

gauge invariance without introducing new fields. It is remarkable that at dimension-5 just one operator is available to build  $\mathcal{L}_5$ . It was found by Weinberg [19] and it is

$$\mathcal{L}_5 = C_5^{rs} \epsilon^{ij} \epsilon^{kl} (l_{ir}^T \mathcal{C} l_{ks}) H_j H_l + \text{h.c.}, \quad (2.30)$$

where  $i, j, k$  and  $l$  are indices of  $SU(2)$ , while  $r$  and  $s$  refer to generation of particles.  $\mathcal{C}$  is the charge conjugation matrix. This operator contains a  $\Delta L = 2$  interaction, that violates the lepton number and furnishes a Majorana mass term to neutrinos after the electroweak breaking. In [20], the authors have shown that all the operators built starting from the SM fields satisfy

$$\frac{1}{2}(\Delta B - \Delta L) \equiv d, \quad (2.31)$$

that makes it clear why for  $d = 5$ , the operator in equation (2.30) does not retain both lepton and baryon numbers.

The scenario of dimension-6 operators is extremely complex, indeed a complete basis, commonly called *Warsaw basis*, was identified quite recently by [21], starting from the results in [22].

#### 2.4.1 SMEFT Corrections to SM

Removing the dimension-5 operator, we can investigate the consequences of  $\mathcal{L}_6$  on observables. In some cases, dimension-6 operators act as a simple shift of SM parameters, however in some others they lead to deeper changes.

As previously said, in EFT is important not only to specify the dimension of the operators, but also the number of insertions of these operators in some diagrams since multiple insertions of low-dimensional operators is equivalent to a single insertion of a higher-dimensional operator. In [23], the authors obtained some compelling results with a single insertion of dimension-6 operators. In the following we analyse some of them.

##### Higgs Sector

If we allow for dimension-6 operators, the Higgs potential, getting a contribution from  $H^6$ , becomes:

$$V(H) = \lambda \left( H^\dagger H - \frac{v^2}{2} \right)^2 - c_H (H^\dagger H)^3,$$

where the coupling constant of  $H^6$  is understood as  $c_H = C_H/\Lambda^2$ . This potential leads to a shift of the vacuum expectation value of Higgs field

$$\langle H^\dagger H \rangle = \frac{v^2}{2} \left( 1 + \frac{3c_H v^2}{4\lambda} \right) \equiv \frac{v_T^2}{2}, \quad (2.32)$$

where the shift term is proportional to the Higgs parameters, i.e.,  $v^2/\lambda$ . The kinetic term gets two corrections

$$\mathcal{L}_{kin} = (D_\mu H)^\dagger (D^\mu H) + c_1 (H^\dagger H) \partial^2 (H^\dagger H) + c_2 (H^\dagger D_\mu H)^* (H^\dagger D_\mu H),$$

once again, the small letters  $c_i$ , with  $i = \{1, 2\}$ , include the cut-off of the theory. In order to correctly normalize it, in unitary gauge we find

$$H = \frac{1}{\sqrt{2}} \begin{pmatrix} 0 \\ (1 + c_3)h + v_T \end{pmatrix},$$

where at first order the coefficients are

$$c_3 \equiv \left(c_1 - \frac{c_2}{4}\right) v^2, \quad v_T \equiv \left(1 + \frac{3c_H v^2}{8\lambda}\right) v. \quad (2.33)$$

Expanding the new Higgs Lagrangian, we observe that dimension-6 operators contribute to Higgs mass as

$$m_H^2 = 2\lambda v_T^2 \left(1 - \frac{3c_H v^2}{2\lambda} + 2c_3\right).$$

### Yukawa Coupling

If dimension-6 operators of Higgs Lagrangian have induced a shift in the parameters, on the contrary, the modification in Yukawa sector appears to be heavier. In particular, introducing the operator  $\psi^2 H^3$ , before the electroweak symmetry breaking the Lagrangian is

$$\begin{aligned} \mathcal{L}_{Yuk}^{(6)} = & - \left( H_j^\dagger \bar{d}_r [Y_d]_{rs} q_{js} + \tilde{H}_j^\dagger \bar{u}_r [Y_u]_{rs} q_{js} + H_j^\dagger \bar{e}_r [Y_e]_{rs} \ell_{js} + \text{h.c.} \right) \\ & + (H^\dagger H) \left( H_j^\dagger \bar{d}_r [c_d^*]_{sr} q_{js} + \tilde{H}_j^\dagger \bar{d}_r [c_u^*]_{sr} q_{js} + H_j^\dagger \bar{e}_r [c_e^*]_{sr} \ell_{js} + \text{h.c.} \right), \end{aligned}$$

where the cut-off is included in the interaction matrices  $c$ . This equation will bring a contribution to the mass of fermions, indeed after the electroweak symmetry breaking the mass of a generic fermion  $\psi$  will be

$$[M_\psi]_{rs} = \frac{v_T}{\sqrt{2}} \left( [Y_\psi]_{rs} - \frac{v^2}{2} [c_\psi^*]_{sr} \right),$$

with  $\psi = \{u, d, e\}$ . If we try to write the interaction term between Higgs and fermions in a Yukawa-like form, i.e.,  $\mathcal{L} = -H\bar{u}\mathcal{Y}q$ , we get

$$[\mathcal{Y}_\psi]_{rs} = \frac{1 + c_3}{v_T} [M_\psi]_{rs} - \frac{v^2}{\sqrt{2}} [c_\psi^*]_{sr},$$

which is no longer proportional to the fermion mass alone. Moreover, given that the mass and Yukawa matrices are not simultaneously diagonalizable, the coupling between the Higgs boson and the fermion  $\psi$  is no more diagonal in flavor.

### Fermi Constant

The introduction of dimension-6 operators in the SM Lagrangian leads, as we saw, to the shift of Higgs parameters, in particular of its  $vev$ . Then, also Fermi constant,  $G_F$ , will be affected by the presence of higher-order operators since it is inversely proportional to the square of  $vev$ , moreover the new Fermi constant is not simply



obtained by replacing  $v \rightarrow v_T$ , indeed at order  $1/\Lambda^2$ , the new constant, renamed  $\mathcal{G}_F$ , is

$$\frac{4\mathcal{G}_F}{\sqrt{2}} = \frac{2}{v_T^2} - (c_{\mu e \mu e}^{ll} + c_{e \mu \mu e}^{ll}) + 2(c_{ee}^{Hl} + c_{\mu\mu}^{Hl}),$$

where the coefficients  $c^{ll}$  comes from the four-lepton interaction of dimension-6 operators, while  $c^{Hl}$  from the exchange of  $W$  bosons. Note that they include the theory cut-off.

## Gauge Bosons

Some dimension-six operators impact on interactions of gauge bosons, both among themselves and with the other particles of SM. The SMEFT theory allows for the following operators

$$\begin{aligned} \mathcal{L}_6^{gauge} = & c_G H^\dagger H G_{\mu\nu}^a G^{a\mu\nu} + c_W H^\dagger H W_{\mu\nu}^i W^{i\mu\nu} + c_B H^\dagger H B_{\mu\nu} B^{\mu\nu} \\ & + c_{WB} H^\dagger \tau^i H W_{\mu\nu}^i B^{\mu\nu} + c_{3G} f^{abc} G_\mu^{a\nu} G_\nu^{b\rho} G_\rho^{c\mu} + c_{3W} \epsilon^{ijk} W_\mu^{i\nu} W_\nu^{j\rho} W_\rho^{k\mu}. \end{aligned}$$

After the electroweak symmetry breaking the operators  $X^2 H^2$  contribute to the kinetic terms of gauge fields as

$$\begin{aligned} \mathcal{L}_{gauge} = & -\frac{1}{2} W_{\mu\nu}^+ W^{-\mu\nu} - \frac{1}{4} W_{\mu\nu}^3 W^{3\mu\nu} - \frac{1}{4} B_{\mu\nu} B^{\mu\nu} - \frac{1}{4} G_{\mu\nu}^a G^{a\mu\nu} \\ & + \frac{v_T^2}{2} c_W W_{\mu\nu}^i W^{i\mu\nu} + \frac{v_T^2}{2} c_B B_{\mu\nu} B^{\mu\nu} - \frac{v_T^2}{2} c_{WB} W_{\mu\nu}^3 B^{\mu\nu}, \end{aligned} \quad (2.34)$$

where the gauge fields are not canonically normalised. In addition, dimension-6 operators lead to a mixing kinetic term between  $W^3$  and  $B$ . As if that were not enough, the mass term of gauge bosons acquires new contributions

$$\mathcal{L}_{mass} = \frac{1}{4} g^2 v_T^2 W_\mu^+ W^{-\mu} + \frac{1}{8} v_T^2 (g W_\mu^3 - g' B_\mu)^2 + \frac{1}{16} v_T^4 c_2 (g W_\mu^3 - g' B_\mu)^2.$$

A redefinition of gauge fields is necessary to restore the diagonal and normalised form of the kinetic terms

$$G_\mu^a = \mathcal{G}_\mu^a (1 + c_G v_T^2), \quad W_\mu^i = \mathcal{W}_\mu^i (1 + c_W v_T^2), \quad B_\mu = \mathcal{B}_\mu (1 + c_B v_T^2).$$

Defining new coupling constants

$$\bar{g}_s = g_s (1 + c_G v_T^2), \quad \bar{g} = g (1 + c_W v_T^2), \quad \bar{g}' = g' (1 + c_B v_T^2),$$

the product  $g_3 G_\mu^i = \bar{g}_3 \mathcal{G}_\mu^i$  is unchanged. Nevertheless, we still have to identify the mass eigenstates for  $W_\mu^3$  and  $B_\mu$ . Taking into account just the EW part of equation (2.34), we have:

$$\begin{aligned} \mathcal{L}_{gauge} = & -\frac{1}{2} \mathcal{W}_{\mu\nu}^+ \mathcal{W}^{-\mu\nu} - \frac{1}{4} \mathcal{W}_{\mu\nu}^3 \mathcal{W}^{3\mu\nu} - \frac{1}{4} \mathcal{B}_{\mu\nu} \mathcal{B}^{\mu\nu} - \frac{v_T^2}{2} c_{WB} \mathcal{W}_{\mu\nu}^3 \mathcal{B}^{\mu\nu} \\ & + \frac{1}{4} \bar{g}^2 v_T^2 \mathcal{W}_\mu^+ \mathcal{W}^{-\mu} + \frac{1}{8} v_T^2 (\bar{g} \mathcal{W}_\mu^3 - \bar{g}' \mathcal{B}_\mu)^2 + \frac{1}{16} v_T^4 c_2 (\bar{g} \mathcal{W}_\mu^3 - \bar{g}' \mathcal{B}_\mu)^2, \end{aligned}$$

and the mass eigenstates are

$$\begin{pmatrix} \mathcal{W}_\mu^3 \\ \mathcal{B}_\mu \end{pmatrix} = \begin{pmatrix} 1 & -\frac{v_T^2 c_{WB}}{2} \\ -\frac{v_T^2 c_{WB}}{2} & 1 \end{pmatrix} \begin{pmatrix} \cos \bar{\theta} & \sin \bar{\theta} \\ -\sin \bar{\theta} & \cos \bar{\theta} \end{pmatrix} \begin{pmatrix} \mathcal{Z}_\mu \\ \mathcal{A}_\mu \end{pmatrix},$$

where

$$\begin{aligned} \tan \bar{\theta} &= \frac{\bar{g}'}{\bar{g}} + \frac{v_T^2}{2} c_{WB} \left( 1 - \frac{\bar{g}'^2}{\bar{g}^2} \right), \\ \sin \bar{\theta} &= \frac{\bar{g}'}{\sqrt{\bar{g}'^2 + \bar{g}^2}} \left( 1 + \frac{v_T^2 c_{WB}}{2} \frac{\bar{g}(\bar{g}^2 - \bar{g}'^2)}{\bar{g}'(\bar{g}^2 + \bar{g}'^2)} \right), \\ \cos \bar{\theta} &= \frac{\bar{g}}{\sqrt{\bar{g}'^2 + \bar{g}^2}} \left( 1 - \frac{v_T^2 c_{WB}}{2} \frac{\bar{g}'(\bar{g}^2 - \bar{g}'^2)}{\bar{g}(\bar{g}^2 + \bar{g}'^2)} \right). \end{aligned}$$

As expected, the photon is still massless since  $U(1)_{EM}$  is unbroken; on the contrary, the masses of heavy bosons of weak interactions become

$$\begin{aligned} M_W^2 &= \frac{\bar{g}'^2 v_T^2}{4}, \\ M_Z^2 &= \frac{v_T^2}{4} (\bar{g}'^2 + \bar{g}^2) + \frac{v_T^2}{8} c_2 (\bar{g}'^2 + \bar{g}^2) + \frac{v_T^4}{2} \bar{g}' \bar{g} c_{WB}. \end{aligned}$$

The covariant derivative is

$$D_\mu = \partial_\mu + i \frac{\bar{g}}{\sqrt{2}} (\mathcal{W}_\mu^+ T^+ + \mathcal{W}_\mu^- T^-) + i \bar{g}_Z (T_3 - \bar{s}^2 Q) \mathcal{Z}_\mu + i \bar{e} Q \mathcal{A}_\mu,$$

where as usual  $Q = T_3 + Y$ . The new coupling constants are

$$\begin{aligned} \bar{e} &= \frac{\bar{g}' \bar{g}}{\sqrt{\bar{g}^2 + \bar{g}'^2}} \left( 1 - \frac{\bar{g}' \bar{g}}{\bar{g}^2 + \bar{g}'^2} v_T^2 c_{WB} \right), \\ \bar{g}_Z &= \frac{\bar{e}}{(\sin \bar{\theta} \cos \bar{\theta})} \left( 1 + \frac{\bar{g}^2 + \bar{g}'^2}{2 \bar{g}' \bar{g}} v_T^2 c_{WB} \right), \\ \bar{s}^2 &= \sin^2 \bar{\theta}. \end{aligned}$$

Finally, the parameter  $\rho$  given by the ratio between the charged and neutral current, also undergoes a modification

$$\sqrt{\rho} \equiv \frac{\bar{g} m_Z}{\bar{g}_Z m_W} = \sqrt{1 + \frac{v_T^2}{2} c_2},$$

where the parameters  $\bar{g}$ ,  $\bar{g}'$ ,  $v_T$ ,  $c_{WB}$  and  $c_2$  can be experimentally fixed through the masses and the couplings of W and Z bosons. The modifications of the coupling between gauge bosons and fermions have been studied in [24, 18].

In this chapter we will see a concrete application of effective field theories in order to study the light-by-light scattering. We will first derive the low-energy effective Lagrangian that, for interacting Dirac fields, is nothing but the famous Euler-Heisenberg Lagrangian, then we will compute the light-by-light scattering at next to leading order in the underlying full theory. The computation will be repeated for the physical QED, to which we will refer as *spinor QED* within this chapter, and for the hypothetical *scalar QED* and *vector QED* where the interacting particles are charged scalars and charged vectors, respectively. Finally, we will match the coefficients of the effective field theory with those of these three different QEDs and we will compute the cross section of the process.

### 3.1 The Euler-Heisenberg Lagrangian

Classical electrodynamics described by Maxwell equations is a linear theory that does not allow for interactions between two electromagnetic fields in vacuum. Nevertheless, if QED at tree level agrees with this picture, higher-order corrections allow the scattering of light-by-light itself. In other words, QED extends classical theory by including also non-linear corrections.

At low energy, the non-linear corrections are described by the Euler-Heisenberg (EH) Lagrangian. The original suggestion for EH theory was given by O. Halpern who firstly realized that photons can be scattered from other photons. Euler and Heisenberg described the process by assuming that degrees of freedom heavier than a certain cut-off  $\Lambda$  can be encoded in new interactions of those fields that survive at energy scales below the cut-off. Since the low-mass scale is represented by the electron mass  $m_e$ , the only surviving field is the photon field.

The Euler-Heisenberg Lagrangian can be derived from QED Lagrangian by integrating out the electron field. Consequently, new interactions among photons arise, that are suppressed by the fourth power of the electron mass, accordingly to the full theory – QED with only electrons – that includes these interactions at next to leading order computations. Since EH Lagrangian must be Lorentz and gauge invariant, every operator directly proportional to the vector potential,  $A_\mu(x)$ , must be excluded in favor of the electromagnetic field strength, as discussed in Appendix A.4.2. Moreover, restricting the analysis up to operators of dimension eight, one

can only have:

$$\mathcal{F}^2, \quad \mathcal{G}^2, \quad \mathcal{F}\mathcal{G}, \quad (3.1)$$

with

$$\mathcal{F} = \frac{1}{4}F^{\mu\nu}F_{\mu\nu} = \frac{1}{2}(\mathbf{B}^2 - \mathbf{E}^2), \quad \text{and} \quad \mathcal{G} = \frac{1}{4}\tilde{F}^{\mu\nu}F_{\mu\nu} = \mathbf{B} \cdot \mathbf{E}, \quad (3.2)$$

where  $\tilde{F}^{\mu\nu} = \frac{1}{2}\epsilon^{\mu\nu\rho\sigma}F_{\rho\sigma}$  is the dual tensor field strength, while  $\mathbf{E}$  and  $\mathbf{B}$  are the electric and magnetic fields. Note that the last term in equation (3.1) is forbidden since it breaks parity invariance.

The EH Lagrangian is composed by the typical kinetic term for photon field plus two operators that describe the interactions between photons

$$\mathcal{L}_{EH} = -\mathcal{F} + \frac{8}{45} \left( \frac{\alpha^2}{m_e^4} \right) \mathcal{F}^2 + \frac{14}{45} \left( \frac{\alpha^2}{m_e^4} \right) \mathcal{G}^2. \quad (3.3)$$

This Lagrangian leads to a direct computation of  $\beta$ -function for QED, Schwinger pair creation, scalar and pseudoscalar decay rates and chiral anomaly, in addition to a straight calculation of light-by-light scattering cross section [25]:

$$\frac{d\sigma}{d\Omega} = \frac{139\alpha^2}{(180\pi)^2} \frac{\omega^6}{m_e^8} (3 + \cos^2\theta)^2, \quad (3.4)$$

with  $\omega = \sqrt{s}/2$  where  $s$  is the square of the energy in the center of mass, and  $\omega/m_e \ll 1$ , while  $\theta$  is the scattering angle between incoming and outgoing directions in the center of mass rest frame.

## 3.2 The Effective Lagrangian

The Euler-Heisenberg Lagrangian in equation (3.3) serves as basic template to build the general effective field theory for interacting photons at low energy. Taking into account just coupling terms, the effective Lagrangian is

$$\mathcal{L}_{eff} = \mathcal{L}_1 + \mathcal{L}_2 \equiv g_1 (F_{\mu\nu}F^{\mu\nu})^2 + g_2 (\tilde{F}_{\mu\nu}F^{\mu\nu})^2, \quad (3.5)$$

that can be visualized by the Feynman diagrams depicted in figure 3.1.



Figure 3.1: Feynman diagrams for the four-photon interactions.

Our purpose is to compute the light-by-light scattering amplitude, both in the effective field theory and in QED in order to identify the values of the two coefficients

$g_1$  and  $g_2$ . We remark that the process occurs at tree level in the EFT and at one-loop in the underlying full theory. The matching procedure will be performed not only for *spinor QED*, but also for *scalar QED* and *vector QED*.

The  $S$ -matrix element of four incoming photons is:

$$\begin{aligned}\langle f|S|i\rangle &= i \int d^4x \langle 0| \left( \prod_{i=1}^4 a_{p_i, \lambda_i} \right) \mathcal{L}_{eff}(x) |0\rangle \\ &= i \mathcal{M} (2\pi)^4 \delta^{(4)}(p_1 + p_2 + p_3 + p_4) \prod_{i=1}^4 \frac{1}{(2\pi)^3 (2\omega_{p_i})^{1/2}},\end{aligned}\tag{3.6}$$

where  $\mathcal{M}$  is the invariant amplitude that can be written as a sum of two pieces

$$\mathcal{M} = \mathcal{M}_1 + \mathcal{M}_2.$$

The addends  $\mathcal{M}_i$ , with  $i = \{1, 2\}$ , are the invariant amplitudes generated by equation (3.6) with  $\mathcal{L}_1$  and  $\mathcal{L}_2$  separately taken. Starting with the first interaction term, we rewrite it to make explicit the dependence on the derivatives of vector potential

$$\begin{aligned}\mathcal{L}_1 &= 4g_1 (\partial_\mu A_\nu \partial^\mu A^\nu \partial_\rho A_\sigma \partial^\rho A^\sigma \\ &\quad - 2\partial_\mu A_\nu \partial^\mu A^\nu \partial_\rho A_\sigma \partial^\sigma A^\rho \\ &\quad + \partial_\mu A_\nu \partial^\nu A^\mu \partial_\rho A_\sigma \partial^\sigma A^\rho).\end{aligned}$$

The quantized vector potential is:

$$A_\mu(x) = \int \frac{d^3p}{(2\pi)^3} \frac{1}{\sqrt{2\omega_p}} \sum_{\lambda=1}^2 \left( \epsilon_\mu^\lambda(p) a_{p,\lambda} e^{-ipx} + \epsilon_\mu^{\lambda*}(p) a_{p,\lambda}^\dagger e^{ipx} \right),$$

thus its first derivative reads

$$\partial_\nu A_\mu(x) = \int \frac{d^3p}{(2\pi)^3} \frac{(-ip_\nu)}{\sqrt{2\omega_p}} \sum_{\lambda=1}^2 \left( \epsilon_\mu^\lambda(p) a_{p,\lambda} e^{-ipx} - \epsilon_\mu^{\lambda*}(p) a_{p,\lambda}^\dagger e^{ipx} \right).$$

From equation (3.6), it is clear that  $\mathcal{M}_1$  is given by the sum over permutations  $\pi$  of four element, since the distinct Wick contractions of the annihilation operators with the vector potentials are  $4! = 24$ . The invariant amplitude is:

$$\begin{aligned}\mathcal{M}_1 &= 4g_1 \sum_{\pi} \left[ (p_{\pi_1} \cdot p_{\pi_2})(\epsilon_{\pi_1} \cdot \epsilon_{\pi_2})(p_{\pi_3} \cdot p_{\pi_4})(\epsilon_{\pi_3} \cdot \epsilon_{\pi_4}) \right. \\ &\quad - 2(p_{\pi_1} \cdot p_{\pi_2})(\epsilon_{\pi_1} \cdot \epsilon_{\pi_2})(p_{\pi_3} \cdot \epsilon_{\pi_4})(p_{\pi_4} \cdot \epsilon_{\pi_3}) \\ &\quad \left. + (p_{\pi_1} \cdot \epsilon_{\pi_2})(p_{\pi_2} \cdot \epsilon_{\pi_1})(p_{\pi_3} \cdot \epsilon_{\pi_4})(p_{\pi_4} \cdot \epsilon_{\pi_3}) \right].\end{aligned}\tag{3.7}$$

Factorizing out the vector polarizations, the amplitude reads

$$\begin{aligned}\mathcal{M}_1 &= \mathcal{M}_1^{\mu\nu\rho\sigma}(p_1, p_2, p_3, p_4) \epsilon_{1\mu}^* \epsilon_{2\nu}^* \epsilon_{3\rho}^* \epsilon_{4\sigma}^* \\ &\equiv \left( \sum_{\pi} \Gamma_1^{\mu\pi_1 \mu\pi_2 \mu\pi_3 \mu\pi_4}(p_{\pi_1}, p_{\pi_2}, p_{\pi_3}, p_{\pi_4}) \right) \Big|_{\mu_i = \mu, \nu, \rho, \sigma} \epsilon_{1\mu}^* \epsilon_{2\nu}^* \epsilon_{3\rho}^* \epsilon_{4\sigma}^*,\end{aligned}$$

where indices inside the brackets have been renamed as  $\mu = \mu_1$ ,  $\nu = \mu_2$ ,  $\rho = \mu_3$  and  $\sigma = \mu_4$ , to write a compact formula. The polarization tensor  $\mathcal{M}_1^{\mu\nu\rho\sigma}$  as well as the tensor  $\Gamma_1^{\mu\pi_1\mu\pi_2\mu\pi_3\mu\pi_4}$ , is a function of photon momenta and Minkowski metric only. Each element of the sum in previous equation is:

$$\begin{aligned} \Gamma_1^{\mu\pi_1\mu\pi_2\mu\pi_3\mu\pi_4}(p_{\pi_1}, p_{\pi_2}, p_{\pi_3}, p_{\pi_4}) &= 4g_1 [(p_{\pi_1} \cdot p_{\pi_2})(p_{\pi_3} \cdot p_{\pi_4})g^{\mu\pi_1\mu\pi_2}g^{\mu\pi_3\mu\pi_4} \\ &\quad - 2(p_{\pi_1} \cdot p_{\pi_2})(p_{\pi_3})^{\mu\pi_4}(p_{\pi_4})^{\mu\pi_3}g^{\mu\pi_1\mu\pi_2} \\ &\quad + (p_{\pi_1})^{\mu\pi_2}(p_{\pi_2})^{\mu\pi_1}(p_{\pi_3})^{\mu\pi_4}(p_{\pi_4})^{\mu\pi_3}]. \end{aligned}$$

For the polarization tensor we get:

$$\begin{aligned} \mathcal{M}_1^{\mu\nu\rho\sigma} &= g_1 [(p_1 \cdot p_2)(p_3 \cdot p_4)g^{\mu\nu}g^{\rho\sigma} + (p_1 \cdot p_3)(p_2 \cdot p_4)g^{\mu\rho}g^{\nu\sigma} \\ &\quad + (p_1 \cdot p_4)(p_2 \cdot p_3)g^{\mu\sigma}g^{\nu\rho} - 2(p_1 \cdot p_2)(p_3)^\sigma(p_4)^\rho g^{\mu\nu} \\ &\quad - 2(p_1 \cdot p_3)(p_2)^\sigma(p_4)^\nu g^{\mu\rho} - 2(p_1 \cdot p_4)(p_2)^\rho(p_3)^\nu g^{\mu\sigma} \\ &\quad + (p_1)^\nu(p_2)^\mu(p_3)^\sigma(p_4)^\rho + (p_1)^\rho(p_2)^\sigma(p_3)^\mu(p_4)^\nu \\ &\quad + (p_1)^\sigma(p_2)^\rho(p_3)^\nu(p_4)^\mu]. \end{aligned} \quad (3.8)$$

Following the same procedure for  $\mathcal{L}_2$ , we obtain the polarization tensor  $\mathcal{M}_2^{\mu\nu\rho\sigma}$ , however its expression is quite long since each term  $\Gamma_2^{\mu_1\mu_2\mu_3\mu_4}$  is

$$\begin{aligned} \Gamma_2^{\mu\pi_1\mu\pi_2\mu\pi_3\mu\pi_4}(p_{\pi_1}, p_{\pi_2}, p_{\pi_3}, p_{\pi_4}) &= -8g_2 [(p_{\pi_1} \cdot p_{\pi_2})(p_{\pi_3} \cdot p_{\pi_4})g^{\mu\pi_1\mu\pi_2}g^{\mu\pi_3\mu\pi_4} \\ &\quad - (p_{\pi_1} \cdot p_{\pi_2})(p_{\pi_3} \cdot p_{\pi_4})g^{\mu\pi_1\mu\pi_4}g^{\mu\pi_2\mu\pi_3} \\ &\quad - 2(p_{\pi_1} \cdot p_{\pi_2})(p_{\pi_3})^{\mu\pi_4}(p_{\pi_4})^{\mu\pi_3}g^{\mu\pi_1\mu\pi_2} \\ &\quad + (p_{\pi_1} \cdot p_{\pi_2})(p_{\pi_3})^{\mu\pi_4}(p_{\pi_4})^{\mu\pi_1}g^{\mu\pi_2\mu\pi_3} \\ &\quad + (p_{\pi_1} \cdot p_{\pi_2})(p_{\pi_3})^{\mu\pi_2}(p_{\pi_4})^{\mu\pi_3}g^{\mu\pi_1\mu\pi_4} \\ &\quad - (p_{\pi_1} \cdot p_{\pi_2})(p_{\pi_3})^{\mu\pi_2}(p_{\pi_4})^{\mu\pi_1}g^{\mu\pi_3\mu\pi_4} \\ &\quad + (p_{\pi_1})^{\mu\pi_2}(p_{\pi_2} \cdot p_{\pi_3})(p_{\pi_4})^{\mu\pi_1}g^{\mu\pi_3\mu\pi_4} \\ &\quad - (p_{\pi_1})^{\mu\pi_2}(p_{\pi_2} \cdot p_{\pi_3})(p_{\pi_4})^{\mu\pi_3}g^{\mu\pi_1\mu\pi_4} \\ &\quad + (p_{\pi_1})^{\mu\pi_2}(p_{\pi_2})^{\mu\pi_3}(p_{\pi_3} \cdot p_{\pi_4})g^{\mu\pi_1\mu\pi_4} \\ &\quad + (p_{\pi_1})^{\mu\pi_2}(p_{\pi_2})^{\mu\pi_1}(p_{\pi_3})^{\mu\pi_4}(p_{\pi_4})^{\mu\pi_3} \\ &\quad - (p_{\pi_1})^{\mu\pi_2}(p_{\pi_2})^{\mu\pi_3}(p_{\pi_3})^{\mu\pi_4}(p_{\pi_4})^{\mu\pi_1}]. \end{aligned}$$

The complete expression for  $M_2^{\mu\nu\rho\sigma}$  is given in equation (A.19). One can prove that the polarization tensor  $\mathcal{M}_1^{\mu\nu\rho\sigma}$  and  $\mathcal{M}_2^{\mu\nu\rho\sigma}$  satisfy the transversality condition since the theory is gauge invariant, see Appendix A.5.

Energy conservation, that is expressed by  $p_1 + p_2 + p_3 + p_4 = 0$  such that all the momenta are incoming, enables us to remove the dependence on  $p_4$  in the total amplitude:

$$\mathcal{M}^{\mu\nu\rho\sigma}(p_1, p_2, p_3) = \mathcal{M}_1^{\mu\nu\rho\sigma}(p_1, p_2, p_3) + \mathcal{M}_2^{\mu\nu\rho\sigma}(p_1, p_2, p_3).$$

Renaming the scalar product in analogy with Mandelstam variables, but taking into account our convention on incoming momenta:

$$\begin{aligned} s &= (p_1 + p_2)^2 = 2p_1 \cdot p_2 \\ t &= (p_1 + p_3)^2 = 2p_1 \cdot p_3 \\ u &= (p_1 + p_4)^2 = (p_2 + p_3)^2 = 2p_2 \cdot p_3 \\ s + t + u &= 2p_1 \cdot p_2 + 2p_1 \cdot p_3 + 2p_1 \cdot p_4 = -2(p_1)^2 = 0. \end{aligned} \quad (3.9)$$

In view of that, the total polarization tensor can be considerably simplified and its complete expression is written in Appendix A.5.

The comparison between the EFT and each one of the QED models takes place at the level of amplitude, therefore their polarization tensors will be compared, in other words we must solve the equation:

$$\mathcal{M}_{eff}^{\mu\nu\rho\sigma}(p_1, p_2, p_3) - \mathcal{M}_{QED}^{\mu\nu\rho\sigma}(p_1, p_2, p_3) = 0 \quad (3.10)$$

where  $\mathcal{M}_{eff}$  is the polarization tensor of the EFT just calculated.

### 3.2.1 Cross-Section

Once the amplitude has been computed, we can go further by calculating the differential cross-section. For an elastic binary process, in the center of mass frame we have:

$$\frac{d\sigma}{d\Omega} = \frac{|\mathcal{M}|^2}{64\pi^2 s}, \quad (3.11)$$

where  $s$  is the square of the energy in the center of mass. Since an experimental setup does not always permit to select polarized light in the initial state, the squared amplitude in the previous formula is averaged on the photon polarizations, namely:

$$|\mathcal{M}|^2 = \frac{1}{4} \sum_{\lambda=1}^2 \mathcal{M}^{\mu\nu\rho\sigma} \mathcal{M}^{\alpha\beta\gamma\delta} \epsilon_{1\mu}^* \epsilon_{2\nu}^* \epsilon_{3\rho}^* \epsilon_{4\sigma}^* \epsilon_{1\alpha} \epsilon_{2\beta} \epsilon_{3\gamma} \epsilon_{4\delta} = \frac{1}{4} \mathcal{M}^{\mu\nu\rho\sigma} \mathcal{M}_{\mu\nu\rho\sigma},$$

where the sum over photon polarizations is  $\sum_{\lambda=1}^2 \epsilon_{\lambda}^{\mu} \epsilon_{\lambda}^{*\nu} = -g^{\mu\nu} + I^{\mu\nu}$ , with  $I^{\mu\nu}$  that is a gauge-dependent part that contracted with a transverse tensor gives a null contribution. The averaged square amplitude is:

$$|\mathcal{M}|^2 = 64 (3g_1^2 - 2g_1g_2 + 3g_2^2) (s^2 + t^2 + st)^2.$$

In the center of mass frame, the dynamics of the system reads

$$\begin{aligned} p'_1 &= (E, 0, 0, \hat{z}E), \\ p'_2 &= (E, 0, 0, -\hat{z}E), \\ p'_3 &= (E, 0, \hat{y}E \sin \theta, \hat{z}E \cos \theta), \\ p'_4 &= (E, 0, -\hat{y}E \sin \theta, -\hat{z}E \cos \theta), \end{aligned} \quad (3.12)$$

where the convention on energy conservation is  $p_1 + p_2 = p_3 + p_4$ , therefore on one hand,  $p'_1$  and  $p'_2$  do match with momenta  $p_1$  and  $p_2$  that appear along the computation, while on the other hand, the momenta  $p'_3$  and  $p'_4$  are of opposite sign respect to  $p_3$  and  $p_4$ . The Mandelstam variables are:

$$\begin{aligned} s &= (p_1 + p_2)^2 = (p'_1 + p'_2)^2 = 4E^2, \\ t &= (p_1 + p_3)^2 = (p'_1 - p'_3)^2 = \frac{s(\cos \theta - 1)}{2}, \end{aligned} \quad (3.13)$$

where  $E = \sqrt{s}/2$  is the photon energy. The differential cross-section in equation (3.11), becomes:

$$\frac{d\sigma}{d\Omega} = \frac{s^3(3g_1^2 - 2g_1g_2 + 3g_2^2)(3 + \cos^2 \theta)^2}{16\pi^2}. \quad (3.14)$$

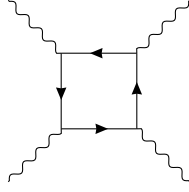


Figure 3.2: The lowest-order contribution to light-by-light scattering in *spinor QED*.

Finally, integrating over the solid angle we get the total cross-section, however, a factor  $1/2!$  must be included to account for indistinguishable particles in final state:

$$\sigma = \frac{1}{2!} \int \frac{d\sigma}{d\Omega} d\Omega = \frac{7s^3(3g_1^3 - 2g_1g_2 + 3g_2^2)}{5\pi}. \quad (3.15)$$

### 3.3 Spinor QED

The Lagrangian for *spinor QED*, whose derivation has been discussed in the first chapter, accounts for an interaction term between the electron and photon fields

$$\mathcal{L}_{int}(x) = -e\bar{\psi}(x)\mathcal{A}(x)\psi(x). \quad (3.16)$$

In QED, the lowest-order contribution to light-by-light-scattering is the box diagram represented in figure 3.2, where the electron is the only particle running in the loop since the theory is at low energy. The  $S$ -matrix is

$$\begin{aligned} \langle f|S|i\rangle &= \frac{1}{4!} \int d^4x_1 d^4x_2 d^4x_3 d^4x_4 \\ &\langle 0| \left( \prod_{i=1}^4 a_{p_i, \lambda_i} \right) \mathcal{T} [\mathcal{L}_{int}(x_1)\mathcal{L}_{int}(x_2)\mathcal{L}_{int}(x_3)\mathcal{L}_{int}(x_4)]|0\rangle, \end{aligned} \quad (3.17)$$

thus, the term inside Dirac brackets can be written as

$$a_1 a_2 a_3 a_4 \mathcal{T}[(\bar{\psi}_1 \mathcal{A}_1 \psi_1)(\bar{\psi}_2 \mathcal{A}_2 \psi_2)(\bar{\psi}_3 \mathcal{A}_3 \psi_3)(\bar{\psi}_4 \mathcal{A}_4 \psi_4)],$$

where  $a_i \equiv a_{p_i, \lambda_i}$  and  $\Psi_i \equiv \Psi(x_i)$  with  $\Psi = \{\bar{\psi}, \psi, \mathcal{A}\}$ . This term allows for  $4!$  different Wick contractions of annihilation operator with photon field, since each  $a_i$  can be contracted with any  $\mathcal{A}_i$ . Moreover, there are still  $4!$  contractions for fermionic operators, however, only 6 of them account for close loops. In the set of these 144 diagrams there is a high redundancy, indeed one can prove that there are only 6 topologically distinct diagrams<sup>1</sup>, thus each diagram is repeated 24 times. This factor cancels the  $1/4!$  of Dyson expansion.

Factorizing out the polarization vectors, and using energy conservation to remove an external momentum, we can parameterise the 6 distinct diagrams as a sum over

<sup>1</sup>When a loop is composed of three-point interaction terms and  $n$  external and indistinguishable particles, the problem of counting distinct diagrams is equivalent to identifying the different arrangements for  $n$  people sitting on a round table.



the combined permutations of indices and momenta, namely

$$\begin{aligned}\mathcal{M}_{1/2} &= \mathcal{M}_{1/2}^{\mu\nu\rho\sigma}(p_1, p_2, p_3, p_4)\epsilon_{1\mu}^*\epsilon_{2\nu}^*\epsilon_{3\rho}^*\epsilon_{4\sigma}^* \\ &= 24 \left( \sum_{\pi} \Gamma^{\mu_{\pi_1}\mu_{\pi_2}\mu_{\pi_3}\sigma}(p_{\pi_1}, p_{\pi_2}, p_{\pi_3}) \right) \Bigg|_{\mu_i=\mu,\nu,\rho} \epsilon_{1\mu}^*\epsilon_{2\nu}^*\epsilon_{3\rho}^*\epsilon_{4\sigma}^*,\end{aligned}\quad (3.18)$$

where, as expected, there are  $3!=6$  permutations.

### 3.3.1 Amplitude Evaluation

Choosing the first configuration  $\pi = 1, 2, 3$ , with  $\mu_i = \{\mu, \nu, \rho\}$  for  $i = \{1, 2, 3\}$ , we can compute the box diagram:

$$\begin{aligned}i\Gamma^{\mu\nu\rho\sigma}(p_1, p_2, p_3) &= -e^4\mu^D \\ &\times \int \frac{d^D l}{(2\pi)^D} \frac{\text{tr}[(\not{q}_0 + m)\gamma^\mu(\not{q}_1 + m)\gamma^\nu(\not{q}_2 + m)\gamma^\rho(\not{q}_3 + m)\gamma^\sigma]}{\prod_{i=0}^3 (q_i^2 - m^2)},\end{aligned}\quad (3.19)$$

where the momenta of virtual electrons are

$$\begin{aligned}q_0 &= l \\ q_1 &= l + p_1 \\ q_2 &= l + p_1 + p_2 \\ q_3 &= l + p_1 + p_2 + p_3.\end{aligned}$$

The box diagram in equation (3.19) is logarithmically divergent; however, the overall amplitude is finite since each of the six permutations contributes with a UV-divergent term that added to the others gives zero. The computation of the diagram has been performed in `Mathematica` powered by the package `FeynCalc`, employing the standard technique of Feynman variables with the aim of simplifying the denominator

$$\frac{1}{\prod_{i=0}^3 (q_i^2 - m^2)} = 6 \int_0^1 dx \int_0^{1-x} dy \int_0^{1-x-y} dz \frac{1}{(l^2 - m^2 [1 + \lambda(s, t)])^4}.$$

The shift  $l \rightarrow l - p_1(x + y + z) - p_2(y + z) - p_3z$  occurred to symmetrize the denominator. The parameter  $\lambda$  depends on Feynman variables and scalar products of the external momenta, with the latter rewritten as a function of Mandelstam variables, according to equation (3.9). Specifically,

$$\lambda(s, t) = \frac{s((x+y)(y+z) - y) + txz}{m^2}$$

Performing the same shift at numerator, we get:

$$\text{tr}[\dots] = \text{tr}[(\not{l} - \not{Q}_0 + m)\gamma^\mu(\not{l} - \not{Q}_1 + m)\gamma^\nu(\not{l} - \not{Q}_2 + m)\gamma^\rho(\not{l} - \not{Q}_3 + m)\gamma^\sigma],$$

where  $Q_i$ , with  $i = \{0, 1, 2, 3\}$ , are linear combinations of the external momenta. At this stage, the structure of  $Q_i$  is not relevant because, in each term of the trace, we have to deal with the number of Dirac matrices on one hand, and the power of

the loop moment on the other. Since integration is made over the whole momentum space, odd powers of  $l_\mu$  are killed by symmetry. Moreover, trace technology leaves alive only terms with an even number of gamma matrices

$$\begin{aligned}
\text{tr}[\dots] = & \text{tr}[\gamma^\alpha \gamma^\mu \gamma^\beta \gamma^\nu \gamma^\gamma \gamma^\rho \gamma^\delta \gamma^\sigma] \left( l_\alpha l_\beta l_\gamma l_\delta + Q_{0\alpha} Q_{1\beta} Q_{2\gamma} Q_{3\delta} \right. \\
& + l_\beta l_\gamma Q_{0\alpha} Q_{3\delta} + l_\beta l_\delta Q_{0\alpha} Q_{2\gamma} + l_\gamma l_\delta Q_{0\alpha} Q_{1\beta} \\
& \left. + l_\alpha l_\beta Q_{2\gamma} Q_{3\delta} + l_\alpha l_\gamma Q_{1\beta} Q_{3\delta} + l_\alpha l_\delta Q_{1\beta} Q_{2\gamma} \right) \\
& + \text{tr}[\gamma^\alpha \gamma^\mu \gamma^\beta \gamma^\nu \gamma^\rho \gamma^\sigma] m^2 (l_\alpha l_\beta + Q_{0\alpha} Q_{1\beta}) \\
& + \text{tr}[\gamma^\alpha \gamma^\mu \gamma^\nu \gamma^\gamma \gamma^\rho \gamma^\sigma] m^2 (l_\alpha l_\gamma + Q_{0\alpha} Q_{2\gamma}) \\
& + \text{tr}[\gamma^\alpha \gamma^\mu \gamma^\nu \gamma^\rho \gamma^\delta \gamma^\sigma] m^2 (l_\alpha l_\delta + Q_{0\alpha} Q_{3\delta}) \\
& + \text{tr}[\gamma^\mu \gamma^\beta \gamma^\nu \gamma^\gamma \gamma^\rho \gamma^\sigma] m^2 (l_\beta l_\gamma + Q_{1\beta} Q_{2\gamma}) \\
& + \text{tr}[\gamma^\mu \gamma^\beta \gamma^\nu \gamma^\rho \gamma^\delta \gamma^\sigma] m^2 (l_\beta l_\delta + Q_{1\beta} Q_{3\delta}) \\
& + \text{tr}[\gamma^\mu \gamma^\nu \gamma^\gamma \gamma^\rho \gamma^\delta \gamma^\sigma] m^2 (l_\gamma l_\delta + Q_{2\gamma} Q_{3\delta}) \\
& + \text{tr}[\gamma^\mu \gamma^\nu \gamma^\rho \gamma^\sigma] m^4.
\end{aligned} \tag{3.20}$$

First of all, Lorentz invariance is invoked to rewrite scalar products of loop momentum since the denominator is an even function of momentum  $l$ , thus

$$\begin{aligned}
\int \frac{d^D l}{(2\pi)^D} l^\mu l^\nu & \rightarrow \int \frac{d^D l}{(2\pi)^D} \frac{l^2 g^{\mu\nu}}{D} \\
\int \frac{d^D l}{(2\pi)^D} l^\mu l^\nu l^\rho l^\sigma & \rightarrow \int \frac{d^D l}{(2\pi)^D} \frac{l^2 (g^{\mu\nu} g^{\rho\sigma} + g^{\mu\rho} g^{\nu\sigma} + g^{\mu\sigma} g^{\nu\rho})}{D(D+2)}
\end{aligned}$$

This simplification reduces the number of Dirac gamma matrices that appear inside a trace. The evaluation of traces has been made according to the equation A.11. The resulting equation is very long; it becomes even longer when the momenta  $Q_i$  are replaced in favor of  $p_i$ . Nevertheless, we can contract repeated indices to display scalar products and introduce Mandelstam variables, as in equation (3.9), to simplify it. The contracted equation shows several terms proportional to the squared of external momenta that can be removed since photons are on-shell. Moreover, we applied the transversality conditions on external photons, that are expressed as:

$$\begin{aligned}
\Gamma^{\mu\nu\rho\sigma}(p_1, p_2, p_3) p_{1\mu} & = 0 \\
\Gamma^{\mu\nu\rho\sigma}(p_1, p_2, p_3) p_{2\nu} & = 0 \\
\Gamma^{\mu\nu\rho\sigma}(p_1, p_2, p_3) p_{3\rho} & = 0,
\end{aligned}$$

that leads to the deletion of those terms proportional to  $p_1^\mu$ ,  $p_2^\nu$  and  $p_3^\rho$ .

At this stage, every term that composes the numerator of the integrand function can be grouped in three ensembles, so that equation (3.19), can be written as:

$$\begin{aligned}
i\Gamma^{\mu\nu\rho\sigma}(p_1, p_2, p_3) = & -6e^4 \mu^D \int_0^1 dx \int_0^{1-x} dy \int_0^{1-x-y} dz \\
& \times \int \frac{d^D l}{(2\pi)^D} \frac{\Gamma_4^{\mu\nu\rho\sigma} + \Gamma_2^{\mu\nu\rho\sigma} + \Gamma_0^{\mu\nu\rho\sigma}}{(l^2 - m^2 [1 + \lambda(s, t)])^4},
\end{aligned}$$

where the subscript of  $\Gamma_i^{\mu\nu\rho\sigma}$  clarifies the proportionality of terms to the loop momentum, for instance  $\Gamma_4^{\mu\nu\rho\sigma}$  is composed of terms proportional to the fourth power of the  $l_\mu$ .

The integration over loop momentum can be performed by the master integration formula, in equation (2.13), which returns

$$\begin{aligned}\Gamma_4^{\mu\nu\rho\sigma} &\propto \int \frac{d^D l}{(2\pi)^D} \frac{(l^2)^2}{(l^2 - m^2[1 + \lambda(s, t)])^4} = \frac{i(\epsilon - 3)(\epsilon - 2)}{3\pi^{2-\epsilon}2^{5-2\epsilon}} \Gamma(\epsilon) ((\lambda + 1)m^2)^{-\epsilon} \\ \Gamma_2^{\mu\nu\rho\sigma} &\propto \int \frac{d^D l}{(2\pi)^D} \frac{(l^2)^1}{(l^2 - m^2[1 + \lambda(s, t)])^4} = -\frac{i}{48\pi^2 m^2 (\lambda + 1)} \\ \Gamma_0^{\mu\nu\rho\sigma} &\propto \int \frac{d^D l}{(2\pi)^D} \frac{(l^2)^0}{(l^2 - m^2[1 + \lambda(s, t)])^4} = \frac{i}{96\pi^2 m^4 (\lambda + 1)^2}.\end{aligned}$$

Unsurprisingly, the integration over the loop momentum produces, at numerator, the same tensor structures obtained for the effective field theory, namely:

$$(g)(g) \quad (g)(p)(p) \quad (p)(p)(p)(p).$$

While  $\Gamma_4^{\mu\nu\rho\sigma}$  and  $\Gamma_0^{\mu\nu\rho\sigma}$  contain only the first and the third kind of structures respectively, the tensor  $\Gamma_2^{\mu\nu\rho\sigma}$  is a mix of first and second type. Therefore, we must separate the  $(g)(g)$  terms of  $\Gamma_2^{\mu\nu\rho\sigma}$ . Summing them with  $\Gamma_4^{\mu\nu\rho\sigma}$ , we get:

$$\begin{aligned}\Gamma_{(g)(g)}^{\mu\nu\rho\sigma} &\equiv \Gamma_4^{\mu\nu\rho\sigma} + \Gamma_{2(g)(g)}^{\mu\nu\rho\sigma} \\ \Gamma_{(g)(p)(p)}^{\mu\nu\rho\sigma} &\equiv \Gamma_{2(g)(p)(p)}^{\mu\nu\rho\sigma} \\ \Gamma_{(p)(p)(p)(p)}^{\mu\nu\rho\sigma} &\equiv \Gamma_0^{\mu\nu\rho\sigma},\end{aligned}\tag{3.21}$$

in this way we can perform a power expansion in the parameter  $\lambda$ , which is performed at second order for  $\Gamma_{(g)(g)}^{\mu\nu\rho\sigma}$ , at first order for  $\Gamma_{(g)(p)(p)}^{\mu\nu\rho\sigma}$  and at zero order for  $\Gamma_{(p)(p)(p)(p)}^{\mu\nu\rho\sigma}$ . Then the integration over Feynman variables is straight.

Finally, the other five diagrams must be compute, however we can parametrize our result as a function of indices, momenta and Mandelstam variable – since they are merely a way of rewriting the scalar products of the external momenta – to obtain other amplitudes without further calculations. The complete amplitude of *spinor QED* is written in equation (A.24).

Comparing the amplitudes of the effective field theory and *spinor QED*, we have:

$$\mathcal{M}^{\mu\nu\rho\sigma}(g_1, g_2) - \mathcal{M}_{1/2}^{\mu\nu\rho\sigma} = 0,\tag{3.22}$$

substituting equation (A.23) and equation (A.24), it leads to the system:

$$\begin{aligned}e^4(10s + 7t) + 5760\pi^2 m^4(g_1 s - g_2(2s + t)) &= 0 \\ 5760\pi^2 m^4 g_2 - 7e^4 &= 0,\end{aligned}$$

whose solutions are:

$$\begin{aligned}g_1 &= \frac{e^4}{1440\pi^2 m^4} = \frac{\alpha^2}{90m^4} \\ g_2 &= \frac{7e^4}{5760\pi^2 m^4} = \frac{7\alpha^2}{360m^4},\end{aligned}\tag{3.23}$$

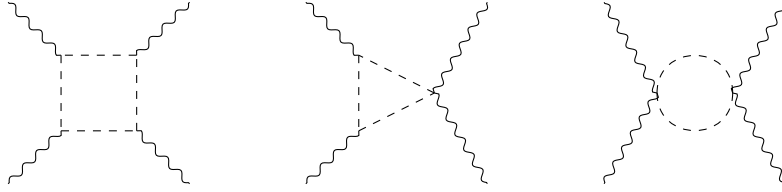


Figure 3.3: The lowest-order contributions to light-by-light scattering in *scalar QED*: box, triangle and bubble diagram, respectively.

from which it follows that  $g_2 = 7/4g_1$ . In other words, the effective Lagrangian for *spinor QED* at low energy is

$$\begin{aligned}\mathcal{L}_{1/2} &= g_1(F_{\mu\nu}F^{\mu\nu})^2 + g_2(\tilde{F}_{\mu\nu}F^{\mu\nu})^2 \\ &= \frac{\alpha^2}{90m^4}(F_{\mu\nu}F^{\mu\nu})^2 + \frac{7\alpha^2}{360m^4}(\tilde{F}_{\mu\nu}F^{\mu\nu})^2 \\ &= \frac{8\alpha^2}{45m^4}\mathcal{F}^2 + \frac{14\alpha^2}{45m^4}\mathcal{G}^2.\end{aligned}$$

which is nothing but the interacting terms of Euler-Heisenberg Lagrangian in equation (3.3).

We can go further by computing the cross-section of light-by-light scattering in *spinor QED*, that follows from (3.14)

$$\frac{d\sigma}{d\Omega} = \frac{139\alpha^4\omega^6}{(180)^2\pi^2m^8}(\cos\theta^2 + 3)^2,$$

in agreement with equation (3.4). The correspondence between our results and those in literature provides support for the employed calculation, that will be used in the following sections to obtain the coefficients for *scalar QED* and *vector QED*.

### 3.4 Scalar QED

The Lagrangian that describes the interaction between a complex scalar field and photon is

$$\mathcal{L}_{int} = -ieA_\mu[\phi^*(\partial^\mu\phi) - (\partial^\mu\phi^*)\phi] + e^2A_\mu A^\mu|\phi|^2, \quad (3.24)$$

which aside to three-point interaction, it allows for four-point interaction vertex:

$$= 2ie^2g_{\mu\nu}.$$

Thus, in *scalar QED* there are three diagrams that contributes to light-by-light scattering, see figure 3.3. These three diagrams, named box, triangle and bubble diagrams, are all ultraviolet divergent. In this case, logarithmic divergence is still

alive when adding up different permutations and only by summing diagrams together we manage to kill it. The computation has been done following the procedure explained for *spinor QED* since no further complications occur.

The comparison with effective field theory leads to the following result:

$$\begin{aligned} g_1 &= \frac{7e^4}{23040\pi^2 m^4} = \frac{7\alpha^2}{1440m^4} \\ g_2 &= \frac{e^4}{23040\pi^2 m^4} = \frac{\alpha^2}{1440m^4}. \end{aligned} \quad (3.25)$$

The effective Lagrangian for the scalar case is:

$$\mathcal{L}_0 = \frac{7\alpha^2}{90m^4} \mathcal{F}^2 + \frac{\alpha^2}{90m^4} \mathcal{G}.$$

From equation (3.14), the differential cross-section is:

$$\frac{d\sigma}{d\Omega} = \frac{17\alpha^4 \omega^6}{64800\pi^2 m^8} (\cos\theta^2 + 3)^2.$$

### 3.5 Vector QED

The Lagrangian that describes the interaction between a vector field  $V_\mu(x)$  and photon is

$$\begin{aligned} \mathcal{L}_{int} &= -ie(A_\mu V_\nu \overset{\leftrightarrow}{\partial}^\mu V^\nu + V_\mu V_\nu^\dagger \overset{\leftrightarrow}{\partial}^\mu A^\nu + V_\mu^\dagger A_\nu \overset{\leftrightarrow}{\partial}^\mu V^\nu) \\ &\quad - e^2(V_\mu V^\dagger{}^\mu A_\nu a^\nu - V_\mu a^\mu V_\nu^\dagger A^\nu), \end{aligned} \quad (3.26)$$

with the usual convention that  $\overset{\leftrightarrow}{\partial}$  gives a minus sign when acts on the left. The Lagrangian for *vector QED* accounts for both three-point and four-point interactions, thus the allowed Feynman diagrams are the box, the triangle and the bubble diagrams, likewise in *scalar QED*. The Lagrangian for *vector QED* is naturally em-

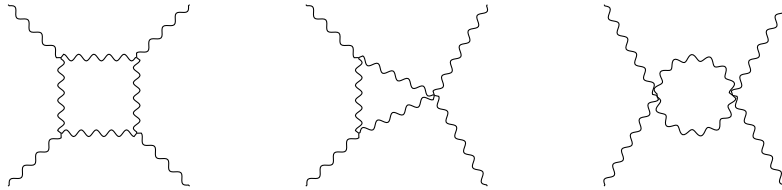


Figure 3.4: The lowest-order contributions to light-by-light scattering in *vector QED*.

bedded in the Standard Model, in fact these interactions can occur between photons and the charged vector bosons of  $SU(2)$  gauge symmetry. Their propagator in  $R_\xi$ -gauge is

$$i\Pi^{\mu\nu}(x) = \frac{-i}{p^2 - m^2} \left( g^{\mu\nu} - \frac{p^\mu p^\nu}{p^2 - \xi m^2} (1 - \xi) \right).$$

The computation of loop diagrams that involve  $W_\mu^\pm$  are typically performed in Feynman-t'Hooft gauge ( $\xi = 1$ ) since it considerably simplifies calculations. However, on the purpose of avoiding Faddeev and Popov ghosts, we worked in unitarity gauge ( $\xi \rightarrow \infty$ ), where the vector propagator reads:

$$i\Pi^{\mu\nu}(x) = \frac{-i}{p^2 - m^2} \left( g^{\mu\nu} - \frac{p^\mu p^\nu}{m^2} \right). \quad (3.27)$$

The computation of diagrams that appear in figure 3.4 is longer than previous cases; in particular, the structure of vector propagator, that brings momentum in the numerator, extremely increases the number of terms that enter in the computation.

The matching procedure leads to:

$$\begin{aligned} g_1 &= \frac{29e^4}{2560\pi^2 m^4} = \frac{29\alpha^2}{160m^4} \\ g_2 &= \frac{27e^4}{2560\pi^2 m^4} = \frac{27\alpha^2}{160m^4}. \end{aligned} \quad (3.28)$$

The effective Lagrangian for the vector case is:

$$\mathcal{L}_1 = \frac{29\alpha^2}{10m^4} \mathcal{F}^2 + \frac{27\alpha^2}{10m^4} \mathcal{G}.$$

From equation (3.14), the differential cross-section is:

$$\frac{d\sigma}{d\Omega} = \frac{393 \alpha^4 \omega^6}{800\pi^2 m^8} (\cos^2 \theta + 3)^2.$$

## 3.6 Conclusions and Outlook

In this chapter, the effective action for low-energy QED has been obtained. The interactions among photons are embedded, at dimension eight, in two effective operators that arise by integrating out the heavy fields. The coefficients of high-dimensional operators are calculated as induced by loop of the heavy particles. The computation not only shows a first application of effective field theories, but also leads to the direct computation of light-by-light scattering in the Standard Model. In particular, the Electroweak sector of SM encodes *vector QED* given that  $SU(2)$  gauge bosons, namely  $W_\mu^\pm$  are electrically charged.

The results of the computation match with literature [26]-[29]. Specifically, in ref. [26] a similar approach has been used, while in ref. [28] and [29] the heat kernel method has been involved to obtain the same result. The outcomes of our calculation are presented in table 3.1, where the coupling constants of effective operator  $\mathcal{F}^2$  and  $\mathcal{G}^2$  are shown, namely  $g_i \equiv \bar{g}_i (\alpha/4m^2)^2$  where  $i = \{1, 2\}$ . The coupling constants increase quite fast with the spin of the particle running in the loop. Assuming that this behavior is kept for larger spins, then light-by-light scattering might represent a preferred channel to investigate high-spin particles, like string excitations or strongly-interacting bound states [30]. Experimentally, light-by-light scattering is extremely difficult to detect, although it has recently been discovered that this reaction is accessible at Large Hadron Collider since a large electromagnetic field strengths is generated by ultra-relativistic colliding lead ions. In ref. [31]

QED models	$\bar{g}_1$	$\bar{g}_2$
scalar	7/90	1/90
spinor	8/45	14/45
vector	29/10	27/10

Table 3.1: Coupling constants of the effective operators  $\mathcal{F}^2$  and  $\mathcal{G}^2$ .

the experimental outcomes of ATLAS are presented. They shown that evidence of this scattering are collected in quasi-real photon interactions from  $480 \mu\text{b}^{-1}$  of ultra-peripheral Pb+Pb collisions at  $\sqrt{s_{NN}} = 5.02 \text{ TeV}$ . In particular, the fiducial cross-section of  $Pb + Pb \rightarrow Pb + Pb + \gamma\gamma$  process was measured and appears to be compatible with SM predictions. The phenomenological analysis of this set up is presented in ref. [34] - [33].

Some extension of effective field theory of EH-type have been proposed, in ref. [35] a generalization from photon to SU(N) boson is investigated while in ref. [27] and [36], an axial coupling of gauge field with fermionic matter has been hypothesized. This interaction allows for the parity-breaking term  $\mathcal{FG}$  in the effective field theory. *Spinor QED* discussed above, appears to be a limit case of such generalized EFT.





In this chapter we will see a concrete application of effective field theory, that will be employed in the description of dark matter; in particular we will present a model where a dark matter candidate, either a Majorana or Dirac spinor, couples to the hypercharge form factor.

The chapter starts with a brief revision of the  $\Lambda$ -CDM model, also known as the *Standard Model of Cosmology*, that gravitationally describes dark matter through the effects of its mass on cosmological objects. Starting from astronomical observation, it is possible to make some assumptions on the nature of dark matter in order to build an effective field theory, that must be tested on experimental outcomes to verify its predictive power. In fact, not only the model must reproduce the estimated relic density abundance of dark matter, but it must also be in agreement with the latest data obtained from direct and indirect detection, as well as collider search, of dark matter.

The mainly reference for this chapter is the article in ref. [1], that was co-authored by the writer of this thesis, that performed, in particular, the analysis and computations given in section 4.4 and 4.5.

## 4.1 The $\Lambda$ -CDM model

In the past forty years our understanding of the Universe has considerably increased thanks to the research in Cosmology and Astrophysics. In particular, several observational data, like rotational curves of galaxies, galaxy merging and accelerated expansion, to name a few, provide indirect support for *dark* nature of the Universe: 95% of its content relies to dark sector, namely dark energy (DE) and dark matter (DM), leaving a measly 5% to baryonic (or ordinary) matter, that is described by the Standard Model of particle physics, presented in chapter 1.

Although many attempts have been made and plenty of speculations have been put forward, a satisfying explanation for dark sector is still missing. Nevertheless, cosmologists have been able to arrange our knowledge on the Universe in a single framework, which has been named the *Standard Model of Cosmology* or  $\Lambda$ -CDM model (where CDM stands for Cold Dark Matter) [48]-[43]. The robustness of the model has been repeatedly questioned since it seems to be constructed with *ad-hoc* assumptions that were invoked in response to observations that falsified the model as it existed at the time [37]. Furthermore, if on one side the particle nature

of dark matter finds a large consensus between cosmologists that support  $\Lambda$ -CDM model [38], on the other side the functional nature of dark energy is still fuzzy and uncertain.

The fundamental hypothesis of  $\Lambda$ -CDM are:

- the cosmological principle, namely homogeneity and isotropy of the Universe;
- the validity of General Relativity (GR);
- the hot Big Bang model history and inflation at the very early stages;
- the dark sector: DE is described by the cosmological constant in Einstein field equations and the majority part of DM is non-relativistic (cold).

The hot Big Bang model history agrees with the observed abundance of light elements, expecting at the same time a relic black body radiation permeating the Universe, that corresponds to the Cosmic Microwave Background (CMB), accidentally discovered by A. Penzias and R. Wilson in 1965. Inflation is a viable solution for flatness of space (at cosmological scales) and to explain the lack of magnetic monopole and it also accounts for the horizon problem<sup>1</sup> explaining the correlation of apparently causally-disconnected regions in CMB.

In General Relativity the dynamics of the space-time is described by the metric tensor  $\tilde{g}_{\mu\nu}$ <sup>2</sup>, whose equations of motion follow from the variation of the Einstein-Hilbert action:

$$S_{EH} = \int d^4x \sqrt{-\tilde{g}} \left[ \frac{R}{16\pi G} + \mathcal{L}_m \right], \quad (4.1)$$

where  $\tilde{g}$  is the determinant of the curved metric,  $R$  is named Ricci scalar,  $G$  is the gravitational Newton constant and  $\mathcal{L}_m$  is the Lagrangian for the matter content of the Universe. The Euler-Lagrange equations of the metric are:

$$R_{\mu\nu} - \frac{1}{2}\tilde{g}_{\mu\nu}R = 8\pi G T_{\mu\nu}, \quad (4.2)$$

which are known as Einstein field equations, where  $T_{\mu\nu}$  is the total-energy momentum tensor. The tensor on the left-hand side is usually renamed Einstein tensor:

$$G_{\mu\nu} \equiv R_{\mu\nu} - \frac{1}{2}\tilde{g}_{\mu\nu}R,$$

and it describes the geometry of space-time. Einstein tensor  $G_{\mu\nu}$  fulfills Bianchi identities, so that  $\nabla_\nu G^{\mu\nu} = 0$ , where  $\nabla_\nu$  is the covariant derivative, that acts on a tensor  $A_\nu^\sigma$  as  $\nabla_\mu A_\rho^\nu = \partial_\mu A_\rho^\nu - \Gamma_{\rho\mu}^\sigma A_\sigma^\nu + \Gamma_{\mu\sigma}^\nu A_\rho^\sigma$ , where  $\Gamma_{\mu\nu}^\rho$  is the Christoffel symbol:

$$\Gamma_{\mu\nu}^\rho = \frac{1}{2}g^{\rho\sigma} (\partial_\mu g_{\nu\sigma} + \partial_\nu g_{\mu\sigma} - \partial_\sigma g_{\mu\nu}).$$

Bianchi identities lead to the conservation of the total energy-momentum tensor:

$$\nabla_\nu T^{\mu\nu} = 0.$$

---

<sup>1</sup>The justification for homogeneity and isotropy of the Universe, according to the cosmological principle, is not fully understood.

<sup>2</sup>In GR, the metric tensor is typically denoted by  $g_{\mu\nu}$  while  $\eta_{\mu\nu}$  stands for the flat metric of Minkowski space-time. Since in this thesis, we adopted particle physics convention, naming the flat metric  $g_{\mu\nu}$ , the curved metric is denoted with  $\tilde{g}_{\mu\nu}$ .

The solution of Einstein equations for an homogeneous, isotropic and adiabatically expanding universe is identified by Friedmann-Lemaître-Robertson-Walker (FLRW) metric:

$$ds^2 = dt^2 - a(t)^2 \left( \frac{dr^2}{1 - kr^2} + r^2 d\Omega^2 \right),$$

where  $a(t)$  is the scale factor and  $k = \{1, 0, 1\}$  is a constant whose values represent a hyperbolic, a flat and a spherical spaces, respectively. Given the symmetries of FLRW metric<sup>3</sup>, the total energy-momentum tensor acquires a diagonal structure:

$$T_{\mu\nu} = \begin{pmatrix} \rho & 0 & 0 & 0 \\ 0 & -P & 0 & 0 \\ 0 & 0 & -P & 0 \\ 0 & 0 & 0 & -P \end{pmatrix},$$

where  $P$  is the pressure and  $\rho$  the energy density. Therefore, the 10 initially equations, embedded in 4.2, are reduced to Friedmann equations:

$$\begin{aligned} H^2 &= \frac{1}{a^2} \left( \frac{da}{dt} \right)^2 = \frac{8\pi G}{3} \rho - \frac{k}{a^2} \\ \frac{dH}{dt} &= \frac{d}{dt} \left( \frac{1}{a} \frac{da}{dt} \right) = -4\pi G (\rho + P) + \frac{k}{a^2}, \end{aligned} \quad (4.3)$$

where  $H$  is the Hubble parameter. Combining the two equations in order to get on the left-hand side the second derivative of the scale parameter  $a(t)$ , we obtain:

$$\frac{d^2 a}{dt^2} = -\frac{4\pi G a}{3} (\rho + 3P),$$

where  $d^2 a/dt^2$  is nothing but an acceleration, namely the Universe acceleration expansion. According to previous equation, when  $\rho + 3P < 0$  the expansion is decelerated and it leads to  $w > -1/3$ , called strong energy condition, where  $w \equiv P/\rho$ . In ordinary matter, the pressure is always positive, thus the observed acceleration of the Universe must be explained with an exotic component, i.e., the cosmological constant  $\Lambda$ , whose state equation is  $w = -1$ , thereby motivating accelerated expansion. Including the cosmological constant, Einstein field equations become:

$$G_{\mu\nu} = 8\pi G T_{\mu\nu} - \tilde{g}_{\mu\nu} \Lambda, \quad (4.4)$$

note that these equations represent the most general modification of Einstein field equations, which are still in agreement with the requirement of diagonal structure of the total energy-momentum tensor, thus preserving also its conservation law, i.e.,  $\nabla_\nu T^{\mu\nu} = 0$  [48].

The generalized version of Friedmann equations follows from (4.4):

$$\begin{aligned} H^2 &= \frac{1}{a^2} \left( \frac{da}{dt} \right)^2 = \frac{8\pi G}{3} \rho - \frac{\Lambda}{3} - \frac{k}{a^2} \\ \frac{dH}{dt} &= \frac{d}{dt} \left( \frac{1}{a} \frac{da}{dt} \right) = -4\pi G (\rho + P) + \frac{k}{a^2}, \end{aligned} \quad (4.5)$$

---

<sup>3</sup>Isotropy and homogeneity imply that the elements  $T^{0i}$  have to vanish while  $T^{ij}$  must be proportional to the 3-metric  $\tilde{g}_{ij}$

where the second equation is unaffected by the introduction of the cosmological constant<sup>4</sup>. The very last set of Friedmann equations can be reworded in the same form of the first one, namely equations (4.3), by shifting density and pressure by a constant value that is proportional to the cosmological constant:

$$\rho \rightarrow \rho + \frac{\Lambda}{8\pi G} \qquad P \rightarrow P - \frac{\Lambda}{8\pi G},$$

which explains why the second Friedmann equation remains unchanged while introducing the cosmological constant. Assuming a flat universe ( $k = 0$ ), we can solve the first equation in (4.5), to get the critical density value that leads to a flat space

$$\rho_c = \frac{3}{8\pi G} H^2. \tag{4.6}$$

Substituting in the original first equation of Friedmann, in (4.3), where  $k$  is still a free parameter, we obtain:

$$H^2 \left( 1 - \frac{\rho}{\rho_c} \right) = -\frac{k}{a^2}.$$

The definition of density parameters

$$\Omega_i = \frac{\rho_i}{\rho_c} \qquad \Omega_{curv} = -\frac{k}{a^2 H^2}, \tag{4.7}$$

where  $i = \{matter, radiation, \Lambda\}$ , allows to separate out the contribution coming from each different substance that permeates the Universe, then equation (4.6) becomes

$$\sum_i \Omega_i + \Omega_{curv} = 1.$$

This equation imposes a condition on the geometrical structure of the universe based on its content: if the density of the universe is lower than the critical value, the curvature of its space-time is negative resulting in a hyperbolic geometry; on the contrary, for a density higher than the critical value the curvature is positive and its geometry is spherical, while a flat space-time requires a density equal to the critical value. At the present time, the best value for these parameters are [39]

$$\begin{aligned} \Omega_m &= 0.3111 \pm 0.0056 \\ \Omega_r &< 5 \cdot 10^{-5} \\ \Omega_\Lambda &= 0.6889 \pm 0.0056 \\ |\Omega_{curv}| &= 0.0007 \pm 0.0019, \end{aligned} \tag{4.8}$$

introducing another puzzling question: why does the content of our Universe exactly coincide with the critical value? Our Universe, at large scale, is therefore flat and its history and evolution can be described by the standard Hot Big Bang theory, considering also a period of inflationary expansion [39].

---

<sup>4</sup>This is not always true, indeed there are several ways to write Friedmann equations, which are not all unchanged by the introduction of  $\Lambda$ .

Density parameters are not fixed in time, their evolution trend can be obtained starting from the total energy-momentum tensor, that in terms of pressure and density is:

$$\frac{d\rho}{dt} = -3H(\rho + P). \quad (4.9)$$

Assuming that each component of the Universe is well-described by this equation, we can integrate it to get the function that describes the evolution of density in time

$$\rho_i(t) = \rho_{i0} \left( \frac{a(t)}{a_0} \right)^{-3(1+w_i)},$$

where  $w_i = \{0, 1/3, -1\}$  for non-relativistic matter, radiation and a cosmological constant, respectively. Thus, each component of the Universe evolves with a simple scaling law, that for matter is  $\rho_m \propto a^{-3}$ , for radiation is  $\rho_r \propto a^{-4}$  and for the  $\Lambda$  is constant  $\rho_\Lambda = 1$ . Hence, the weight of each component changes in time, resulting in a sequence of stages where the Universe was ‘dominated’ by different components. Since the scale factor increases with time, at the early stages radiation was predominant, but due to its faster dilution compared to matter, during the Universe expansion, it was definitively defeated by matter at the equivalence red-shift, where  $\rho_m(t_{eq}) = \rho_r(t_{eq})$ . In the same way, at some point in the past, called red-shift of matter-cosmological constant, the latter has exceeded the former and the Universe has started an era of accelerated expansion.

## 4.2 Indirect Evidences of Dark Matter

In the previous section, we mentioned matter as a single component of the Universe, however, the value in (4.8) is understood as the sum of two contributions: the baryon (or ordinary) matter ( $\Omega_b$ ) and cold dark matter ( $\Omega_c$ ). In particular, the Planck collaboration obtained [39]:

$$\begin{aligned} \Omega_c h^2 &= 0.1200 \pm 0.0012 \\ \Omega_b h^2 &= 0.0224 \pm 0.0001, \end{aligned} \quad (4.10)$$

where  $h$  is defined from  $H_0 = 100h \text{ km s}^{-1} \text{ Mpc}^{-1}$  and named dimensionless Hubble constant<sup>5</sup>. Almost 84% of the Universe matter content belongs to dark matter, whose origin is still unknown, although there are several experimental evidences, that find a good explanation because of dark matter. In fact, DM was firstly introduced as a viable solution to explain the rotational velocity of hydrogen-cloud in the external region of galaxies. In the non-relativistic limit, the dynamics of galaxy is well described by Newton’s gravity and the expected velocity of rotating objects around galaxy must be proportional to  $(M/r)^{1/2}$ , where  $M$  is the mass of the gravitational source that sets in rotational motion the hydrogen-clouds, whose distance from the galaxy center is  $r$ . Thus, once all the observed matter as been counted in  $M$ , the expected behavior of velocity is rapidly decreasing in distance,  $v \propto r^{-1/2}$ . Nevertheless, data suggest that the speed of hydrogen-clouds is greater than expected, leading to the hypothesis that some dark mass has not been counted. The issue of missing matter has been also found in gravitational lensing since

<sup>5</sup>The current estimation [39] for Hubble constant is  $H_0 = (67.4 \pm 0.5) \text{ km s}^{-1} \text{ Mpc}^{-1}$ .

light traveling from far away sources might be deflected in space regions where no lightning object has been observed.

Dark matter also represents a solution for structure formation after the inflation period, when density fluctuations have been created, while background density was diluted because of Universe's expansion. If the perturbation density of a certain region of space exceeds a critical overdensity relative to the background, that region starts to collapse, giving rise to a gravitational bound state. In a universe with only ordinary matter, all the anisotropies would be washed out since matter interacts with radiation that was dominant in the early stages, as we saw in the previous section. On the contrary, the scenario of weakly (or absent) interactions between dark matter and radiation can explain structure formation since, in this case, dark matter dominates the gravitational potential, that acts on ordinary matter collapsing it. In fact, the initial anisotropies of dark matter began to grow through a sequence of merging, leading to the formation of dark matter halos and thereby to galaxies formation in their center [40].

The nature of DM is still unknown, astronomical observations suggest that dark matter permeating the galaxies belongs to the *cold* type. The adjective *cold* means that dark matter moves slowly compared to the speed of light, in other words, it can be treated as non-relativistic object. Theoretically, there are many proposals on the particle nature of DM, some candidates are:

- Weakly-interacting massive particles (WIMPs): originally introduced in [41], WIMPs are not included in the Standard Model and they interact at least gravitationally with SM sector. Like particles in the SM, WIMPs candidates are expected to be thermally created in the early stages. Some theories consider also new interactions, weaker than the weak force, that couples WIMPs with SM. Therefore, WIMPs detection is really challenging and currently no particles belonging to this class have been discovered.
- Neutrinos: the experiments on neutrino's oscillations confirmed that the mass of neutrinos is small but not zero, in contrast with SM that fixes at zero their mass, thus the cosmic neutrino background has been considered as candidate for DM. However, there are several problems in considering neutrino as DM candidate. Since neutrinos follow Fermi-Dirac distribution they have a maximum phase-space density, which implies a maximum space density that cannot explain the high dark matter density estimated for dwarf irregular galaxies and dwarf spheroidals galaxies.
- Supersymmetric particles: SM does not accounts for any fundamental relationship between fermions and bosons. Such a relation has been proposed in the field of supersymmetry, where fermions and bosons constitute particles multiplets. The hypothesis is that supersymmetry holds at very high energy, while at low-energy scale it is broken. The Minimal Supersymmetric Standard Model (MSSM) has been proposed as a model of broken supersymmetry, where each fermion of SM has a superpartner that belongs to boson and vice-versa. The soft supersymmetry breaking allows for masses of the superpartner different from their SM counterparts. The most general gauge invariant Lagrangian, including these fields, contains operators that violate both lepton and baryon numbers, leading to proton decay at weak scale. Nevertheless, proton

is a stable particle, thus conservation of R-parity must be imposed. In other words, superpartners must have negative R-parity and must interact in pairs, in this way the ensemble of superpartners must, at least, contains one stable particle that is the dark matter candidate [42].

- Axions-like particles: originally introduced as a feasible solution for the Strong CP problem, as we will see in the next chapter, ALPs are now back in vogue as DM candidates.

The only non-particular proposal concerns

- Primordial black holes (PBHs): PBHs are hypothetical black holes that could have formed in the very early stages of the Universe, in a period when radiation was dominant. The recent detection of gravitational waves from the collaborations LIGO and VIRGO have given credence to this theory.

We remark that, despite an increasing experimental efforts in searching for dark matter, none of the above candidates have been discovered, nor other new particles. Thus, DM remains an open problem of physics both theoretically and experimentally.

### 4.3 Effective Field Theory Approach

The model building procedure requires some preliminary assumptions in order to identify the interaction operators that couple dark matter with particles of the SM. For instance, of particular interest are the interactions of dark matter with photon, given its status as primary messenger of astrophysical and cosmological probes. UV models can generate these interactions at tree-level through extremely small couplings, and are known as milli-charged dark matter [65, 66, 67, 68, 184]. If we assume dark matter to be electrically neutral, the general framework for describing these interactions is via electromagnetic form factors, which couple dark matter directly to the electromagnetic field strength tensor [70, 71, 74]. These are theoretically and experimentally well motivated, and arise in a plethora of models [141, 142, 183]

Heavy mediators that couple SM to dark matter are a popular explanation for the relative weakness of its interactions. Allowing the use of an effective field theory approach to assess the scenario in a fairly model independent way [53, 50, 51, 54, 147]. The effective operators give a good description when the energy scale of the considered processes is well below the masses of the mediating particles, and their interactions respect the low-energy symmetries of the SM. The appropriate choice of such symmetries is a crucial aspect for a consistent EFT description, and ultimately depends on the relevant scales of the calculation at hand. In this chapter we focus on the EFT for electromagnetic form factors, treating them as local, higher-dimensional operators mediated by heavy new physics.

First of all, we must choose the correct symmetry for the low-energy EFT. In fact, to couple the stable gauge singlet of dark matter with photon, there are two viable solutions: the electromagnetic symmetry group, i.e.,  $U(1)_{EM}$ , or the full electroweak symmetry group, namely  $SU(2)_L \times U(1)_Y$ . In the first case, this results in the operators  $O^{\mu\nu} F_{\mu\nu}$  while in the other case in  $O^{\mu\nu} B_{\mu\nu}$ , where  $O^{\mu\nu}$  is a

gauge singlet combination (usually a bilinear) of dark matter fields<sup>6</sup>. As we saw in chapter 1, the hypercharge form factor is a linear combinations of electromagnetic form factors and the corresponding  $Z$  boson operator, weighted by appropriate factors of the sine and cosine of the Weinberg angle. This relation is preserved in the EFT:

$$\begin{aligned} C O^{\mu\nu} B_{\mu\nu} &= C^\gamma O^{\mu\nu} F_{\mu\nu} + C^Z O^{\mu\nu} Z_{\mu\nu}, \\ C^\gamma &= C \cos \theta_w \\ C^Z &= -C \sin \theta_w, \end{aligned} \tag{4.11}$$

where the factors  $C$  denote generic Wilson coefficients. The choice between the two theories is motivated by the observation that we are able to test these models over a wide range of energy scales, even higher than the EW scale, thanks to collider experiments, thus the most appropriate theory is the one with the hypercharge form factor. Furthermore, the dark matter mass itself is a free parameter and determines the relevant scale for thermal freeze-out and indirect detection constraints. Naturally, at energies far below the electroweak scale the  $Z$  boson degree of freedom decouples and the two descriptions are identical. At this low-energy scale, relevant scattering process involving dark matter field might occur, however, the description with the hypercharge form factor still holds.

In literature, the EFT with electromagnetic form factor for dark matter have been studied in direct and indirect detection as well as at colliders even far beyond its validity limit, extending to the TeV range [70, 71, 72, 73, 181, 74, 165, 166, 76, 167, 162, 77, 69, 158, 182, 99, 159]. Nevertheless, it is clear that the appropriate EFT have to involve the hypercharge form factor since the relevant energies can be considerably higher than the electroweak scale.

The employment of a wrong theory leads to an ambiguous treatment of some processes involving dark matter fields, such as the  $\chi\chi \rightarrow W^+W^-$  channel, which was treated with a non-univocal approach by different authors:

- by ignoring it, as the author of ref. [69] did, even if  $\gamma \rightarrow W^+W^-$  is a vertex of SM and must appear in annihilation processes;
- by assuming that the theory and its outcomes were correct, as in ref. [99] where the  $\chi\chi \rightarrow W^+W^-$  channel was employed to identify collider limits in the energy region above 80 GeV, where the electromagnetic form factors predict a large and unphysical growth, which occurs when an EFT is pushed beyond its validity region.

These treatments are in tension with each other and we argue that the issue must be resolved by employing the hypercharge form factors. Involving the operator  $B_{\mu\nu}$ , it alters the phenomenology described in [69], since the largest experimentally observable effects come in the form of resonant features around the  $Z$ -boson mass and additional constraints from  $Z$ -boson invisible decay width can be investigated. The hypercharge form factors also restore the full SM gauge invariance, thus the behavior of  $\chi\chi \rightarrow W^+W^-$  channel appears to be smooth even at high energies, where the  $Z$ -mediated diagrams dominates the process, resulting in a total annihilation cross-section. Ultimately, the most stringent limits usually come from either

---

<sup>6</sup>The stability of dark matter ensures that, otherwise one can couple the dark matter field to neutrinos as in ref. [163, 164].



direct detection or colliders, so modifications of indirect detection limits do not have extreme consequences. Nevertheless, annihilation plays a central role in the relic density calculation, and we will see that the relic line of dark matter depends on the chosen form factor.

## 4.4 Comparing EFTs: Hypercharge vs Electromagnetic

The EFT framework relies on the presence of decoupled, new physics at an arbitrary high-energy scale, identified by  $\Lambda$ , that in the low-energy limit leaves behind the light particles of SM plus a dark matter field. The latter is assumed to be a fermionic singlet that interacts with the photon and the  $Z$  boson through effective interactions, that involve the hypercharge gauge boson. Up to dimension-6, the operators of the EFTs are

$$\mathcal{L}_{\text{Majorana}}^{\chi} = \frac{\mathcal{C}_{\mathcal{A}}}{2\Lambda^2} \bar{\chi} \gamma^{\mu} \gamma^5 \chi \partial^{\nu} B_{\mu\nu}, \quad (4.12)$$

if the dark matter field is understood as a Majorana particle denoted by  $\chi$ , while

$$\begin{aligned} \mathcal{L}_{\text{Dirac}}^{\psi} = & 2\mathcal{L}_{\text{Majorana}}^{\chi \rightarrow \psi} + \frac{\mathcal{C}_{\mathcal{M}}}{2\Lambda} \bar{\psi} \sigma^{\mu\nu} \psi B_{\mu\nu} \\ & + \frac{\mathcal{C}_{el}}{2\Lambda} i \bar{\psi} \sigma^{\mu\nu} \gamma^5 \psi B_{\mu\nu} + \frac{\mathcal{C}_{cr}}{\Lambda^2} \bar{\psi} \gamma^{\mu} \psi \partial^{\nu} B_{\mu\nu}, \end{aligned} \quad (4.13)$$

for a Dirac fermion labeled by  $\psi$ <sup>7</sup>. The  $\mathcal{C}_i$ , with  $i = \{\mathcal{A}, \mathcal{M}, el, cr\}$ , are the dimensionless Wilson coefficients for the dimension-6 anapole moment, the dimension-5 the electric and magnetic dipole moments and the dimension-6 charge radius operator, respectively. In ref. [83, 84], the authors demonstrated that for Majorana particles the only non-zero hypercharge interaction is the anapole moment. The relation of Wilson coefficients to usual electromagnetic form factors, denoted by the ‘ $\gamma$ ’ superscript, can be found through equation (4.11).

We have implemented this effective field theory into `FeynRules` [80] and obtained the model files in the UFO format [81], which will be used in the rest of the analysis<sup>8</sup>.

To highlight the types of interactions and scatterings that the dark matter form factors mediate, figure 4.1 depicts all possible Feynman diagrams for dark matter annihilation into two states of the SM, via a single insertion of the operators in equations (4.12) and (4.13), that is to say at leading order in the EFT expansion.

### 4.4.1 Electromagnetic Form Factors Beyond their Limits

We have introduced the form factor operators and claimed the use of the hypercharge variants to safely explore the phenomenology of an EFT that aims to couple a dark matter candidate with the fields of SM via annihilation channels only. In this section, we will discuss two explicit examples in which the employment of the hypercharge or the electromagnetic operators leads to significant phenomenological consequences; in particular the latter argues for the use of photon-only operators beyond their validity.

<sup>7</sup>Dark matter particle is denoted by  $\chi$  whenever does not need to be specified.

<sup>8</sup>The model files are publicly available at <https://feynrules.irmp.ucl.ac.be/wiki/EWFF4DM>.

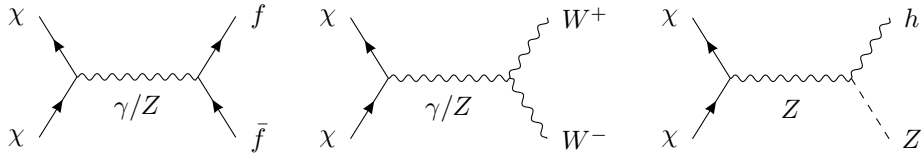


Figure 4.1: Dark matter annihilation diagrams. The coupling to photon and  $Z$  boson are defined in equations (4.12) and (4.13), considering only one vertex insertion of the hypercharge EFT.

### Annihilation of Dark Matter into $W$ Bosons

The first example to analyzed the differences between the two EFT descriptions is the  $\chi\chi \rightarrow W^+W^-$  scattering process. For dark matter masses above  $m_W$ , the  $\chi\chi \rightarrow W^+W^-$  annihilation channel plays an important role in fixing the thermal relic abundance; besides that, a recent phenomenological study [99] has found the vector boson fusion (VBF) process to be a sensitive probe of ‘anapole’ dark matter for the EFT with the electromagnetic form factor, which corresponds to the photon version of the  $\mathcal{C}_A$  operator in equation (4.12). This process embeds the  $W^+W^- \rightarrow \chi\chi$  amplitude, leading to a striking signature of two very forward jets recoiling against the missing energy, reflecting the production of a pair of neutral, stable particles.

Specifically, we made the computations for a pair of Majorana matter candidate that interacts via the anapole moment operator. This form factor describes the interaction between a gauge current, corresponding to the photon or  $B$  fields, with the current of the dark matter candidate. The middle diagram in figure 4.1 accounts for the contribution to this scattering process. It is simplest to first compute the contribution of the photon-only anapole moment, arising from the EFT with the electromagnetic form factor where the mediator of the interaction is the photon and its Wilson coefficient is  $\mathcal{C}_A^\gamma$ . The amplitude of the process, with incoming momenta  $p_1, p_2$  and outgoing momenta  $p_3, p_4$ , is

$$i\mathcal{M}_A^\gamma = -\frac{\mathcal{C}_A^\gamma i e}{\Lambda^2 k^2} \bar{v}(p_2, m_\chi) (k^2 \gamma^\mu \gamma^5 - k^\mu \not{k} \gamma^5) u(p_1, m_\chi) T_\mu^{\rho\sigma} \varepsilon_\rho(p_3) \varepsilon_\sigma^*(p_4), \quad (4.14)$$

where  $k = p_1 + p_2$ ,  $u, v$  and  $\varepsilon$  are the spinors and polarization vectors for  $\chi$  and  $W^\pm$  respectively, and the tensor structure of the  $W^+W^-\gamma$  vertex has been abbreviated by  $T^{\mu\rho\sigma}$ . The high-energy limit ( $m_W^2, m_\chi^2 \ll s < \Lambda^2$ ) of the corresponding squared matrix element (summed and averaged over final and initial polarization states) is

$$|\mathcal{M}_A^\gamma|^2 \sim \frac{2\pi\alpha_{EW}}{9m_W^4} \left( \frac{\mathcal{C}_A^\gamma}{\Lambda^2} \right)^2 s^4 \sin^2\theta + O(s^3), \quad (4.15)$$

where  $s = k^2$  is the square of the center of mass energy,  $\theta$  is the scattering angle and  $\alpha_{EW}$  the EW fine structure constant. The result in equation (4.15) implies a growth in energy of the underlying amplitude of  $|\mathcal{M}_A| \sim s^2$ . Nevertheless, at the amplitudes level we expect that the contribution coming from a dimension-6 operator is proportional, at most, to  $s$ . This is because the only scales present in the high-energy limit are  $\Lambda$  and  $s$ , furthermore  $2 \rightarrow 2$  amplitudes are dimensionless,

meaning that a dimension-6 operator should yield a  $s/\Lambda^2$  behavior. One can realize that the amplitude in equation (4.15) does not admit a clean high-energy limit, since it is diverging for  $m_W \rightarrow 0$ . Using the partial wave analysis, as in ref. [170], the lowest partial wave of the helicity amplitude for the longitudinal  $W$  boson configuration violates unitarity at a centre of mass energy

$$\sqrt{s} \gtrsim 4.3 \sqrt{m_Z \frac{\Lambda}{\sqrt{\mathcal{C}_A^\gamma}}}, \quad (4.16)$$

which implies that unitarity is violated below the cutoff ( $\sqrt{s} \lesssim \Lambda$ ), for

$$\Lambda \gtrsim \frac{1.7 \text{ TeV}}{\sqrt{\mathcal{C}_A^\gamma}}. \quad (4.17)$$

Altogether, these results suggest that the treatment of this amplitude in the EFT with electromagnetic form factor is incomplete. This can be traced back to the fact that the photon-only anapole operator must be strictly used at energy scales where the  $W$  boson field is not a low-energy degree of freedom, i.e., below the EW scale. Instead, using the hypercharge anapole operator in its place yields a result with the correct high-energy behavior for a dimension-6 operator. The annihilation process mediated by  $Z$  boson when combined with the former contribution, as described in equation (4.11), exactly cancels the leading high-energy behavior of equation (4.14), resulting in the amplitude

$$i \mathcal{M}_A = \frac{\mathcal{C}_A}{\Lambda^2} \frac{i e m_Z^2 c_W}{k^2 (k^2 - m_Z^2)} \bar{v}(p_2, m_\chi) (k^2 \gamma^\mu \gamma^5 - k^\mu \not{k} \gamma^5) u(p_1, m_\chi) T_\mu^{\rho\sigma} \varepsilon_\rho(p_3) \varepsilon_\sigma^*(p_4), \quad (4.18)$$

whose matrix element squared, in the high-energy limit, reads

$$|\mathcal{M}_A|^2 \sim \frac{2\pi\alpha_{EW}}{c_W^2} \left( \frac{\mathcal{C}_A}{\Lambda^2} \right)^2 s^2 \sin^2 \theta + O(s). \quad (4.19)$$

Now the partial wave unitarity bounds take a more familiar form

$$\sqrt{s} \gtrsim 18.9 \frac{\Lambda}{\sqrt{\mathcal{C}_A}}, \quad (4.20)$$

from which we get the violation of unitarity below the cutoff only for the implausibly non-perturbative values of  $\mathcal{C}_A \gtrsim 360$ . Therefore, the annihilation process into  $W$  bosons has been partly ‘unitarized’ by using the appropriate EFT description.

In summary, since the relevant energy scale for the scattering process  $\chi\chi \rightarrow W^+W^-$  is around or above the EW scale, the appropriate low-energy symmetry of an EFT approach to new physics is  $SU(2)_L \times U(1)_Y$ . The photon-only anapole contribution to this process manifestly does not respect this symmetry, being only  $U(1)_{EM}$  invariant. This violation of gauge invariance leads to two additional powers of ‘anomalous’ energy growth, contradicting the expectations dictated by dimensional analysis. The behavior described for the electromagnetic anapole moment is also common to other form factor operator contributions to this scattering

and only the corresponding hypercharge form factors are able to restore the gauge invariance and the high-energy limit. The charge radius operator gives identical predictions in this channel, with the same consequences for unitarity violation and resulting bounds on  $\mathcal{C}_{cr}^\gamma$  as equations (4.16) and (4.17) that are relaxed for  $\mathcal{C}_{cr}$  as in equation (4.20). Similar conclusions can be reached about dimension-5 operators. In ref. [56], analogous effects due to non-gauge-invariant descriptions of dark matter contact interactions with quarks and their unitarity-violating effects in mono- $W$  production have been pointed out.

The implications of the different approaches are discussed in section 4.5 in the context of collider phenomenology in section 4.6.1 where the thermal relic abundance will be calculated. In the former, we will see that the above computation leads to the VBF production cross-section of  $\chi\chi$  at the LHC being overestimated by several orders of magnitude while in the latter, the relic abundance predictions when  $m_\chi \gtrsim m_W$  are drastically modified.

### Dark Matter Coupling to $Z$ Boson

The second aspect of the electromagnetic vs hypercharge form factors is related to the fact that, as previously mentioned, the hypercharge operators introduce an additional dark matter coupling, in particular with  $Z$  boson. Since these can be viewed as a ‘completion’ of the photon channel, for all the interesting phenomenological aspects of electromagnetic form factors one generically expects a  $Z$  boson form factor coupling of a similar magnitude. This involves a series of other experimental and theoretical probes of such dark matter models. The first major consequence is a  $Z$ -funnel shape, peaking at  $m_\chi \sim 45$  GeV, in the thermal relic density as a function of  $m_\chi$ , which alters the relationship between direct detection constraints and preferred regions for producing the correct relic density. The second consequence is that, for  $m_\chi < 45$  GeV, the model can now be constrained by invisible  $Z$  decays. Indirect LEP constraints on an additional invisible partial width,  $\Gamma_{inv}$ , place a strong bound of  $\Gamma_{inv} < 2$  MeV which can potentially have a significant impact on the viable parameter space. The partial decay widths of  $Z$  boson into the dark matter field, mediated by hypercharge form factors, are:

$$\begin{aligned}
\Gamma_{\mathcal{A}}^Z &= \frac{\mathcal{C}_{\mathcal{A}}^2 s_W^2 m_Z^2 (m_Z^2 - 4m_\chi^2)^{3/2}}{24\pi\Lambda^4} \\
\Gamma_{cr}^Z &= \frac{\mathcal{C}_{cr}^2 s_W^2 m_Z^2 \sqrt{m_Z^2 - 4m_\psi^2} (m_Z^2 + 2m_\psi^2)}{12\pi\Lambda^4} \\
\Gamma_{el}^Z &= \frac{\mathcal{C}_{el}^2 s_W^2 (m_Z^2 - 4m_\psi^2)^{3/2}}{24\pi\Lambda^2} \\
\Gamma_{\mathcal{M}}^Z &= \frac{\mathcal{C}_{\mathcal{M}}^2 s_W^2 \sqrt{m_Z^2 - 4m_\psi^2} (m_Z^2 + 8m_\psi^2)}{24\pi\Lambda^2}.
\end{aligned} \tag{4.21}$$

This constraint from LEP corresponds to  $\Lambda/C_{\mathcal{A}}^{1/2} \gtrsim 315$  GeV for the anapole moment and  $\Lambda/C_{cr}^{1/2} \gtrsim 370$  GeV for charge radius, while for both dimension-5 interactions, we have  $\Lambda/C_5 \gtrsim 1$  TeV. These are shown together with the other considered constraints in section 4.7.

Variable	Cut	Variable	Cut
$ \eta(j) $	$> 3.0$	$ \Delta\eta $	$> 7.0$
$p_T(j)$	$> 30.0$ GeV	$E_T^{miss}$	$> 175.0$ GeV
$N(j)$	$\geq 2$	$m_{jj}$	$> 500.0$ GeV

Table 4.1: Summary of the kinematic selection criteria imposed in vector boson fusion analysis.

Relying on the consideration of scattering of dark matter with  $W$  boson, one could argue that the phenomenology of dark matter models is properly described by electromagnetic form factors for  $m_\chi < m_W$ ; however, the hypercharge form factors predict a correlation between the couplings mediated by photons and those mediated by  $Z$  bosons, such that their relic density predictions differ from those of the electromagnetic form factors and that additional  $Z$ -decay constraints can be applied to the model for all masses below 45 GeV.

In conclusion, we have shown that the hypercharge form factors are the suitable description for these models of dark matter effective interactions and that, on the contrary, the electromagnetic form factors do not appear to furnish an adequate picture in any range of dark matter masses. The former provides a consistent framework for calculating the dark matter production, annihilation and scattering processes relevant for theoretically and experimentally testing this scenario.

## 4.5 Collider Searches of Dark Matter

In this section we revisit the potential for the LHC to probe the parameter space of dark matter assuming that the EFT with electromagnetic form factors can correctly describe the physics of the processes.

Reversing the annihilation diagrams of figure 4.1 suggests a number of potential production modes of dark matter particles, that can be explored at hadron colliders, including the traditional ‘mono- $X$ ’ searches via the  $q\bar{q}$  initial state and the vector boson fusion mediated by the  $W^+W^-$ -initiated sub-amplitude. Several of these have been studied, in literature, as a probe of the anapole dark matter coupling,  $\mathcal{C}_A^\gamma$  [75, 77, 99]. As argued in section 4.4.1, although the VBF channel has been shown to be particularly sensitive to the electromagnetic anapole form factor, the consistency of the  $W^+W^- \rightarrow \chi\chi$  amplitude requires the reformulation of the electromagnetic EFT in terms of the hypercharge form factor, particularly for dark matter masses above  $m_W$ .

We begin with a reappraisal of the  $W^+W^- \rightarrow \chi\chi$  channel, quantifying the difference in sensitivity with respect to the photon and the hypercharge form factors. The partial ‘unitarization’ of the  $W^+W^- \rightarrow \chi\chi$  sub amplitude that occurs when going from photon to hypercharge form factor results in a drastic loss of sensitivity, to the point that mono-jet searches become the most stringent probes. Subsequently, we proceed with the interpretation of the latest CMS mono-jet search [134], which represents the strongest known limit from collider searches on electroweak form factors for dark matter, as well as projections for the high-luminosity LHC. Our analyses are performed in `Madgraph5_aMC@NLO` [58], where parton-level Monte Carlo sim-

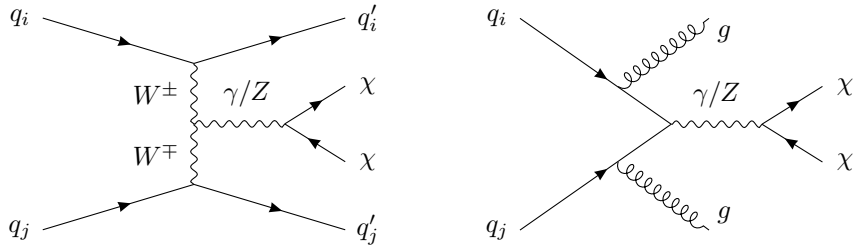


Figure 4.2: Examples of Feynman diagrams for  $pp \rightarrow \chi\chi jj$  mediated by EW form factors for dark matter. On the left the pure-EW contributions, on the right the mixed QCD/EW contributions.

ulations are generated for proton-proton collisions at a center of mass energy of  $\sqrt{s} = 13$  TeV, using the UFO model that we have created. The event samples were analyzed with `MadAnalysis5` [57].

#### 4.5.1 Electromagnetic EFT in Vector Boson Fusion

The dark matter production mode involving vector boson fusion as intermediate state, exhibits a striking signature of missing energy along with a high invariant mass pair of forward jets, well-separated in rapidity. It is particularly well-known for being the most sensitive and direct way to search for invisible Higgs decay modes and has also been used to constrain dark matter production via the Higgs-portal interaction through both on- and off-shell probes [60, 62, 61, 63, 59]. More generally, it offers a unique way to probe the interactions of a light dark sector with the EW gauge bosons via  $W^+W^- \rightarrow \chi\chi$  scattering. In section 4.4.1, our study of the different behavior of this amplitude between the hypercharge and electromagnetic form factors suggests that the two different effective field theories will lead to very different phenomenology in this channel. The latter exhibits a rapid energy growth, beyond the expectations for a dimension-6 operators, that highlights the breakdown of unitarity due to gauge symmetry violation at energies above the  $W$  mass. In this section, we quantify the impact in the change from electromagnetic to hypercharges on the prospects of constraints for dark matter in the VBF processes.

The starting point for our analysis is provided by [99], in which authors identified VBF processes as a very promising constrain to  $\mathcal{C}_A^\gamma$ . Their phenomenological analysis of signal and background distributions identified efficient selection criteria to determine the phase space region in which the VBF signal dominates. These are summarized in table 4.1 and correspond to the familiar requirements of two jets with a large separation in rapidity,  $|\Delta\eta|$ , as well as a large invariant mass  $m_{jj}$  and a significant missing energy. Our main goal is to quantify the difference between the limits outlined for the electromagnetic and hypercharge versions of each operator. Therefore, we replicate a simple version of the kinematical analysis, taking into account the dominant source of SM background, namely  $Z + \text{jets}$  with the  $Z$  boson decaying into neutrinos.

At tree-level, the signal process  $pp \rightarrow \chi\chi jj$  has two contributions of different coupling order, shown in figure 4.2. The first one is the pure-EW contribution,

arising at  $O(\alpha_{EW}^3)$ , which includes the ‘true’ VBF topology, and represents the target of this analysis. The second contribution, arising at  $O(\alpha_S^2\alpha_{EW})$  describes two QCD emissions from the underlying Drell-Yan-like production of the  $\chi\chi$  final state. We noticed that, before applying VBF selection criteria, the total cross-section of the latter process is much larger compared to that of the former. Once the tight selection of table 4.1 are imposed, in the electromagnetic anapole case the signal rate is dominated by vector boson fusion topology; however, this is no longer true for the hypercharge case.

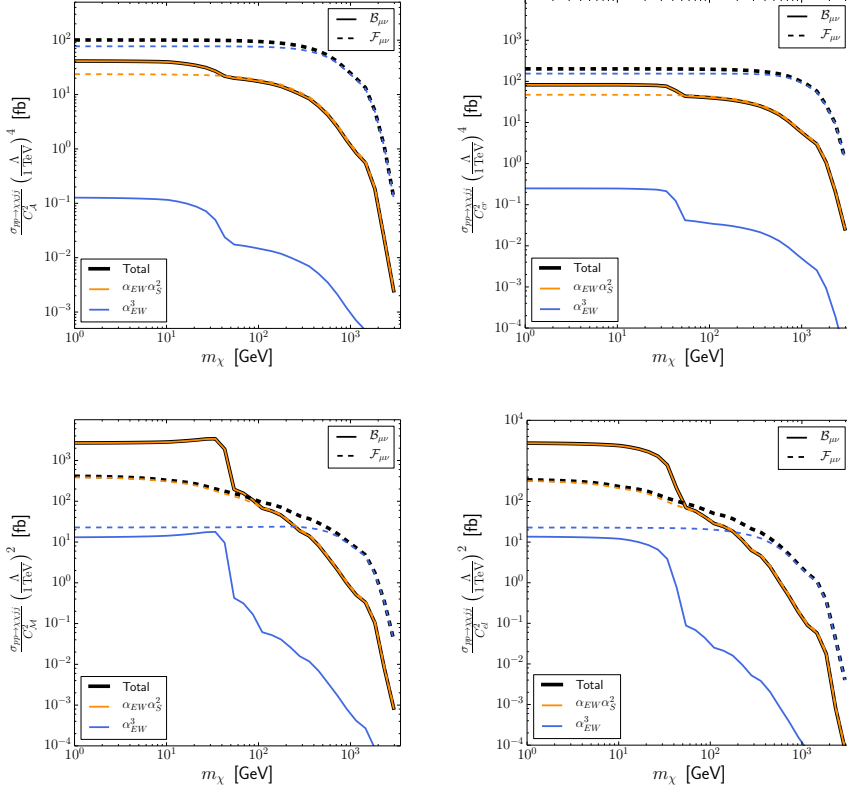


Figure 4.3: The  $pp \rightarrow \chi\chi jj$  cross-sections predicted by the hypercharge (solid line) and electromagnetic versions (dashed line) form factors. The anapole moment in top left panel, the charge radius in top right, the magnetic dipole moment in bottom left and the electric dipole moment in bottom right. The mixed QCD/EW contribution is represented in orange, pure-EW contribution in blue and total process in black. The rates are obtained for  $C_i = 1$  and  $\Lambda = 1$  TeV.

The two upper panels of figure 4.3 depict the cross-sections of hypercharge and electromagnetic dimension-6 operators, for the two separate contributions (the orange line for mixed QCD/EW contribution and the blue line for the pure-EW contribution) and their sum (the black line) as a function of dark matter mass. The cross-sections are estimated before VBF cuts were applied, with the only requirement of a di-jet invariant mass of 100 GeV, to avoid on-shell vector bosons

contributing two jets through their hadronic decays. We find that in the electromagnetic case the VBF contribution and the QCD-emission topology have roughly the same magnitude. On the contrary, in the hypercharge case the mixed QCD/EW contribution dominates the inclusive cross-section. Furthermore, in all hypercharge cases, the cross-section exhibits a feature at 45 GeV, coming from the newly-present on-shell  $Z \rightarrow \chi\chi$  contribution. The plots, especially in the hypercharge case, show that the mixed QCD/EW contribution, which is approximately three orders of magnitude greater than the pure-EW contribution, can no longer be correctly neglected in the determination of the sensitivity even though it comes from a different type of process compared to the one originally being targeted. In the lower panels of figure 4.3, we show the same plot for cross-sections involving dimension-5 operators. In this case, the purely VBF contribution is suppressed even for the electromagnetic form factors. The two contributions have comparable magnitudes only in the limit of large dark matter masses.

After the stringent VBF selection, we find that for low values of dark matter masses, the signal rate is almost equally divided between the pure-EW and mixed QCD/EW contributions. Conversely, as dark matter mass increases, the latter comes to completely dominate the signal cross-section.

For the purpose of estimate the sensitivity, we performed a cut-and-count analysis assuming an integrated luminosity of  $3000 \text{ fb}^{-1}$  collected at the LHC. We endorsed the following definition of signal significance

$$z = \frac{s}{\sqrt{s + b + (b/4)^2}},$$

where  $s$  and  $b$  denote the number of signal and background events in the signal region, respectively. The measure includes a 25% relative systematic uncertainty on the background expectation, which is motivated in ref. [99] as being typical for LHC in vector boson fusion searches. The critical value,  $z = 2$  is used to determine the 95% confidence level (C.L.) exclusion limit of a given operator in the scale  $\Lambda$  divided by the appropriate power of the Wilson coefficient.

The limits plotted in figure 4.4, quantify the drastic loss in sensitivity for all the hypercharge form factors. Note that one of the major difference between our analysis and that of [99] is related to the fact that we do not perform a binned-likelihood fit of the di-jet invariant mass distribution after the initial VBF selection cuts. While this is expected to somewhat improve the overall sensitivity, our main concern here is the difference between the electromagnetic and hypercharge form factors, as well as the fact that the loss in sensitivity defeats the justification for considering this channel.

At TeV scale, the constraints for dimension-6 operators are reduced by an order of magnitude, while for dimension-5 case, the loss is about a factor of 3 below  $m_Z/2$  and again an order of magnitude above. We found that the drop in cross-section for the pure EW contribution is compounded by a loss in efficiency of the extreme VBF selection employed in this analysis, which on the contrary was optimized for dimension-6 operators for electromagnetic form factors, leading to a further worsening of prospects for this particular set of cuts. Therefore, the obtained sensitivity is not likely to be optimal for the hypercharge operators. Nevertheless, given the quartic(quadratic) dependence of the dimension-6(5) signal cross-section on the cutoff scale  $\Lambda$ , it is extremely unrealistic that an optimization of signal to back-



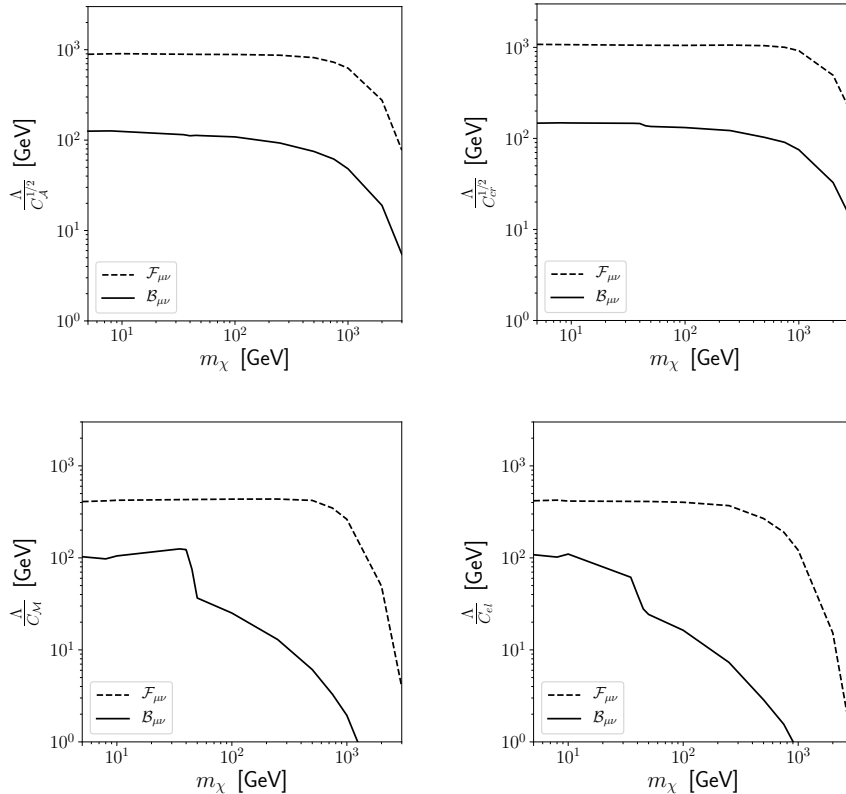


Figure 4.4: Vector boson fusion constraints for the electromagnetic (black dashed) and hypercharge (black solid) form factors. The anapole moment in top left panel, the charge radius in top right, the magnetic dipole moment in bottom left and the electric dipole moment in bottom right.

ground would gain the orders of magnitude needed to recover comparable sensitivity. Finally, relatively weak constraints also mean that the validity of the effective description is more likely to break down, considering the typical energy scales involved in vector boson fusion processes at the LHC. For this reason, we have not considered this option, but rather alternative options for collider constraints on these scenarios.

A remarkably observation is that, in contrast with pure-EW contribution to  $\chi\chi + 2j$ , the mixed QCD/EW cross-section is largely unaffected by the switch from electromagnetic to hypercharge form factors. This is because the underlying new physics process is  $q\bar{q} \rightarrow \chi\chi$ , as opposed to  $W^+W^- \rightarrow \chi\chi$  in the EW process, see figure 4.2. In the case of dimension-6 form factors, the two considered operators can be removed by the photon/hypercharge gauge field equations of motion, or the appropriate redefinition of fields

$$\partial^\nu F_{\mu\nu} = eJ_\mu^{\text{EM}} \quad \partial^\rho B_{\rho\mu} = eJ_\mu^Y, \quad (4.22)$$

where  $J_\mu^{\text{EM}}$  and  $J_\mu^Y$  are the electromagnetic and hypercharge currents, respectively.

These consist mostly of fermion bilinears, in other words both types of operators have a component that can be described by a linear combination of  $q\bar{q}\chi\chi$  contact interactions. These four-fermion operators prompt the mixed QCD/EW process, such that the electromagnetic and hypercharge operators are expected to have similar predictions up to  $O(1)$  factors of ratios of linear combinations of gauge charges and quark-antiquark parton luminosities.

Operators of dimension-5 cannot be eliminated by equations of motion, therefore they can only be understood as momentum dependent interactions between neutral gauge fields and a pair of dark matter particles. Once again, in this case we do not expect a significant difference when switching from electromagnetic to hypercharge form factor, apart from the observed additional on-shell  $Z$  component of the cross-section in  $q\bar{q} \rightarrow \chi\chi$  scattering. The reason why the  $W^+W^- \rightarrow \chi\chi$  channel is so suppressed is that hypercharge form factors partly unitarize this scattering process. Moreover, even for electromagnetic form factors of dimension-5 the vector boson fusion channel is not particularly effective, and even more for their hypercharge counterparts.

In the case of hypercharge form factors, the clear dominance of the  $q\bar{q} \rightarrow \chi\chi$  scattering lead us to the conclusion that this set of interactions is most likely to be better constrained by processes that explicitly target this amplitude, the most obvious of which is the well-known mono- $X$  channel.

## 4.5.2 The Latest on the Mono-jet Signature

The most rudimentary collider searches, which do not have explosive repercussions of gauge violation, are likely to be the most promising. Naturally, the mono-jet searches have been widely studied in the context of the effective operators, see [75] for the anapole interaction and [173, 177, 178, 174, 51, 179, 180, 150, 175, 149, 148, 176, 147] for more generic dark matter EFT research. In this section, we provide an update of these bounds using the results of the most recent CMS analysis [134] with a luminosity of  $35.9 \text{ fb}^{-1}$  as well as a projection into the high-luminosity LHC. As previously argued, unlike with VBF processes, the growth of off-shell  $\gamma/Z$  does not play a key role in either the electromagnetic or EW form factors, leading to similar limits for both operator types. Nevertheless, the discussion up to this point should have already convinced the reader that the interactions with the  $B$  field are the only ones that are physically significant, and so we present only these results.

The selection criteria of the CMS analysis on the single jet are,  $p_{jet}^T > 250 \text{ GeV}$  and  $|\eta| < 2.5$ . The missing transverse energy distribution  $p_T^{\text{miss}}$ , equal to the jet  $p_T$  at leading order, is then used to constrain the production of invisible particles produced in association with a single jet or a boosted, hadronic vector boson. For the purpose of calculate the current and future limits we used the binned  $\chi^2$  statistic,

$$\chi^2 \equiv (\mathbf{n}_{\text{exp}} + \kappa \mathbf{n}_{\text{sig}} - \mathbf{n}_{\text{obs}}) \cdot \mathbf{V}^{-1} \cdot (\mathbf{n}_{\text{exp}} + \kappa \mathbf{n}_{\text{sig}} - \mathbf{n}_{\text{obs}}), \quad (4.23)$$

comparing data ( $\mathbf{n}_{\text{obs}}$ ) with the expected distribution of SM background reported by the analysis ( $\mathbf{n}_{\text{exp}}$ ), incorporating the predicted shape of the dark matter signal contribution ( $\mathbf{n}_{\text{sig}}$ ). The new physics interaction is labeled by  $\kappa = (c/\Lambda^2)^2$  and  $\kappa = (c/\Lambda)^2$  for dimension-6 and dimension-5 interactions respectively, and the covariance matrix for data  $\mathbf{V}$  includes the reported statistical and systematic uncertainties for the  $p_T^{\text{miss}}$  distribution and their correlations. The shape of the signal

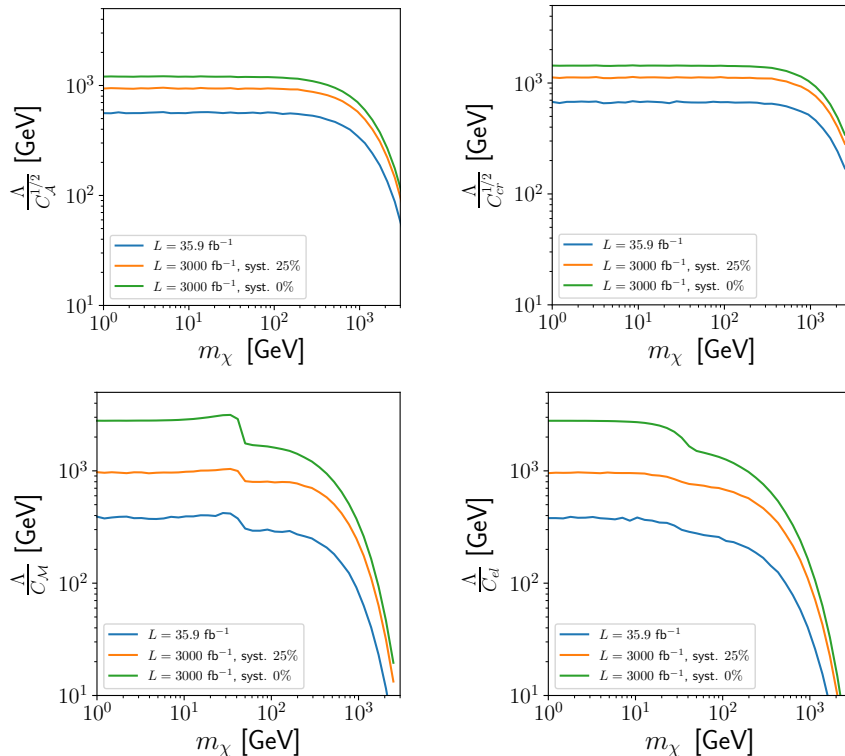


Figure 4.5: The current mono-jet LHC constraint (blue) and projected high luminosity LHC reach with 25% (orange) and 0% (green) systematic uncertainty. The anapole moment in top left panel, the charge radius in top right, the magnetic dipole moment in bottom left and the electric dipole moment in bottom right.

distribution depends only on dark matter mass since the coupling strength, called  $\kappa$ , can be factorized out from the process. Since the observables linearly depend on the parameter of interest, the  $\Delta\chi^2$  can be written as

$$\Delta\chi^2(\kappa) = (\kappa - \kappa_{min}) \cdot \mathbf{F} \cdot (\kappa - \kappa_{min}), \quad (4.24)$$

where  $\kappa_{min}$  is the value of  $\kappa$  that minimizes  $\chi^2$  and  $\mathbf{F}$  is the Fisher information matrix that encodes the shape of the likelihood in  $\kappa$  around its maximum for a given  $m_\chi$ . It depends on the normalized signal for each value of dark matter mass and the covariance matrix  $\mathbf{V}$ . Imposing the critical value of  $\Delta\chi^2 = 3.84$ , we derived through this form the upper limits on  $\kappa$ .

The limits depicted in figure 4.5 provide the most update results for dark matter candidate that couples to the fields of SM through hypercharge form factors of dimension-6 and dimension-5. They are within an order of magnitude of each other, with charge radius interaction reaching the strongest limit. The constraints outlined for dimension-6 form factors start to decrease around  $m_\chi \sim 1$  TeV, while for dimension-5 they already degrade at  $m_\chi \sim 300$  GeV. The reason for this lies in the fact that the dimension-6 operators grow faster with energy and populate

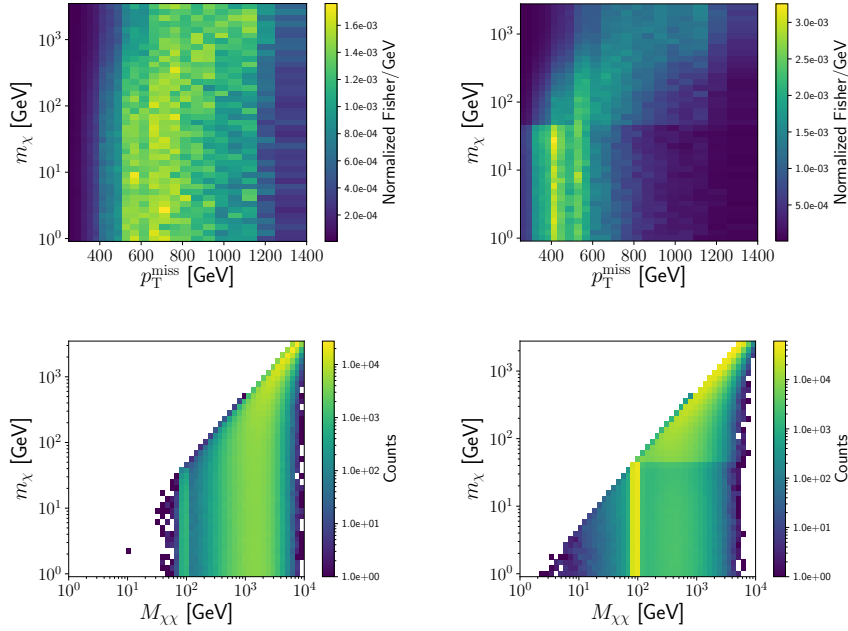


Figure 4.6: 2D heatmap showing how Fisher information per GeV is distributed over the  $p_T^{\text{miss}}$ . The Fisher information is normalized to 1 for each value of  $m_\chi$ . The anapole moment in top left panel, the charge radius in top right panel. In lower panels (anapole moment on the left and charge radius on the right) we plotted the invariant mass bins of the mono-jet search.

more easily the high- $p_T$  bins of the distribution, where systematic uncertainties in the background expectations are less important. In the same plot we also show the projections for  $3 \text{ ab}^{-1}$  of LHC data, assuming either reduced (25%) or no (0%) systematic uncertainties. The former is considered a reasonable expectation, considering the improvements in theoretical and experimental methods over the next 15 years. High-energy bins are also less sensitive to variations in the systematic errors of the background. Therefore, for dimension-5 operators, the expected sensitivities are much more sensitive to variations in the assumed systematic uncertainties. This picture is highlighted by the top row in figure 4.6, which shows how the Fisher information, and therefore the constraining power, is distributed over bins as a function of  $m_\chi$ . This visualization is only possible without including the correlations between uncertainties of different bins, which has an overall small effect on our limits. One can notice a clear bias for lower  $p_T$  for dimension-5 form factors, particularly at  $m_\chi$  below the  $m_Z/2$ .

A crucial aspect that must be considered when dealing with collider data to identify the limits for an EFT is whether the energy, at which we are working, is sufficiently below the new physics scale  $\Lambda$ . The subtleties associated with this aspect have been examined [173, 51, 172, 49, 135, 55] and have led to the adoption of simplified models [136, 160, 171]. Since the EFT approach does not predict, ‘*a priori*’, the values of the Wilson coefficients,  $\mathcal{C}$ , and constraints apply to the

combination  $\mathcal{C}/\Lambda^n$ , one is technically safe from such worries up to a point. It is only when matching these operators with the UV underlying theory that care must be taken. An approximate version of the argument would take the highest bin value, used in the analysis, and require  $\Lambda > p_T^{\text{max}}$ . Therefore limits, such as

$$C/\Lambda^n < \text{limit}, \quad (4.25)$$

can be recast as a lower bound on the Wilson coefficient that admits a valid interpretation

$$C_j > \left( \frac{\text{max bin}}{\text{limit}} \right)^2 \quad \text{and} \quad C_j > \left( \frac{\text{max bin}}{\text{limit}} \right), \quad (4.26)$$

for dimension-6 and dimension-5 form factors, respectively. Taking the maximum bin of 1.4 TeV, it returns a minimum  $C \sim O(1)$ . However, looking at figure 4.6 we realize that most of the information belongs to the lower energy bins, which might give more space for lower values of  $C$  and  $\Lambda$  to be consistent with these results.

In the light of the above, the  $p_T^{\text{miss}}$  does not represent the only energy scale of the process that can be used to examine its validity. The  $\chi\chi$  invariant mass, although not observable, is presumably a more accurate representation of the energy being probed, given that can be identified with the momentum flow through the effective vertex. One would roughly associate this quantity with  $2m_\chi$ , since particle pair production are inclined to occur close to the kinematic threshold. Nevertheless, for dark matter masses below a few hundred GeV, the high-energy of the LHC collisions coupled with the valence quark PDF in the initial state and the energy dependence of the interactions bias this quantity to much higher-than-expected values. The bottom row of figure 4.6 exhibits the distribution of invariant mass,  $M_{\chi\chi}$ , for different values of  $m_\chi$ . We found that for dimension-6 operators and dark matter masses up to 500 GeV, which is the expected that restores  $m_{\chi\chi} \sim 2m_\chi$ , many signal events populate the invariant masses around 1 TeV. For dimension-5, the dominant value for  $M_{\chi\chi}$  is  $\sim m_Z$  when  $m_\chi \lesssim 45$  GeV, above which the behavior is similar to dimension-6. This is consistent with our previous analysis from the Fisher information in the case of low dark matter masses, but requires caution in interpreting the limits when  $m_\chi$  reaches  $O(\text{TeV})$  and beyond; for instance, using equation 4.26 with the aforementioned estimates of  $m_{\chi\chi}$ , yields minimum Wilson coefficients of around  $C_5 \gtrsim 0.03$  for the dimension-5 operators in the low mass case, when  $m_\chi < 45$  GeV. For the dimension-6 operators, the higher typical scale leads to  $C_6 \gtrsim 1$  for  $m_\chi < 1$  TeV, above which the limits are significantly weakened anyway. Overall, the sensitivity of the collider lends itself to interpretations in relatively strongly coupled scenarios and would not be sufficient to allow for loop-induced Wilson coefficients, as is often the case for EW form factors induced by weakly coupled UV completions.

## 4.6 DM Phenomenology in hypercharge EFT

In this section we present the dark matter phenomenology of the hypercharge EFT theories. We show the interplay among the most constraining direct and indirect searches for dark matter and discuss the prospects for detection by estimating the sensitivity of future probes to the model parameter space.

### 4.6.1 Dark Matter Production

A fundamental issue that must be addressed in any model describing dark matter concerns its formation in the primordial stages of the Universe. In our analysis, we assume that this is achieved via the standard thermal freeze-out mechanism. Initially, the interactions between the dark matter and the particles of SM were effective enough to keep it in thermal equilibrium with SM plasma. Subsequently, when the expansion of the Universe dilutes dark matter enough, annihilations become ineffective and the dark matter freezes out with a relic density  $\Omega_\chi$ . The proportionality between relic density and the cross section is

$$\Omega_\chi h^2 \propto \frac{1}{\langle \sigma_{\text{ann}} v \rangle}, \quad (4.27)$$

where  $\langle \sigma_{\text{ann}} v \rangle$  is the thermally averaged annihilation cross-section evaluated at the freeze-out temperature.

Dark matter annihilation into particles of SM is described differently between the two considered EFT models, referring back to figure 4.1: in the hypercharge case  $\chi\chi \rightarrow \text{SM SM}$  processes are also mediated by the  $Z$  boson in  $s$ -channel, whose contribution can potentially be resonant, while this is not the case for the electromagnetic form factors. In figure 4.7, we show the annihilation cross-section into various final states composed by particles of SM as a function of the center-of-mass energy ( $\sqrt{s}/2$ ). In this case, the analysis has been conducted for the charge radius operator; however, qualitatively the picture is similar for all the other form factors. The first astonishing difference between gauge invariant and violating cases, is the  $Z$ -funnel shape that appears when we consider the coupling with  $B$  field, leading to the conclusions: (i) the use of the photon-only channel is not accurate already at energies around 15 GeV, (ii) the  $Z$  resonance dominates  $\langle \sigma_{\text{ann}} v \rangle$  roughly in the range between 15 and 60 GeV and includes the  $\chi\chi \rightarrow \nu_l \nu_l$  process with a similar relevance to annihilation into quarks, while this channel is not present in the case of the electromagnetic form factors. The second deviation between the EFT models for dark matter is found above the  $Z$ -funnel, where the hypercharge  $\langle \sigma_{\text{ann}} v \rangle$  returns a proper energy dependence ( $\propto s$ ), while the electromagnetic operator shows an annihilation cross-section growing in energy with a gradient greater than  $s$ , as previously discussed in section 4.4.1. At high energies, the annihilation channel is dominated by fermionic final states for the hypercharge form factors; on the contrary, in the electromagnetic case the predominant process is that with  $W^+W^-$  as final state. The discrepancies highlighted between the two EFT models lead to different suitable parameter space regions when searching for relic abundance. For a given dark matter mass, we compute the effective coupling that provides the correct relic density by making use of MadDM 3.0 [79] and matching the value of  $\Omega_\chi h^2$  to that measured by the Planck satellite [78].

In the left panel of figure 4.8 we plot the results for the dimension-6 interactions. The results confirm figure 4.7 to the extent that electromagnetic and hypercharge interactions start to diverge around  $m_\chi \sim 30$  GeV for the whole  $Z$ -funnel and that above  $m_\chi \sim 90$  GeV the electromagnetic anapole has a steeper gradient. Given that for dark matter masses the generic thermal relic bound, calculated by using partial wave analysis for a generic  $s$ -wave cross-section [82], is 100 TeV, we plotted the result up to this value. Nevertheless, all anapole interactions are  $p$ -wave hence

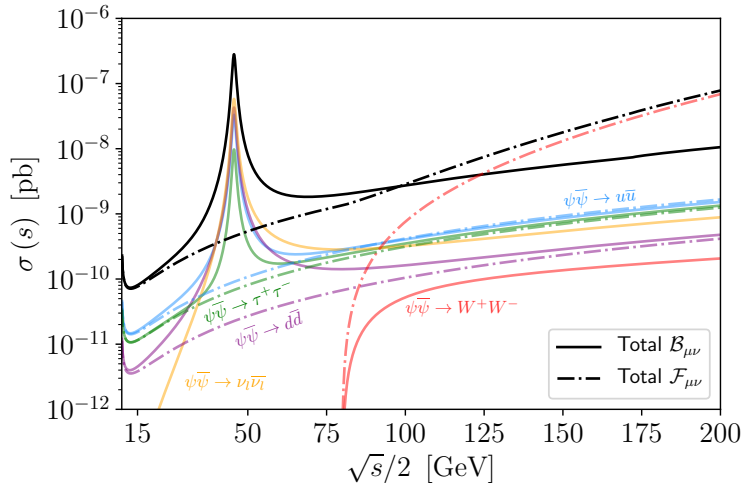


Figure 4.7: Annihilation cross-sections as a function of the center-of-mass energy for charge radius coupling. Solid lines stand for hypercharge form factor, while dotted lines for electromagnetic form factor. Different contributions are shown in different color as labeled. The dark matter mass is set to  $m_\chi = 10$  GeV, the Wilson coefficient is  $\mathcal{C}_{cr} = 1.0$  and  $\Lambda = 10$  TeV.

partial wave unitarity might break down at higher dark matter masses with respect to the case of  $s$ -wave unitarity, see *e.g.* [145].

We also consider naive perturbativity limits on the parameter space by taking,

$$\frac{\mathcal{C}_6}{\Lambda^2} s \leq 4\pi \quad \text{and} \quad \frac{\mathcal{C}_5}{\Lambda} \sqrt{s} \leq 4\pi, \quad (4.28)$$

for dimension-6 and dimension-5 vertices respectively. For the annihilation process we set  $\sqrt{s} \sim 2m_\chi$  to get the relations,

$$\frac{m_\chi}{\sqrt{\pi}} \leq \frac{\Lambda}{\sqrt{\mathcal{C}_6}} \quad \text{and} \quad \frac{m_\chi}{2\pi} \leq \frac{\Lambda}{\mathcal{C}_5}. \quad (4.29)$$

These constraints (depicted as grey areas in figure 4.8) are a loose statement on whether it makes sense to treat the effective couplings perturbatively. Beyond these regions, one may worry that loop contributions could be comparable to the tree-level ones that we have computed. They are independent of the scale of new physics  $\Lambda$  since one can always compensate any restriction by varying the Wilson coefficients  $\mathcal{C}_j$ . If one is prepared to make more specific assumptions, *i.e.*, to understand how this actual term relates to a complete UV model, different constraints can be derived.

The left panel in figure figure 4.8 highlights that for relic density obtained in the hypercharge EFTs, the perturbative description of the scattering starts to break down around a dark matter mass of  $\sim 6$  TeV for the anapole moment and of  $\sim 20$  TeV for the charge radius.

For both dimension-6 operators, the annihilation processes in the  $s$ -channel, shown in figure 4.1, are the only ones available. It is tempting to also consider  $t$ -

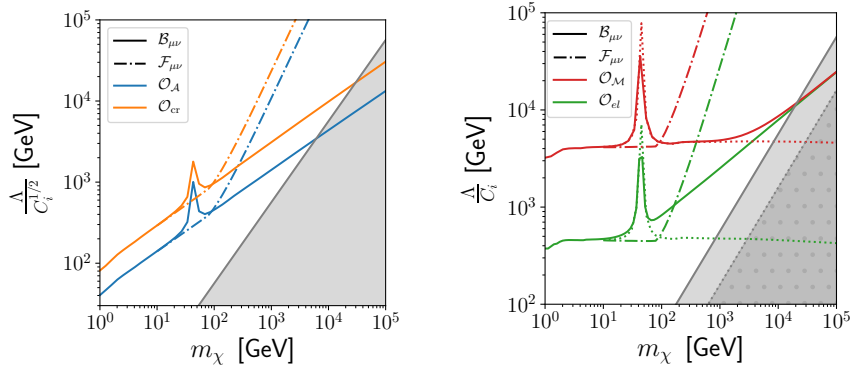


Figure 4.8: Values of  $\Lambda/\sqrt{\mathcal{C}_i}$  that yield to the estimated relic density abundance (colored lines) as a function of dark matter masses. The plot on the left is for dimension-6 operators (blue for the anapole moment and orange for the charge radius), while the plot on the right is for dimension-5 operators (red for the magnetic moment and green for the electric dipole moment). Solid and dot-dashed lines stand for hypercharge and electromagnetic form factors, respectively. Dotted lines are for hypercharge interactions that do not include double insertion contributions, i.e., the pure dimension-5. The grey region denotes the breakdown of perturbativity for the EFT theories: the solid grey region for dimension-6 (in both panels), the dotted region for a single insertion of dimension-5 operators.

channel and  $u$ -channel processes with two effective vertices, as shown in figure 4.9. These annihilation processes give rise to di-photon or  $\gamma Z$  final states, which are prominent for dark matter line searches [113, 112], as well as the  $ZZ$  final state, which contributes, for instance, to continuum gamma ray searches. From the EFT perspective, however, care should be taken when considering processes at higher orders in Wilson coefficients. In fact, higher order contributions to a process with multiple insertions of low-dimensional operators can be of the same order in  $\Lambda^{-n}$  as a single insertion of high-dimensional operators, although these are typically neglected. It could also happen that a multiple insertion diagram can be fully described in terms of a single insertion of a high-dimensional operator. In fact, multiple insertions of an EFT operator in, e.g., loop calculations require the theory to be renormalized to higher orders in  $\Lambda^{-n}$ . These effects are truly of higher dimension and be considered as operators of a higher dimension.

From equation (4.13), it appears the annihilation processes  $\chi\chi \rightarrow \gamma\gamma, \gamma Z, ZZ$  can only be described by double insertions of dimension-5 operators, while there is not a corresponding single insertion of dimension-6 operator that mediates the same interactions. Therefore, up to  $\Lambda^{-2}$ , these processes are described only by the square of the dimension-5 couplings. New operator contributions only arise starting at dimension-7, in the form of so-called Rayleigh operators,  $\chi\chi F^{\mu\nu} F_{\mu\nu}$  [165, 166, 168]. In agreement with the above, it is justified to include ‘double insertions’ as part of the model, i.e., to consider the magnetic and electric dipoles up to dimension-6, when describing the new physics contributions to dark matter annihilation onto neutral gauge bosons.



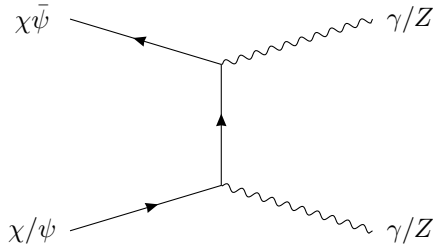


Figure 4.9: Annihilation channels of dimension-6 or dimension-8. They occur through multiple insertion of effective vertices. Possible final states are  $\gamma\gamma$ ,  $\gamma Z$  and  $ZZ$ .

In the following of the analysis we will consider the phenomenology of the pure dimension-5 operators and their double insertions separately, to study the parameter regions in which each type of contribution is relevant. In the right panel of figure 4.8, we plotted the correct relic abundance lines for both the magnetic and electric dipole interactions (red and green respectively). We show the curves for both the electromagnetic (black dot-dashed) and hypercharge field strength tensors (black dotted) this time including the double insertion processes (black solid). The phenomenology is rather similar to the case of the dimension-6 operators, except that for the hypercharge dimension-5 operators the value of  $\Lambda/\mathcal{C}_j$  becomes flat at large dark matter masses. In fact, dimension-5 operators do not grow with energy while dimension-6 operators grow  $\propto s$ . Therefore at large dark matter masses, above  $10^3$  GeV or 100 GeV for the magnetic and electric vertex respectively, the processes described by a double insertion of dimension-6 double start to dominate the hypercharge EFT model. The additional diagrams grow with energy and the relic lines exhibit a slope similar to anapole and charge radius cases. Given their respective energy growths, the single and double insertion scenarios have different perturbativity bounds depicted by the grey regions. As expected, dimension-6 bounds cover more the parameter space. In the right panel of figure 4.8, we notice that for the magnetic dipole, including the double insertion processes slightly restrains the viable parameter space for thermal relic: the dark matter mass upper bound due to perturbative unitarity of 30 TeV for dimension-5 operator only becomes 20 TeV for dimension-6 vertices. On the contrary, the parameter space of the electric dipole is enlarged, shifting the upper bound of perturbative unitarity on the dark matter mass from 3 TeV up to 20 TeV.

A crucial aspect of the unphysical growth in the cross-section registered for the photon-only interactions, is that the steep gradient in figure 4.8 makes it appear that the correct relic density can be obtained to arbitrarily high values of  $m_\chi$ . However, this is not realistic since the  $W^+W^-$  scattering cross-section violates unitarity at much lower masses.

As we remarked at the beginning of the section, the computation of the relic density abundance of dark matter relic is based on the thermal freeze-out assumption with the standard cosmological history. In figure 4.8, the region below the black curve denotes under-abundant dark matter, while that above it denotes over-abundant. In the latter case its annihilation cross-section is small and dark matter

decouples too early from the thermal bath with a large abundance; the later it decouples the more dark matter undergoes matter suppression.

In the next section we will assume that the dark matter candidate accounts for all dark matter regardless of abundance resulting from thermal freeze-out. In particular, this assumption concerns the local dark matter densities that enter the fluxes computations for indirect and direct detection experiments. For instance, in the case of under-abundant dark matter this scenario could be realized by additional non-thermal contributions to dark matter production, such as the late gravitino decay in supersymmetric models, which is a popular mechanism to augment the neutralino relic density and bring it to Planck measured value [124]. Over-abundant dark matter could be accommodated by a non-standard cosmological history which for instance modifies the expansion rate of the Universe, see ref. [143], or UV completion of phenomenological models could provide more efficient annihilations at early times, ref. [125] and references therein.

Furthermore, there exist alternative scenarios that can reproduce the correct relic density, such as the freeze-in mechanism [122, 121] and forbidden dark matter [123], which might highlight different regions of the EFT model parameter space. Nevertheless, those scenarios typically select dark matter candidates which are fairly light, close or below the GeV mass scale. This region is in great tension with the measurements of the  $Z$  boson invisible decay width for the hypercharge EFT model; however, a throughout analysis of the phenomenology due to the freeze-in mechanism is beyond our research.

#### 4.6.2 Direct Searches

Direct dark matter searches expect to measure the recoil of target nuclei hit by a dark matter particle passing through the underground detectors. The momentum transfer in elastic collision is limited by kinematics and the galactic escape velocity, named  $v_{\text{esc}}$ , in detector frame

$$q_{\text{max}}^2 = 4\mu_{\chi T}^2 v_{\text{esc}}^2, \quad (4.30)$$

where  $\mu_{\chi T}$  is the reduced mass of the incoming dark matter and the target nucleus. The largest value of  $q^2$  is achieved in the large  $m_{\chi}$  limit, with  $v_{\text{esc}} \sim 700 \text{ km s}^{-1}$  [186] and results in  $q \leq 500 \text{ MeV}$ . This value, is well above most of the signal, which instead falls in the range between 1 and 10 MeV. Therefore, results for the electromagnetic moments will be directly applicable to the hypercharge EFT model, since the  $B$  field strength tensor is simply related to both photon and  $Z$  boson as highlighted by equation (4.11). In the following, we briefly review how the non-relativistic operators relevant for direct detection are obtained from the EW EFT operators in equations (4.12) and (4.13).

The computation of direct detection contribution for dimension-5 operators, has to include the scattering amplitude with the full propagator. The interaction vertices that couple quarks with photon and  $Z$  field are

$$\mathcal{L}_{\text{int}} \supset eQ_q \bar{q} A_{\mu} q + \frac{g}{4c_W} \bar{q} \gamma^{\mu} (V_q - A_q \gamma^5) q Z_{\mu}, \quad (4.31)$$

where  $g$  is the EW coupling and  $Q_q$  is the electromagnetic charge. Moreover,  $V_q$  and  $A_q$  are the vector and axial coupling respectively, and they describe the interactions

between quarks and  $Z$  field. According to ref. [94], their parametrization is

$$V_q = 2(-2Q_q s_W^2 + T_q^3) \quad \text{and} \quad A_q = 2T_q^3, \quad (4.32)$$

where  $T_q^3$  is the weak isospin number. Since the pure vector coupling with  $Z$  boson has the same structure as that for photon, it will produce the same responses from nucleons  $O^{\text{DD}}$  as outlined in ref. [97, 98, 64, 69]. However, a fundamental difference is related to the coefficients of such operators, which for the  $Z$  field, have a suppression factor

$$\frac{C_{B\mu\gamma\mu}^{\text{N}}}{C_{A\mu\gamma\mu}^{\text{N}}} = \frac{1}{4m_W^2} \frac{V_N}{Q_N}, \quad (4.33)$$

if the couplings in the Lagrangian, namely equation (4.12) and equation (4.13), are assumed to be the same. The super and sub scripts  $N$  refer nucleon interaction, namely the parameters  $V_N$  and  $Q_N$  are summed values from quark coefficients  $V_q$  and  $Q_q$ , respectively. In reference [185], the author quote the exact value of these parameters. As expected, the axial vector couplings give rise to novel responses compared to the photon case<sup>9</sup>; however, due to the suppression coming from the mediator, the contributions are sub-dominant.

For the electromagnetic EFT, the computations involving dimension-6 operators are simplified since we can make use of the equations of motion

$$\partial^\nu F_{\mu\nu} = eJ_\mu^{\text{EM}} \approx e \sum_{q=u,d,s} Q_q \bar{q}\gamma_\mu q, \quad (4.34)$$

where the approximation is because we are interested in calculating low-energy scattering with nucleons. For  $B$  field, there is a similar expression

$$\partial^\rho B_{\rho\mu} = \frac{1}{2} g' H^\dagger i \overleftrightarrow{D}_\mu H + g' (J_\mu^{\text{EM}} - J_\mu^3), \quad (4.35)$$

where  $J_\mu^3$  is the current  $J_\mu^3 = \sum_i \bar{f}_i^L \gamma^\mu T^3 f_i^L$ ,  $H$  is the Higgs field,  $T^3$  is the weak isospin value of the fermion  $f$  and  $g'$  is the hypercharge coupling. After the EW-symmetry breaking, equation (4.35) becomes

$$\partial^\rho B_{\rho\mu} = \frac{egv^2}{4} Z_\mu + g' (J_\mu^{\text{EM}} - J_\mu^3), \quad (4.36)$$

where  $v$  is the Higgs vacuum expectation value and  $g$  is the weak charge. Using the  $Z$  equation of motion

$$Z_\nu = \frac{e}{s_W} \Pi^{\mu\nu} J_\mu^Z = \frac{e}{s_W} \Pi^{\mu\nu} (J_\mu^3 - s_W^2 J_\mu^{\text{EM}}),$$

where  $\Pi^{\mu\nu}$  is the  $Z$  propagator, and expanding in the large  $m_Z$  limit, at the lowest order the result from the photon field is recovered

$$\partial^\rho B_{\rho\mu} \approx ec_W J_\mu^{\text{EM}} + O\left(\frac{q^2}{m_Z^2}\right),$$

---

<sup>9</sup>In the non-relativistic formalism of [98], these responses are the operators  $O_9$  and  $O_{14}$ .

which is the relevant term at the energy scales of direct detection. Since the effects of interactions mediated by  $Z$  are weaker than that mediated by the photon, the results are equivalent to previous works, in which dark matter interactions in the non-relativistic effective theory basis go like

$$\begin{aligned}
\bar{\chi}i\sigma^{\mu\nu}\gamma^5\chi B_{\mu\nu} &\rightarrow Q_N e \frac{4}{q^2} m_\chi m_N^2 O_{11}^{DD} \\
\bar{\chi}\sigma^{\mu\nu}\chi B_{\mu\nu} &\rightarrow 2em_\chi m_N \left[ \frac{Q_N}{4m_\chi} O_1^{DD} + Q_N m_N \frac{O_5^{DD}}{q^2} \right. \\
&\quad \left. + \frac{g_N}{2m_N} \left( O_4^{DD} - \frac{m_N^2 O_6^{DD}}{q^2} \right) \right] \\
\bar{\chi}\gamma^\mu\chi\partial^\nu B_{\mu\nu} &\rightarrow 4m_\chi m_N e Q_N O_1^{DD} \\
\bar{\chi}\gamma^\mu\gamma^5\chi\partial^\nu B_{\mu\nu} &\rightarrow 4m_\chi m_N e (2Q_N O_8^{DD} - g_N O_9^{DD}),
\end{aligned}$$

where the factors  $Q_N$ ,  $m_N$  and  $g_N$  are the charge, mass and the magnetic moments of the nucleons respectively. In the basis defined above,  $O_1^{DD}$  is the canonical spin-independent interaction which receives a coherent contribution from the nucleons in the target nucleus by way of  $A^2$ , where  $A$  is the atomic number. The same occurs for  $O_{11}^{DD}$  which, however, is also momentum suppressed. Thus, it directly follows that the anapole response will be the weakest.

Making use of the tool called RAPIDD [85], we recast the current exclusion limit by XENON1T [86] as well as future LZ [87, 88] projected sensitivity in terms of the hypercharge EFT model. For the purpose of match with results coming from colliders and indirect searches, we present the 95% C.L. exclusions and projections, as opposed to the direct detection community standard of 90% confident level. XENON1T has the strongest exclusion limit at intermediate and large dark matter masses while LZ will probably be the most sensitive detector in the same mass range, built in the near future. For the XENON1T results, we make use of the prescription given in appendix A of reference [69]. We adopted the same procedure to derive the projected limit for the LZ experiment and for an exposure of 1000 days, as LZ will be a dual phase time projection chamber consisting of 5.6 tons of xenon similar to XENON1T. Our result is in agreement with that obtained in appendix D of [89]. In order to evaluate the sensitivity of direct detection at low dark matter masses, we simulate the SuperCDMS experiment following [108, 109, 110, 107]. In particular, we used the high-voltage design of the experiment, which will be able to access very low threshold energies, thus enabling greater sensitivity to light dark matter.

We have not included any current bounds in the parameter space below  $m_\chi \sim 6$  GeV, which would likely come from CRESST-III [152, 151] or DarkSide-50 [153]. The situation here is more complicated and could even be most constrained through electron recoils. In reference [154, 161], the authors computed the electron recoil bounds for anapole, magnetic and electric moments and shown that for  $m_\chi \sim 1$  GeV, Xenon1T [86] results are the most sensitive. The interplay between electronic and nuclear recoils, as well as the multitude of ongoing experiments, is left to a potential future work.

In figure 4.10, we reported the constraints at 95% C.L. and future reach from direct detection for the hypercharge EFT model. We found that the basic picture

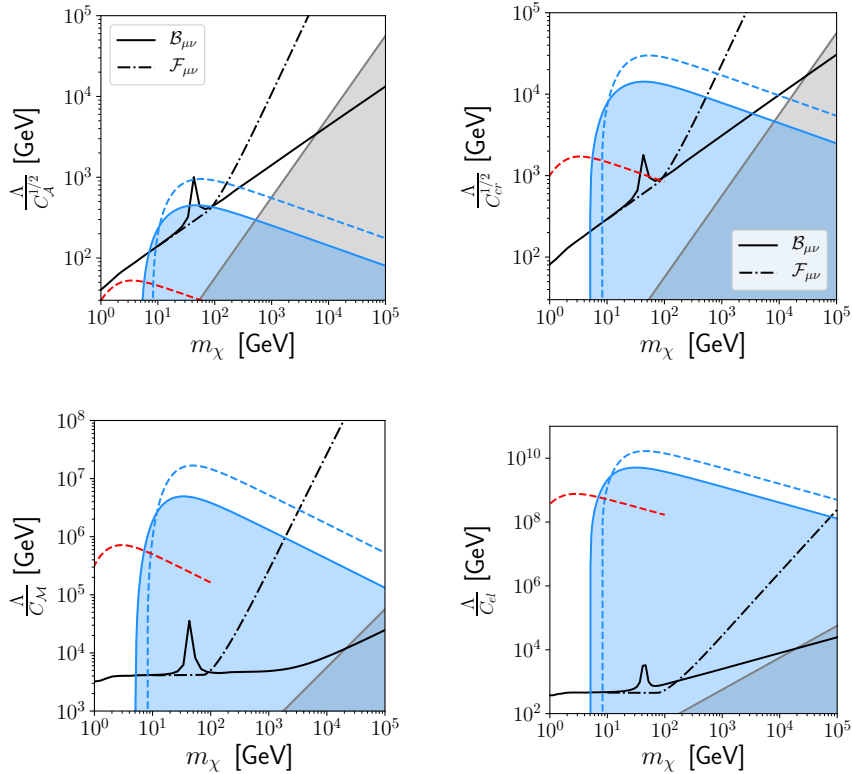


Figure 4.10: Direct detection limits at 95% confidence level (C.L.) on  $\Lambda/c_j$  (or  $\Lambda/c_j^{1/2}$ ) as a function of the dark matter mass  $m_\chi$ , coming from the current XENON1T exclusion limit (**blue**) as well as projected sensitivities of the future LZ experiment (blue dashed) and SuperCDMS (red dashed). The top left panel for the anapole moment, top right panel for charge radius, bottom left panel for magnetic moment and bottom right panel for the electric dipole moment form factors, respectively. Notice that the scale of the y-axis has been altered from figure 4.8 due to the strength of the direct detection limits.

does not change with respect to the case of the photon-only interaction [69] barring a few remarks. The blue shaded region shows that current constraints from XENON1T are able to exclude large regions of viable parameter space. In fact, the black solid lines, that predict the correct dark matter abundance via freeze-out, are completely ruled out for the magnetic and electric dipole moments, as previous works [146] already obtained. Our finding is that even considering the extra dimension-6 contributions, it is not possible to escape constraints.

### 4.6.3 Indirect Searches

Indirect searches of dark matter rely on the annihilation into particles of the Standard Model, which subsequently decay, shower and hadronise to lead to a continuum spectrum of gamma rays, cosmic rays (positrons and antiprotons) and neutrinos,

likewise presented in reference [129]. Alternatively, dark matter can annihilate, as we previously said, into the di-photon or  $\gamma Z$  final state, producing the smoking-gun signature of a sharp gamma-ray line feature at the dark matter mass [126, 127, 128]. In this section, we derive exclusion bounds for our models using the continuum annihilation spectra, including the  $ZZ$  final state, and the  $\gamma\gamma$ ,  $\gamma Z$  line final states. The latter three annihilation channels come from the double insertion diagrams as represented in figure 4.9, with the last two being peculiar to the hypercharge form factors.

All annihilations share a typical energy scale that is fixed by the dark matter mass, as the late time environments that provide the strongest constraints (for example, dwarf spheroidal galaxies, dSPhs, and the Galactic Centre) are much cooler than at the time of freeze-out, being characterized by relative velocities  $v/c$  ranging roughly from  $10^{-5}$  to  $10^{-3}$ . The fact that the annihilation cross-section is either an  $s$ -wave or  $p$ -wave is extremely important to determine the mapping that indirect constraints draw in the parameter space of the hypercharge EFT models. We have analytically calculated the (velocity averaged) annihilation cross-sections for all operators in (4.12) and (4.13) and reported in table A.1, Appendix A.6, their expression obtained in the limit of massless particles of the SM. These expressions are in agreement with reference [69]. As already noted, the anapole moment is  $p$ -wave, hence, we cannot further consider this form factor in this section. The electric dipole moment annihilation into fermions and gauge bosons of SM is suppressed by  $p$ -wave, while the related dimension-6 operator, leading to  $\gamma\gamma$ ,  $\gamma Z$  and  $ZZ$ , are not suppressed and therefore accounted in this analysis. Conversely, the magnetic dipole and the charge radius interactions are  $s$ -wave, meaning that their annihilation strength is unaltered throughout the thermal history of the Universe.

From table A.1, in the high-energy limit operators manifest a hierarchy between the  $f\bar{f}$  and  $W^+W^-(Zh)$  final states, which differs only by factors of their respective hypercharges, as already shown in figure 4.7. This is supported by figure 4.11, which shows, in the left panel, these branching ratios for the charge radius form factor. Nevertheless, all operators (neglecting, at this stage, the double insertions) have qualitatively the same trend. We have included dashed lines for the electromagnetic moment to highlight the need for taking the gauge invariant interaction.

The effect of interpreting indirect detection limits in the context of hypercharge instead of photon-only EFT models is represented for the charge radius interaction on the right panel of figure 4.11: the most constraining bounds for the hypercharge form factors are those identified by Fermi-LAT dSph, while in the case of photon-only operators cosmic-ray antiprotons [102] from AMS 02 originating from  $W^+W^-$  are predominant. It is not surprising, at this stage, that by taking the gauge violating effective interactions, indirect constraints become larger and larger as the mass of the dark matter increases, even surpassing the strong sensitivity of the direct detection constraints, which was set around 500 GeV. In literature [69], it has been claimed that the  $W^-W^+$  final state is sub-dominant, which is not the case for the electromagnetic interaction. Their results, considering final states composed by fermionic particles only are much more in line with the one obtained with a correct treatment of the hypercharge operators, as these final states clearly dominate the annihilation cross-section, while bosonic final states have  $\text{BR} \simeq 10^{-2}$ . The most peculiar aspect is the appearance of both the  $Z$ -funnel region, in figures 4.7 and 4.11, and the presence of more annihilation channels in the case of hypercharge EFT.

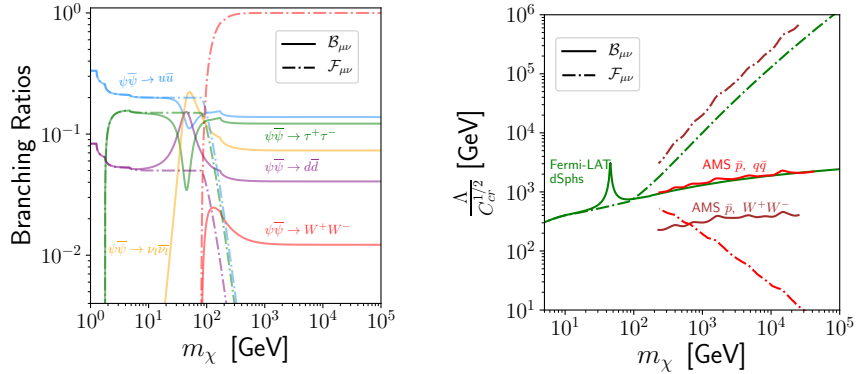


Figure 4.11: On the left, the branching ratios of the velocity averaged annihilation cross-section into all possible final states of SM as a function of the dark matter mass, for the charge radius effective interaction. The line and color scheme is the same as figure 4.7. On the right, the exclusion limits (excluded the region below the curve) at 95% C.L. coming from Fermi-LAT dwarf spheroidal galaxies [79] (Fermi-LAT dSphs) and AMS 02 cosmic ray measurements [102] (AMS  $\bar{p}$ , for the  $q\bar{q}$  and  $W^+W^-$  final states) in the plane  $\Lambda/C_{cr}^{1/2}$  versus the dark matter mass. The results are shown for both the cases of hypercharge (solid) and photon only (dashed) EFT dark matter model (dashed) as labeled.

The monochromatic neutrino channel is relevant for indirect detection, since it is considered a clean astrophysical messenger and its branching ratio is remarkable ( $\sim 0.1$ ) at high energies and dominates in the  $Z$ -funnel region. The inclusion of double insertions of dimension-5 operators, as discussed in section 4.6.1, is both legitimate and correct. This predictably complicates the picture, since, for instance, the branching ratio of a specific annihilation channel no longer depends solely on the mass of dark matter. Now some annihilation processes are proportional to different powers of the effective coupling, namely

$$\frac{\langle\sigma v\rangle_{\gamma\gamma}}{\langle\sigma v\rangle_{f\bar{f}}} \propto \frac{\Lambda^2}{\mathcal{C}_j^2}, \quad (4.37)$$

meaning that bigger couplings lead to the di-photon channel dominating for low values of dark matter mass. In figure 4.12, we reported the results for two specific values of  $\Lambda/C_i$ . The relative branching ratios of  $\gamma\gamma$ ,  $\gamma Z$  and  $ZZ$  are the same in both cases, since predicted by the breaking of the EW symmetry. Nevertheless, the onset of dimension-6 operator is delayed to larger dark matter masses for larger  $\Lambda/C_i$ , as expected from (4.37). Notice that the  $\gamma\gamma$  final state has the largest branching ratio, strictly followed by  $\gamma Z$ , while the  $ZZ$  final state is one order of magnitude lower.

Before going into the details of how the indirect detection constraints delimit the parameter space of the model, we briefly outline what exclusion constraints have been considered in the analysis and how they have been recast for effective moments.

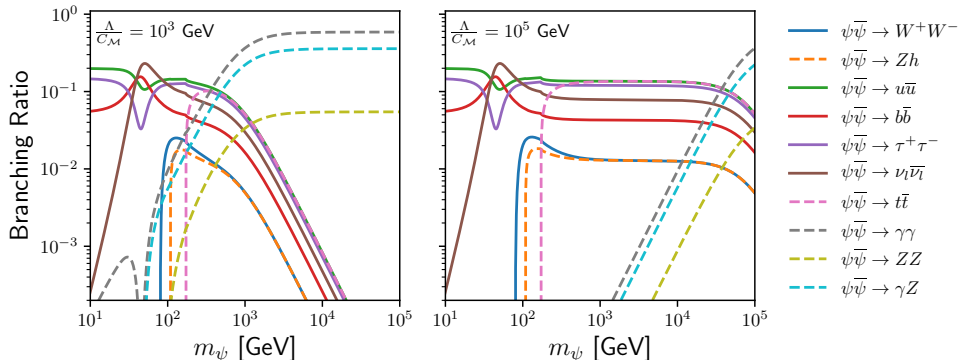


Figure 4.12: On the left, the branching ratios of the velocity averaged annihilation cross-section into all possible final states composed by particles of SM as a function of the dark matter mass, for the magnetic effective interaction with  $\Lambda/\mathcal{C}_{\mathcal{M}} = 10^3$ , including dimension-6 contributions. The line and color scheme is the same as figure 4.7. On the right, the same as left for  $\Lambda/\mathcal{C}_{\mathcal{M}} = 10^5$ .

### Charged Lepton and Quark Final States

We consider the 95% C.L. gamma-ray continuum bounds from Fermi-LAT dSphs and antiproton bounds from AMS 02 (AMS  $\bar{p}$ ).

The dSph Fermi-LAT constraint has been obtained using `MadDM`, which performs a statistical analysis to set the limit given our specific model. For future constraints coming from land and space based telescopes on gamma-ray measurements from dSphs we have considered the Cherenkov Telescope Array (CTA) [103] and the Large Synoptic Survey Telescope (LSST) + Fermi-LAT white paper [104]. For CTA, we obtained a projection by using the sensitivity for the  $\tau^+\tau^-$  annihilation channel shown in reference [103], which is the most constraining for the hypercharge EFT models. The LSST+Fermi-LAT (LSST+LAT) projection assumes that it is accurate to scale the  $b\bar{b}$  projection to other fermionic channels. A more accurate analysis would probably yield better projections, but that is beyond the scope of our analysis. Whenever relevant, we included into the gamma-ray continuum limits the contribution of the  $ZZ$  and  $\gamma Z$  final states (the latter contribution is scaled by 1/2 to take into account the fact that only one  $Z$  boson is emitted).

Antiproton bounds have been obtained from [102], by rescaling each final state with the BR obtained from models. Notice that astrophysical uncertainties are extremely large, and even when profiled out their inclusion makes an envelope that can shift the bound up or down by a factor of approximately four. Nonetheless, these are competitive bounds for dark matter masses larger than 250 GeV.

Finally, we also consider the Planck limits [111] on dark matter annihilating into  $e^+e^-$ , which, at extremely low dark matter masses, are competitive with dSphs bounds. These bounds are due to the annihilations of dark matter that injects electromagnetically interacting particles during the dark ages, which can potentially modify the residual ionisation fraction, enlarge the last scattering surface and modify the anisotropies of the cosmic microwave background.



## Neutrino Exclusion Limits

A comprehensive study on the constraints from dark matter to neutrinos from the Galactic Center or from the diffuse isotropic background has been performed in reference [101], from which we took the constraints of Antares [116]. The IceCube constraints are a combination of [117] together with [118], which are obtained for neutrino lines. Future projections from the neutrino telescopes KM3NeT [114] and Hyper-Kamiokande [115] are also shown, again derived in the most optimistic scenario of neutrino lines. The experimental constraints have usually been obtained for a NFW dark matter density profile hypothesis [132, 133]. Each limit has been rescaled accordingly with the branching ratio into neutrino lines of the model. All bounds are shown at 90% confidence level. The  $ZZ$  and  $\gamma Z$  final states produce a continuum neutrino spectrum, thus a rescaling of the above-mentioned limits and projections is not correct. The implementation of this final state would imply a full recasting of experimental limits using their likelihoods; however, this goes beyond the scope of this analysis and our results remain unchanged especially because as the  $ZZ$  contribution into neutrinos is a subdominant component anyway.

## Gamma-ray Lines

We have considered two lines searches at 95% C.L. from the Galactic Center by Fermi-LAT [113] (Fermi  $\gamma\gamma, \gamma Z$ ) and HESS [112] (HESS  $\gamma\gamma, \gamma Z$ ), both obtained with the Einasto dark matter density profile assumption [131]. The experimental exclusion bounds have been rescaled again by the corresponding branching ratio of the processes  $\psi\bar{\psi} \rightarrow \gamma\gamma, \gamma Z$  (the latter being divided by two since each annihilation emits just one photon). Additionally, we shown the projected sensitivity for line searches towards the Galactic Center for CTA (assuming consistently an Einasto dark matter density profile) from [130] (CTA  $\gamma\gamma, \gamma Z$ ).

We shown in figure 4.13 the constraints from indirect searches as well as the reach of future probes for hypercharge EFT models, in a comprehensive fashion. By considering first the results for the magnetic dipole at dimension-5 only (top left panel) we realized that current dSph Fermi-LAT limits are the most constraining, together with cosmic-ray antiproton bounds at high masses. We obtained that the current neutrino bounds are substantially weaker than that of Fermi-LAT and AMS  $\bar{p}$ . It is important to notice, however, that future experiments such as KM3NeT will be competitive with CTA for heavy dark matter while LSST discovery of new dSphs will increase the current Fermi-LAT bounds (LSST+Fermi-LAT). Moreover, complementary across annihilation channels will prove important in the event of positive signal. The description is qualitatively unchanged for the charge radius operator (bottom right panel).

As discussed above, the magnetic dipole phenomenology should be considered up to dimension-6, this shown in the top right panel. When the branching ratio of  $\langle\sigma v\rangle_{\gamma\gamma, \gamma Z}$  start to dominate, all continuum searches weaken, as expected from figure 4.12, and this occurs accordingly to equation (4.37). Up to this certain mass value, the magnetic dipole behaves like a pure dimension-5 operator, while above it the HESS limit dominates in constraining the model parameter space. The experimental sensitivity from continuum searches, however, does not completely drop to zero, as it is still powered by the  $ZZ$  final state. Here, for simplicity, we only shown the behavior of the dominant Fermi-LAT dSph limit.

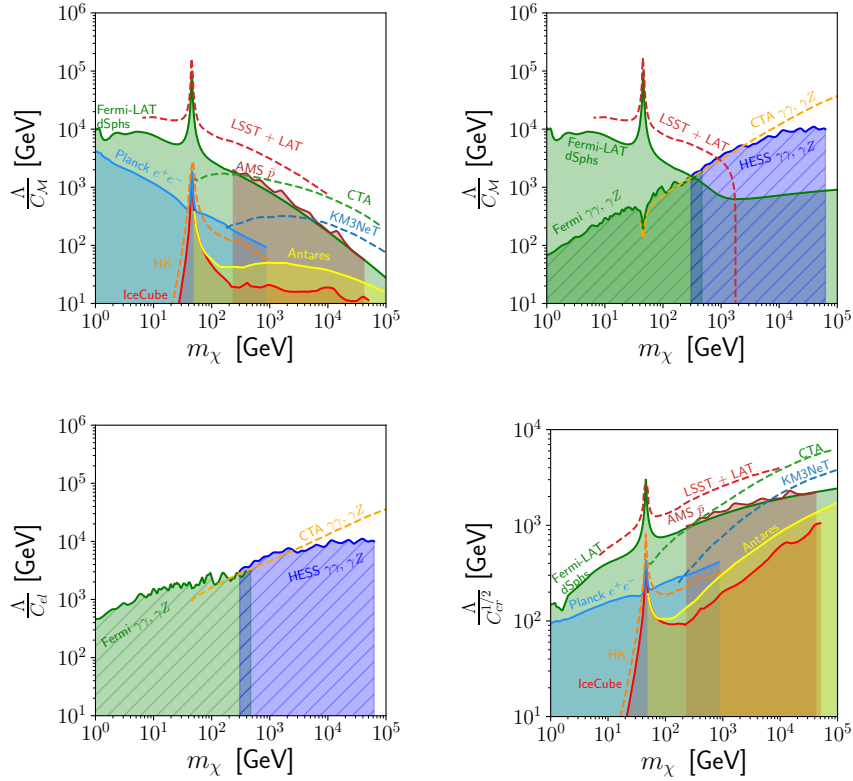


Figure 4.13: In the top left panel, the indirect detection constraints for the magnetic hypercharge moment interaction in the plane  $\Lambda/C_M$  and dark matter mass  $m_\chi$ . In the top right panel, the same as left but including the dimension-6 operator leading to the di-photon final state. In the bottom left panel, the same as top right for the electric dipole form factor, notice that only di-photon exclusion bounds are relevant for this operator. In the bottom right panel, the same as top left for the charge radius interaction. The experimental constraints shown by shaded region are actual bounds, while dashed lines are projected sensitivities, as in figure 4.10. Gamma-ray continuum bounds: Fermi-LAT dwarf spheroidal galaxies [79] (green), CTA projection [103] (green) and LSST+Fermi-LAT dwarf spheroidal galaxies sensitivity [104] (dark red); Neutrino bounds: IceCube [118] (red), Antares [101, 116] (yellow), Hyper-Kamiokande (HK) [115] (orange) and KM3NeT [114] (blue). Additional constraints: Planck [111] (light blue), AMS 02 cosmic rays [102] (brown), gamma-ray lines from the Galactic Centre from Fermi-LAT [113] (green), HESS [112] (dark blue) and expected CTA sensitivity [130]. Unlike figure 4.10 the relic density curve is not shown to avoid additional cluttering. Details on the CL of each exclusion limit are provided in the text.

The projected sensitivity of CTA only slightly improves the sensitivity of gamma-ray line searches to the magnetic moment operator at very large dark matter masses. Notice that the LSST+Fermi-LAT sensitivity drops artificially to zero since it is obtained from a  $b\bar{b}$  final state and could not be easily translated into a  $ZZ$  ones.

We do not expect that our conclusion will change when this bound is included, as the same portion of the parameter space is already excluded by HESS. The case of the electric dipole interaction (bottom left) is peculiar since, as stated above, the diphoton and  $\gamma Z$  channels are the only  $s$ -wave interactions; therefore, this introduces the possibility of constraining the model via indirect probes which would not be possible otherwise. Furthermore, one must notice that unlike the magnetic and charge radius form factors, there is no  $Z$ -peak (or dip for the line searches), due to the  $p$ -wave suppression of  $Z$  mediating diagrams. In this case, we have not considered the  $ZZ$  gamma-ray continuum because it would give a subdominant contribution as for the magnetic dipole operator, showing only the effect of line finding.

## 4.7 Conclusions and Outlooks

In this chapter we started with a revisit of the *Standard Model of Cosmology*, focusing in particular on the reasons for the introduction of dark matter. Subsequently, we introduce an effective field theory where that couples the photon with a new fermionic field  $\chi$  both Dirac and Majorana, i.e., the dark matter candidate. The only effective interaction which is not zero for Majorana dark matter is the anapole moment at dimension-6 while for Dirac dark matter the magnetic and electric dipole at dimension-5 and the charge radius at dimension-6 also exist.

These so-called electromagnetic form factors might have seemed to be thoroughly studied in literature, however, at certain energies the EFT treatment has not been properly addressed, leading to wrong conclusions. Our analysis amends these issues and results in a proper mapping of the operator parameter space in the light of current and future dark matter and collider searches. The results from each section are collated and presented together in figure 4.14, to summarize our main findings and bring to light possible caveats.

Starting with the primary issue, a naive treatment of the electromagnetic operator, dark matter coupling to  $F_{\mu\nu}$ , signals gauge-violating processes at large energies or dark matter masses. Gauge invariance is simply restored by coupling the dark matter to the  $U(1)_Y$  gauge boson  $B_{\mu\nu}$  of the Standard Model instead of the photon at energies above the  $W$  boson mass. This is dictated by the proper choice of low-energy symmetries of the EFT given the energy scales of the processes relevant for dark matter phenomenology. The price or maybe the recompense of the consistent description is a set of interactions for dark matter with the  $Z$  boson. An immediate consequence is that constraints apply from the  $Z$  invisible decay width, having fundamental consequences for the parameter space at low dark matter masses. The description also leads to a richer set of final states, namely  $Z\gamma$  &  $ZZ$  in addition to  $\gamma\gamma$ , for indirect detection via the dimension-5 interactions.

This issue is represented in the plots by the relic density lines (black) from both the  $F_{\mu\nu}$  and  $B_{\mu\nu}$  and tells us that the gauge violating annihilation cross-sections leads to a completely different picture for where viable thermal dark matter candidates are in parameter space. Furthermore, the  $Z$ -width bound from LEP (green region) closes the window of freeze-out dark matter for masses  $\lesssim 45$  GeV for all but the magnetic dipole. The gauge violating process, namely  $W^+W^- \rightarrow \chi\chi$ , also provides large and unphysical contributions in collider experiments, which would

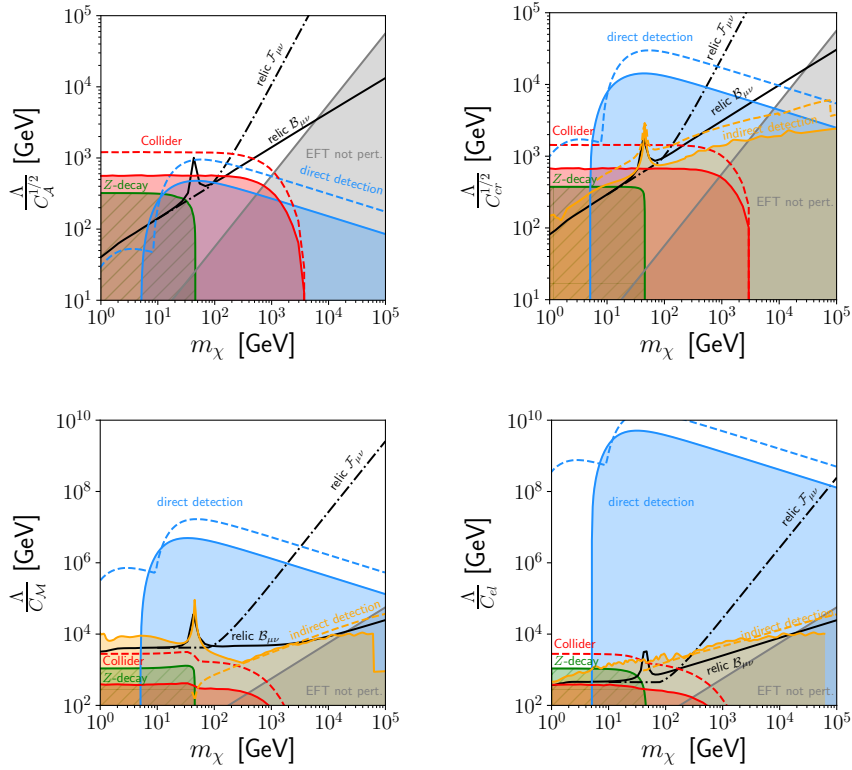


Figure 4.14: Summary of the most constraining search from direct (blue), indirect (yellow) detection and collider searches (red for LHC searches and green for LEP searches) in the plane  $\Lambda/c_A^{1/2}$  versus  $m_\chi$ . Current experimental bounds are denoted with solid lines and shaded regions, while projected sensitivities are shown with dashed lines. The relic density with denoted by a black line for the hypercharge (solid) and electromagnetic (dot-dashed) scenarios. In the top left panel the analysis for the anapole moment form factor, in the top right panel for the charge radius and in the bottom pannels for the magnetic (left) and electric (right) dipoles, respectively.

lead to incorrect conclusions concerning the most sensitive searches (cf. VBF instead of mono-jet searches, as described in section 4.5). The same scattering process would lead to the incorrect impression that indirect detection experiments have a better sensitivity that direct searches for high values of dark matter mass. The hypercharge form factors correctly describe the electromagnetic effective interaction of dark matter at energies relevant for dark matter and collider searches, therefore we only focus on those.

The search that is most dominant in figure 4.14 is direct detection. These experiments (here shown XENON1T and projected LZ and SuperCDMS sensitivities) are able to cover almost all the parameter space up until the perturbative limit for the EFT for magnetic and electric dipoles. Generally speaking, direct detection is the strongest current constraint above  $m_\chi \sim 6$  GeV for all but the anapole interaction.

Notice that for direct detection the pure electromagnetic description is valid, as the relevant energies are much below the EW scale.

At low masses, direct detection is likely more sensitive than  $Z$  invisible decay width for all interactions but the anapole moment. Above  $m_\chi \sim 100$  GeV, experimental sensitivity can be improved by analyzing recoil energies up to 500 keV as shown in ref. [93]. This is of particular relevance for the anapole interaction since improvements in this region could constrain the thermal freeze-out scenario.

It is important, however, to remark that astrophysical assumptions are at play in these bounds. For instance, there is a plausible level of uncertainty in the density of dark matter in the solar system, see e.g. [157, 156, 137, 144, 155]. Since the limits for direct detection are so sensitive in the case of dimension-5 operators, it is still likely that direct detection remains the most constraining search also in the case of huge variation of the local density. The only region which might escape direct detection is eventually the low  $m_\chi$  region for the magnetic dipole, where indirect limits (Fermi-LAT dSphs) dutifully cover the relic line and overcome as well the  $Z$ -decay bound.

Astrophysical uncertainty is certainly at play in indirect searches as well, but in a completely different domain. Limits on the continuum of gamma rays coming from the Fermi-LAT telescope are derived from a set of dwarf spheroidal galaxies, which are dark matter dominated objects. The argument used to weaken limits in direct detection experiments is simply not available in the indirect case. For this reason, the complementary nature of the two searches is important, in particular since large portions of the thermal relic line is covered by indirect searches in the cases of magnetic, electric and charge radius interactions.

The strongest mono-jet bounds from section 4.5.2 and their high luminosity projections are shown in figure 4.14 as “collider bounds”. When we compare our new mono-jet bounds to other dark matter searches, we achieve competitive results apart from the impressive hierarchy between the direct detection sensitivity to dimension-5 operators and all others. The best case is for the dimension-6 operators, since for the anapole interaction the constraints currently are more sensitive for the whole valid parameter space. We also point out that these limits either already, or will eventually surpass those coming from invisible  $Z$  decays in all cases. We notice an interesting complementarity between the high-luminosity LHC and direct detection bounds not only for the anapole but also for the charge radius interaction, which was not naively expected given the fact that it induces spin-independent nucleon scattering.

One limitation of these results is that our analysis focuses only on one interaction at a time, rather than allowing all operators to vary at once. In such a global study, renormalization group running and operator mixing may well change significantly the picture, since dark matter annihilation,  $Z$ -decay, collider production and nuclear scattering all take place at different scales (see Refs. [54, 95, 89, 96] for relevant studies). Nevertheless, the results presented here can provide useful inputs to a global DM-EFT analysis, in order to properly assess how much parameter space is left for a thermally produced dark matter candidate. In this case, the Dirac dark matter scenario will be severely precluded by dimension-5 moments, with no good reason, ‘*a priori*’ to suppress them. Therefore, data seems to be pushing us towards a Majorana dark matter candidate.

Finally, we also tried to assess the validity of the EFT description given the

sensitivity obtained by each experiment. We used naive perturbativity arguments to suggest regions in which predictions are not expected to be reliable. The validity issue is especially important for the collider bounds, since a range of energies are naturally probed by the LHC. Therein we discuss the viable range of Wilson coefficients that admit a valid EFT interpretation, concluding that couplings of order one are required. In other words, a thermal relic produced by loops is perhaps not compatible with a viable EFT interpretation. On the contrary, tree level processes via a  $U(1)'$ -mixing are unavailable to Majorana particles. The assumption of a simple thermal history of dark matter can lead to the construction of exotic models, whose implications can only be evaluated after a comprehensive global analysis.

In this chapter effective field theories will be employed to extend the Standard Model of particle physics by including a new physical state that belongs to the class of axion-like particles (ALPs).

The chapter starts with the description of the *Strong CP problem*, whose most known solution is the Peccei-Quinn theory of axions. Nevertheless, the idea of R. Peccei and H. Quinn appears to be extremely ductile and not strictly related to the scope for which it was originally proposed. This leads to a class of theories that include axions without considering the strong CP problem, therefore the name ‘axion-like particles’ is preferred to axion alone.

In our EFT, ALPs interact with every particle in SM. A unitarity rotation, whose phase is proportional to the ALP itself, will lead to a Lagrangian where the coupling between ALP and heavy fermions is preferred, thus bringing to a top-philic theory, whose phenomenology is studied.

## 5.1 The Strong CP Problem

In section 1.2.2, we said that the most general Lagrangian for Quantum Chromodynamics is equation (1.9). Nevertheless, there is a further Lorentz and gauge invariant term that can be added

$$\mathcal{L}_{QCD} \supset \frac{\theta g_s^2}{32\pi^2} G_{\mu\nu}^a \tilde{G}^{\mu\nu a}, \quad (5.1)$$

which is  $C$ -conserving, but violates  $P$ ,  $T$  and  $CP$  symmetries. Even if this term can be written as a total derivative

$$\partial^\mu K_\mu = G\tilde{G}, \quad \text{with} \quad K_\mu = \epsilon_{\mu\nu\rho\sigma} \left( A_\nu^a G_{\rho\sigma}^a - \frac{2}{3} f^{abc} A_\nu^a A_\rho^b A_\sigma^c \right),$$

it cannot be neglected since the statement that  $G_{\mu\nu}^a$  vanishes faster than  $1/r^2$  does not lead  $A_\mu$  to vanish faster than  $1/r$  for  $r \rightarrow \infty$ , where  $r$  is the Euclidean distance [188]. The term in equation (5.1) is called *instanton* and causes  $\theta$  to have physical effects<sup>1</sup>. The instanton term not only is allowed, but also required since it

<sup>1</sup>In the Abelian case  $K_\mu = \epsilon_{\mu\nu\rho\sigma} A^\nu F^{\rho\sigma}$ , thus the request for  $F_{\mu\nu}$  of falling faster than  $1/r^2$ , leads to  $A$  falling faster than  $1/r$ . Even in  $SU(2)$  an analogous term to that in equation (5.1) is allowed, however, we can remove it by using symmetries that are anomalously violated and, i.e., the baryon and lepton number.

may be generated by a divergent loop, making  $\theta$  necessary for the renormalization.

The angle  $\theta$  changes by performing a chiral rotation, thus it cannot appear in any observable of the theory. In fact, starting from the Yukawa matrices of quarks, introduced in equation (1.21), namely

$$\begin{aligned} Y_u &= U_u M_u K_u^\dagger, \\ Y_d &= U_d M_d K_d^\dagger, \end{aligned} \quad (5.2)$$

and performing a chiral transformation of the right-handed spinors we can remove the  $K_u$  and  $K_d$  matrices, while a generic rotation simplifies  $U_u$  and  $U_d$ , thus we have:

$$\theta_p = \arg \det [K_u K_d] = -\arg \det [Y_u Y_d], \quad (5.3)$$

since  $\det [M_u M_d]$  is real. After two rotations the CP-violating term reads:

$$\mathcal{L}_{QCD} \supset \frac{\bar{\theta} g_s^2}{32\pi^2} G_{\mu\nu}^a \tilde{G}^{\mu\nu a}, \quad (5.4)$$

where we defined  $\bar{\theta} = \theta - \theta_p$ , the chiral rotation contemporary shifts  $\theta$  and  $\theta_p$ , leaving their difference unchanged, i.e.,  $\bar{\theta}$ . In other words, the angle  $\bar{\theta}$  is an observable of the theory<sup>2</sup> and we commonly refer to it as *strong CP phase*.

The effects of  $\bar{\theta}$  could be observed in pions theory, since the vacuum energy becomes proportional to this angle [189]

$$E(\bar{\theta}) = V^3 (m_u + m_d) \cos \bar{\theta} = f_\pi^2 m_\pi^2 \cos \bar{\theta}, \quad (5.5)$$

where  $V^3 = \langle \bar{u}u \rangle = \langle \bar{d}d \rangle$ . The strong CP phase impacts on neutron physics, where it causes an electric dipole moment for neutron, that is directly proportional to  $\bar{\theta}$  [189], namely  $d_n = \bar{\theta} (3 \times 10^{-16} \text{e} \cdot \text{cm})$ . The current experimental bound for the neutron electric dipole moment is  $d_n = 1.8 \times 10^{-26} \text{e} \cdot \text{cm}$  [190], so that:

$$\bar{\theta} < 10^{-10}.$$

### 5.1.1 Axions and Axion-like Particles

The hypothetical solutions to the Strong CP problem include theories of massless quark [191], spontaneous CP violation [192, 193] and axions [194], to name a few. On one hand, the theory of massless quark just moves the problem from smallness of  $\bar{\theta}$  to smallness of  $m_u$  – being up the lightest quark – as there is no symmetry that fixes its value to zero while the spontaneous CP violation does not represent an intriguing model since it forces all breaking terms to be included in Yukawa matrices, as the full theory respects CP symmetry. On the other hand, axions represents a compelling solution to the Strong CP problem. A new spontaneously broken symmetry  $U_{PQ}(1)$  must be added to the Standard Model [194] in order to generate a new Goldstone boson  $a(x)$  that cancels the effects of  $\bar{\theta}$ . In particular the effective Lagrangian of axions is:

$$\mathcal{L} = (\partial_\mu a)^2 + \left( \bar{\theta} - \frac{a}{f_a} \right) \frac{g_s^2}{32\pi^2} G_{\mu\nu}^a \tilde{G}^{\mu\nu a}, \quad (5.6)$$

<sup>2</sup>If quarks are massless than  $\det [M_u M_d] = 0$ , thus  $\bar{\theta}$  becomes unphysical.



where  $f_a$  is named axion decay constant. The vacuum energy, in equation (5.5), becomes:

$$E(a, \bar{\theta}) = f_a^2 m_\pi^2 \cos\left(\bar{\theta} - \frac{a(x)}{f_a}\right),$$

which is a potential for the axion field. The vacuum expectation value is  $\langle a \rangle = f_a \bar{\theta}$ . This potential also accounts for a tight relationship between the mass and the axion decay constant. Expanding the previous equation, we get:

$$m_a = \frac{m_\pi f_\pi}{f_a}, \quad (5.7)$$

that can be constrained by cosmological and astrophysical bounds that squeeze the axion mass in the range  $10^{-4}\text{eV} < m_a < 10^{-2}\text{eV}$ . Moreover, even neutron dipole moment finds a solution in the theory of axions, since  $d_n \propto \bar{\theta} - a(x)/f_a = 0$ .

The Peccei-Quinn symmetry not only allows for interactions between the axion and gauge fields:

$$\mathcal{L}_a = \frac{a}{f_a} \frac{g_s^2}{32\pi^2} G\tilde{G} + \frac{a}{f_W} \frac{g^2}{32\pi^2} W\tilde{W} + \frac{a}{f_B} \frac{g'^2}{32\pi^2} B\tilde{B}, \quad (5.8)$$

but also for derivative couplings with SM fermions and the Higgs field, as we will see in the next section. Unlike the interaction with gluon field, the coupling with electromagnetic and weak bosons is model dependent. Many efforts were made in order to define boundaries for those coupling and, unless complex models are introduced, both couplings with fermion and with photon seems weaker compared to the interaction with gluon [189]-[196]. Practically, the coupling with photon is the easiest to probe and many experiments have been carried out in this direction to search for axion although the magnitude of the interaction is completely uncorrelated to the Strong CP problem. Thus, one has to wonder why we are forcing the new particle to solve the strong CP problem if we are looking for couplings that have nothing to do with it. Because of this reason, axions have been overshadowed by the Axions-Like Particles (ALPs).

In following sections we will exclusively study ALPs, treating them as new scalar or pseudoscalar field and ignoring the Strong CP problem.

## 5.2 Effective Field Theory of ALP

Assuming that ALP is a new gauge singlet, described by a scalar or pseudoscalar field  $a(x)$ , whose couplings with SM fields are, at the classical level, protected by an approximate shift symmetry  $a \rightarrow a + c$ , which is broken by the mass term  $m_a$ . Up to dimension-5 operators, the most general Lagrangian is [197]:

$$\begin{aligned} \mathcal{L}_{\text{ALP}} = & \frac{1}{2} \partial_\mu a \partial^\mu a - \frac{1}{2} m_a^2 a^2 + i c_H \partial_\mu a (H^\dagger \overleftrightarrow{D}^\mu H) \\ & + c_g a G_{\mu\nu}^a \tilde{G}^{a\mu\nu} + c_w a W_{\mu\nu}^i \tilde{W}^{i\mu\nu} + c_b a B_{\mu\nu} \tilde{B}^{\mu\nu} \\ & + \sum_{\psi=L,Q} c_\psi \partial^\mu a (\psi^\dagger \overleftrightarrow{\sigma}_\mu \psi) + \sum_{\psi=e,u,d} c_\psi \partial^\mu a (\psi^\dagger \sigma_\mu \psi), \end{aligned} \quad (5.9)$$

where  $c_i = C_i/\Lambda$ , for some energy cut-off  $\Lambda$ . We choose to introduce the cut-off instead of using the ALP decay constant  $f_a$ , for the purpose of working with dimensionless coupling constants, namely  $C_g$ ,  $C_w$  and  $C_b$ . They embeds the coefficients of equation (5.8), so that for gluon interaction, we have  $C_g/\Lambda = \alpha_s^2/(8\pi f_a)$ .

### 5.2.1 Phase Redefinition of SM Fields

The Lagrangian in equation (5.9) provides democratic interactions between ALP and fields of the Standard Model, however, performing a rotation, whose phase is proportional to ALP itself, of fermions and Higgs fields we will end up with a new Lagrangian which could provide information about couplings involving the ALP, which, at that point, could encourage specific channels of interaction. In flavor basis, the phase redefinition is realized as a unitary rotation, that for fermions is proportional to  $3\times 3$  Hermitian matrices  $\mathbf{q}_\psi$

$$\begin{aligned}\psi_i &\rightarrow [e^{i\mathbf{q}_\psi a}]_{ij} \psi_j, \\ H &\rightarrow e^{iq_H a} H.\end{aligned}$$

The technicalities of calculation are presented in section A.7.1, here we only report the result:

$$\begin{aligned}\mathcal{L}_{\text{SM}} &\rightarrow \mathcal{L}_{\text{SM}} - (\partial_\mu a) \sum_{\psi=L,Q} (\psi^\dagger \bar{\sigma}^\mu \psi) \mathbf{q}_\psi - (\partial_\mu a) \sum_{\psi=e,u,d} (\psi^\dagger \sigma^\mu \psi) \mathbf{q}_\psi \\ &\quad - ia (\ell^\dagger H e_R) (\mathbf{Y}_e \cdot \mathbf{q}_e - \mathbf{q}_L \cdot \mathbf{Y}_e + q_H \mathbf{Y}_e) + \text{h.c.} \\ &\quad - ia (q^\dagger H d_R) (\mathbf{Y}_d \cdot \mathbf{q}_d - \mathbf{q}_Q \cdot \mathbf{Y}_d + q_H \mathbf{Y}_d) + \text{h.c.} \\ &\quad - ia (q^\dagger \tilde{H} u_R) (\mathbf{Y}_u \cdot \mathbf{q}_u - \mathbf{q}_Q \cdot \mathbf{Y}_u - q_H \mathbf{Y}_u) + \text{h.c.} \\ &\quad - iq_H (\partial^\mu a) (H^\dagger \overleftrightarrow{D}^\mu H) + O(a^2) + O[(\partial a)^2]\end{aligned}\tag{5.10}$$

The switch from flavor basis to mass basis is achieved by the rotation

$$\begin{aligned}\psi_L &\rightarrow \mathbf{U}_\psi \cdot \psi_L, \\ \psi_R &\rightarrow \mathbf{V}_\psi \cdot \psi_R,\end{aligned}$$

that transforms equation (5.10) as

$$\begin{aligned}\mathcal{L}_{\text{SM mass}} &\rightarrow \mathcal{L}_{\text{SM mass}} - (\partial_\mu a) \sum_{\psi=L,Q} (\psi^\dagger \bar{\sigma}^\mu \psi) \tilde{\mathbf{q}}_\psi - (\partial_\mu a) \sum_{\psi=e,u,d} (\psi^\dagger \sigma^\mu \psi) \tilde{\mathbf{q}}_\psi \\ &\quad - \frac{ia\sqrt{2}}{v} (\ell^\dagger H e_R) (\mathbf{M}_e \cdot \tilde{\mathbf{q}}_e - \tilde{\mathbf{q}}_{L,e} \cdot \mathbf{M}_e + q_H \mathbf{M}_e) + \text{h.c.} \\ &\quad - \frac{ia\sqrt{2}}{v} (q^\dagger H d_R) (\mathbf{M}_d \cdot \tilde{\mathbf{q}}_d - \tilde{\mathbf{q}}_{Q,d} \cdot \mathbf{M}_d + q_H \mathbf{M}_d) + \text{h.c.} \\ &\quad - \frac{ia\sqrt{2}}{v} (q^\dagger \tilde{H} u_R) (\mathbf{M}_u \cdot \tilde{\mathbf{q}}_u - \tilde{\mathbf{q}}_{Q,u} \cdot \mathbf{M}_u - q_H \mathbf{M}_u) + \text{h.c.} \\ &\quad - iq_H (\partial^\mu a) (H^\dagger \overleftrightarrow{D}_\mu H) + O(a^2) + O[(\partial a)^2],\end{aligned}\tag{5.11}$$

where we defined the parameters

$$\begin{aligned}\tilde{\mathbf{q}}_{Q,u} &= \mathbf{U}_u^\dagger \cdot \mathbf{q}_Q \cdot \mathbf{U}_u, & \tilde{\mathbf{q}}_u &= \mathbf{V}_u^\dagger \cdot \mathbf{q}_u \cdot \mathbf{V}_u, \\ \tilde{\mathbf{q}}_{Q,d} &= \mathbf{U}_d^\dagger \cdot \mathbf{q}_Q \cdot \mathbf{U}_d, & \tilde{\mathbf{q}}_d &= \mathbf{V}_d^\dagger \cdot \mathbf{q}_d \cdot \mathbf{V}_d, \\ \tilde{\mathbf{q}}_{L,e} &= \mathbf{U}_e^\dagger \cdot \mathbf{q}_L \cdot \mathbf{U}_e, & \tilde{\mathbf{q}}_e &= \mathbf{V}_e^\dagger \cdot \mathbf{q}_e \cdot \mathbf{V}_e,\end{aligned}$$

and the masses matrices as

$$\mathbf{M}_\psi = \frac{v}{\sqrt{2}} \mathbf{U}_\psi^\dagger \cdot \mathbf{Y}_\psi \cdot \mathbf{V}_\psi.$$

The non-invariant measure of path integral for fermions introduces the Fujikawa anomaly [198], which is realized as a shift of the coupling constants between ALP and gauge fields [197]:

$$\begin{aligned}C_b \rightarrow C_B &\equiv C_b - \frac{\alpha_Y}{8\pi} \sum \left( \frac{\mathbf{q}_Q}{3} - \frac{8\mathbf{q}_u}{3} - \frac{2\mathbf{q}_d}{3} + \mathbf{q}_L - 2\mathbf{q}_e \right) \\ C_w \rightarrow C_W &\equiv C_w - \frac{\alpha_2}{8\pi} \sum (3\mathbf{q}_Q + \mathbf{q}_L) \\ C_g \rightarrow C_G &\equiv C_g - \frac{\alpha_s}{8\pi} \sum (2\mathbf{q}_Q - \mathbf{q}_u - \mathbf{q}_d)\end{aligned}\tag{5.12}$$

The new theory for ALP is given by the sum of equation (5.9) and equation (5.11). The former has not been rotated since each one of its term is already proportional to ALP – or to partial derivative of the ALP – thus every further term that the phase rotation would produce is already counted in  $O(a^2)$  – or in  $O[(\partial a)^2]$ . Rewriting the Hermitian matrices that performed the phase redefinition

$$\tilde{\mathbf{q}}_\psi = \frac{\tilde{\mathbf{C}}_\psi}{\Lambda}, \quad q_H = \frac{\tilde{C}_H}{\Lambda},$$

and taking into account also Fujikawa anomaly, the effective Lagrangian becomes:

$$\begin{aligned}\mathcal{L}_{\text{ALP}}^Y &= \frac{1}{2} \partial_\mu a \partial^\mu a - \frac{1}{2} m_a^2 a^2 \\ &+ \frac{C_B}{\Lambda} a B_{\mu\nu} \tilde{B}^{\mu\nu} + \frac{C_W}{\Lambda} a W_{\mu\nu}^i \tilde{W}^{i\mu\nu} + \frac{C_G}{\Lambda} a G_{\mu\nu}^a \tilde{G}^{a\mu\nu} \\ &+ \sum_{\psi=L,Q} \left( \frac{C_\psi}{\Lambda} - \frac{\tilde{C}_\psi}{\Lambda} \right) \partial^\mu a (\psi \bar{\sigma}_\mu \psi) + \sum_{\psi=e,u,d} \left( \frac{C_\psi}{\Lambda} - \frac{\tilde{C}_\psi}{\Lambda} \right) \partial^\mu a (\psi^\dagger \sigma_\mu \psi) \\ &+ ia \left( \frac{C_e}{\Lambda} (\ell^\dagger H e_R) + \frac{C_d}{\Lambda} (q^\dagger H d_R) + \frac{C_u}{\Lambda} (q^\dagger \tilde{H} u_R) + \text{h.c.} \right) \\ &+ i \left( \frac{C_H}{\Lambda} - \frac{\tilde{C}_H}{\Lambda} \right) \partial_\mu a \left( H^\dagger \overleftrightarrow{D}^\mu H \right).\end{aligned}$$

where the capital  $C_i$ , for  $i = \{e, u, d\}$ , are defined as

$$\begin{aligned}\mathbf{C}_e &= \mathbf{y}_d (\tilde{\mathbf{C}}_e - \tilde{\mathbf{C}}_L + \tilde{C}_H), \\ \mathbf{C}_u &= \mathbf{y}_d (\tilde{\mathbf{C}}_u - \tilde{\mathbf{C}}_Q - \tilde{C}_H), & \mathbf{y}_\psi &= \frac{\sqrt{2}}{v} \mathbf{M}_f, \\ \mathbf{C}_d &= \mathbf{y}_d (\tilde{\mathbf{C}}_d - \tilde{\mathbf{C}}_Q + \tilde{C}_H).\end{aligned}\tag{5.13}$$

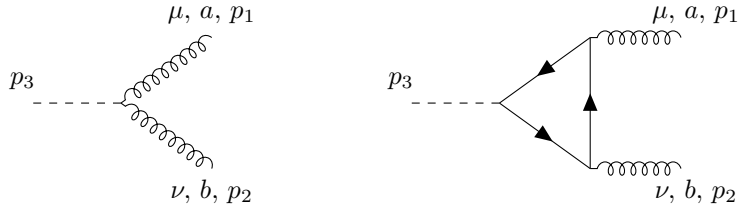


Figure 5.1: The lowest-order contributions to  $ALP \rightarrow gg$  scattering process.

One may already have noticed that since the parameters of the phase rotation, in equation (5.2.1), are free, we can fix them at the values of the original couplings; those that appear in equation (5.9), to get

$$\begin{aligned} \mathcal{L}_{\text{ALP}}^Y = & \frac{1}{2} \partial_\mu a \partial^\mu a - \frac{1}{2} m_a^2 a^2 + \frac{C_B}{\Lambda} a B_{\mu\nu} \tilde{B}^{\mu\nu} + \frac{C_W}{\Lambda} a W_{\mu\nu}^i \tilde{W}^{i\mu\nu} + \frac{C_G}{\Lambda} a G_{\mu\nu}^a \tilde{G}^{a\mu\nu} \\ & + ia \left( \frac{C_e}{\Lambda} (\ell^\dagger H e_R) + \frac{C_d}{\Lambda} (q^\dagger H d_R) + \frac{C_u}{\Lambda} (q^\dagger \tilde{H} u_R) + \text{h.c.} \right), \end{aligned} \quad (5.14)$$

where we have no longer used the convention of bold symbol for matrices. Despite this Lagrangian is equivalent to that in equation (5.9), it allows us to look at ALP theory from a different point of view, the interactions between the ALP and the fermions are proportional to Yukawa coupling; this also explains the superscript  $Y$  in the previous equation.

## 5.2.2 Comparing Effective Field Theories

In previous section we obtained a new Lagrangian for ALP field. The computation has been rigorously executed and starting from the most general Lagrangian for ALP, where interactions with fermions of SM are encoded in derivative operators of ALP field itself, we ended up with new couplings that connect ALP and fermions through Yukawa-like operators. We now have to investigate whether the two theories really describe the same physics.

In this section, we will prove the equivalence of the two Lagrangians by calculating the amplitude of a specific process in both theories, namely  $ALP \rightarrow gg$ . Without losing generality we can choose  $C_g = 0$ , so that in Lagrangian with derivative coupling the process can only take place at 1-loop. Moreover, equation (5.12) can be simplified in

$$C_G = -\frac{\alpha_s}{8\pi} \sum (2q_Q - q_u - q_d). \quad (5.15)$$

In the theory with Yukawa-like couplings Feynman diagrams that contribute to the amplitude of  $ALP \rightarrow gg$  are depicted in figure 5.1. we have made is that the loop diagram is proportional to the mass of the particle running through it, so we compute the loop for a top quark. From Lagrangian (5.14), we get the required

interaction vertices

$$\begin{aligned}\mathcal{V}_{ALP\,gg}^Y &= \frac{2iC_G}{\Lambda} \delta^{ab} \epsilon_{\mu\nu\rho\sigma} (p_1^\rho p_2^\sigma - p_1^\sigma p_2^\rho), \\ \mathcal{V}_{ALP\,tt}^Y &= \frac{C_t v}{\sqrt{2}\Lambda} \delta^{ab} \gamma^5.\end{aligned}\tag{5.16}$$

The tree-level amplitude is straight:

$$i\mathcal{M}_{\text{tree}} = \frac{4iC_G}{\Lambda} \delta^{ab} \epsilon_{\mu\nu\rho\sigma} p_1^\rho p_2^\sigma \epsilon^\mu(p_1) \epsilon^\nu(p_2).\tag{5.17}$$

By slightly deviating from our main purpose, we can obtain the decay width of the process without many efforts. The squared amplitude is:

$$|\mathcal{M}_{\text{tree}}|^2 = \frac{256C_G^2}{\Lambda^2} (p_1 \cdot p_2)^2,$$

and the dynamics in the center of mass frame reads

$$\begin{aligned}p_1 &= (m_a/2, m_a/2, 0, 0), \\ p_2 &= (m_a/2, -m_a/2, 0, 0), \\ p_3 &= (m_a, \vec{0}),\end{aligned}$$

thus leading to the decay width:

$$d\Gamma = \frac{2C_G^2}{\Lambda^2\pi} m_a^3$$

The computation of the decay width was made by taking into account that the final state presents two identical particles, therefore a factor of 1/2 must be included in the integration over the solid angle. Since we have implemented both EFT theories in `FeynRules` [80] and obtained the model files in UFO format [81] that were upload on `Madgraph5_aMC@NLO` [58], we checked this result by fixing the parameters.

Coming back to the matching between the two effective field theories, we have to compute the amplitude at next to leading order with a top quark running in the loop. Our convention on energy conservation is fixed by  $p_1 + p_2 = p_3$ , with the momenta of gluons that are outgoing while the ALP momentum is incoming. The amplitude of the loop diagram is:

$$\begin{aligned}i\mathcal{M}_{\text{loop}} &= -\epsilon_\mu(p_1) \epsilon_\nu(p_2) \int \frac{d^D l}{(2\pi)^D} \frac{v \gamma^5 C_t \delta^{ab}}{\sqrt{2}\Lambda} \frac{i(\not{l} - \not{p}_1 + m_t)}{(l - p_1)^2 - m_t^2} \\ &\quad \times (ig_s \gamma^\mu T^{g_1}) \frac{i(\not{l} + m_t)}{l^2 - m_t^2} (ig_s \gamma^\nu T^{g_2}) \frac{i(\not{l} + \not{p}_2 + m_t)}{(l + p_2)^2 - m_t^2} + \left(1 \leftrightarrow 2\right) \\ &\quad \left(\mu \leftrightarrow \nu\right)\end{aligned}$$

where  $\mathcal{M}_{\text{loop}}$  is made of two addends since gluons of the final state can be exchanged among themselves. This amplitude appears superficially divergent. However, the result must be UV finite. Lorentz invariance and symmetry under the exchange of  $1 \leftrightarrow 2$  and  $\mu \leftrightarrow \nu$ , which is nothing but Bose statistics, suggests that there are only two allowed structures, which are  $p_1^\nu p_2^\mu$  and  $\epsilon^{\mu\nu\rho\sigma} p_{1\rho} p_{2\sigma}$ . In both cases, the amplitudes will be, at worst, proportional to  $p^2 \int d^4 l / l^5$  which means they are not

divergent. Making use of dimensional regularization, we have to deal with the issue of  $\gamma^5$  and  $\epsilon^{\mu\nu\rho\sigma}$  extensions, as they are specific objects of four-dimensional space. In this thesis, we overcome this problem by adopting the KKS-scheme, whose main rules are given in Appendix A.2.1.

After trace resolution, we can write the amplitude as a function of Passarino-Veltman scalar integrals (PaVe), see Appendix A.8, to get

$$i\mathcal{M}_{\text{loop}} = \frac{ig_s^2 C_t v m_t \delta^{ab}}{(2\pi)^2 \sqrt{2}\Lambda} \epsilon^\mu(p_1) \epsilon^\nu(p_2) \epsilon^{\mu\nu\rho\sigma} p_{1\rho} p_{2\sigma} C_0(-p_1, p_2, m_t, m_t, m_t)$$

Finally, summing up tree-level and one-loop amplitudes, we get the desired result for the Lagrangian that carries Yukawa-like interactions

$$\begin{aligned} i\mathcal{M}^Y &= i\mathcal{M}_{\text{tree}} + i\mathcal{M}_{\text{loop}} \\ &= \frac{2i\delta^{g_1 g_2}}{\Lambda} \epsilon_\mu(p_1) \epsilon_\nu(p_2) \epsilon^{\mu\nu\rho\sigma} p_{1\rho} p_{2\sigma} \\ &\quad \left( 2C_G + \frac{g_s^2 C_t v m_t}{2(2\pi)^2 \sqrt{2}} C_0(-p_1, p_2, m_t, m_t, m_t) \right). \end{aligned} \quad (5.18)$$

On the contrary, the computation for the Lagrangian with derivative coupling is more complicated. As previously said, since the coupling with gluon is fixed at zero, the scattering process  $ALP \rightarrow gg$  occurs, at least, at one-loop. In this case, the interaction vertex involved in the computation couples the ALP with the top quark:

$$\mathcal{V}_{ALP tt}^D = \frac{C_{top} \delta^{ab}}{\Lambda} \not{p}_3 P_+, \quad (5.19)$$

where the projectors are, as usual, given by  $P_\pm = (\mathbf{1} \pm \gamma^5)/2$ . Then the amplitude reads:

$$\begin{aligned} i\mathcal{M}^D &= -\epsilon^\mu(p_1) \epsilon^\nu(p_2) \int \frac{d^D l}{(2\pi)^D} \frac{C_{top} \delta^{ab} \not{p}_3 P_+}{\Lambda} \frac{i(\not{l} - \not{p}_1 + m_t)}{(l-p_1)^2 - m_t^2} \\ &\quad \times (ig_s \gamma^\mu T^{g_1}) \frac{i(\not{l} + m_t)}{l^2 - m_t^2} (ig_s \gamma^\nu T^{g_2}) \frac{i(\not{l} + \not{p}_2 + m_t)}{(l+p_2)^2 - m_t^2} + \left( 1 \leftrightarrow 2 \right)_{\mu \leftrightarrow \nu}. \end{aligned}$$

The computation of the trace is quite hard and long, in addition many stratagems are required to obtain the result. First of all, distinguishing terms according to the presence or absence of  $\gamma^5$ , we get:

$$\text{tr}[\dots] = \frac{1}{2} C_{top} \left( \text{tr}[\dots]_{no \gamma^5} + \text{tr}[\dots]_{\gamma^5} \right).$$

A simple shrewdness tells that the contribution of the first term must be null: looking at equation (5.18), we realize that the complete result is proportional to Levi-Civita tensor, which cannot come from a trace without  $\gamma^5$ . Our hypothesis was checked with `FeynCalc`: a divergent result was obtained from the integration of the term that does not carry  $\gamma^5$ , however, the result is fully anti-symmetrical under the exchange  $\mu \leftrightarrow \nu$  and  $1 \leftrightarrow 2$ . The loop diagram where gluons of the final state have been exchanged provides for such contribution, thus removing the divergence and resulting in a zero net result.

The trace involving  $\gamma^5$  results in

$$\begin{aligned}\text{tr}[\dots]_{\gamma^5} = & \text{tr}[\gamma^\rho \gamma^5 \gamma^\alpha \gamma^\mu \gamma^\beta \gamma^\nu \gamma^\gamma] (p_1 + p_2)_\rho (l - p_1)_\alpha l_\beta (l + p_2)_\gamma \\ & + \text{tr}[\gamma^\rho \gamma^5 \gamma^\alpha \gamma^\mu \gamma^\nu] (l - p_1)_\alpha (p_1 + p_2)_\rho m_t^2 \\ & + \text{tr}[\gamma^\rho \gamma^5 \gamma^\mu \gamma^\beta \gamma^\nu] l_\beta (p_1 + p_2)_\rho m_t^2 \\ & + \text{tr}[\gamma^\rho \gamma^5 \gamma^\mu \gamma^\nu \gamma^\gamma] (l + p_2)_\gamma (p_1 + p_2)_\rho m_t^2,\end{aligned}$$

The last three terms – those proportional to the mass of top quark – can be recast according to the rules provided by KKS-scheme, while the first term was settled by the trick suggested in [208]. The idea consists in rewriting the momentum of ALP particle as:

$$p_{3\rho} = (p_1 + p_2)_\rho = (l - l + p_1 + p_2)_\rho = -(l - p_1)_\rho + (l + p_2)_\rho,$$

in such a way that the simplification  $(l - q)(l - q) = (l - q)^2$  can be applied to decrease the number of Dirac matrices involved in the trace. The whole trace then turns to:

$$\begin{aligned}\text{tr}[\dots] = & \frac{C_{top}}{2} (-4i \epsilon^{\mu\nu\rho\sigma} ((l - p_1)^2 - m_t^2) p_{2\rho} l_\sigma - 4i \epsilon^{\mu\nu\rho\sigma} ((l + p_2)^2 - m_t^2) p_{1\rho} l_\sigma \\ & + 8i (g^{\rho\alpha} \epsilon^{\mu\beta\nu\gamma} - g^{\rho\mu} \epsilon^{\alpha\beta\nu\gamma} + g^{\rho\beta} \epsilon^{\alpha\mu\nu\gamma} - g^{\rho\nu} \epsilon^{\alpha\mu\beta\gamma} + g^{\rho\gamma} \epsilon^{\alpha\mu\beta\nu}) \\ & \times (l + p_2)_\rho (l - p_1)_\alpha l_\beta (l + p_2)_\gamma \\ & + 8i m_t^2 \epsilon^{\mu\nu\rho\sigma} p_{1\rho} p_{2\sigma}).\end{aligned}$$

The first line is null since each term gives rise to an integrand function that is composed by either odd terms in the loop momentum – once the shift at denominator will take place – or tensor that are symmetric under the exchange of two indices, therefore the contraction with Levi-Civita symbol returns a null result. Moreover, the usual simplification for product of even number of loop momentum is applied, however, combined with a further trick that helps in the solution of the integral:

$$l_\rho l_\beta p_{1\alpha} p_{2\gamma} \rightarrow \frac{l^2}{D} g_{\rho\beta} p_{1\alpha} p_{2\gamma} = \frac{(l^2 - m_t^2) + m_t^2}{D} g_{\rho\beta} p_{1\alpha} p_{2\gamma}. \quad (5.20)$$

The amplitude, written in terms of Passarino-Veltman scalar integral, contains both  $B_0$  and  $C_0$ . Since the former does not appear in equation (5.18), we can solve it (the procedure is given in Appendix A.8) to get

$$\begin{aligned}i\mathcal{M}^D = & \frac{i \delta^{ab} g_s^2 C_{top}}{8\pi^2 \Lambda} \epsilon^\mu(p_1) \epsilon^\nu(p_2) \epsilon^{\mu\nu\rho\sigma} p_{1\rho} p_{2\sigma} \\ & \times (1 + 2m_t^2 C_0(-p_1, p_2, m_t, m_t, m_t)) + O(\epsilon)\end{aligned} \quad (5.21)$$

The matching between the two theories is performed by equating the amplitude in equation (5.18), that comes from the Lagrangian with Yukawa-like interactions, with that of equation (5.21), which is obtained by the Lagrangian with derivative couplings

$$\begin{aligned}C_G = & \frac{g_s^2}{32\pi^2} C_{top}, \\ C_t = & \frac{\sqrt{2} m_t}{v} C_{top}.\end{aligned} \quad (5.22)$$

In other words, the two theories reproduce the same physics if their coupling constants are related by these relations. Making use of equation (5.15), we can check that

$$C_G = 0 - \frac{\alpha_s}{8\pi}(-q_u) = \frac{\alpha_s}{8\pi} C_{top},$$

while from equation (5.13), we obtain

$$C_t = \mathbf{y}_d \tilde{\mathbf{c}}_u = \frac{\sqrt{2} m_t}{v} C_{top}.$$

in agreement with equation (5.22).

In conclusion, the computation shows that the original Lagrangian, in equation (5.9), not only represents the most general theory of ALP up to dimension-5, but it also considers interactions with fermions of SM through derivative couplings that, ‘*a priori*’, do not discriminate between flavors. Nevertheless a simple phase redefinition of SM fields, whose phase is proportional to the ALP itself, gives rise to a new Lagrangian, namely equation (5.14), that is completely equivalent to the previous in describing physics, but which encourages coupling with heavy fermions. Emphasizing this behavior, we can formulate a top-philic theory for the ALP.

### 5.3 Top-philic Axions-like Particles

In the Lagrangian with Yukawa-like interactions we choose to switch off all the couplings except for that with top quark. Including the top quark, kinetic term and its interaction with the gluon field, the effective field theory is

$$\begin{aligned} \mathcal{L}_{EFT} = & \bar{t} (i\not{\partial} - m_t + g_s \not{G}^a T^a) t \\ & + \frac{1}{2} \partial_\mu a \partial^\mu a - \frac{1}{2} m_a^2 a^2 - \frac{C_t v}{\sqrt{2} \Lambda} \bar{t} (i\gamma^5 a) t, \end{aligned} \quad (5.23)$$

where Yukawa-like coupling has been recast by the  $vev$  of the Higgs field.

#### 5.3.1 Renormalization of ALP theory

Since our purpose is to make predictions up to next to leading order in the ALP theory, we have to renormalize the Lagrangian. The renormalization procedure of the ALP sector requires the introduction of the following counter-terms:

$$\begin{aligned} a^0 &= \sqrt{Z_a} a^R, & t^0 &= \sqrt{Z_2} t^R, & m_a^0 &= Z_{m_a} m_a^R, \\ m_t^0 &= Z_{m_t} m_t^R, & C_t^0 &= Z_{C_t} C_t. \end{aligned}$$

The renormalization of Yukawa-like coupling is fixed by that of the coupling constant between ALP and top quark, such as  $Z_Y = Z_{C_t} Z_2 \sqrt{Z_a}$ . Following the canonical procedure, we introduce the  $\delta$  parameters

$$Z_i \equiv 1 + \delta_i$$



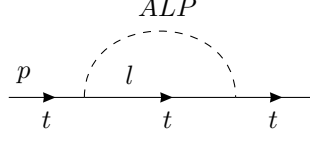


Figure 5.2: The self-interaction of quark top in the ALP top-philic theory.

where  $i = \{a, 2, m_a, m_t, Y\}$ . The EFT Lagrangian then becomes:

$$\begin{aligned}
\mathcal{L}_{EFT} = & \bar{t} (i\not{\partial} - m_t + g_s \not{G}^a T^a) t_j + \frac{1}{2} \partial_\mu a \partial^\mu a - \frac{1}{2} m_a^2 a^2 \\
& - \frac{C_t v}{\sqrt{2} \Lambda} \bar{t} (i\gamma^5 a) t + \delta_2 \bar{t} (i\not{\partial} + g_s \not{G}^a T_{ij}^a) t - (\delta_2 + \delta_{m_t}) m_t \bar{t} t \quad (5.24) \\
& + \frac{1}{2} \delta_a \partial_\mu a \partial^\mu a - \frac{1}{2} (\delta_a + \delta_{m_a}) m_a^2 a^2 - \frac{C_t v}{\sqrt{2} \Lambda} \delta_Y \bar{t} (i\gamma^5 a) t,
\end{aligned}$$

where we dropped the superscript  $R$  as it is not necessary to provide any further clarification. The renormalized theory also includes the following rules

$$\begin{aligned}
\text{---} \otimes \text{---} &= i (p^2 \delta_a - (\delta_a + \delta_{m_a}) m_a^2), \\
\text{---} \otimes \text{---} &= i (\not{p} \delta_2 - (\delta_2 + \delta_{m_t}) m_t) \delta^{ij},
\end{aligned}$$

while the counter-term of vertices are the same as equation (5.16) multiplied by  $\delta_2$  and  $\delta_Y$ , respectively. Our main goal is to make predictions on the top quark physics, assuming that ALP is involved in the interaction of this field; thus we need to compute the counter-term strictly related to top quark only, namely  $\delta_2$  and  $\delta_m$

### Wave Functions

The renormalization procedure of ALP sector, up to one-loop corrections, requires the computation of 1PI diagrams of top quark propagator. At this level of accuracy, the whole set of 1PI is composed by two diagrams: the top self-interaction and the counter-term; then the complete propagator of the top quark is

$$iG(\not{p}) = \frac{i}{\not{p} - m_t + \Sigma(\not{p})}, \quad (5.25)$$

where the sum of 1PI diagrams is  $\Sigma(\not{p}) \equiv i\Sigma_{ALP}(\not{p}) + i(\not{p}\delta_2 - (\delta_2 + \delta_{m_t}) m_t)$ , where  $\Sigma_{ALP}(\not{p})$  is the top quark self energy in the theory of ALP, whose Feynman diagram is depicted in figure 5.2. The on-shell renormalization scheme fixes the singularity of the propagator at the physical mass and its residue must be equal to the imaginary unit:

$$\not{p} + \Sigma(\not{p})|_{m_t} = m_t, \quad \lim_{\not{p} \rightarrow m_t} \frac{i(\not{p} - m_t)}{\not{p} - m_t + \Sigma(\not{p})} = i.$$

These conditions set the counter-terms

$$\delta_{m_t} = \frac{1}{m_t} \Sigma_{alP}(m_t), \quad \delta_2 = -\frac{d}{d\not{p}} \Sigma_{alP}(\not{p})|_{m_t}, \quad (5.26)$$

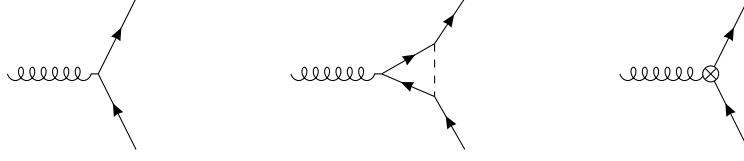


Figure 5.3: Feynman diagrams involved in the computation of the counter-term for the interaction between gluon and top quark.

The computation of the diagram can be easily addressed with Feynman variables

$$i\Sigma_{ALP}(\not{p}) = -i \frac{C_t^2 v^2}{2\Lambda^2} \delta^{ac} \frac{\mu^{2\epsilon}}{(4\pi)^{2-\epsilon}} \int_0^1 dx (m_t - \not{p}x) \frac{\Gamma(\epsilon)}{\Delta^\epsilon},$$

where, as usual, we have set  $D = 4 - 2\epsilon$ . Factorizing out  $\delta^{ac}$ , since it appears in the propagator, and applying the conditions of equation (5.26), we get

$$\begin{aligned} \delta_{m_t} &= -\frac{C_t^2 v^2}{64\pi^2 \Lambda^2} \left( \frac{1}{\epsilon} + \log\left(\frac{\tilde{\mu}^2}{m_t^2}\right) + x^2 + 1 - (x^2 - 2)x^2 \log x \right. \\ &\quad \left. + x^3 \sqrt{x^2 - 4} \log\left(\frac{\sqrt{x^2 - 4} + x}{2}\right) \right), \\ \delta_2 &= -\frac{C_t^2 v^2}{64\pi^2 \Lambda^2} \left( \frac{1}{\epsilon} + \log\left(\frac{\tilde{\mu}^2}{m_t^2}\right) + 3x^2 + 1 + (4 - 3x^2)x^2 \log x \right. \\ &\quad \left. - \frac{(10x^3 - 3x^5)}{\sqrt{x^2 - 4}} \log\left(\frac{\sqrt{x^2 - 4} + x}{2}\right) \right), \end{aligned} \quad (5.27)$$

where we defined  $x = m_a/m_t$  and  $\tilde{\mu}^2 \equiv 4\pi\mu^2 e^{-\gamma_E}$ . In the  $\overline{\text{MS}}$ -scheme the two counter-terms are equal:

$$\delta_2 = \delta_{m_t} = -\frac{C_t^2 v^2}{64\pi^2 \Lambda^2} \frac{1}{\epsilon}. \quad (5.28)$$

### Interaction Vertex

Since in ALP theory the gluon field and the strong coupling do not require to be renormalized, the counter-term of top wave function automatically fixes that of gluon-top interaction. This can be directly derived from equation (5.24). Nevertheless one can check this statement by a direct computation of  $\delta_G$ , that mathematically means to compute the Feynman diagrams represented in figure 5.3. The vertex structure is the same as that obtained by Schwinger in his famous computation for the QED vertex correction, which is fixed by Lorentz invariance and Gordon identity

$$\Gamma^\mu = \gamma^\mu F_1(k^2) + \frac{i\sigma^{\mu\nu}}{2m_t} k_\nu F_2(k^2)$$

where  $k_\nu$  denotes the photon momentum. In addition, in our case we only need to consider the color charge. Since the computation is merely a check of the result obtained in equation (5.27) we do not show it.

## 5.4 NLO amplitude of $\bar{q}q \rightarrow \bar{t}t$

A simple process, where ALP theory might be tested, is  $\bar{q}q \rightarrow \bar{t}t$  scattering, that at next-to-leading order involves the loop diagram in figure 5.4. The counter-term

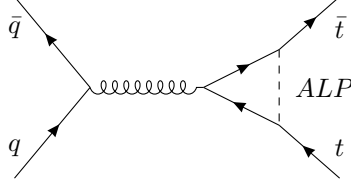


Figure 5.4: The next-to-leading order diagram for the scattering process  $\bar{q}q \rightarrow \bar{t}t$ .

$\delta_2$  computed in previous section is necessary to remove the divergent terms from the amplitude. The computation, which is quite long and complex, was made in `Mathematica` powered by the package `FeynCalc`, by making use of Passarino-Veltman reduction technique. Nevertheless, the following  $C_0$  scalar integral will show up in the solution

$$\begin{aligned} C_0 &\equiv C_0(s, m_t^2, m_t^2, m_t^2 m_t^2, x^2 m_t^2) \\ &= \frac{1}{i\pi^2} \int d^4l \frac{1}{(l^2 - m_t^2)((l + \sqrt{s})^2 - m_t^2)((l + m_t)^2 - x^2 m_t^2)}, \end{aligned}$$

where  $x = m_a/m_t$ . The `X-package` returns the full solution of this integral<sup>3</sup>, that we simplified by operating an expansion series over  $x$  in each Di-Logarithm that appears in the solution, the series has been truncated at  $O(x)$ , however, since the coefficient of  $C_0$  is proportional to  $x^2$ , the full amplitude will be a  $O(x^3)$ . Additionally, the properties of Di-Log

$$\begin{aligned} \text{Li}_2\left(\frac{1}{1-z}\right) &= \text{Li}_2(z) - \frac{1}{2} \log^2(1-z) + \log(-z) \log(1-z) + \frac{\pi^2}{6}, \\ \text{Li}_2\left(\frac{z}{z-1}\right) &= -\text{Li}_2(z) - \frac{1}{2} \log^2(1-z), \end{aligned}$$

have been applied to simplify the computation that results in

$$\begin{aligned} C_0 &= -\frac{1}{3} (12\text{Li}_2(z) - 12i \log(x)(\pi - i \log(z)) - 3 \log^2(z) + 6 \log(1-z) \log(z) \\ &\quad - 6i\pi \log(z) + 6i\pi \log(1-z) + 6 \log(1-z) \log(-z) + 4\pi^2) \end{aligned}$$

where

$$z = \frac{1-v}{1+v} \quad \text{and} \quad v = \sqrt{1 - \frac{4m_t^2}{s}}, \quad (5.29)$$

<sup>3</sup>The computation can be also performed by Feynman variables techniques, however, the computation is far from being straight and it requires specific steps, as for instance a shift on the inner Feynman variable that linearizes the denominator of the integrand function respect to external variable. Then the order of integration can be reversed according to Fubini's theorem.

with  $s = (p_{\bar{q}} + p_q)^2$ , therefore the condition  $s \geq 4m_t^2$  can be rendered as  $0 \leq v < 1$  and  $0 < z \leq 1$ , with  $z$  that reaches its maximum value when the energy involved in the process achieves its minimum.

The NLO amplitude, which is given by the sum of tree-level diagram, one loop diagram and its counter-term, at order  $O(x^3)$  is written in equation (A.30).

### 5.4.1 Scalar Axion-like Particles

The results shown up to this point have been obtained by considering ALP as a pseudoscalar field, however, we can repeat every computation for a scalar particle.

Starting from Yukawa vertex:

$$\begin{aligned} V &\approx g\bar{\psi}\phi\psi && \text{scalar case} \\ V &\approx g\bar{\psi}(i\gamma^5)\phi\psi && \text{pseudo-scalar case} \end{aligned}$$

Comparing the second line of this equation with the interaction term in equation (5.23), we get:

$$g \equiv -\frac{C_{qt}v}{\sqrt{2}\Lambda},$$

therefore, the theory for scalar ALP is:

$$\mathcal{L}_{EFT} = \bar{t}(i\cancel{\partial} - m_t + g_s G^a T^a) t_j + \frac{1}{2}\partial_\mu a \partial^\mu a - \frac{1}{2}m_a^2 a^2 - \frac{C_t v}{\sqrt{2}\Lambda} \bar{t} a t. \quad (5.30)$$

The interaction vertex between ALP and top quark is

$$\mathcal{V}_s^Y = -\frac{iC_t v}{\sqrt{2}\Lambda} \delta^{ab}. \quad (5.31)$$

The same renormalization procedure described for pseudoscalar case can be repeated for scalar ALP. The counter-terms are

$$\begin{aligned} \delta_{m_t} &= \frac{C_t^2 v^2}{64\pi^2 \Lambda^2} \left( \frac{3}{\epsilon} + 3 \log\left(\frac{\tilde{\mu}^2}{m_t^2}\right) - x^2 + 7 + (x^2 - 6)x^2 \log(x) \right. \\ &\quad \left. + x(4 - x^2) \sqrt{x^2 - 4} \log\left(\frac{\sqrt{x^2 - 4} + x}{2}\right) \right) \\ \delta_2 &= \frac{C_t^2 v^2}{64\pi^2 \Lambda^2} \left( -\frac{1}{\epsilon} - \log\left(\frac{\tilde{\mu}^2}{m_t^2}\right) - 3x^2 + 7 + (3x^2(x^2 - 4) + 8) \log(x) \right. \\ &\quad \left. - \frac{3x(x^4 - 6x^2 + 8)}{\sqrt{x^2 - 4}} \log\left(\frac{\sqrt{x^2 - 4} + x}{2}\right) \right). \end{aligned} \quad (5.32)$$

Even for scalar case we proved that in the  $\overline{\text{MS}}$ -scheme the equality  $\delta_2 = \delta_G$  still holds.

The NLO amplitude of the scattering process  $\bar{q}q \rightarrow \bar{t}t$  was obtained also in scalar theory and its expression is given in equation (A.32)

### 5.4.2 Massless Limit

An interesting case of study is the ALP massless theory. We computed the ALP massless limit for the NLO amplitude of  $q\bar{q} \rightarrow t\bar{t}$  in both pseudoscalar and scalar theories.

From literature [3], we know that the amplitude of a process involving the real emission of a massless scalar particle is divergent, however, this infrared divergency is absorbed by the NLO amplitude of the same process without the real emission. In fact, in perturbation theory real emission graphs are of the same order as one-loop amplitudes.

Since the NLO amplitude, computed above, represents the regulator of the process with a real ALP emission, we expected that its massless limit is divergent for the scalar theory, indeed

$$\begin{aligned} \lim_{m_a \rightarrow 0} i\mathcal{M}_{scalar} &= \infty, \\ \lim_{m_a \rightarrow 0} i\mathcal{M}_{pseudo} &= T_{a_1 a_2}^{g_1} T_{a_3 a_4}^{g_1} \bar{v}(p_2) \gamma_\mu u(p_1) \\ &\quad \times \bar{u}(p_3) \frac{z(i \log(z) - \pi) (m_t(z+1)^2 \gamma^\mu - 2iz(p_3 + p_4)^\mu)}{64\pi^4 m_t^3 (z-1)(z+1)^3} v(p_4), \end{aligned}$$

which confirms that the real emission amplitude of a scalar ALP particle presents an IR divergence.

## 5.5 Yukawa Potential in the non-Relativistic Limit

In this section we will compute the behavior of the Yukawa potential between two top quarks that interact by exchanging an ALP particle, both in the pseudo-scalar and scalar theory. The result is obtained in the non-relativistic (NR) limit. We will proceed by computing the amplitudes in the effective field theory, then we will apply the non-relativistic limit and by comparing with the Born approximation for non-relativistic quantum theory, we will obtain the Yukawa potential.

In the effective field theory of top-philic ALP, the interaction occurs when a *top quark* and an *anti-top quark* exchanges a virtual ALP, hence the scattering process can take place either through *s-channel* and *t-channel*.

First of all, we must check the sign of Wick contraction. Starting from the s-channel (time flows from left to the right), without taking care of the coupling constant that could be imaginary or real:

The diagram shows an s-channel exchange of an ALP particle between a top quark and an anti-top quark. On the left, an incoming top quark with momentum  $p$  and an incoming anti-top quark with momentum  $q$  meet at a vertex. A dashed line representing the ALP particle with momentum  $k$  connects this vertex to another vertex on the right. From the right vertex, an outgoing top quark with momentum  $p'$  and an outgoing anti-top quark with momentum  $q'$  emerge. The diagram is equated to a mathematical expression involving a time-ordered product of two fermion bilinears:

$$= \langle \mathbf{p}', \mathbf{q}' | (1/2!) \int d^4x (\bar{\psi}\psi)_x \int d^4y (\bar{\psi}\psi)_y | \mathbf{p}, \mathbf{q} \rangle \quad (5.33)$$

where the factor  $(1/2!)$  coming from Taylor series of the time-ordering product is always canceled by the  $2!$  ways of realize the Wick contraction. The initial and final

states are labeled as:

$$|\mathbf{p}, \mathbf{q}\rangle \sim a_{\mathbf{p}}^{\dagger} a_{\mathbf{q}}^{\dagger} |0\rangle \quad \langle \mathbf{p}, \mathbf{q}| \sim \langle 0| a_{\mathbf{q}} a_{\mathbf{p}}$$

so that  $(|\mathbf{p}, \mathbf{q}\rangle)^{\dagger} = \langle \mathbf{p}, \mathbf{q}|$ . Where  $a_{\mathbf{p}}^{s\dagger}$  and  $a_{\mathbf{p}}^s$  are the creation and annihilation operators of the particle. Thus,

$$|\mathbf{p}, s\rangle = \sqrt{2E_{\mathbf{p}}} a_{\mathbf{p}}^{s\dagger} |0\rangle \quad \langle \mathbf{p}, s| = \langle 0| a_{\mathbf{p}}^s \sqrt{2E_{\mathbf{p}}}$$

with the usual normalization convention

$$\langle \mathbf{p}, s | \mathbf{q}, r \rangle = (2\pi)^3 \delta^3(\mathbf{p} - \mathbf{q}) \delta_{rs}. \quad (5.34)$$

The quantized Dirac fermion and anti-fermion are

$$\begin{aligned} \psi(x) &= \int \frac{d^3p}{(2\pi)^3} \frac{1}{\sqrt{2E_{\mathbf{p}}}} \sum_s (a_{\mathbf{p}}^s u^s(p) e^{-ipx} + b_{\mathbf{p}}^{s\dagger} v^s(p) e^{ipx}), \\ \bar{\psi}(x) &= \int \frac{d^3p}{(2\pi)^3} \frac{1}{\sqrt{2E_{\mathbf{p}}}} \sum_s (a_{\mathbf{p}}^{s\dagger} \bar{u}^s(p) e^{ipx} + b_{\mathbf{p}}^s \bar{v}^s(p) e^{-ipx}), \end{aligned}$$

where  $b_{\mathbf{p}}^{s\dagger}$  and  $b_{\mathbf{p}}^s$  are the creation and annihilation operators for the antiparticles. The initial and final states embedding a particle or an antiparticle generated by the Dirac field are

$$\begin{aligned} \psi(x) | \mathbf{p}, s \rangle &= u^s(p) e^{-ipx} |0, \rangle & \langle \mathbf{p}, s | \psi(x) &= \langle 0 | v^s(p) e^{ipx}, \\ \bar{\psi}(x) | \mathbf{p}, s \rangle &= \bar{v}^s(p) e^{-ipx} |0, \rangle & \langle \mathbf{p}, s | \bar{\psi}(x) &= \langle 0 | \bar{u}^s(p) e^{ipx}, \end{aligned}$$

where the normal modes  $u(x)$  and  $\bar{u}(x)$  decode for an incoming and outgoing particles respectively, while  $\bar{v}(x)$  and  $v(x)$  decode for an incoming and outgoing antiparticles.

To untangle the operators in the amplitude we can move each field functions close to the corresponding operator, taking into account the anti-commutation relation for Dirac field. After the integrations over the space-time points and the transferred momentum, we obtain the amplitude in the s-channel:

$$i\mathcal{M}^s = (2\pi)^4 \delta^4(p + q - p' - q') \frac{i}{k^2 - m_a^2} \bar{v}(q) u(p) \bar{u}(p') v(q'), \quad (5.35)$$

where  $p$  and  $q$  are the incoming momenta and  $p'$  and  $q'$  the outgoing momenta. The energy conservation reads  $k = p + q$  or  $k = p' + q'$ , where  $k$  is the four-momentum of the ALP.

Following the same procedure for the t-channel, we get:

$$i\mathcal{M}^t = -(2\pi)^4 \delta^4(p + q - p' - q') \frac{i}{k^2 - m_a^2} \bar{u}(p') u(p) \bar{v}(q) v(q'), \quad (5.36)$$

note that the energy conservation now is  $k = p - p'$  and  $k = q' - q$ . In particular, expression (5.36) agrees with literature [3], where authors usually calculate the Yukawa-interaction for processes that involve only particles, as  $p + q \rightarrow p' + q'$ . They find a positive untangled amplitude, however it is well-known that the trade

of a pair of particles for a pair of anti-particles introduces a minus sign. Summing the two amplitudes:

$$i\mathcal{M} = i(2\pi)^4 \delta^4(p + q - p' - q') \times \left( \frac{1}{(p+q)^2 - m_a^2} \bar{v}(q) u(p) \bar{u}(p') v(q') - \frac{1}{(p-p')^2 - m_a^2} \bar{u}(p') u(p) \bar{v}(q) v(q') \right).$$

Note that up to this point, we did not specify if the ALP involved in the computation is a scalar or a pseudoscalar field. We can easily make this distinction by introducing the vertex operator between ALP and Dirac spinors. Since vertex operators are:

$$\mathcal{V}_{PS} = \frac{C_t v}{\sqrt{2}\Lambda} \gamma^5, \quad \mathcal{V}_S = -i \frac{C_t v}{\sqrt{2}\Lambda}, \quad (5.37)$$

the amplitudes become

$$i\mathcal{M}_{PS} = i \left( \frac{C_t v}{\sqrt{2}\Lambda} \right)^2 (2\pi)^4 \delta^4(p + q - p' - q') \times \left( \frac{1}{(p+q)^2 - m_a^2} \bar{v}(q) \gamma^5 u(p) \bar{u}(p') \gamma^5 v(q') - \frac{1}{(p-p')^2 - m_a^2} \bar{u}(p') \gamma^5 u(p) \bar{v}(q) \gamma^5 v(q') \right), \quad (5.38)$$

$$i\mathcal{M}_S = i \left( \frac{C_t v}{\sqrt{2}\Lambda} \right)^2 (2\pi)^4 \delta^4(p + q - p' - q') \times \left( \frac{1}{(p+q)^2 - m_a^2} \bar{v}(q) u(p) \bar{u}(p') v(q') - \frac{1}{(p-p')^2 - m_a^2} \bar{u}(p') u(p) \bar{v}(q) v(q') \right).$$

In order to perform the NR limit, the spinors chains must be evaluated. The suitable form of Dirac spinors to work in the NR limit is:

$$u_s(p) = \sqrt{\frac{E_{\mathbf{p}} + m}{2E_{\mathbf{p}}}} \begin{pmatrix} \chi_s \\ \frac{\mathbf{p} \cdot \boldsymbol{\sigma}}{E_{\mathbf{p}} + m} \chi_s \end{pmatrix} \quad v_s(-q) = \sqrt{\frac{E_{\mathbf{q}} + m}{2E_{\mathbf{q}}}} \begin{pmatrix} \frac{-\mathbf{q} \cdot \boldsymbol{\sigma}}{E_{\mathbf{q}} + m} \eta_r \\ \eta_r \end{pmatrix}$$

where  $\chi$  and  $\eta$  are 2-components spinors. The appropriate representation of gamma matrices to perform the NR limit is Dirac representation:

$$\gamma^0 = \begin{pmatrix} \mathbf{1} & 0 \\ 0 & -\mathbf{1} \end{pmatrix}, \quad \gamma^5 = \begin{pmatrix} 0 & \mathbf{1} \\ \mathbf{1} & 0 \end{pmatrix}.$$

In NR limit  $E_{\mathbf{p}'} \approx E_{\mathbf{p}} \approx m_t$ , thus:

$$\bar{u}_{s'}(p') u_s(p) = \chi_{s'}^\dagger \left( 1 - \frac{(\mathbf{p}' \cdot \boldsymbol{\sigma}_z)(\mathbf{p} \cdot \boldsymbol{\sigma}_z)}{4m_t^2} \right) \chi_s,$$

where  $\sigma_z$  are nothing but Pauli matrices for the top quark. For the anti-top we have:

$$\bar{v}_r(q) v_{r'}(q') = -\eta_r^\dagger \left( 1 - \frac{(\mathbf{q} \cdot \boldsymbol{\sigma}_{\bar{z}})(\mathbf{q}' \cdot \boldsymbol{\sigma}_{\bar{z}})}{4m_t^2} \right) \eta_{r'},$$

where  $\sigma_{\bar{x}}$  are the Pauli matrices for the anti-top quark. The corresponding spinor chains in the pseudoscalar case are:

$$\begin{aligned}\bar{u}_{s'}(p') \gamma^5 u_s(p) &= \chi_{s'}^\dagger \frac{(\mathbf{p} - \mathbf{p}') \cdot \boldsymbol{\sigma}_z}{2m_t} \chi_s = \chi_{s'}^\dagger \frac{\mathbf{k}^t \cdot \boldsymbol{\sigma}_x}{2m_t} \chi_s, \\ \bar{v}_r(q) \gamma^5 v_{r'}(q') &= \eta_r^\dagger \frac{(\mathbf{q}' - \mathbf{q}) \cdot \boldsymbol{\sigma}_{\bar{z}}}{2m_t} \eta_{r'} = \eta_r^\dagger \frac{\mathbf{k}^t \cdot \boldsymbol{\sigma}_{\bar{x}}}{2m_t} \eta_{r'},\end{aligned}$$

where  $\mathbf{k}^t$  stands for the transferred momentum in t-channel. Thus, in scalar case there is an extra minus sign compared to pseudoscalar case. For s-channel, we have:

$$\begin{aligned}\bar{v}_r(q) u_s(p) &= -\eta_r^\dagger \frac{(\mathbf{p} + \mathbf{q}) \cdot \boldsymbol{\sigma}}{2m_t} \chi_s = -\eta_r^\dagger \frac{\mathbf{k}^s \cdot \boldsymbol{\sigma}}{2m_t} \chi_s, \\ \bar{u}_{s'}(p') v_{r'}(q') &= -\chi_{s'}^\dagger \frac{(\mathbf{p}' + \mathbf{q}') \cdot \boldsymbol{\sigma}}{2m_t} \eta_{r'} = -\chi_{s'}^\dagger \frac{\mathbf{k}^s \cdot \boldsymbol{\sigma}}{2m_t} \eta_{r'}, \\ \bar{v}_r(q) \gamma^5 u_s(p) &= -\eta_r^\dagger \left( 1 + \frac{(\mathbf{q} \cdot \boldsymbol{\sigma}_{\bar{z}})(\mathbf{p} \cdot \boldsymbol{\sigma}_z)}{4m_t^2} \right) \chi_s, \\ \bar{u}_{s'}(p') \gamma^5 v_{r'}(q') &= \chi_{s'}^\dagger \left( 1 + \frac{(\mathbf{p}' \cdot \boldsymbol{\sigma}_z)(\mathbf{q}' \cdot \boldsymbol{\sigma}_{\bar{z}})}{4m_t^2} \right) \eta_{r'},\end{aligned}$$

here  $\mathbf{k}^s$  stands for the transferred momentum in s-channel. Now the extra minus sign appears in pseudo-scalar case, thus the sign of the two amplitudes, up to this point, is the same.

Furthermore, in NR limit holds:

$$\begin{aligned}(k^t)^2 &= (p - p')^2 \approx (0, \mathbf{p} - \mathbf{p}')^2 = -(\mathbf{k}^t)^2, \\ (k^s)^2 &= (p + q)^2 \approx (2m_t, 0)^2 = 4m_t^2,\end{aligned}$$

therefore, the scalar propagators read:

$$\begin{aligned}t - \text{channel}) \quad & \frac{1}{k^2 - M_a^2} \approx -\frac{1}{(\mathbf{k}^t)^2 + M_a^2} \\ s - \text{channel}) \quad & \frac{1}{k^2 - M_a^2} \approx \frac{1}{4m_t^2 - M_a^2}\end{aligned}$$

Substituting these results in equation (5.38), we can obtain the amplitudes in the non-relativistic limit. Since our ALP is a light particle, we have  $2m_t \gg M_a$ , thus the amplitudes can be truncated at order  $O(1/(4m_t^2)^2)$ , this results in a complete suppression of the s-channel in scalar case, while only its leading order survives in pseudoscalar case. Comparing the amplitudes with Born approximation of quantum mechanics

$$\langle f | iT | i \rangle = -i\tilde{V}(\mathbf{k}) (2\pi)^4 \delta(E_f - E_i) \delta(\mathbf{p}_f - \mathbf{p}_i),$$

we will obtain the Yukawa potentials. The comparison must take into account the normalisation prescription of initial and final states, that in quantum mechanics is  $\langle \mathbf{p} | \mathbf{q} \rangle = (2\pi)^3 \delta(\mathbf{p} - \mathbf{q})$ , which is equivalent to the normalisation of our quantum field theory, given by equation (5.34). Moreover, to remove the bi-spinor we must notice that choosing their value, we are fixing the initial and final helicity states, hence:

$$\chi_s^\dagger \eta_r = \eta_r^\dagger \chi_s = \delta_{sr} \qquad \chi_s^\dagger [M]_{2 \times 2} \eta_r = [M]_{sr}$$



Setting  $\mathbf{k} \equiv \mathbf{k}^t$

$$\begin{aligned}\tilde{V}_{PS}(\mathbf{k}) &= - \left( \frac{C_t v}{\sqrt{2} \Lambda} \right)^2 \left( - \frac{\delta_{s r} \delta_{s' r'}}{4m_t^2} + \frac{[\mathbf{k} \cdot \boldsymbol{\sigma}_z]_{s' s} [\mathbf{k} \cdot \boldsymbol{\sigma}_{\bar{z}}]_{r r'}}{(\mathbf{k}^2 + m_a^2) 4m_t^2} \right), \\ \tilde{V}_S(\mathbf{k}) &= - \left( \frac{C_t v}{\sqrt{2} \Lambda} \right)^2 \frac{1}{\mathbf{k}^2 + m_a^2} \\ &\quad \times \left( \delta_{s s'} \delta_{r r'} - \frac{\delta_{r r'} [(\mathbf{p}' \cdot \boldsymbol{\sigma}_z) (\mathbf{p} \cdot \boldsymbol{\sigma}_z)]_{s' s}}{4m_t^2} - \frac{\delta_{s s'} [(\mathbf{q} \cdot \boldsymbol{\sigma}_{\bar{z}}) (\mathbf{q}' \cdot \boldsymbol{\sigma}_{\bar{z}})]_{r r'}}{4m_t^2} \right).\end{aligned}$$

### Yukawa Potential for Scalar ALP

Making use of relation (A.4), we can simplify the second term in the bracket of the scalar potential. Then performing a Fourier transformation, we obtain the potential as a function of space-time coordinates. Changing from linear to polar coordinates, then  $d^3k \rightarrow dk d\theta d\varphi k^2 \sin\theta$ , with  $k \in [-\infty, +\infty]$ ,  $\theta \in [0, \pi]$  and  $\varphi \in [0, 2\pi]$ . The integration is now straight, and the potential is

$$\begin{aligned}V_S(\mathbf{x}) &= - \left( \frac{C_t v}{\sqrt{2} \Lambda} \right)^2 \frac{e^{-m_a x}}{4\pi x} \delta_{s s'} \delta_{r r'} \\ &\quad + \left( \frac{C_t v}{\sqrt{2} \Lambda} \right)^2 \frac{e^{-m_a x}}{4\pi x} \left[ \frac{\delta_{s s'} \delta_{r r'} (\mathbf{p}^2 + \mathbf{q}^2)}{4m_t^2} \right. \\ &\quad \left. - i \left( m_a + \frac{1}{x} \right) \left( \frac{\delta_{r r'} [(\hat{\mathbf{x}} \cdot \boldsymbol{\sigma}_z) (\mathbf{p} \cdot \boldsymbol{\sigma}_z)]_{s' s}}{4m_t^2} - \frac{\delta_{s s'} [(\mathbf{q} \cdot \boldsymbol{\sigma}_{\bar{z}}) (\hat{\mathbf{x}} \cdot \boldsymbol{\sigma}_{\bar{z}})]_{r r'}}{4m_t^2} \right) \right],\end{aligned}\tag{5.39}$$

where  $\partial^i x = x^i/x = \hat{x}^i$ . The first addend returns the well-known Yukawa potential of an interaction mediated by a scalar particle. In agreement with literature, the potential is universally attractive. On the contrary, the other terms, that represent higher-order corrections introduce a repulsive adjustment – being of opposite sign.

### Yukawa Potential for Pseudoscalar ALP

For the purpose of obtaining the pseudoscalar potential, we have to replicate the procedure employed in scalar case

$$V_{PS}(\mathbf{x}) = \left( \frac{C_t v}{\sqrt{2} \Lambda} \right)^2 \left( \frac{\delta_{s r} \delta_{s' r'} \delta^{(3)}(\mathbf{x})}{4m_t^2} + \frac{[\boldsymbol{\nabla} \cdot \boldsymbol{\sigma}_z]_{s' s} [\boldsymbol{\nabla} \cdot \boldsymbol{\sigma}_{\bar{z}}]_{r r'}}{4m_t^2} \frac{e^{-m_a x}}{4\pi x} \right),$$

where the derivatives of the second term can be rewritten as:

$$\begin{aligned}V_{PS}(\mathbf{x}) &= \left( \frac{C_t v}{\sqrt{2} \Lambda} \right)^2 \frac{m_a^2 e^{-M_a x}}{(4m_t^2) 12\pi x} \\ &\quad \times \left[ [S_{z\bar{z}}]_{s' s r r'} \left( 1 + \frac{3}{m_a x} + \frac{3}{(m_a x)^2} \right) + [\boldsymbol{\sigma}_z]_{s' s} \cdot [\boldsymbol{\sigma}_{\bar{z}}]_{r r'} \right],\end{aligned}\tag{5.40}$$

for a more detailed explanation, see Appendix A.7.2. In previous equation, the spin tensor operator  $S_{12} = 3(\boldsymbol{\sigma}_1 \cdot \hat{\mathbf{x}})(\boldsymbol{\sigma}_2 \cdot \hat{\mathbf{x}}) - \boldsymbol{\sigma}_1 \cdot \boldsymbol{\sigma}_2$  has been introduced, with Pauli

matrices; the latter represent the top and anti-top spins. Given that the spin value is  $1/2$  for both particle and anti-particle, the total spin of the system belongs to  $S = \{0, 1\}$ . Assuming that spins are oriented along  $\hat{\mathbf{x}}$ , then  $(\boldsymbol{\sigma}_z \cdot \hat{\mathbf{x}})$  and  $(\boldsymbol{\sigma}_{\bar{z}} \cdot \hat{\mathbf{x}})$  can only be  $\pm 1/2$ , consequently  $(\boldsymbol{\sigma}_z \cdot \boldsymbol{\sigma}_{\bar{z}})$  can take the values  $\pm 1/4$ , depending on the relative alignment. Accordingly to that, the spin tensor operator belongs to  $S_{z\bar{z}} = \{-1/2, 1/2\}$ , with the negative value for the anti-aligned configuration.

In conclusion, the overall sign of the pseudo-scalar potential depends on the relative alignment of spins in the initial states: when the spins of the top quark is anti-aligned to that of anti-top, the total spin sums zero and an attractive potential with an overall negative sign arises ( $S = 0$  and  $S_{z\bar{z}} = -1/2$ ); on the contrary, when the spin of the top quark is aligned to that of anti-top, a repulsive potential with positive overall sign ( $S = 1$  and  $S_{z\bar{z}} = 1/2$ ) rules the interaction.

## 5.6 Conclusions and Outlook

In this section we started by presenting the Strong CP Problem, which most famous solution relies on the introduction of a new spontaneously broken symmetry, i.e.,  $U_{PQ}(1)$ , whose Goldstone boson is called axion. Subsequently, we saw that experimental efforts in the searching for axions are mostly investigating its interaction with photon field, that has nothing in common with Strong CP problem, thus paving the way for ALP theories. In particular we presented the most general Lagrangian for ALP up to dimension-5 operators, that involves democratic operators that couple ALP field with fermions of the SM. A phase rotation of the latter, including also Higgs field, yields to a new theory that is completely equivalent to the previous from the physical point of view, but which highlights that ALP coupling with heavy fermions are preferred.

The new top-philic theories – one for scalar and one for pseudoscalar ALP – were renormalized in order to compute NLO amplitudes, as we did for  $\bar{q}q \rightarrow \bar{t}t$ , and cross-section that can be compared with experimental data in order to set the free parameters of the Lagrangian, namely the mass of the ALP and the coupling constant for the interaction with top quark. Both EFTs were implemented into `FeynRules` to generate the model files in the UFO format, which have been upload on `Madgraph5_aMC@NLO` and a preliminary analysis was already performed. Specifically, with the theories of ALP we tried to recover the discrepancy between experimental data and theory prediction highlighted by both ATLAS and CMS in the scattering process  $pp \rightarrow \bar{t}t$ . Each top rapidly decays in a bottom quark by emitting a  $W$  boson, which in turn leptonically decays<sup>4</sup> in a pair of a charged and a neutral leptons. The signature of the final state is then a pair of charged leptons plus some missing energy of the two undetected neutral leptons. In particular ATLAS and CMS measured the differential cross-section as a function of the di-lepton  $\Delta\phi$ , i.e., the azimuthal angle between the two charged leptons in the final state. The results of their analysis can be found for in [199, 199], however, the state of art of this discrepancy stands out from figure 5.5 [201]. The lower plot shows that within the Standard Model at NNLO, the expected behavior of cross-section is increasing as the azimuthal angle between the two charged leptons grows, while data

<sup>4</sup>The  $W^\pm$  boson can decay in a leptonic or hadronic state, thus a selection occurs to record the necessary data. Moreover the letonic decay is easiest to track at LHC.

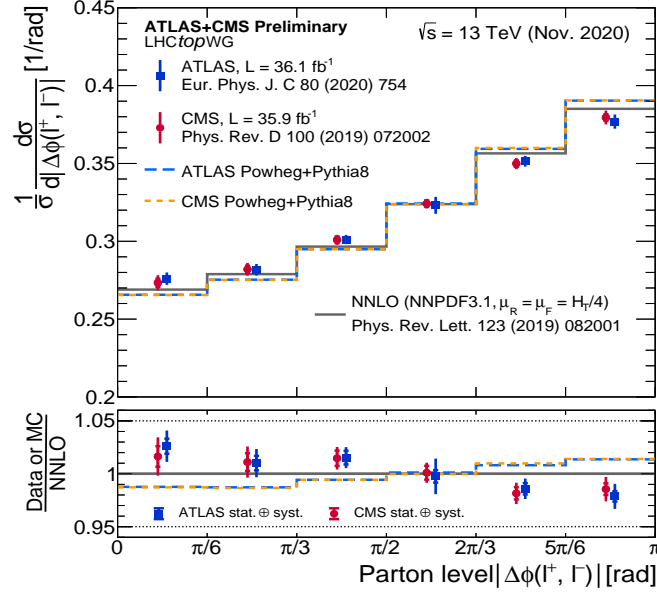


Figure 5.5: Normalized differential cross-section as function of the di-lepton  $\Delta\phi$ . The charged leptons are produced by the scattering process  $pp \rightarrow \bar{t}t$ , at  $\sqrt{s} = 13$  TeV where the pairs of top quarks decay weakly and  $W^\pm$  decays in turn in a leptonic final state. The plot is taken from the LHCPHysics Web [201].

records the opposite trend. Including ALP in the theory, the main process becomes  $pp \rightarrow \bar{t}t ALP$ , that keeps the signature of the original scattering since ALP is undetected. Thus, we can fix the free parameters of the theory by fitting experimental data, however, a preliminary result shows that adding a pseudoscalar ALP to SM, the divergence deepens; on the contrary, by adding a scalar ALP the discrepancy becomes narrower, suggesting that our investigations should be directed primarily towards the latter.

In conclusion, the research on axions-like particles – not necessarily restricted to a top-philic theory – has a lot of potential since it might represent a compelling solution to more than one open problem in fundamental physics. In addition to those mentioned in this thesis, not only ALPs are suitable as dark matter candidate [189, 202] but also several proposals have been made to solve the enigmatic question of the anomalous magnetic moment of the muon (muon  $g - 2$ ), by mainly exploring the phenomenology of coupling with photons [204, 203, 205], which generates a NNLO contribution to muon  $g - 2$ . Axions and ALPs are also included in specific supersymmetric theories where PQ symmetry breaking is often related to supersymmetry breaking [206].



# Conclusions

The Standard Model of particle physics is not only an elegant framework for compactly describing three of the four fundamental interactions, but it has also proven to be very successful in predicting experimental data. Nevertheless, several phenomena, from dark matter to baryon asymmetry, do not find any explanation within SM. This theory, in fact, might be understood as a low-energy effective description of Nature which approximates an underlying more comprehensive theory. Besides that, the lack of direct evidences of new physics at LHC, probably because of an insufficient energy level, further complicates theoretical research. It would be inaccurate to state that deviations from predictions have not already been observed since small discrepancies occur in many sectors of SM, from leptonic universality, through top quark physics to muon  $g - 2$ , to name a few. At present time, however, there is no conclusive confirmation of new physics; with a deviation of approximately  $4\sigma$ , muon  $g - 2$  is the measurement with the largest deviation from the theoretical prediction and it could be a window for new physics in the next future. In the meantime, we are forced to conduct a thorough search in data to identify additional deviations. This suggests that effective field theory might represent the suitable facility to address with open problems of physics because higher-order operators could account for small deviations.

In this thesis, we applied the effective field theory approach to three different topics. Firstly, we demonstrated that light-by-light scattering might represent a preferred channel to look for higher-spin particles, like string excitations or strongly-interacting bound states, since the coefficients of effective vertices are highly dependent on the spin of the particle running in the loop. Light-by-light scattering is extremely difficult to detect, although it has recently been discovered that it is accessible at LHC since a large electromagnetic field strengths is generated by ultra-relativistic colliding lead ions, therefore more precise experimental data will be available in the near future.

Furthermore, we employed EFTs in the description of Dark Matter. Hypothesising an interaction between a new fermionic dark matter field and an hypercharge form factor, we were able to address the issue of gauge invariance at high scales already identified as a problem in previous works. Available implementations with the electromagnetic form factors have a limited region of validity well below the electroweak scale. Moreover, we proved that dark matter coupling to  $F_{\mu\nu}$ , signals gauge-violating processes at high energies. On the contrary, the gauge invariance is restored by coupling dark matter with the  $B$  gauge boson. The choice to couple dark matter with the hypercharge field is ruled by the relevant energy scale ac-

cessible by processes involving dark matter, which can be way larger than the EW scale. Besides photon annihilation channel, the hypercharge EFT involves the  $Z$  boson channel. A direct consequence is that the constraint coming from the invisible decay width of  $Z$  boson affects the parameters region of low dark matter masses. Moreover, in the gauge-violating theory, the process  $W^+W^- \rightarrow \chi\chi$  provides large unphysical contributions in collider experiments, which would lead to the incorrect result that indirect detection experiments have a better sensitivity than direct searches for high values of dark matter masses. Thus, the hypercharge form factors correctly describe the electromagnetic effective interactions of dark matter at energies relevant for dark matter and collider searches.

Finally, we studied a new physics model featuring axion-like particles. Specifically, we started with the most general Lagrangian, up to dimension-5 operators, that democratically couples an ALP to each SM field. Performing a chiral rotation of SM matter fields and Higgs doublet, we obtain a reformulation of the theory, completely equivalent to the previous one, which however highlights that the couplings of ALPs with heavy fermions are preferred. Hence, we switched to a top-philic theory for ALP and investigated its phenomenological implications, focusing on next-to-leading-order processes that involves ALPs in loops,  $\bar{t}t$  interaction mediated by ALP and distribution of proton-proton collisions where a pair of top quarks constitutes the final states.

Effective field theories have proven to be a suitable tool for search of physics beyond the Standard Model. On one hand, they introduce the advantage of a quite model independent description; on the other hand, by admitting high-dimensional operators they contribute to a natural explanation of small deviations from the four-dimensional theory. In fact, as long as direct evidence of new physics is missing, the efforts should be concentrated on indirect searches, whose limit is determined by both accuracy of measurements and precision of the theoretical calculations. This thesis provides a further proof that EFT can be employed in the development of new theories that, implementing the Standard Model, will lead to a better understanding of Nature.







## A.1 Pauli Matrices

Pauli matrices were identified at first by W. Pauli while obtaining the Schrödinger-Pauli equation<sup>1</sup> for a non-relativistic quantum particle with 1/2-spin. In fact, introducing Pauli matrices the equation assumes a more compact form.

Pauli matrices are a set of three  $2 \times 2$  matrices

$$\sigma_1 = \begin{pmatrix} 0 & 1 \\ 1 & 0 \end{pmatrix} \quad \sigma_2 = \begin{pmatrix} 0 & -i \\ i & 0 \end{pmatrix} \quad \sigma_3 = \begin{pmatrix} 1 & 0 \\ 0 & -1 \end{pmatrix}. \quad (\text{A.1})$$

It is straight to prove that Pauli matrices are Hermitian and unitary:

$$\sigma_i = \sigma_i^\dagger \quad \sigma_i^{-1} = \sigma_i^\dagger,$$

from which follows

$$\sigma_1^2 = \sigma_2^2 = \sigma_3^2 = -i\sigma_1\sigma_2\sigma_3 = \mathbf{1}.$$

In addition,  $\sigma$  matrices have null trace and  $\det \sigma_i = -1$ .

Pauli matrices satisfy the following commutation and anti-commutations relations

$$[\sigma_i, \sigma_j] = 2i\epsilon_{ijk}\sigma_k \quad \{\sigma_i, \sigma_j\} = 2i\delta_{ij}\mathbf{1}, \quad (\text{A.2})$$

whose sum leads to

$$\sigma_i\sigma_j = \delta_{ij}\mathbf{1} + i\epsilon_{ijk}\sigma_k. \quad (\text{A.3})$$

Contracting with the components of the 3-vectors  $a_i$  and  $b_j$  (that commutes with  $\sigma_i$ )

$$(\mathbf{a} \cdot \boldsymbol{\sigma})(\mathbf{b} \cdot \boldsymbol{\sigma}) = (\mathbf{a} \cdot \mathbf{b})\mathbf{1} + i(\mathbf{a} \times \mathbf{b}) \cdot \boldsymbol{\sigma} \quad (\text{A.4})$$

where  $\boldsymbol{\sigma} = (\sigma_1, \sigma_2, \sigma_3)$ , while in the Minkowski space-time they form, together with the identity matrix, the following four-vectors

$$\sigma^\mu = (\mathbf{1}, \boldsymbol{\sigma}) \quad \bar{\sigma}^\mu = (\mathbf{1}, -\boldsymbol{\sigma}).$$

Moreover, the set composed by identity matrix and Pauli matrices, form a basis for the  $2 \times 2$  Hermitian matrices. The commutation relation in equation (A.2) is equivalent to that of Lie Algebra of the group  $SU(2)$ . Pauli matrices are indeed proportional to the generators of the fundamental representation of  $SU(2)$ , thus they span the  $su(2)$  algebra.

<sup>1</sup>Schrödinger-Pauli equation represents the non-relativistic limit of Dirac equation.

## A.2 Dirac Matrices

Dirac matrices, commonly named gamma matrices, are a set of four  $4 \times 4$  matrices labelled by  $\gamma^\mu$ , that spans the matrix representation of Clifford algebra  $Cl_{1,3}(\mathbb{R})$ , defined by the anti-commutation relation:

$$\{\gamma^\mu, \gamma^\nu\} = 2g^{\mu\nu}\mathbb{1}, \quad (\text{A.5})$$

where  $\gamma^\mu = (\gamma^0, \gamma^1, \gamma^2, \gamma^3)$ .

Dirac matrices can be expressed in different representations; however, the most used is Weyl (or chiral) representation, in which Dirac matrices are

$$\gamma^0 = \begin{pmatrix} 0 & \mathbb{1} \\ \mathbb{1} & 0 \end{pmatrix} \quad \gamma^1 = \begin{pmatrix} 0 & \sigma_1 \\ -\sigma_1 & 0 \end{pmatrix} \quad \gamma^2 = \begin{pmatrix} 0 & \sigma_2 \\ -\sigma_2 & 0 \end{pmatrix} \quad \gamma^3 = \begin{pmatrix} 0 & \sigma_3 \\ -\sigma_3 & 0 \end{pmatrix}.$$

In a more compact way, we can write

$$\gamma^\mu = \begin{pmatrix} 0 & \bar{\sigma}^\mu \\ \sigma^\mu & 0 \end{pmatrix} \quad (\text{A.6})$$

In addition, we can define the fifth Dirac matrix as

$$\gamma^5 \equiv i\gamma^0\gamma^1\gamma^2\gamma^3 = \frac{i}{4!}\epsilon^{\mu\nu\rho\sigma}\gamma_\mu\gamma_\nu\gamma_\rho\gamma_\sigma \quad (\text{A.7})$$

which commutes with all the other gamma matrices

$$\{\gamma^\mu, \gamma^5\} = 0. \quad (\text{A.8})$$

The matrix  $\gamma^5$  is unitary and Hermitian, therefore its square is equal to the identity matrix. Moreover the trace of four Dirac matrices and  $\gamma^5$  returns:

$$\text{tr}[\gamma^5\gamma^\mu\gamma^\nu\gamma^\rho\gamma^\sigma] = -4i\epsilon^{\mu\nu\rho\sigma},$$

while any trace involving an even number of matrices  $\gamma^5$  is null. The cyclic property can be used when several  $\gamma^5$  appear in a trace in order to mash them together and use  $(\gamma^5)^2 = \mathbb{1}$ .

### A.2.1 Dirac Matrices in D-dimensions

The loop computation presented in this thesis are performed in dimensional regularisation, therefore we need to extend the definition of gamma matrices to a space of D-dimensions. We still continue to use the Greek letter  $\gamma$  to refer at Dirac matrices, thus the dimension of the space will be explicitly stated in the description.

In D-dimension the generalisation of equation (A.5) is:

$$\{\gamma^\mu, \gamma^\nu\} = 2g^{\mu\nu}\mathbb{1}_{d \times d}. \quad (\text{A.9})$$

It is easy to prove that the following rules hold for Dirac matrices in a D-dimensional space:

$$\begin{aligned} \gamma_\mu\gamma^\mu &= d \\ \gamma^\mu\gamma^\nu\gamma_\mu &= -(2-d)\gamma^\nu \\ \gamma^\mu\gamma^\nu\gamma^\rho\gamma_\mu &= (d-4)\gamma^\nu\gamma^\rho + 4g^{\nu\rho} \\ \gamma^\mu\gamma^\nu\gamma^\rho\gamma^\sigma\gamma_\mu &= -2\gamma^\sigma\gamma^\rho\gamma^\nu - (d-4)\gamma^\nu\gamma^\rho\gamma^\sigma \\ \gamma^\mu\gamma^\nu\gamma^\rho\gamma^\sigma\gamma^\epsilon\gamma_\mu &= 2\gamma^\epsilon\gamma^\nu\gamma^\rho\gamma^\sigma + 2\gamma^\sigma\gamma^\rho\gamma^\nu\gamma^\epsilon - (d-4)\gamma^\nu\gamma^\rho\gamma^\sigma\gamma^\epsilon, \end{aligned} \quad (\text{A.10})$$

and so on. Dirac matrices are engaged in the computation of  $S$ -matrix element for scattering processes that involve fermionic fields. In particular, if a specific process occurs at next to leading order with a fermionic loop, the number of Dirac matrices in the trace might be very large. Nevertheless, there are many properties of gamma matrices that can help us in the computation. First of all, the trace of an odd number of Dirac matrices is null

$$\text{tr}[\gamma^{\mu_1} \dots \gamma^{\mu_{2n-1}}] = 0,$$

while for an even number of gammas we have:

$$\begin{aligned} \text{tr}[\gamma^\mu \gamma^\nu] &= 4 g^{\mu\nu} \\ \text{tr}[\gamma^\mu \gamma^\nu \gamma^\rho \gamma^\sigma] &= 4 (g^{\mu\nu} g^{\rho\sigma} - g^{\mu\rho} g^{\nu\sigma} + g^{\mu\sigma} g^{\nu\rho}) \\ \text{tr}[\gamma^\mu \gamma^\nu \gamma^\rho \gamma^\sigma \gamma^\epsilon \gamma^\eta] &= 4 (g^{\eta\rho} g^{\mu\nu} g^{\epsilon\sigma} - g^{\eta\sigma} g^{\mu\nu} g^{\epsilon\rho} + g^{\mu\nu} g^{\rho\sigma} g^{\epsilon\eta} \\ &\quad - g^{\eta\nu} g^{\mu\rho} g^{\epsilon\sigma} + g^{\eta\sigma} g^{\mu\rho} g^{\epsilon\nu} + g^{\eta\nu} g^{\mu\sigma} g^{\epsilon\rho} \\ &\quad - g^{\eta\rho} g^{\mu\sigma} g^{\epsilon\nu} + g^{\eta\mu} g^{\nu\rho} g^{\epsilon\sigma} - g^{\eta\sigma} g^{\nu\rho} g^{\epsilon\mu} \\ &\quad + g^{\mu\sigma} g^{\nu\rho} g^{\epsilon\eta} - g^{\eta\mu} g^{\nu\sigma} g^{\epsilon\rho} + g^{\eta\rho} g^{\nu\sigma} g^{\epsilon\mu} \\ &\quad - g^{\mu\rho} g^{\nu\sigma} g^{\epsilon\eta} + g^{\eta\mu} g^{\rho\sigma} g^{\epsilon\nu} - g^{\eta\nu} g^{\rho\sigma} g^{\epsilon\mu}) \\ \text{tr}[\gamma^{\mu_1} \dots \gamma^{\mu_{2n}}] &= 4 \sum_{\pi} (-1)^{\sigma(\pi)} g^{\mu_{i_1} \mu_{j_1}} \dots g^{\mu_{i_n} \mu_{j_n}}. \end{aligned} \quad (\text{A.11})$$

where  $1 = i_1 < \dots < i_n$  and  $i_k < j_k$ , while  $\pi$  are the permutations of  $i_1, j_1, \dots, i_n, j_n$ . Thus, the extension of gamma matrices to a  $D$ -dimensional space is quite straight. On the contrary, problems arise when we try to extend  $\gamma^5$ , which definition is still that of equation (A.7). In fact, the main property of this matrix, namely equation (A.8), crashes against cyclic property of trace. These two rules cannot simultaneously hold in a coherent extension of  $\gamma^5$ . Thus, there are two possible path we can follow:

- KKS-scheme: retains the anti-commutation property in equation (A.8),
- BMHV-scheme: retains the trace cyclic property.

In this thesis, we embrace the KKS-scheme [207]-[208], whose main rules are

I) first rule:

$$\{\gamma^\mu, \gamma^5\} = 0,$$

II) second rule:

$$\begin{aligned} \text{tr}[\gamma^{\mu_1} \dots \gamma^{\mu_{2n-1}} \gamma^5] &= 0 \\ \text{tr}[\gamma^\mu \gamma^\nu \gamma^\rho \gamma^\sigma \gamma^5] &= -4i \epsilon^{\mu\nu\rho\sigma} \\ \text{tr}[\gamma^{\mu_1} \dots \gamma^{\mu_{2n}} \gamma^5] &= 4 \sum_{\pi} (-1)^{\sigma(\pi)} \epsilon^{\mu_{i_{n+1}} \mu_{i_{n+2}} \mu_{j_{n+1}} \mu_{j_{n+2}}} \\ &\quad \times g^{\mu_{i_1} \mu_{j_1}} \dots g^{\mu_{i_{n+2}} \mu_{j_{n+2}}}, \end{aligned}$$

where  $1 = i_1 < \dots < i_{n+2}$  and  $i_k < j_k$ , while  $\pi$  are the permutations of  $i_1, j_1, \dots, i_{n+2}, j_{n+2}$ ,

- III) third rule: when an odd number of  $\gamma^5$  appears in a trace, cyclic property cannot be used,
- IV) fourth rule: if a specific process is given by several diagrams, all the traces must be read starting from the same vertex, that will be called *reading point*,
- V) fifth rule: the anomalous graphs, of a theory involving an anomalous axial current, must be read starting from an axial vector vertex in order to fulfill the usual convention of conserved vector currents. When there are several axial vector vertices, the Bose symmetric choice of the reading prescription must be used.

For more details see reference [207].

### A.3 Gell-Mann Matrices

Gell-Mann matrices are eight linearly independent  $3 \times 3$  Hermitian matrices of null trace. They are half of the generators of the group  $SU(3)$  in the fundamental representation

$$T^a = \frac{\lambda^a}{2}$$

with  $a, b, c = \{1, \dots, 8\}$ . Explicitly, those matrices are

$$\begin{aligned} \lambda_1 &= \begin{pmatrix} 0 & 1 & 0 \\ 1 & 0 & 0 \\ 0 & 0 & 0 \end{pmatrix} & \lambda_2 &= \begin{pmatrix} 0 & -i & 0 \\ i & 0 & 0 \\ 0 & 0 & 0 \end{pmatrix} & \lambda_3 &= \begin{pmatrix} 1 & 0 & 0 \\ 0 & -1 & 0 \\ 0 & 0 & 0 \end{pmatrix} \\ \lambda_4 &= \begin{pmatrix} 0 & 0 & 1 \\ 0 & 0 & 0 \\ 1 & 0 & 0 \end{pmatrix} & \lambda_5 &= \begin{pmatrix} 0 & 0 & -i \\ 0 & 0 & 0 \\ i & 0 & 0 \end{pmatrix} & \lambda_6 &= \begin{pmatrix} 0 & 0 & 0 \\ 0 & 0 & 1 \\ 0 & 1 & 0 \end{pmatrix} \\ \lambda_7 &= \begin{pmatrix} 0 & 0 & 0 \\ 0 & 0 & -i \\ 0 & i & 0 \end{pmatrix} & \lambda_8 &= \frac{1}{\sqrt{3}} \begin{pmatrix} 1 & 0 & 0 \\ 0 & 1 & 0 \\ 0 & 0 & -2 \end{pmatrix}. \end{aligned}$$

Gell-Mann matrices are nothing but the generalisation of Pauli matrices for  $SU(3)$ , indeed they satisfy the commutation relation

$$[\lambda_a, \lambda_b] = 2if^{abc}\lambda_c$$

where  $f^{abc}$  are the structure constants of  $SU(3)$ , that are completely anti-symmetric and real quantities.

Since Gell-Mann matrices satisfy the Jacobi identity:

$$[\lambda^a, [\lambda^b, \lambda^c]] + [\lambda^b, [\lambda^c, \lambda^a]] + [\lambda^c, [\lambda^a, \lambda^b]] = 0,$$

then structure constants obey to

$$f^{abd}f^{dce} + f^{bcd}f^{dae} + f^{cad}f^{dbe} = 0.$$

## A.4 Embedding Particles in Fields

In this appendix we discuss the key principles that link real particles to fields. Since the present thesis is mostly based on model building it is useful to introduce this topic for the purpose of obtain, for every types of fields, the basic Lagrangian that serve as basis on which more complex theories can be built. Analogous discussion can be found in *Peskin & Schroeder* [3] or *Schwartz* [4].

Elementary particles are characterised by dynamical quantities such as momentum and spin projection along an axis, that can be modified by boosts or rotations, and by intrinsic quantum number that identify the particle. Mathematically, we can associate each particle to a set of states  $|\psi\rangle$ , that under a Poincaré transformation  $\mathcal{P}$  transforms only among themselves to preserve quantum numbers:

$$|\psi\rangle \rightarrow \mathcal{P}|\psi\rangle.$$

A set of elements that satisfy this property is called representation of Poincaré group. Well-known examples are the scalar field  $\phi(x)$  and the vector field  $V_\mu(x)$ . For any given representation, we can define a basis  $\{|\psi_i\rangle\}$  where the index  $i$  can be discrete or continuous:

$$|\psi_i\rangle \rightarrow \mathcal{P}_{ij}|\psi_j\rangle.$$

Schur's lemma states that if is not possible to identify a subset of states that transforms only among themselves, then the representation  $\{|\psi\rangle\}$  is called *irreducible*.

A predictable quantum field theory also requires unitary since the matrix elements  $\mathcal{M}$  must be Poincaré invariant:

$$\mathcal{M} = \langle\psi_1|\psi_2\rangle = \langle\psi'_1|\psi'_2\rangle = \langle\psi_1|\mathcal{P}^\dagger\mathcal{P}|\psi_2\rangle = \mathcal{M}' \quad \Rightarrow \quad \mathcal{P}^\dagger\mathcal{P} = 1,$$

thus, particles are understood as irreducible unitary representations of the Poincaré group.

In 1939 Wigner classified all irreducible unitary representations of Poincaré group labelling them by the mass  $m$  and the spin number  $j$ , therefore it can only acquire half-integer numbers, namely  $j = \{0, 1/2, 1, 3/2, \dots\}$ . He also demonstrated that the number of allowed states for each representation is:

$$j > 0 \Rightarrow \begin{cases} 2j + 1 & \text{for } m > 0 \\ 2 & \text{for } m = 0 \end{cases} \quad \text{while} \quad j = 0 \Rightarrow \{1 \ \forall m.$$

The irreducible unitary representations of Poincaré group are infinite-dimensional while we are used to deal with finite-dimensional and reducible representation such as scalar, vector and tensor representations. In fact, the vector representation, that brings four degrees of freedom, is the direct sum of the 1-spin and the 0-spin states. Therefore, we must find a prescription to embed particles, i.e., the irreducible unitary representations, in scalar, vector and tensor representations. The simple idea to overcome this problem is to make the finite representations dependent on the momentum, in this way they turn to infinite-dimensional representations as the momentum can assume infinite different values. Namely, the representation of the full Poincaré group is induced by the so-called *little group*, where the momentum is fixed. The little group is finite-dimensional and has unitary representations.

### A.4.1 The Scalar Field

Starting from the spin  $j = 0$  particle, the embedding procedure aims to include one degree of freedom in the real scalar field  $\phi(x)$ . The Lorentz invariant kinetic and massive terms are:

$$\mathcal{L} = \frac{1}{2} \partial_\mu \phi \partial^\mu \phi - \frac{1}{2} m^2 \phi^2, \quad (\text{A.12})$$

this Lagrangian also transforms covariantly under translations. The related equation of motion is  $(\partial^2 - m^2) \phi = 0$ , whose solution is:

$$\phi(x) = e^{-ipx}, \quad \text{with } p^2 = m^2.$$

The classical energy density, i.e., the zero-zero component of the energy-momentum tensor, is:

$$\mathcal{E} = \frac{\partial \mathcal{L}}{\partial \dot{\phi}} \dot{\phi} - \mathcal{L} = \frac{1}{2} \left[ (\partial_t \phi)^2 + (\nabla \phi)^2 + m^2 \phi^2 \right],$$

being positive defined and bounded by 0 from below, tells us that the overall sign of Lagrangian in equation (A.12) is the correct one.

### A.4.2 The Vector Field

The four-dimensional vector field  $A^\mu(x)$  is the smallest field that can embed massive 1-spin particles, as they bring three degrees of freedom. In this case, a prescription to remove the superfluous degree must be identified.

Leaving aside this problem, we can first try to guess the Lagrangian and then verify that it propagates the right number of modes. Inspired by the scalar field we can guess that the Lagrangian for the vector theory is:

$$\mathcal{L} = -\frac{1}{2} \partial_\mu A_\nu \partial^\mu A^\nu - \frac{1}{2} m^2 A_\nu A^\nu, \quad (\text{A.13})$$

whose equations of motion are  $(\partial^2 + m^2) V_\mu = 0$ , that bring four propagation modes. Hence, Lagrangian in equation (A.13) does not describe a massive 1-spin particle but four scalar 0-spin states, that are  $V_0, V_1, V_2, V_3$ . In other words, the four vector has been decomposed as  $4 = 1 \oplus 1 \oplus 1 \oplus 1$ . The associated classical energy density is:

$$\begin{aligned} \mathcal{E} = T_{00} &= \frac{\partial \mathcal{L}}{\partial (\partial_0 A_\mu)} \partial_0 A_\mu - \mathcal{L} \\ &= -\frac{1}{2} \left[ (\partial_0 A_0)^2 + (\nabla A_0)^2 + m^2 A_0^2 \right] + \frac{1}{2} \left[ (\partial_0 \mathbf{A})^2 + (\nabla \mathbf{V})^2 + m^2 \mathbf{A}^2 \right], \end{aligned}$$

which is not positive definite, thus Lagrangian in equation (A.13) cannot even describe any physics.

In four dimensions other operators can serve as kinetic term, likewise  $A_\mu \partial^\mu \partial^\nu A_\nu$  and  $A_\mu \partial^2 A^\mu$ . Including both of them, the new Lagrangian is:

$$\mathcal{L} = \frac{c_1}{2} A_\mu \partial^2 A^\mu + \frac{c_2}{2} A_\mu \partial_\mu \partial_\nu A^\nu + \frac{1}{2} m^2 A_\mu A^\mu, \quad (\text{A.14})$$

where  $c_1$  and  $c_2$  are free coefficients. As long as  $c_2 \neq 0$ , the term  $\partial_\nu A^\nu$  forces  $A^\nu$  to transform as a vector. The equations of motion are:

$$c_1 \partial^2 A_\mu + c_2 \partial_\mu \partial_\nu A^\nu + m^2 A_\mu = 0,$$

whose derivative is  $[(c_1 + c_2) \partial^2 + m^2] (\partial_\mu A^\mu) = 0$ . If  $c_1 = -c_2$  and  $m \neq 0$ , then we get  $\partial_\mu A^\mu = 0$ , which reduces by one the degrees of freedom of  $A^\mu$ . The four vector has been decomposed as  $4 = 3 \oplus 1$ , with the extra degree corresponding to a 0-spin mode, while the others reproduce the 1-spin massive particle. The equation  $\partial_\mu A^\mu = 0$  is Lorentz invariant, this guarantees that the extra degree of freedom is completely removed from the representation.

Fixing  $c_1 = -c_2 = 1$  for convenient, equation (A.14) becomes:

$$\begin{aligned} \mathcal{L} &= \frac{1}{2} A_\mu \partial^2 A^\mu - \frac{1}{2} A_\mu \partial^\mu \partial_\nu A^\nu + \frac{1}{2} m^2 A_\mu A^\mu \\ &= -\frac{1}{4} F_{\mu\nu} F^{\mu\nu} + \frac{1}{2} m^2 A_\mu A^\mu, \end{aligned} \quad (\text{A.15})$$

where  $F_{\mu\nu} = \partial_\mu A_\nu - \partial_\nu A_\mu$ . The equations of motion are still  $(\partial^2 + m^2)A_\mu = 0$ , which have solutions:

$$A_\mu = \sum_i \int \frac{d^3 p}{(2\pi)^3} \epsilon_\mu^i(p) \tilde{v}_i(\mathbf{p}) e^{ipx},$$

with  $\omega_p = \sqrt{\mathbf{p}^2 + m^2}$ . The vectors  $\epsilon_\mu^i(p)$  form a basis and they are named polarizations. As we were looking for a basis that automatically leads to  $\partial_\mu V^\mu = 0$ , the number of basis element is three, thus  $i$  runs over 1, 2, 3. The condition is directly embedded if the polarization vectors satisfy:

$$p_\mu \epsilon_\mu^i(\mathbf{p}) = 0.$$

Once the momentum  $p^\mu$ , with  $p^2 = m^2$ , is fixed, the previous equation has three independent solutions, that are the momentum-dependent polarization vectors  $\epsilon_\mu^i(p)$ , with the conventional normalisation  $\epsilon_\mu^* \epsilon^\mu = -1$ . For an explicit solution, we can take  $p_\mu$  as pointing in the  $z$ -direction:

$$p^\mu = (E, 0, 0, p_z), \quad \text{with} \quad E^2 - p_z^2 = m^2.$$

The solutions of equation (A.4.2) are:

$$\epsilon_\mu^1 = (0, 1, 0, 0), \quad \epsilon_\mu^2 = (0, 0, 1, 0) \quad \text{and} \quad \epsilon_\mu^L = \left( \frac{p_z}{E}, 0, 0, \frac{E}{m} \right).$$

The vectors  $\epsilon_\mu^1$  and  $\epsilon_\mu^2$  are named *transverse* polarizations, while the third vector is called *longitudinal* polarization. The integration of the polarizations, that are momentum dependent, against Fourier components  $\tilde{v}_i(\mathbf{p})$  gives rise to the space of vectors satisfying the equations of motion; this vector field forms an infinite-dimensional unitary representation of Poincaré group.

We must notice that in the high-energy limit, the longitudinal polarization becomes

$$\epsilon_\mu^L \sim \frac{E}{m} (1, 0, 0, 1).$$

The cross section of a process, that involving these two modes, behaves as  $d\sigma \sim g^2(\epsilon^L)^2 \sim g^2 \frac{E^2}{m^2}$ , with  $g$  coupling constant. The cross section – being a probability – is bounded by 1, then if we are able to reach sufficiently high energies,  $d\sigma \sim 1$  that means  $E \sim m/g$ . Taking a mass value  $m \sim 100$  GeV, close to the mass of weak bosons, and  $g \sim 0.1$ , then  $E \sim 1$  TeV is the energy scale at which theory begins to fail.

Not all the 1-spin states that appear in Nature are massive particle, photons and gluons are indeed massless bosons. One could think that performing the limit  $m_{V_\mu} \rightarrow 0$  for the massive case, is enough to describe massless 1-spin particles, however this limit is not smooth. Anyhow, the limit works for the Lagrangian:

$$\mathcal{L} = -\frac{1}{4} F_{\mu\nu} F^{\mu\nu}, \quad (\text{A.16})$$

while the constraint  $m^2 (\partial_\mu A^\mu) = 0$  is automatically fulfilled, restoring the 0-spin mode that we removed. The massless limit  $m \rightarrow 0$  leads to  $\epsilon_\mu^L \rightarrow \infty$ , since light-vector momentum became  $p_\mu \rightarrow (E, 0, 0, E)$ , as  $p_z \rightarrow E$ . In addition, the 1-spin massless particle has only two physical polarization states, thus we have to remove two extra polarizations. The Lagrangian in equation (A.16) already propagates two modes, indeed it must satisfy the property of gauge invariance, that the massive term breaks. The equation (A.16) is invariant under the transformation:

$$A_\mu(x) \rightarrow A_\mu(x) + \partial_\mu f(x), \quad (\text{A.17})$$

which means that the physical system of a massless 1-spin particle is mathematically described by a class of vector fields that differs one from each other by the total derivative of a scalar function  $f(x)$ . The equations of motion are  $\partial^2 A_\mu - \partial_\mu (\partial_\nu A^\nu) = 0$ , or in components:

$$\begin{aligned} \partial_i^2 A_0 - \partial_0 \partial_i A_i &= 0, \\ \partial^2 A_i - \partial_i (\partial_0 A_0 - \partial_i A_i) &= 0. \end{aligned}$$

Taking the gradient of the spatial components of equation (A.17), i.e.,  $\partial_i A_i(x) \rightarrow \partial_i A_i(x) + \partial_i^2 f(x)$ , and choosing  $f(x)$  such that its second space derivate is null, then if  $\partial_i A_i(x)$  is not singular, we are free to set  $\partial_i A_i(x) = 0$ , named *Coulomb gauge*. The first equation of motion becomes:

$$\partial_i^2 A_0 = 0,$$

which is satisfied by  $A_0(x) \rightarrow A_0(x) + \partial_t f(x)$ , i.e., the zero component of gauge transformation, allowing us to set  $A_0 = 0$  which completely eliminates on degree of freedom from  $A_\mu$ . The other equations of motion are:

$$\partial^2 A_i = 0,$$

that bring three propagation modes that will be reduced by one imposing the constraint  $\partial_i A_i = 0$ . Turning into Fourier space

$$A_\mu(x) = \int \frac{d^4 p}{(2\pi)^4} \epsilon_\mu(p) e^{ipx},$$



the equations of motion become  $p^2 = 0$ , while the gauge choice  $\partial_i A_i = 0$  and the constraint  $A_0 = 0$  lead to  $p_i \epsilon_i = 0$  and  $\epsilon_0 = 0$  respectively. Choosing the inertial reference frame where  $p_\mu = (E, 0, 0, E)$ , the two solutions of the equations of motion are:

$$\epsilon_\mu^1 = (0, 1, 0, 0), \quad \epsilon_\mu^2 = (0, 0, 1, 0),$$

which are the linear polarizations of light. Another viable basis for the transverse polarizations of light is composed by the helicity eigenstates, that are the circular polarizations:

$$\epsilon_\mu^R = \frac{1}{\sqrt{2}} (0, 1, i, 0), \quad \epsilon_\mu^L = \frac{1}{\sqrt{2}} (0, 1, -i, 0).$$

Thus, the theory we built stands as the right theory for massless 1-spin particle, as it propagates only two degrees of freedom.

There are many choices for gauge, a familiar one is  $\partial_\mu A^\mu = 0$ , called *Lorentz gauge*. This gauge, being Lorentz invariant, leads to three polarization vectors that satisfy  $p_\mu \epsilon^\mu = 0$ , that are

$$\epsilon_\mu^1 = (0, 1, 0, 0), \quad \epsilon_\mu^2 = (0, 0, 1, 0), \quad \epsilon_\mu^f = (1, 0, 0, 1),$$

where we recognize the transverse polarizations plus the so-called forward polarization. The latter vector does not correspond to any physical state as it is even not normalizable, with  $(\epsilon_\mu^f)^* \epsilon^{f\mu} = 0$ .

### A.4.3 The Spinor Field

A general solution of Dirac equation is not an irreducible representation of the Lorentz group. The commutation relation

$$[\gamma^5, S^{\mu\nu}] = 0,$$

with  $S^{\mu\nu} = \frac{i}{4} [\gamma^\mu, \gamma^\nu]$ , provides the existence of eigenvectors of  $\gamma^5$ , associated to different eigenvalues, that do not mix under Lorentz transformations. Moreover, the block-diagonal form of boost and rotation generators for Dirac field

$$S^{0j} = \frac{i}{4} [\gamma^0, \gamma^j] = -\frac{i}{2} \begin{pmatrix} \sigma^j & 0 \\ 0 & -\sigma^j \end{pmatrix},$$

$$S^{ij} = \frac{i}{4} [\gamma^i, \gamma^j] = \frac{i}{2} \epsilon^{ijk} \begin{pmatrix} \sigma^k & 0 \\ 0 & \sigma^k \end{pmatrix},$$

is another confirmation that Dirac spinor is reducible. Schur's Lemma removes all doubt by establishing that for an irreducible representation, the property in equation (A.4.3) must be a prerogative of the identity matrix only.

The Dirac spinor, often called bispinor, is indeed given by the sum of one left-handed and one right-handed Weyl spinor:

$$\psi_D(x) = \begin{pmatrix} \psi_L(x) \\ \psi_R(x) \end{pmatrix} = \begin{pmatrix} \psi_{L1}(x) \\ \psi_{L2}(x) \\ \psi_{R1}(x) \\ \psi_{R2}(x) \end{pmatrix}, \quad \psi_L(x) = \begin{pmatrix} \psi_{L1}(x) \\ \psi_{L2}(x) \end{pmatrix}, \quad \psi_R(x) = \begin{pmatrix} \psi_{R1}(x) \\ \psi_{R2}(x) \end{pmatrix},$$

where left-handed and right-handed spinors are two non-equivalent representation of Lorentz group.

Since the group algebra  $so(1, 3)$ , is equivalent to the direct sum of two algebras generated by the group  $SU(2)$

$$so(1, 3) = su(2) \oplus su(2),$$

each representation of Lorentz group can be labelled by two semi-integer number as  $\mathcal{T}_{(m, n)}$ , with  $(2m + 1)(2n + 1)$  independent states. Making use of this notation, the left-handed Weyl spinor belongs to  $\mathcal{T}_{(\frac{1}{2}, 0)}$  representation, while the right-handed to  $\mathcal{T}_{(0, \frac{1}{2})}$  [210].

As before, we try to write down the Lagrangian starting the kinetic and mass terms, that can be proportional to  $\psi_R^\dagger \psi_R$ , thus

$$\mathcal{L} = \psi_R^\dagger \partial^2 \psi_R + m_W^2 \psi_R^\dagger \psi_R,$$

which do not satisfy Lorentz invariant, likewise the left-handed spinor. Hence, a mass term for the Weyl spinor is not allowed. On the contrary, combining the left-handed and the right-handed spinors in the same term we get

$$\mathcal{L} = m_{Dirac} \left( \psi_L^\dagger \psi_R + \psi_R^\dagger \psi_L \right),$$

where  $m_{Dirac} \in \mathbb{R}$ , is the mass for a Dirac spinor. The kinetic term is:

$$\mathcal{L} = \psi_L^\dagger \partial^2 \psi_R + \psi_R^\dagger \partial^2 \psi_L,$$

that is real and invariant, but it propagates a couple of scalars instead of a spinor, similarly to what happens with the vector field  $V^\mu$  that propagates four scalar until we contract it with  $\partial_\mu$ . Going further, we can look at  $\psi_R^\dagger \sigma_i \psi_R$  that behaves like a spatial vector, thus we can simply build a four-vector as  $A_R^\mu = (\psi_R^\dagger \psi_R, \psi_R^\dagger \boldsymbol{\sigma} \psi_R)$ , while for the left-handed spinor  $V_L^\mu = (\psi_L^\dagger \psi_L, -\psi_L^\dagger \boldsymbol{\sigma} \psi_L)$ . Defining

$$\sigma^\mu \equiv (\mathbf{1}, \boldsymbol{\sigma}), \quad \bar{\sigma}^\mu \equiv (\mathbf{1}, -\boldsymbol{\sigma}),$$

the two terms become  $A_R^\mu = \psi_R^\dagger \sigma^\mu \psi_R$  and  $V_L^\mu = \psi_L^\dagger \bar{\sigma}^\mu \psi_L$ , that contracted with  $\partial_\mu$  give rise to the Lagrangian:

$$\mathcal{L} = i\psi_R^\dagger \partial_\mu \sigma^\mu \psi_R + i\psi_L^\dagger \partial_\mu \bar{\sigma}^\mu \psi_L + m_{Dirac} \left( \psi_L^\dagger \psi_R + \psi_R^\dagger \psi_L \right)$$

notice that if we had applied the derivative in front of each term we would get a total derivative. The imaginary unit has been introduced to make the Lagrangian hermitian. In terms of Dirac field, the previous Lagrangian turns to:

$$\mathcal{L} = \bar{\psi} (i\gamma^\mu \partial_\mu - m) \psi \tag{A.18}$$

where  $\bar{\psi} = \psi^\dagger \gamma^0 = (\psi_R^\dagger, \psi_L^\dagger)$  and

$$\gamma^\mu = \begin{pmatrix} 0 & \sigma^\mu \\ \bar{\sigma}^\mu & 0 \end{pmatrix}$$

The EOM of this Lagrangian is Dirac equation  $(i\gamma^\mu \partial_\mu - m)\psi = 0$ , thus it really propagates a Dirac spinor. In addition to Dirac equation, spinors satisfy also the Klein-Gordon equation  $(\partial^2 + m^2)\psi(x) = 0$ , whose solutions are plane-waves:

$$\psi_s(x) = \int \frac{d^3p}{(2\pi)^3} u_s(p) e^{ipx},$$

with  $p_0 = \sqrt{\mathbf{p}^2 + m^2} > 0$ . Even solutions with negative energies are allowed, but those are understood as anti-particles of positive energies:

$$\chi_s(x) = \int \frac{d^3p}{(2\pi)^3} v_s(p) e^{ipx},$$

again with  $p_0 = \sqrt{\mathbf{p}^2 + m^2} > 0$ . The polarizations of particles and anti-particles are the spinors  $u_s(p)$  and  $v_s(p)$  respectively. Since they are momentum-dependent, the search for an explicit solution requires the setting of the momentum. For example, in the rest frame  $p^\mu = (m, 0, 0, 0)$  the solutions are

$$u_s = \begin{pmatrix} \xi_s \\ \xi_s \end{pmatrix}, \quad v_s = \begin{pmatrix} \eta_s \\ -\eta_s \end{pmatrix},$$

for any two-component spinors  $\xi_s$  and  $\eta_s$ , a viable choice is  $\xi_1 = \eta_1 = \begin{pmatrix} 1 \\ 0 \end{pmatrix}$  and  $\xi_2 = \eta_2 = \begin{pmatrix} 0 \\ 1 \end{pmatrix}$ . For a momentum pointing along the z-axis  $p^\mu = (E, 0, 0, p_z)$ , the polarizations are:

$$u_s(p) = \begin{pmatrix} \sqrt{p \cdot \sigma} \xi_s \\ \sqrt{p \cdot \bar{\sigma}} \xi_s \end{pmatrix}, \quad v_s(p) = \begin{pmatrix} \sqrt{p \cdot \sigma} \eta_s \\ -\sqrt{p \cdot \bar{\sigma}} \eta_s \end{pmatrix}.$$

In conclusion, an infinite representation for Dirac spinor has been found, a remark is necessary, the representation is not irreducible as it is given by the direct sum of two non-equivalent Weyl spinor, one of left and one of right chirality.

## A.5 Light-by-light Formulas

The complete formula for the polarization tensor  $M_2^{\mu\nu\rho\sigma}$  is

$$\begin{aligned}
\mathcal{M}_2^{\mu\nu\rho\sigma} = & 32g_2 \left( -2(p_4)^\mu (p_3)^\nu (p_2)^\rho (p_1)^\sigma + (p_3)^\mu (p_4)^\nu (p_2)^\rho (p_1)^\sigma \right. \\
& + (p_2)^\mu (p_3)^\nu (p_4)^\rho (p_1)^\sigma + 2(p_4)^\mu g^{\nu\rho} (p_2 \cdot p_3) (p_1)^\sigma \\
& - g^{\mu\rho} (p_4)^\nu (p_2 \cdot p_3) (p_1)^\sigma - g^{\mu\nu} (p_4)^\rho (p_2 \cdot p_3) (p_1)^\sigma \\
& - (p_3)^\mu g^{\nu\rho} (p_2 \cdot p_4) (p_1)^\sigma + g^{\mu\rho} (p_3)^\nu (p_2 \cdot p_4) (p_1)^\sigma \\
& - (p_2)^\mu g^{\nu\rho} (p_3 \cdot p_4) (p_1)^\sigma + g^{\mu\nu} (p_2)^\rho (p_3 \cdot p_4) (p_1)^\sigma \\
& + (p_4)^\mu (p_3)^\nu (p_1)^\rho (p_2)^\sigma - 2(p_3)^\mu (p_4)^\nu (p_1)^\rho (p_2)^\sigma \\
& + (p_3)^\mu (p_1)^\nu (p_4)^\rho (p_2)^\sigma + (p_2)^\mu (p_4)^\nu (p_1)^\rho (p_3)^\sigma \\
& + (p_4)^\mu (p_1)^\nu (p_2)^\rho (p_3)^\sigma - 2(p_2)^\mu (p_1)^\nu (p_4)^\rho (p_3)^\sigma \\
& + (p_4)^\mu (p_3)^\nu g^{\rho\sigma} (p_1 \cdot p_2) + (p_3)^\mu (p_4)^\nu g^{\rho\sigma} (p_1 \cdot p_2) \\
& - (p_3)^\mu g^{\nu\sigma} (p_4)^\rho (p_1 \cdot p_2) - g^{\mu\sigma} (p_3)^\nu (p_4)^\rho (p_1 \cdot p_2) \\
& - (p_4)^\mu g^{\nu\rho} (p_3)^\sigma (p_1 \cdot p_2) - g^{\mu\rho} (p_4)^\nu (p_3)^\sigma (p_1 \cdot p_2) \\
& + 2g^{\mu\nu} (p_4)^\rho (p_3)^\sigma (p_1 \cdot p_2) - (p_2)^\mu (p_4)^\nu g^{\rho\sigma} (p_1 \cdot p_3) \\
& + (p_4)^\mu g^{\nu\sigma} (p_2)^\rho (p_1 \cdot p_3) - g^{\mu\sigma} (p_4)^\nu (p_2)^\rho (p_1 \cdot p_3) \\
& + (p_2)^\mu g^{\nu\sigma} (p_4)^\rho (p_1 \cdot p_3) - (p_4)^\mu g^{\nu\rho} (p_2)^\sigma (p_1 \cdot p_3) \\
& + 2g^{\mu\rho} (p_4)^\nu (p_2)^\sigma (p_1 \cdot p_3) - g^{\mu\nu} (p_4)^\rho (p_2)^\sigma (p_1 \cdot p_3) \\
& - (p_2)^\mu (p_3)^\nu g^{\rho\sigma} (p_1 \cdot p_4) - (p_3)^\mu g^{\nu\sigma} (p_2)^\rho (p_1 \cdot p_4) \\
& + 2g^{\mu\sigma} (p_3)^\nu (p_2)^\rho (p_1 \cdot p_4) + (p_3)^\mu g^{\nu\rho} (p_2)^\sigma (p_1 \cdot p_4) \\
& - g^{\mu\rho} (p_3)^\nu (p_2)^\sigma (p_1 \cdot p_4) + (p_2)^\mu g^{\nu\rho} (p_3)^\sigma (p_1 \cdot p_4) \\
& - g^{\mu\nu} (p_2)^\rho (p_3)^\sigma (p_1 \cdot p_4) - (p_4)^\mu (p_1)^\nu g^{\rho\sigma} (p_2 \cdot p_3) \\
& - (p_4)^\mu g^{\nu\sigma} (p_1)^\rho (p_2 \cdot p_3) + g^{\mu\sigma} (p_4)^\nu (p_1)^\rho (p_2 \cdot p_3) \\
& + g^{\mu\sigma} (p_1)^\nu (p_4)^\rho (p_2 \cdot p_3) - 2g^{\mu\sigma} g^{\nu\rho} (p_1 \cdot p_4) (p_2 \cdot p_3) \\
& + g^{\mu\rho} g^{\nu\sigma} (p_1 \cdot p_4) (p_2 \cdot p_3) + g^{\mu\nu} g^{\rho\sigma} (p_1 \cdot p_4) (p_2 \cdot p_3) \\
& - (p_3)^\mu (p_1)^\nu g^{\rho\sigma} (p_2 \cdot p_4) + 2(p_3)^\mu g^{\nu\sigma} (p_1)^\rho (p_2 \cdot p_4) \\
& - g^{\mu\sigma} (p_3)^\nu (p_1)^\rho (p_2 \cdot p_4) + g^{\mu\rho} (p_1)^\nu (p_3)^\sigma (p_2 \cdot p_4) \\
& - g^{\mu\nu} (p_1)^\rho (p_3)^\sigma (p_2 \cdot p_4) + g^{\mu\sigma} g^{\nu\rho} (p_1 \cdot p_3) (p_2 \cdot p_4) \\
& - 2g^{\mu\rho} g^{\nu\sigma} (p_1 \cdot p_3) (p_2 \cdot p_4) + g^{\mu\nu} g^{\rho\sigma} (p_1 \cdot p_3) (p_2 \cdot p_4) \\
& + 2(p_2)^\mu (p_1)^\nu g^{\rho\sigma} (p_3 \cdot p_4) - (p_2)^\mu g^{\nu\sigma} (p_1)^\rho (p_3 \cdot p_4) \\
& - g^{\mu\sigma} (p_1)^\nu (p_2)^\rho (p_3 \cdot p_4) - g^{\mu\rho} (p_1)^\nu (p_2)^\sigma (p_3 \cdot p_4) \\
& + g^{\mu\nu} (p_1)^\rho (p_2)^\sigma (p_3 \cdot p_4) + g^{\mu\sigma} g^{\nu\rho} (p_1 \cdot p_2) (p_3 \cdot p_4) \\
& \left. + g^{\mu\rho} g^{\nu\sigma} (p_1 \cdot p_2) (p_3 \cdot p_4) - 2g^{\mu\nu} g^{\rho\sigma} (p_1 \cdot p_2) (p_3 \cdot p_4) \right)
\end{aligned} \tag{A.19}$$

The complete formula for the total tensor polarization, where the momentum  $p_4$  has been removed by energy conservation, i.e.,  $p_1 + p_2 + p_3 = -p_4$ , is:

$$\begin{aligned}
M^{\mu\nu\rho\sigma} = & 32g_1 (g^{\mu\sigma} g^{\nu\rho} (p_1 \cdot p_2)^2 + g^{\mu\nu} g^{\rho\sigma} (p_1 \cdot p_2)^2 + g^{\mu\sigma} g^{\nu\rho} (p_1 \cdot p_3)^2 \\
& + g^{\mu\rho} g^{\nu\sigma} (p_1 \cdot p_3)^2 + (p_2)^\rho (p_3)^\nu g^{\mu\sigma} (p_1 \cdot p_2) \\
& + (p_2)^\sigma (p_3)^\mu g^{\nu\rho} (p_1 \cdot p_2) + 2g^{\mu\sigma} g^{\nu\rho} (p_1 \cdot p_2) (p_1 \cdot p_3) \\
& + (p_2)^\rho (p_3)^\mu g^{\nu\sigma} (p_1 \cdot p_3) + (p_2)^\rho (p_3)^\nu g^{\mu\sigma} (p_1 \cdot p_3) \\
& + (p_2)^\sigma (p_3)^\mu g^{\nu\rho} (p_1 \cdot p_3) + (p_2)^\sigma (p_3)^\nu g^{\mu\rho} (p_1 \cdot p_3) \\
& + 2(p_2)^\rho (p_2)^\sigma (p_3)^\mu (p_3)^\nu) \\
& + 32g_2 (-g^{\mu\sigma} g^{\nu\rho} (p_1 \cdot p_2)^2 + 2g^{\mu\rho} g^{\nu\sigma} (p_1 \cdot p_2)^2 - g^{\mu\nu} g^{\rho\sigma} (p_1 \cdot p_2)^2 \\
& - g^{\mu\sigma} g^{\nu\rho} (p_1 \cdot p_3)^2 - g^{\mu\rho} g^{\nu\sigma} (p_1 \cdot p_3)^2 + 2g^{\mu\nu} g^{\rho\sigma} (p_1 \cdot p_3)^2) \quad (\text{A.20}) \\
& - 2(p_2)^\rho (p_2)^\sigma g^{\mu\nu} (p_1 \cdot p_2)^2 - 2(p_3)^\mu (p_3)^\nu g^{\rho\sigma} (p_1 \cdot p_2) \\
& + 2(p_2)^\rho (p_3)^\mu g^{\nu\sigma} (p_1 \cdot p_2) - 3(p_2)^\rho (p_3)^\nu g^{\mu\sigma} (p_1 \cdot p_2) \\
& - 3(p_2)^\sigma (p_3)^\mu g^{\nu\rho} (p_1 \cdot p_2) + 2(p_2)^\sigma (p_3)^\nu g^{\mu\rho} (p_1 \cdot p_2) \\
& - 4g^{\mu\sigma} g^{\nu\rho} (p_1 \cdot p_2) (p_1 \cdot p_3) + 2g^{\mu\rho} g^{\nu\sigma} (p_1 \cdot p_2) (p_1 \cdot p_3) \\
& + 2g^{\mu\nu} g^{\rho\sigma} (p_1 \cdot p_2) (p_1 \cdot p_3) - (p_2)^\rho (p_3)^\mu g^{\nu\sigma} (p_1 \cdot p_3) \\
& - (p_2)^\rho (p_3)^\nu g^{\mu\sigma} (p_1 \cdot p_3) - (p_2)^\sigma (p_3)^\mu g^{\nu\rho} (p_1 \cdot p_3) \\
& - (p_2)^\sigma (p_3)^\nu g^{\mu\rho} (p_1 \cdot p_3) - 2(p_2)^\rho (p_2)^\sigma (p_3)^\mu (p_3)^\nu)
\end{aligned}$$

The total polarization tensor  $\mathcal{M}^{\mu\nu\rho\sigma}$ , likewise its two components  $\mathcal{M}_1^{\mu\nu\rho\sigma}$  and  $\mathcal{M}_2^{\mu\nu\rho\sigma}$ , satisfies the property of transversality:

$$\mathcal{M}^{\mu_1\mu_2\mu_3\mu_4} p_{i\mu_i} = 0 \quad (\text{A.21})$$

where  $i = \{1, 2, 3\}$  since the fourth momentum has been removed yet.

Renaming the scalar product in analogy with Mandelstam variables, but taking into account our convention on incoming momenta:

$$\begin{aligned}
s &= (p_1 + p_2)^2 = 2p_1 \cdot p_2 \\
t &= (p_1 + p_3)^2 = 2p_1 \cdot p_3 \\
u &= (p_1 + p_4)^2 = (p_2 + p_3)^2 = 2p_2 \cdot p_3 \\
s + t + u &= 2p_1 \cdot p_2 + 2p_1 \cdot p_3 + 2p_1 \cdot p_4 = -2(p_1)^2 = 0,
\end{aligned} \quad (\text{A.22})$$

the total polarization tensor becomes

$$\begin{aligned}
\mathcal{M}^{\mu\nu\rho\sigma} = & g^{\mu\sigma} g^{\nu\rho} (8g_1 s^2 + 16g_1 st + 8g_1 t^2 - 8g_2 s^2 - 32g_2 st - 8g_2 t^2) \\
& + g^{\mu\rho} g^{\nu\sigma} (8g_1 t^2 + 16g_2 s^2 + 16g_2 st - 8g_2 t^2) \\
& + g^{\mu\nu} g^{\rho\sigma} (8g_1 s^2 - 8g_2 s^2 + 16g_2 st + 16g_2 t^2) \\
& + (p_1)^\nu (p_1)^\rho (32g_2 s + 32g_2 t) g^{\mu\sigma} + (p_1)^\nu (p_1)^\sigma (-16g_2 s - 16g_2 t) g^{\mu\rho} \\
& + (p_1)^\rho (p_1)^\sigma (-16g_2 s - 16g_2 t) g^{\mu\nu} - 32g_2 t (p_2)^\mu (p_2)^\rho g^{\nu\sigma} \\
& + 16g_2 t (p_2)^\mu (p_2)^\sigma g^{\nu\rho} + 16g_2 t (p_2)^\rho (p_2)^\sigma g^{\mu\nu} \\
& - 32g_2 s (p_3)^\mu (p_3)^\nu g^{\rho\sigma} + 16g_2 s (p_3)^\mu (p_3)^\sigma g^{\nu\rho} \\
& + 16g_2 s (p_3)^\nu (p_3)^\sigma g^{\mu\rho} + (p_1)^\nu (p_2)^\mu (16g_2 s - 16g_1 s) g^{\rho\sigma} \\
& + (p_1)^\sigma (p_2)^\mu g^{\nu\rho} (-16g_1 s - 16g_1 t + 16g_2 s + 32g_2 t) \\
& + (p_1)^\nu (p_2)^\sigma g^{\mu\rho} (16g_1 t - 16g_2 s - 32g_2 t) \\
& + (p_1)^\sigma (p_3)^\mu g^{\nu\rho} (-16g_1 s - 16g_1 t + 32g_2 s + 16g_2 t) \\
& + (p_1)^\rho (p_3)^\sigma g^{\mu\nu} (16g_1 s - 32g_2 s - 16g_2 t) \\
& + (p_1)^\rho (p_3)^\mu (16g_2 t - 16g_1 t) g^{\nu\sigma} \\
& + (p_2)^\rho (p_3)^\nu g^{\mu\sigma} (16g_1 s + 16g_1 t - 16g_2 s - 16g_2 t) \\
& + (p_2)^\sigma (p_3)^\nu g^{\mu\rho} (16g_1 t + 16g_2 s - 16g_2 t) \\
& + (p_2)^\rho (p_3)^\sigma g^{\mu\nu} (16g_1 s - 16g_2 s + 16g_2 t) \\
& + (p_1)^\rho (p_2)^\mu (-32g_2 s - 32g_2 t) g^{\nu\sigma} + (p_1)^\rho (p_2)^\sigma (16g_2 s + 16g_2 t) g^{\mu\nu} \\
& + 32g_2 t (p_1)^\nu (p_2)^\rho g^{\mu\sigma} - 16g_2 t (p_1)^\sigma (p_2)^\rho g^{\mu\nu} + 32g_2 s (p_1)^\rho (p_3)^\nu g^{\mu\sigma} \\
& - 16g_2 s (p_1)^\sigma (p_3)^\nu g^{\mu\rho} + (p_1)^\nu (p_3)^\mu (-32g_2 s - 32g_2 t) g^{\rho\sigma} \\
& + (p_1)^\nu (p_3)^\sigma (16g_2 s + 16g_2 t) g^{\mu\rho} + 32g_2 s (p_2)^\rho (p_3)^\mu g^{\nu\sigma} \\
& - 16g_2 s (p_2)^\sigma (p_3)^\mu g^{\nu\rho} + 32g_2 t (p_2)^\mu (p_3)^\nu g^{\rho\sigma} - 16g_2 t (p_2)^\mu (p_3)^\sigma g^{\nu\rho} \\
& + (32g_2 - 32g_1) [(p_1)^\sigma (p_2)^\mu (p_2)^\rho (p_3)^\nu + (p_1)^\sigma (p_2)^\rho (p_3)^\mu (p_3)^\nu \\
& + (p_1)^\nu (p_1)^\rho (p_2)^\sigma (p_3)^\mu + (p_1)^\rho (p_2)^\sigma (p_3)^\mu (p_3)^\nu \\
& + (p_1)^\nu (p_1)^\rho (p_2)^\mu (p_3)^\sigma + (p_1)^\nu (p_2)^\mu (p_2)^\rho (p_3)^\sigma] \\
& - 32g_2 [(p_1)^\rho (p_1)^\sigma (p_2)^\mu (p_3)^\nu + (p_1)^\nu (p_1)^\sigma (p_2)^\rho (p_3)^\mu \\
& + (p_1)^\rho (p_2)^\mu (p_2)^\sigma (p_3)^\nu + (p_1)^\nu (p_2)^\rho (p_2)^\sigma (p_3)^\mu \\
& + (p_1)^\rho (p_2)^\mu (p_3)^\nu (p_3)^\sigma + (p_1)^\nu (p_2)^\rho (p_3)^\mu (p_3)^\sigma],
\end{aligned} \tag{A.23}$$

which contains 45 different structures.

The complete amplitude of *spinor QED* is:

$$\begin{aligned}
M_{1/2}^{\mu\nu\rho\sigma} = & g^{\mu\nu} g^{\rho\sigma} \left( -\frac{e^4 s^2}{240\pi^2 m^4} + \frac{7e^4 st}{360\pi^2 m^4} + \frac{7e^4 t^2}{360\pi^2 m^4} \right) \\
& + g^{\mu\rho} g^{\nu\sigma} \left( \frac{7e^4 s^2}{360\pi^2 m^4} + \frac{7e^4 st}{360\pi^2 m^4} - \frac{e^4 t^2}{240\pi^2 m^4} \right) \\
& + g^{\mu\sigma} g^{\nu\rho} \left( -\frac{e^4 s^2}{240\pi^2 m^4} - \frac{e^4 st}{36\pi^2 m^4} - \frac{e^4 t^2}{240\pi^2 m^4} \right) \\
& + \frac{e^4}{360\pi^2 m^4} \left( 14(s+t)(p_1)^\nu (p_1)^\rho g^{\mu\sigma} - 7(s+t)(p_1)^\nu (p_1)^\sigma g^{\mu\rho} \right. \\
& \quad - 7(s+t)(p_1)^\rho (p_1)^\sigma g^{\mu\nu} + 3s(p_1)^\nu (p_2)^\mu g^{\rho\sigma} \\
& \quad + 14(p_1)^\nu (p_2)^\rho g^{\mu\sigma} - (7s-10t)(p_1)^\nu (p_2)^\sigma g^{\mu\rho} \\
& \quad + 7(s+t)(p_1)^\rho (p_2)^\sigma g^{\mu\nu} - 14(s+t)(p_1)^\rho (p_2)^\mu g^{\nu\sigma} \\
& \quad + (3s+10t)(p_1)^\sigma (p_2)^\mu g^{\nu\rho} - 7t(p_1)^\sigma (p_2)^\rho g^{\mu\nu} \\
& \quad - 14(s+t)(p_1)^\nu (p_3)^\mu g^{\rho\sigma} + 7(s+t)(p_1)^\nu (p_3)^\sigma g^{\mu\rho} \\
& \quad + 3t(p_1)^\rho (p_3)^\mu g^{\nu\sigma} + 14s(p_1)^\rho (p_3)^\nu g^{\mu\sigma} \\
& \quad - (10s+7t)(p_1)^\rho (p_3)^\sigma g^{\mu\nu} + (10s+3t)(p_1)^\sigma (p_3)^\mu g^{\nu\rho} \\
& \quad - 7s(p_1)^\sigma (p_3)^\nu g^{\mu\rho} - 14t(p_2)^\mu (p_2)^\rho g^{\nu\sigma} \\
& \quad + 7t(p_2)^\mu (p_2)^\sigma g^{\nu\rho} + 7t(p_2)^\rho (p_2)^\sigma g^{\mu\nu} \\
& \quad + 14t(p_2)^\mu (p_3)^\nu g^{\rho\sigma} - 7t(p_2)^\mu (p_3)^\sigma g^{\nu\rho} \\
& \quad + 14s(p_2)^\rho (p_3)^\mu g^{\nu\sigma} - 3(s+t)(p_2)^\rho (p_3)^\nu g^{\mu\sigma} \\
& \quad - (3s-7t)(p_2)^\rho (p_3)^\sigma g^{\mu\nu} - 7s(p_2)^\sigma (p_3)^\mu g^{\nu\rho} \\
& \quad + (7s-3t)(p_2)^\sigma (p_3)^\nu g^{\mu\rho} - 14s(p_3)^\mu (p_3)^\nu g^{\rho\sigma} \\
& \quad \left. + 7s(p_3)^\mu (p_3)^\sigma g^{\nu\rho} + 7s(p_3)^\nu (p_3)^\sigma g^{\mu\rho} \right) \\
& - \frac{7e^4}{180\pi^2 m^4} \left( (p_1)^\rho (p_1)^\sigma (p_2)^\mu (p_3)^\nu + (p_1)^\nu (p_1)^\sigma (p_2)^\rho (p_3)^\mu \right. \\
& \quad + (p_1)^\rho (p_2)^\mu (p_2)^\sigma (p_3)^\nu + (p_1)^\nu (p_2)^\rho (p_2)^\sigma (p_3)^\mu \\
& \quad \left. + (p_1)^\rho (p_2)^\mu (p_3)^\nu (p_3)^\sigma + (p_1)^\nu (p_2)^\rho (p_3)^\mu (p_3)^\sigma \right) \\
& + \frac{e^4}{60\pi^2 m^4} \left( (p_1)^\sigma (p_2)^\mu (p_2)^\rho (p_3)^\nu + (p_2)^\rho (p_3)^\mu (p_3)^\nu (p_1)^\sigma \right. \\
& \quad + (p_1)^\nu (p_1)^\rho (p_2)^\sigma (p_3)^\mu + (p_1)^\rho (p_2)^\sigma (p_3)^\mu (p_3)^\nu \\
& \quad \left. + (p_1)^\nu (p_2)^\rho (p_2)^\sigma (p_3)^\mu + (p_1)^\nu (p_2)^\mu (p_2)^\rho (p_3)^\sigma \right)
\end{aligned} \tag{A.24}$$

## A.6 Dark Matter Table

Analytic expressions for the cross-section ( $\sigma$ ), and velocity-weighted, non-relativistic annihilation cross-sections ( $\sigma v$ ), for dimension-5 and dimension-6 operators of the hypercharge EFT for Dirac dark matter.

Opr.	$\psi\bar{\psi} \rightarrow XX$	$\sigma_{XX}(s \gg m_f, m_Z)$	$(\sigma v)_{XX}$
$O_{\mathcal{M}}$	$f\bar{f}$	$\frac{(3-2\beta^2)e^2 N_c C_{\mathcal{M}}^2 Y_f^2}{48\pi\beta\Lambda^2 c_W^2}$	$\frac{e^2 N_c C_{\mathcal{M}}^2 Y_f^2}{16\pi\Lambda^2 c_W^2}$
	$W^+W^-, Zh$	$\frac{(3-2\beta^2)e^2 C_{\mathcal{M}}^2}{384\pi\beta c_W^2 \Lambda^2}$	$\frac{e^2 C_{\mathcal{M}}^2}{128\pi c_W^2 \Lambda^2}$
	$\gamma\gamma$	$\frac{C_{\mathcal{M}}^4 c_W^4 s \left( (9-7\beta^2)\beta^2 - 6\beta(\beta^2-1)^2 \tanh^{-1}(\beta) \right)}{96\pi\beta^3 \Lambda^4}$	$\frac{c_W^4 C_{\mathcal{M}}^4 m_\psi^2}{8\pi\Lambda^4}$
	$\gamma Z$	$\frac{\frac{s_W^2}{c_W^2} \left( 2\sigma_{\gamma\gamma} + 3(\beta^2-1) \log\left(\frac{3+\beta}{1-\beta}\right) \right)}{c_W^2}$	$\frac{s_W^2}{c_W^2} 2(\sigma v)_{\gamma\gamma}$
$O_{el}$	$f\bar{f}$	$\frac{e^2 \beta N_c C_{el}^2 Y_f^2}{48\pi c_W^2 \Lambda^2}$	$\frac{e^2 N_c C_{el}^2 Y_f^2}{48\pi c_W^2 \Lambda^2} \cdot v^2$
	$W^+W^-, Zh$	$\frac{e^2 \beta C_{el}^2}{384\pi c_W^2 \Lambda^2}$	$\frac{e^2 C_{el}^2}{384\pi c_W^2 \Lambda^2} v^2$
	$\gamma\gamma$	$\frac{C_{el}^4 c_W^4 s \left( (9-7\beta^2)\beta^2 - 6\beta(\beta^2-1)^2 \tanh^{-1}(\beta) \right)}{96\pi\beta^3 \Lambda^4}$	$\frac{c_W^4 C_{el}^4 m_\psi^2}{8\pi\Lambda^4}$
	$\gamma Z$	$\frac{\frac{s_W^2}{c_W^2} \left( 2\sigma_{\gamma\gamma} + 3(\beta^2-1) \log\left(\frac{3+\beta}{1-\beta}\right) \right)}{c_W^2}$	$\frac{s_W^2}{c_W^2} 2(\sigma v)_{\gamma\gamma}$
$O_{cr}$	$f\bar{f}$	$\frac{(3-\beta^2)e^2 s N_c C_{cr}^2 Y_f^2}{48\pi\beta c_W^2 \Lambda^4}$	$\frac{e^2 N_c C_{cr}^2 Y_f^2 m_\psi^2}{4\pi c_W^2 \Lambda^4}$
	$W^+W^-, Zh$	$\frac{(3-\beta^2)e^2 s C_{cr}^2}{384\pi\beta c_W^2 \Lambda^4}$	$\frac{e^2 C_{cr}^2 m_\psi^2}{32\pi c_W^2 \Lambda^4}$
$O_A$	$f\bar{f}$	$\frac{e^2 s \beta C_A^2 N_c Y_f^2}{24\pi\Lambda^4 c_W^2}$	$\frac{e^2 C_A^2 N_c Y_f^2 m_\chi^2}{6\pi\Lambda^4 c_W^2} \cdot v^2$
	$W^+W^-, Zh$	$\frac{e^2 s \beta C_A^2}{192c_W^2 \pi\Lambda^4}$	$\frac{e^2 C_A^2 m_\chi^2}{48\pi\Lambda^4 c_W^2} \cdot v^2$

Table A.1: Analytic expressions for the cross-section ( $\sigma$ ), and velocity-weighted, non-relativistic annihilation cross-sections ( $\sigma v$ ) into SM final states ( $XX$ ), for dimension-5 and dimension-6 operators of the hypercharge EFT for Dirac dark matter. The cross-section is provided in the high-energy limit with massless SM particles,  $\beta^2 = (1 - 4m_\psi^2/s)$  and  $N_c$  is the number of colors. In the low velocity limit  $\beta \approx v$ , so cross-sections that are  $s$ -wave will be  $O(1/\beta)$  at the lowest order. The  $\psi\bar{\psi} \rightarrow ZZ$  annihilation cross-section is given by  $(s_W^4/c_W^4)\sigma_{\gamma\gamma}$ . The Majorana anapole can be obtained by dividing the Dirac anapole moment by two, following equations (4.12) and (4.13).



## A.7 ALPs Computations

### A.7.1 Explicit Calculation of Phase Redefinition

Performing an ALP-dependent phase redefinition of the Higgs and the fermion fields in the SM Lagrangian, that in flavor basis is realized as a unitary rotation whose phase is proportional to the  $3 \times 3$  Hermitian matrices  $\mathbf{q}_\psi$

$$\begin{aligned}\psi_i &\rightarrow [e^{i\mathbf{q}_\psi^i a}]_{ij} \psi_j, \\ H &\rightarrow e^{i\mathbf{q}_H a} H,\end{aligned}$$

we can obtain more details, compared with those following from equation (5.9), on the phenomenology of ALP. The phase redefinition affects each term of SM Lagrangian except for those that are pure gauges.

Since left-handed and right-handed fermions undergo different couplings, we have chosen to use Weyl basis in this computation, thus we must have to switch from Dirac to Weyl spinor in each term of the Lagrangian. For instance, term kinetic term of the left-handed spinor turns to:

$$\bar{\psi}_L \gamma_\mu \partial^\mu \psi_L = \psi_L^\dagger \gamma_0 \gamma_\mu \partial^\mu \psi_L = \begin{pmatrix} \psi_L^\dagger & 0 \end{pmatrix} \begin{pmatrix} 0 & \mathbb{1} \\ \mathbb{1} & 0 \end{pmatrix} \begin{pmatrix} 0 & \sigma_\mu \\ \bar{\sigma}_\mu & 0 \end{pmatrix} \partial^\mu \begin{pmatrix} \psi_L \\ 0 \end{pmatrix} = \psi_L^\dagger \bar{\sigma}_\mu \partial^\mu \psi_L.$$

The adopted notation might be a little misunderstanding since the same symbol  $\psi_L$  has been used to denote both the Dirac and the Weyl spinor, however we made this choice to avoid extra subscripts. A similar computation can be done for the right-handed spinors. Thus:

$$\begin{aligned}\bar{\psi}_L \not{\partial} \psi_L &\rightarrow \psi_L^\dagger \bar{\sigma}^\mu \partial_\mu \psi_L, \\ \bar{\psi}_R \not{\partial} \psi_R &\rightarrow \psi_R^\dagger \sigma^\mu \partial_\mu \psi_R.\end{aligned}$$

The phase redefinition of the right-handed spinor leads to:

$$\begin{aligned}\mathcal{L}_{\psi_R} &\rightarrow i \left( [e^{i\mathbf{q}_{\psi_R} a}]_{ij} \psi_{Rj} \right)^\dagger (\sigma^\mu D_\mu) \left( [e^{i\mathbf{q}_{\psi_R} a}]_{ik} \psi_{Rk} \right) \\ &= \mathcal{L}_{\psi_R} - (\partial_\mu a) \psi_{Ri}^\dagger [\mathbf{q}_{\psi_R}]_{ij} \sigma^\mu \psi_{Rj} + O[(\partial a)^2],\end{aligned}\tag{A.25}$$

where the covariant derivative is  $D_\mu = \partial_\mu - ig_s G_\mu^a T^a - ig' Y_{\psi_R} B_\mu$  and the subscript  $\psi_R$  runs over the right-handed fields  $e$ ,  $u$  and  $d$ . The computation was performed by using the Hermitian transpose of the transformation matrix

$$\left( [e^{i\mathbf{q}_\psi a}]_{ij} \right)^\dagger \simeq \left( [\mathbb{1} + ia \mathbf{q}_\psi]_{ij} \right)^\dagger = [\mathbb{1}]_{ij} - ia [\mathbf{q}_\psi]_{ij} \simeq [e^{-i\mathbf{q}_\psi a}]_{ij},$$

and the derivative of an exponential matrix

$$\partial_\mu [e^{i\mathbf{q}_\psi a}]_{ij} = i (\partial_\mu a) [e^{i\mathbf{q}_\psi a}]_{ij} = i (\partial_\mu a) [e^{i\mathbf{q}_\psi a}]_{ij} [\mathbf{q}_\psi]_{kj}.$$

The phase redefinition of the left-handed spinor fields leads to an analogous formula of equation (A.25) since the only difference is that the covariant derivative now reads  $D_\mu = \partial_\mu - ig_s G_\mu^a T^a - ig W_\mu^a \tau^a - ig' Y_{\psi_L} B_\mu$ , thus we get:

$$\mathcal{L}_{\psi_L} \rightarrow \mathcal{L}_{\psi_L} - (\partial_\mu a) \psi_{Li}^\dagger [\mathbf{q}_{\psi_L}]_{ij} \bar{\sigma}^\mu \psi_{Lj} + O[(\partial a)^2],\tag{A.26}$$

where  $\psi_L$  takes the values  $L$  and  $Q$ . Summing together the equations (A.25) and (A.25) for all the flavor, we obtain the complete transformation of the Lagrangian that describes the interaction between fermions and gauge fields:

$$\begin{aligned} \mathcal{L}_{\text{int}} &\rightarrow \mathcal{L}_{\text{int}} - (\partial_\mu a) \sum_{\psi=L,Q} [\mathbf{q}_\psi]_{ij} \psi_i^\dagger \bar{\sigma}^\mu \psi_j \\ &\quad - (\partial_\mu a) \sum_{\psi=e,u,d} [\mathbf{q}_\psi]_{ij} \psi_i^\dagger \sigma^\mu \psi_j + O[(\partial a)^2]. \end{aligned} \quad (\text{A.27})$$

Turning to Higgs Lagrangian, the phase redefinition acts as

$$\begin{aligned} \mathcal{L}_H &\rightarrow (D_\mu(e^{iq_H a} H))^\dagger (D^\mu(e^{iq_H a} H)) + m_H^2 H^\dagger H - \lambda(H^\dagger H)^2 \\ &= \mathcal{L}_H - iq_H (\partial^\mu a) (H^\dagger \overset{\leftrightarrow}{D}_\mu H) + O[(\partial a)^2], \end{aligned} \quad (\text{A.28})$$

where the mass term and the potential are not affected by the rotation since they are composed by the Higgs field and his Hermitian transpose.

Finally, we have to transform the Yukawa terms of the SM Lagrangian. This time, left-handed and right-handed Weyl spinors are mixed in the same Lagrangian term, therefore we need to distinguish between the two types of particles that compose the  $SU(2)$  doublet: the upper particles (up-like quarks and neutral leptons), and lower particles (down-like quarks and charged leptons). Starting with the case of lower particles, in particular for charged leptons:

$$\mathcal{L}_{Yuk,e} \rightarrow -\mathbf{Y}_{ij}^e L_\ell^\dagger [e^{-i\mathbf{q}_L a}]_{\ell i} e^{iq_H a} H [e^{i\mathbf{q}_e a}]_{jk} e_R^k + h.c.,$$

expanding in Taylor series:

$$\begin{aligned} \mathcal{L}_{Yuk,e} &\rightarrow -\mathbf{Y}_{ij}^e L_\ell^\dagger ([\mathbb{1}]_{\ell i} - [i\mathbf{q}_L a]_{\ell i}) (1 + iq_H a) H ([\mathbb{1}]_{jk} + [i\mathbf{q}_e a]_{jk}) e_R^k + h.c. \\ &= \mathcal{L}_{Yuk,e} - ia \left( \mathbf{Y}_{ik}^e [\mathbf{q}_e]_{kj} - \mathbf{Y}_{kj}^e [\mathbf{q}_L]_{ik} + q_H \mathbf{Y}_{ij}^e \right) L_i^\dagger H e_R^j + h.c. + O(a^2). \end{aligned}$$

While for the up-like quarks, we have:

$$\begin{aligned} \mathcal{L}_{Yuk,u} &\rightarrow -\mathbf{Y}_{ij}^u q_\ell^\dagger [e^{-i\mathbf{q}_Q a}]_{\ell i} e^{-iq_H a} \tilde{H} [e^{i\mathbf{q}_u a}]_{jk} u_R^k + h.c. \\ &= \mathcal{L}_{Yuk,u} - ia \left( \mathbf{Y}_{ik}^u [\mathbf{q}_u]_{kj} - \mathbf{Y}_{kj}^u [\mathbf{q}_Q]_{ik} - q_H \mathbf{Y}_{ij}^u \right) q_i^\dagger \tilde{H} u_R^j + h.c. + O(a^2). \end{aligned}$$

Summarizing our result, the phase redefinition in the complete Yukawa Lagrangian leads to

$$\begin{aligned} \mathcal{L}_{Yuk} &\rightarrow \mathcal{L}_{Yukawa} - ia \left( \mathbf{Y}_{ik}^e [\mathbf{q}_e]_{kj} - \mathbf{Y}_{kj}^e [\mathbf{q}_L]_{ik} + q_H \mathbf{Y}_{ij}^e \right) \ell_i^\dagger H e_R^j + h.c. \\ &\quad - ia \left( \mathbf{Y}_{ik}^d [\mathbf{q}_d]_{kj} - \mathbf{Y}_{kj}^d [\mathbf{q}_Q]_{ik} + q_H \mathbf{Y}_{ij}^d \right) q_i^\dagger H d_R^j + h.c. \\ &\quad - ia \left( \mathbf{Y}_{ik}^u [\mathbf{q}_u]_{kj} - \mathbf{Y}_{kj}^u [\mathbf{q}_Q]_{ik} - q_H \mathbf{Y}_{ij}^u \right) q_i^\dagger \tilde{H} u_R^j + h.c. + O(a^2). \end{aligned}$$

Forgetting for the moment the non invariant measure of the path integral, the

SM Lagrangian under the phase rotation of fields turns to:

$$\begin{aligned}
\mathcal{L}_{\text{SM}} \rightarrow & \mathcal{L}_{\text{SM}} - (\partial_\mu a) \left( \sum_{\psi=L,Q} [q_\psi]_{ij} \psi_i^\dagger \bar{\sigma}^\mu \psi_j + \sum_{\psi=e,u,d} [q_\psi]_{ij} \psi_i^\dagger \sigma^\mu \psi_j \right) \\
& - ia \left( \mathbf{Y}_{ik}^e [\mathbf{q}_e]_{kj} - \mathbf{Y}_{kj}^e [\mathbf{q}_L]_{ik} + q_H \mathbf{Y}_{ij}^e \right) \ell_i^\dagger H e_R^j + \text{h.c.} \\
& - ia \left( \mathbf{Y}_{ik}^d [\mathbf{q}_d]_{kj} - \mathbf{Y}_{kj}^d [\mathbf{q}_Q]_{ik} + q_H \mathbf{Y}_{ij}^d \right) q_i^\dagger H d_R^j + \text{h.c.} \\
& - ia \left( \mathbf{Y}_{ik}^u [\mathbf{q}_u]_{kj} - \mathbf{Y}_{kj}^u [\mathbf{q}_Q]_{ik} - q_H \mathbf{Y}_{ij}^u \right) q_i^\dagger \tilde{H} u_R^j + \text{h.c.} \\
& - iq_H (\partial^\mu a) (H^\dagger \overleftrightarrow{D}^\mu H) + O(a^2) + O[(\partial a)^2].
\end{aligned} \tag{A.29}$$

The amplitude of the scattering process  $\bar{q}q \rightarrow \bar{t}t$  at NLO in the ALP theory, is given by the sum of the tree-level, the one-loop diagram involving ALP and its counter-term:

$$\begin{aligned}
i\mathcal{M}_{NLO} = & T_{a_1 a_2}^{g_1} T_{a_3 a_4}^{g_1} \bar{v}(p_2) \gamma_\mu u(p_1) \\
& \times \bar{u}(p_3) \left[ \frac{iz\gamma^\mu}{192\pi^4 (z^2 - 1)^3 m_t^2} \left( 48x^2 z^2 \text{Li}_2(z) + 24zx^2 z \log(1 - z) \right. \right. \\
& \times (\log(-z) + \log(z) + i\pi) - 6i\pi x^2 z(z(z + 10) + 1) + 3i\pi (z^2 - 1)^2 \\
& + 3\log(z) + 16\pi^2 x^2 z^2 + 3z(-\log(z)(2x^2(z^2 + 4i\pi z + 10z + 1) \\
& + 4x^2 z \log(z) - z(z^2 - 2))) + 3x^2(3z^4 - 2z^3 + 2z - 3) \\
& \left. \left. + 12x^2 \log(x)(z^4 - 4i\pi z^2 - 4z^2 \log(z) - 1) \right) \right. \\
& + \frac{z^2 \sigma^{\mu\nu} (p_3 + p_4)_\nu}{96\pi^4 (z^2 - 1)^3 m_t^3} \left( 12x^2 z \text{Li}_2(z) + 3i\pi(z(-6x^2 + z - 2) + 1) \right. \\
& + 3x^2(z^2 - 1) + 4\pi^2 x^2 z + 6x^2 \log(x)(z^2 - 2i\pi z - 2z \log(z) - 1) \\
& + 6x^2 z \log(1 - z)(\log(-z) + \log(z) + i\pi) \\
& \left. \left. - 3z \log(z)(x^2 \log(z) + (6 + 2i\pi)x^2 - z + 2) + 3\log(z) \right) \right] v(p_4),
\end{aligned} \tag{A.30}$$

where the incoming quarks are labeled by the subscripts 1 and 2, so that their momenta and colors are  $p_1, a_1$  and  $p_2, a_2$  respectively, while the outgoing pair of quarks top are labeled by the indices 3 and 4. The color index of the gluon field is  $g_1$ . Moreover, the variables  $x$  and  $z$  are:

$$x = m_a/m_t, \quad z = \frac{1 - v}{1 + v} \quad \text{with} \quad v = \sqrt{1 - \frac{4m_t^2}{s}}. \tag{A.31}$$

The condition  $s \geq 4m_t^2$ , where  $s = (p_{\bar{q}} + p_q)^2$ , can be rendered as  $0 \leq v < 1$  and  $0 < z \leq 1$ , with  $z$  that reaches its maximum value when the energy involved in the process achieves its minimum.

In the scalar ALP theory, where the interaction vertex between the ALP and the top quark is:

$$V_s^Y = \frac{iC_t v}{\sqrt{2}\Lambda} \delta^{ab},$$

the NLO amplitude – still at  $O(x^3)$  – is:

$$\begin{aligned}
i\mathcal{M}_{NLO} = & T_{a_1 a_2}^{g_1} T_{a_3 a_4}^{g_1} \bar{v}(p_2) \gamma_\mu u(p_1) \\
& \times \bar{u}(p_3) \left[ \frac{izm_t \gamma^\mu}{192\pi^4 (z^2 - 1)^3 m_t^3} \left( 144x^2 z^2 Li_2(z) + (z - 1)^2 48z Li_2(z) \right. \right. \\
& + 36x^2 \log(x) (z^4 - 4i\pi z^2 - 4z^2 \log(z) - 1) \\
& - 3x^2 z (3(z + 2)z^2 - 16\pi^2 z + 2i\pi(z(z + 10) + 1) - 6) \\
& + 72x^2 i\pi z^2 (\log(2 - 2z) - \log(2z)) \\
& - 6x^2 z (-12i\pi z \log(1 - z) + \log(z) + z \log(z)(z + 6 \log(z) + 10)) + 3 \\
& + 6\pi x(z - 1)(z + 1)(z(3z + 2) + 3) - 24z^2 + 16\pi^2 z + 3i\pi((z - 14)z + 1) \\
& + 24i(z - 1)^2 \pi z (\log(2 - 2z) - \log(2z)) + 3 \log(z) + 24 \\
& + 24(z - 1)^2 \log(x) (-z^2 - 2i\pi z - 2z \log(z) + 1) \\
& \left. \left. + 24(z - 1)^2 i\pi z \log(1 - z) + 3(z - 1)^4 z(z - 4 \log(z) - 14) \log(z) \right) \right] \\
& + \frac{6z^2 \sigma^{\mu\nu} (p_3 + p_4)_\nu}{192\pi^4 (z^2 - 1)^3 m_t^3} \left( 12x^2 z Li_2(z) - 3x^2 (z^2 - 1) \right. \\
& - i\pi (6x^2 z + 4ix (z^2 - 1) + 3(z - 1)^2) \\
& + 6x^2 (z^2 - 2i\pi z - 1) \log(x) + 4\pi^2 x^2 z - 3 \log(z) \\
& + 6x^2 z \log(1 - z) (\log(-z) + i\pi) - 6x^2 i\pi z \log(z) - 3x^2 z \log^2(z) \\
& \left. \left. - 3z \log(z) (-2x^2 \log(1 - z) + 2x^2 + 4x^2 \log(x) + z - 2) \right) \right] v(p_4).
\end{aligned} \tag{A.32}$$

## A.7.2 Derivatives in Pseudo-Scalar Potential

The pseudoscalar potential is

$$V_{PS}(\mathbf{x}) = \left( \frac{C_t v}{\sqrt{2} \Lambda} \right)^2 \left( \frac{\delta_{sr} \delta_{s'r'} \delta^{(3)}(\mathbf{x})}{4m_t^2} + \frac{[\nabla \cdot \boldsymbol{\sigma}_z]_{s's} [\nabla \cdot \boldsymbol{\sigma}_z]_{r'r'}}{4m_t^2} \frac{e^{-m_a x}}{4\pi x} \right),$$

Recalling that Del operator is  $\nabla = (\partial_1, \partial_2, \partial_3)$ , we can label its components as  $\partial_i$  where  $i = \{1, 2, 3\}$ , therefore:

$$\begin{aligned}
\partial^i \partial^j \left( \frac{e^{-M_a |x|}}{x} \right) = & e^{-M_a |x|} \partial^i \partial^j \left( \frac{1}{|x|} \right) \\
& + \partial^i \left( e^{-M_a |x|} \right) \partial^j \left( \frac{1}{|x|} \right) + \partial^i \left( \frac{1}{|x|} \right) \partial^j \left( e^{-M_a |x|} \right) \\
& + \frac{1}{|x|} \partial^i \partial^j \left( e^{-M_a |x|} \right)
\end{aligned}$$

Moreover, we must notice that  $|x| = (x_1^2 + x_2^2 + x_3^2)^{1/2}$  and  $\partial^i |x| = x^i / |x| \equiv \hat{x}^i$ . The first term is singular and not derivable in  $x = 0$ , therefore we start evaluating

it for  $|x| \neq 0$ :

$$\begin{aligned} e^{-M_a |x|} \partial^i \partial^j \left( \frac{1}{|x|} \right) &= e^{-M_a |x|} \partial^i \left( -\frac{x^j}{|x|^2} \right) \\ &= e^{-M_a |x|} \left( \frac{3x^i x^j}{|x|^5} - \frac{\delta^{ij}}{|x|^3} \right) \\ &= e^{-M_a |x|} \left( \frac{3\hat{x}^i \hat{x}^j - \delta^{ij}}{|x|^3} \right) \end{aligned}$$

while in the coordinates' origin we have  $|x| = 0$  and  $i = j$ , thus:

$$e^{-M_a |x|} \partial^i \partial^j \left( \frac{1}{|x|} \right) = e^{-M_a |x|} \frac{\delta^{ij}}{3} \nabla^2 \left( \frac{1}{|x|} \right) = e^{-M_a |x|} \frac{\delta^{ij}}{3} (-4\pi \delta^3(\mathbf{x}))$$

this result follows from the evaluation of  $\nabla^2(1/|x|)$  which is null for each value of  $|x| \neq 0$  and equals to  $-4\pi$  for  $|x| = 0$ . To obtain this result in a faster way lets write the Laplacian operator in polar coordinates:

$$\nabla^2 = \frac{1}{r^2} \partial_r (r^2 \partial_r) + \frac{1}{r^2 \sin \theta} \partial_\theta (\sin \theta \partial_\theta) + \frac{1}{r^2 \sin^2 \theta} \partial_\phi^2$$

Only its first term survives when applied on a function of the radius only:

$$\nabla^2(1/r) = \frac{1}{r^2} \partial_r (r^2 \partial_r(1/r)) = \frac{1}{r^2} \partial_r (-1) = 0$$

However, to evaluate this Laplacian in  $r = 0$  we can integrate our function  $1/r$  on a sphere volume pointed in the origin. Using Gauss theorem:

$$\int_V \nabla^2(1/r) dV = \int_S \nabla(1/r) dS$$

now we only need to evaluate the Del operator and write the infinitesima sphere surface as  $dS = \hat{r} dA = \hat{r} r^2 \sin \theta d\theta d\phi$ , thus:

$$\int_V \nabla^2(1/r) dV = \int_0^\pi d\theta \int_0^{2\pi} d\phi (-\mathbf{r}/r^3) \hat{r} r^2 \sin \theta = -4\pi$$

therefore, we get that the Laplacian of  $1/r$  is null for all the value of  $r \neq 0$ , but its integral over a sphere volume is equal to  $-4\pi$ . Thus, it must be different from zero in the center of coordinates space, thus we can conclude that  $\nabla^2(1/r) = -4\pi \delta^3(\mathbf{r})$ .

Coming back to our computation, the first term is:

$$e^{-M_a |x|} \partial^i \partial^j \left( \frac{1}{|x|} \right) = e^{-M_a |x|} \left( \frac{3\hat{x}^i \hat{x}^j - \delta^{ij}}{|x|^3} - \frac{4}{3} \pi \delta^3(\mathbf{x}) \delta^{ij} \right) \quad (\text{A.33})$$

The second and third term are straight and they can be analysed together:

$$\partial^i \left( e^{-M_a |x|} \right) \partial^j \left( \frac{1}{|x|} \right) + \partial^i \left( \frac{1}{|x|} \right) \partial^j \left( e^{-M_a |x|} \right) = 2e^{-M_a |x|} M_a \frac{\hat{x}^i \hat{x}^j}{|x|^2} \quad (\text{A.34})$$

The derivative of last is:

$$\begin{aligned}
\frac{1}{|x|} \partial^i \partial^j \left( e^{-M_a |x|} \right) &= \frac{1}{|x|} \partial^i \left( -M_a e^{-M_a |x|} \partial^j |x| \right) \\
&= \frac{e^{-M_a |x|}}{|x|} \left( M_a^2 (\partial^i |x|) (\partial^j |x|) - M_a \partial^i \partial^j |x| \right) \\
&= \frac{e^{-M_a |x|}}{|x|} \left( M_a^2 \hat{x}^i \hat{x}^j - M_a \partial^i (x^j / |x|) \right) \\
&= \frac{e^{-M_a |x|}}{|x|} \left( M_a^2 \hat{x}^i \hat{x}^j - \frac{M_a}{|x|} \delta^{ij} + \frac{M_a}{|x|} \hat{x}^i \hat{x}^j \right)
\end{aligned} \tag{A.35}$$

Summing together equations (A.33) - (A.35)

$$\begin{aligned}
\partial^i \partial^j \left( \frac{e^{-M_a |x|}}{|x|} \right) &= \frac{M_a^2 e^{-M_a |x|}}{3|x|} \left[ (3\hat{x}^i \hat{x}^j - \delta^{ij}) \left( 1 + \frac{3}{M_a |x|} + \frac{3}{(M_a |x|)^2} \right) + \delta^{ij} \right] \\
&\quad - \frac{4\pi}{3} \delta^3(\mathbf{x}) \delta^{ij}
\end{aligned}$$

## A.8 Passarino Veltman Scalar Integrals

The Passarino-Veltman scalar integrals are defined as

$$\begin{aligned}
B_0(q_{10}, m_0, m_1) &= \frac{\mu^{(4-D)}}{i(\pi)^{D/2}} \int d^D l \frac{1}{(l^2 - m_0^2)((l + q_1)^2 - m_1^2)} \\
C_0(q_{10}, q_{20}, m_0, m_1, m_2) &= \frac{\mu^{(4-D)}}{i(\pi)^{D/2}} \int d^D l \frac{1}{(l^2 - m_0^2)((l + q_1)^2 - m_1^2)((l + q_2)^2 - m_2^2)}
\end{aligned}$$

In chapter 3 and 5, we many of these integrals enter in computations. While an explicit solution for  $C_0$  is quite hard to obtain when all its parameters are non null, the same does not hold for  $B_0$ , which can be easily solved with Feynman variables. Furthermore, this integral is involved in computations where the particle that running in the loop does not change its flavor, thus  $m_0 = m_1 = m$

$$\begin{aligned}
B_0(p, m, m) &= \mu^{(4-D)} \int \frac{d^D l}{i(\pi)^{D/2}} \int_0^1 dx \frac{1}{[(l^2 - m^2)(1-x) + ((l+p)^2 - m^2)x]^2} \\
&= \mu^{(4-D)} \int \frac{d^D l}{i(\pi)^{D/2}} \int_0^1 dx \frac{1}{(l^2 + 2lxp - m^2)^2} \\
&= \mu^{(4-D)} \frac{(2\pi)^D}{i(\pi)^{D/2}} \int \frac{d^D l}{(2\pi)^D} \int_0^1 dx \frac{1}{(l^2 - m^2)^2}
\end{aligned}$$

where the second equality has been obtained by performing the shift  $l \rightarrow l - px$ . The integration over loop momentum is now straight:

$$B_0(p, m, m) = \mu^\epsilon \frac{(2\pi)^D}{i(\pi)^{D/2}} \frac{i\Gamma(2 - \frac{D}{2})}{(4\pi)^{D/2}} (m^2)^{-2+D/2} = \frac{1}{\epsilon} - \gamma_E - \log \frac{m^2}{\mu^2} + O(\epsilon). \tag{A.36}$$

# Bibliography

- [1] C. Arina, A. Cheek, K. Mimasu and L. Pagani, *Eur. Phys. J. C* **81** (2021) no.3, 223 doi:10.1140/epjc/s10052-021-09010-1 [arXiv:2005.12789 [hep-ph]].
- [2] P. A. M. Dirac, *Proc. Roy. Soc. Lond. A* **114** (1927), 243 doi:10.1098/rspa.1927.0039
- [3] M. E. Peskin and D. V. Schroeder, *An Introduction to quantum field theory*, Addison-Wesley Publishing Company, 1995.
- [4] M. D. Schwartz, *Quantum Field Theory and the Standard Model*, Cambridge University Press, New York, 2014.
- [5] R. P. Feynman and M. Gell-Mann, *Phys. Rev.* **109** (1958), 193-198 doi:10.1103/PhysRev.109.193
- [6] S. L. Glashow, *Nucl. Phys.* **22** (1961), 579-588 doi:10.1016/0029-5582(61)90469-2
- [7] A. Salam, *Conf. Proc. C* **680519** (1968), 367-377 doi:10.1142/9789812795915\_0034
- [8] F. Englert and R. Brout, *Phys. Rev. Lett.* **13** (1964), 321-323 doi:10.1103/PhysRevLett.13.321
- [9] P. W. Higgs, *Phys. Rev. Lett.* **13** (1964), 508-509 doi:10.1103/PhysRevLett.13.508
- [10] S. Weinberg, *Phys. Rev. Lett.* **19** (1967), 1264-1266 doi:10.1103/PhysRevLett.19.1264
- [11] G. 't Hooft, *Nucl. Phys. B* **35** (1971), 167-188 doi:10.1016/0550-3213(71)90139-8
- [12] A. V. Manohar, doi:10.1093/oso/9780198855743.003.0002 [arXiv:1804.05863 [hep-ph]].
- [13] D. B. Kaplan, [arXiv:nucl-th/0510023 [nucl-th]].
- [14] W. Skiba, doi:10.1142/9789814327183\_0001 [arXiv:1006.2142 [hep-ph]].
- [15] C. P. Burgess, *Ann. Rev. Nucl. Part. Sci.* **57** (2007), 329-362 doi:10.1146/annurev.nucl.56.080805.140508 [arXiv:hep-th/0701053 [hep-th]].

- [16] B. Gripaios, [arXiv:1506.05039 [hep-ph]].
- [17] I. Z. Rothstein, [arXiv:hep-ph/0308266 [hep-ph]].
- [18] I. Brivio and M. Trott, Phys. Rept. **793** (2019), 1-98 doi:10.1016/j.phys-rep.2018.11.002 [arXiv:1706.08945 [hep-ph]].
- [19] S. Weinberg, Phys. Rev. Lett. **43** (1979), 1566-1570 doi:10.1103/PhysRevLett.43.1566
- [20] A. Kobach, Phys. Lett. B **758** (2016), 455-457 doi:10.1016/j.physletb.2016.05.050 [arXiv:1604.05726 [hep-ph]].
- [21] B. Grzadkowski, M. Iskrzynski, M. Misiak and J. Rosiek, JHEP **10** (2010), 085 doi:10.1007/JHEP10(2010)085 [arXiv:1008.4884 [hep-ph]].
- [22] W. Buchmuller and D. Wyler, Nucl. Phys. B **268** (1986), 621-653 doi:10.1016/0550-3213(86)90262-2
- [23] R. Alonso, E. E. Jenkins, A. V. Manohar and M. Trott, JHEP **04** (2014), 159 doi:10.1007/JHEP04(2014)159 [arXiv:1312.2014 [hep-ph]].
- [24] G. Buchalla, O. Cata and G. D'Ambrosio, Eur. Phys. J. C **74** (2014) no.3, 2798 doi:10.1140/epjc/s10052-014-2798-2 [arXiv:1310.2574 [hep-ph]].
- [25] W. Heisenberg and H. Euler, Z. Phys. **98** (1936) no.11-12, 714-732 doi:10.1007/BF01343663 [arXiv:physics/0605038 [physics]].
- [26] F. Přeučil and J. Hořejší, J. Phys. G **45** (2018) no.8, 085005 doi:10.1088/1361-6471/aace90 [arXiv:1707.08106 [hep-ph]].
- [27] M. Ghasemkhani, V. Rahmanpour, R. Bufalo and A. Soto, [arXiv:2109.11411 [hep-th]].
- [28] S. Fichtel and G. von Gersdorff, JHEP **03** (2014), 102 doi:10.1007/JHEP03(2014)102 [arXiv:1311.6815 [hep-ph]].
- [29] C. Baldenegro, S. Fichtel, G. von Gersdorff and C. Royon, JHEP **06** (2017), 142 doi:10.1007/JHEP06(2017)142 [arXiv:1703.10600 [hep-ph]].
- [30] S. Fichtel, G. von Gersdorff, B. Lenzi, C. Royon and M. Saimpert, JHEP **02** (2015), 165 doi:10.1007/JHEP02(2015)165 [arXiv:1411.6629 [hep-ph]].
- [31] M. Aaboud *et al.* [ATLAS], Nature Phys. **13** (2017) no.9, 852-858 doi:10.1038/nphys4208 [arXiv:1702.01625 [hep-ex]].
- [32] D. d'Enterria and G. G. da Silveira, Phys. Rev. Lett. **111** (2013), 080405 [erratum: Phys. Rev. Lett. **116** (2016) no.12, 129901] doi:10.1103/PhysRevLett.111.080405 [arXiv:1305.7142 [hep-ph]].
- [33] M. Klusek-Gawenda, P. Lebiedowicz and A. Szczurek, Phys. Rev. C **93** (2016) no.4, 044907 doi:10.1103/PhysRevC.93.044907 [arXiv:1601.07001 [nucl-th]].
- [34] J. Ellis, N. E. Mavromatos and T. You, Phys. Rev. Lett. **118** (2017) no.26, 261802 doi:10.1103/PhysRevLett.118.261802 [arXiv:1703.08450 [hep-ph]].



- [35] J. Quevillon, C. Smith and S. Touati, Phys. Rev. D **99** (2019) no.1, 013003 doi:10.1103/PhysRevD.99.013003 [arXiv:1810.06994 [hep-ph]].
- [36] K. Yamashita, X. Fan, S. Kamioka, S. Asai and A. Sugamoto, PTEP **2017** (2017) no.12, 123B03 doi:10.1093/ptep/ptx157 [arXiv:1707.03308 [hep-ph]].
- [37] D. Merritt, Stud. Hist. Phil. Sci. B **57** (2017), 41-52 doi:10.1016/j.shpsb.2016.12.002 [arXiv:1703.02389 [physics.hist-ph]].
- [38] S. Funk, Proc. Nat. Acad. Sci. **112** (2015), 2264 doi:10.1073/pnas.1308728111 [arXiv:1310.2695 [astro-ph.HE]].
- [39] N. Aghanim *et al.* [Planck], Astron. Astrophys. **641** (2020), A6 [erratum: Astron. Astrophys. **652** (2021), C4] doi:10.1051/0004-6361/201833910 [arXiv:1807.06209 [astro-ph.CO]].
- [40] J. F. Navarro, C. S. Frenk and S. D. M. White, Astrophys. J. **462** (1996), 563-575 doi:10.1086/177173 [arXiv:astro-ph/9508025 [astro-ph]].
- [41] G. Steigman and M. S. Turner, Nucl. Phys. B **253** (1985), 375-386 doi:10.1016/0550-3213(85)90537-1
- [42] E. A. Baltz, eConf **C040802** (2004), L002 [arXiv:astro-ph/0412170 [astro-ph]].
- [43] P. Coles and F. Lucchin, *Cosmology: The Origin and evolution of cosmic structure*, John Wiley & Sons Inc, 2002
- [44] S. Dodelson, *Modern Cosmology*, Academic Press, Amsterdam, 2003.
- [45] V. Mukhanov, *Physical Foundations of Cosmology*, Cambridge University Press, Oxford, 2005.
- [46] S. Weinberg, *Cosmology*, Oxford University Press, 2008.
- [47] B. F. Schutz, *A FIRST COURSE IN GENERAL RELATIVITY*, Cambridge Univ. Pr., Cambridge, UK, 1985.
- [48] S. Weinberg, *Gravitation and Cosmology: Principles and Applications of the General Theory of Relativity*, John Wiley and Sons, New York, 1972.
- [49] G. Busoni, A. De Simone, E. Morgante and A. Riotto, Phys. Lett. B **728** (2014), 412-421 doi:10.1016/j.physletb.2013.11.069 [arXiv:1307.2253 [hep-ph]].
- [50] M. Beltran, D. Hooper, E. W. Kolb, Z. A. C. Krusberg and T. M. P. Tait, JHEP **09** (2010), 037 doi:10.1007/JHEP09(2010)037 [arXiv:1002.4137 [hep-ph]].
- [51] P. J. Fox, R. Harnik, J. Kopp and Y. Tsai, Phys. Rev. D **85** (2012), 056011 doi:10.1103/PhysRevD.85.056011 [arXiv:1109.4398 [hep-ph]].
- [52] G. Bertone, D. Hooper and J. Silk, Phys. Rept. **405** (2005), 279-390 doi:10.1016/j.physrep.2004.08.031 [arXiv:hep-ph/0404175 [hep-ph]].

- [53] Q. H. Cao, C. R. Chen, C. S. Li and H. Zhang, *JHEP* **08** (2011), 018 doi:10.1007/JHEP08(2011)018 [arXiv:0912.4511 [hep-ph]].
- [54] S. Matsumoto, S. Mukhopadhyay and Y. L. S. Tsai, *JHEP* **10** (2014), 155 doi:10.1007/JHEP10(2014)155 [arXiv:1407.1859 [hep-ph]].
- [55] M. Bauer, A. Butter, N. Desai, J. Gonzalez-Fraile and T. Plehn, *Phys. Rev. D* **95** (2017) no.7, 075036 doi:10.1103/PhysRevD.95.075036 [arXiv:1611.09908 [hep-ph]].
- [56] N. F. Bell, Y. Cai, J. B. Dent, R. K. Leane and T. J. Weiler, *Phys. Rev. D* **92** (2015) no.5, 053008 doi:10.1103/PhysRevD.92.053008 [arXiv:1503.07874 [hep-ph]].
- [57] E. Conte and B. Fuks, *Int. J. Mod. Phys. A* **33** (2018) no.28, 1830027 doi:10.1142/S0217751X18300272 [arXiv:1808.00480 [hep-ph]].
- [58] J. Alwall, R. Frederix, S. Frixione, V. Hirschi, F. Maltoni, O. Mattelaer, H. S. Shao, T. Stelzer, P. Torrielli and M. Zaro, *JHEP* **07** (2014), 079 doi:10.1007/JHEP07(2014)079 [arXiv:1405.0301 [hep-ph]].
- [59] J. Heisig, M. Krämer, E. Madge and A. Mück, *JHEP* **03** (2020), 183 doi:10.1007/JHEP03(2020)183 [arXiv:1912.08472 [hep-ph]].
- [60] N. Craig, H. K. Lou, M. McCullough and A. Thalapillil, *JHEP* **02** (2016), 127 doi:10.1007/JHEP02(2016)127 [arXiv:1412.0258 [hep-ph]].
- [61] H. Han, J. M. Yang, Y. Zhang and S. Zheng, *Phys. Lett. B* **756** (2016), 109-112 doi:10.1016/j.physletb.2016.03.010 [arXiv:1601.06232 [hep-ph]].
- [62] M. Endo and Y. Takaesu, *Phys. Lett. B* **743** (2015), 228-234 doi:10.1016/j.physletb.2015.02.042 [arXiv:1407.6882 [hep-ph]].
- [63] M. Ruhdorfer, E. Salvioni and A. Weiler, *SciPost Phys.* **8** (2020), 027 doi:10.21468/SciPostPhys.8.2.027 [arXiv:1910.04170 [hep-ph]].
- [64] E. Del Nobile, *Phys. Rev. D* **98** (2018) no.12, 123003 doi:10.1103/PhysRevD.98.123003 [arXiv:1806.01291 [hep-ph]].
- [65] B. Holdom, *Phys. Lett. B* **166** (1986), 196-198 doi:10.1016/0370-2693(86)91377-8
- [66] B. Holdom, *Phys. Lett. B* **178** (1986), 65-70 doi:10.1016/0370-2693(86)90470-3
- [67] S. A. Abel and B. W. Schofield, *Nucl. Phys. B* **685** (2004), 150-170 doi:10.1016/j.nuclphysb.2004.02.037 [arXiv:hep-th/0311051 [hep-th]].
- [68] B. Batell and T. Gherghetta, *Phys. Rev. D* **73** (2006), 045016 doi:10.1103/PhysRevD.73.045016 [arXiv:hep-ph/0512356 [hep-ph]].
- [69] B. J. Kavanagh, P. Panci and R. Ziegler, *JHEP* **04** (2019), 089 doi:10.1007/JHEP04(2019)089 [arXiv:1810.00033 [hep-ph]].

- [70] M. Pospelov and T. ter Veldhuis, Phys. Lett. B **480** (2000), 181-186 doi:10.1016/S0370-2693(00)00358-0 [arXiv:hep-ph/0003010 [hep-ph]].
- [71] K. Sigurdson, M. Doran, A. Kurylov, R. R. Caldwell and M. Kamionkowski, Phys. Rev. D **70** (2004), 083501 [erratum: Phys. Rev. D **73** (2006), 089903] doi:10.1103/PhysRevD.70.083501 [arXiv:astro-ph/0406355 [astro-ph]].
- [72] V. Barger, W. Y. Keung and D. Marfatia, Phys. Lett. B **696** (2011), 74-78 doi:10.1016/j.physletb.2010.12.008 [arXiv:1007.4345 [hep-ph]].
- [73] T. Banks, J. F. Fortin and S. Thomas, [arXiv:1007.5515 [hep-ph]].
- [74] C. M. Ho and R. J. Scherrer, Phys. Lett. B **722** (2013), 341-346 doi:10.1016/j.physletb.2013.04.039 [arXiv:1211.0503 [hep-ph]].
- [75] Y. Gao, C. M. Ho and R. J. Scherrer, Phys. Rev. D **89** (2014) no.4, 045006 doi:10.1103/PhysRevD.89.045006 [arXiv:1311.5630 [hep-ph]].
- [76] E. Del Nobile, G. B. Gelmini, P. Gondolo and J. H. Huh, JCAP **06** (2014), 002 doi:10.1088/1475-7516/2014/06/002 [arXiv:1401.4508 [hep-ph]].
- [77] A. Alves, A. C. O. Santos and K. Sinha, Phys. Rev. D **97** (2018) no.5, 055023 doi:10.1103/PhysRevD.97.055023 [arXiv:1710.11290 [hep-ph]].
- [78] P. A. R. Ade *et al.* [Planck], Astron. Astrophys. **594** (2016), A13 doi:10.1051/0004-6361/201525830 [arXiv:1502.01589 [astro-ph.CO]].
- [79] F. Ambrogi, C. Arina, M. Backovic, J. Heisig, F. Maltoni, L. Mantani, O. Mattelaer and G. Mohlabeng, Phys. Dark Univ. **24** (2019), 100249 doi:10.1016/j.dark.2018.11.009 [arXiv:1804.00044 [hep-ph]].
- [80] A. Alloul, N. D. Christensen, C. Degrande, C. Duhr and B. Fuks, Comput. Phys. Commun. **185** (2014), 2250-2300 doi:10.1016/j.cpc.2014.04.012 [arXiv:1310.1921 [hep-ph]].
- [81] C. Degrande, C. Duhr, B. Fuks, D. Grellscheid, O. Mattelaer and T. Reiter, Comput. Phys. Commun. **183** (2012), 1201-1214 doi:10.1016/j.cpc.2012.01.022 [arXiv:1108.2040 [hep-ph]].
- [82] K. Griest and M. Kamionkowski, Phys. Rev. Lett. **64** (1990), 615 doi:10.1103/PhysRevLett.64.615
- [83] Ia. B. Zel'Dovich, Soviet Journal of Experimental and Theoretical Physics, **6** (1958), 1184 Provided by the SAO/NASA Astrophysics Data System.
- [84] E. E. Radescu, Phys. Rev. D **32** (1985), 1266 doi:10.1103/PhysRevD.32.1266
- [85] D. G. Cerdeño, A. Cheek, E. Reid and H. Schulz, JCAP **08** (2018), 011 doi:10.1088/1475-7516/2018/08/011 [arXiv:1802.03174 [hep-ph]].
- [86] E. Aprile *et al.* [XENON], Phys. Rev. Lett. **121** (2018) no.11, 111302 doi:10.1103/PhysRevLett.121.111302 [arXiv:1805.12562 [astro-ph.CO]].
- [87] D. S. Akerib *et al.* [LZ], [arXiv:1509.02910 [physics.ins-det]].

- [88] B. J. Mount, S. Hans, R. Rosero, M. Yeh, C. Chan, R. J. Gaitskell, D. Q. Huang, J. Makkinje, D. C. Malling and M. Pangilinan, *et al.* [arXiv:1703.09144 [physics.ins-det]].
- [89] F. D’Eramo, B. J. Kavanagh and P. Panci, *JHEP* **08** (2016), 111 doi:10.1007/JHEP08(2016)111 [arXiv:1605.04917 [hep-ph]].
- [90] A. Albert *et al.* [Fermi-LAT and DES], *Astrophys. J.* **834** (2017) no.2, 110 doi:10.3847/1538-4357/834/2/110 [arXiv:1611.03184 [astro-ph.HE]].
- [91] A. Geringer-Sameth, S. M. Koushiappas and M. Walker, *Astrophys. J.* **801** (2015) no.2, 74 doi:10.1088/0004-637X/801/2/74 [arXiv:1408.0002 [astro-ph.CO]].
- [92] M. Ackermann *et al.* [Fermi-LAT], *Phys. Rev. Lett.* **115** (2015) no.23, 231301 doi:10.1103/PhysRevLett.115.231301 [arXiv:1503.02641 [astro-ph.HE]].
- [93] N. Bozorgnia, D. G. Cerdeño, A. Cheek and B. Penning, *JCAP* **12** (2018), 013 doi:10.1088/1475-7516/2018/12/013 [arXiv:1810.05576 [hep-ph]].
- [94] G. Arcadi, Y. Mambrini and F. Richard, *JCAP* **03** (2015), 018 doi:10.1088/1475-7516/2015/03/018 [arXiv:1411.2985 [hep-ph]].
- [95] F. D’Eramo and M. Procura, *JHEP* **04** (2015), 054 doi:10.1007/JHEP04(2015)054 [arXiv:1411.3342 [hep-ph]].
- [96] Q. H. Cao, A. K. Wei and Q. F. Xiang, *Chin. Phys. C* **44** (2020) no.11, 113105 doi:10.1088/1674-1137/abae53 [arXiv:2006.12768 [hep-ph]].
- [97] J. Fan, M. Reece and L. T. Wang, *JCAP* **11** (2010), 042 doi:10.1088/1475-7516/2010/11/042 [arXiv:1008.1591 [hep-ph]].
- [98] A. L. Fitzpatrick, W. Haxton, E. Katz, N. Lubbers and Y. Xu, *JCAP* **02** (2013), 004 doi:10.1088/1475-7516/2013/02/004 [arXiv:1203.3542 [hep-ph]].
- [99] A. Flórez, A. Gurrola, W. Johns, J. Maruri, P. Sheldon, K. Sinha and S. R. Starko, *Phys. Rev. D* **100** (2019) no.1, 016017 doi:10.1103/PhysRevD.100.016017 [arXiv:1902.01488 [hep-ph]].
- [100] J. Kumar and D. Marfatia, *Phys. Rev. D* **88** (2013) no.1, 014035 doi:10.1103/PhysRevD.88.014035 [arXiv:1305.1611 [hep-ph]].
- [101] C. A. Argüelles, A. Diaz, A. Kheirandish, A. Olivares-Del-Campo, I. Safa and A. C. Vincent, *Rev. Mod. Phys.* **93** (2021) no.3, 035007 doi:10.1103/RevModPhys.93.035007 [arXiv:1912.09486 [hep-ph]].
- [102] A. Cuoco, J. Heisig, M. Korsmeier and M. Krämer, *JCAP* **04** (2018), 004 doi:10.1088/1475-7516/2018/04/004 [arXiv:1711.05274 [hep-ph]].
- [103] B. S. Acharya *et al.* [CTA Consortium], doi:10.1142/10986 [arXiv:1709.07997 [astro-ph.IM]].
- [104] A. Drlica-Wagner *et al.* [LSST Dark Matter Group], [arXiv:1902.01055 [astro-ph.CO]].

- [105] H. Zhan and J. A. Tyson, Rept. Prog. Phys. **81** (2018) no.6, 066901 doi:10.1088/1361-6633/aab1bd [arXiv:1707.06948 [astro-ph.CO]].
- [106] S. Ando, B. J. Kavanagh, O. Macias, T. Alves, S. Broersen, S. Delnoij, T. Goldman, J. Groefsema, J. Kleverlaan and J. Lenssen, *et al.* JCAP **10** (2019), 040 doi:10.1088/1475-7516/2019/10/040 [arXiv:1905.07128 [astro-ph.CO]].
- [107] N. Bozorgnia, A. Fattahi, C. S. Frenk, A. Cheek, D. G. Cerdeno, F. A. Gómez, R. J. J. Grand and F. Marinacci, JCAP **07** (2020), 036 doi:10.1088/1475-7516/2020/07/036 [arXiv:1910.07536 [astro-ph.GA]].
- [108] R. Agnese *et al.* [SuperCDMS], Phys. Rev. D **95** (2017) no.8, 082002 doi:10.1103/PhysRevD.95.082002 [arXiv:1610.00006 [physics.ins-det]].
- [109] F. Kahlhoefer, S. Kulkarni and S. Wild, JCAP **11** (2017), 016 doi:10.1088/1475-7516/2017/11/016 [arXiv:1707.08571 [hep-ph]].
- [110] T. Bringmann *et al.* [GAMBIT Dark Matter Workgroup], Eur. Phys. J. C **77** (2017) no.12, 831 doi:10.1140/epjc/s10052-017-5155-4 [arXiv:1705.07920 [hep-ph]].
- [111] T. R. Slatyer, Phys. Rev. D **93** (2016) no.2, 023527 doi:10.1103/PhysRevD.93.023527 [arXiv:1506.03811 [hep-ph]].
- [112] L. Rinchuso [H.E.S.S.], EPJ Web Conf. **209** (2019), 01023 doi:10.1051/epjconf/201920901023 [arXiv:1901.05299 [astro-ph.HE]].
- [113] M. Ackermann *et al.* [Fermi-LAT], Phys. Rev. D **91** (2015) no.12, 122002 doi:10.1103/PhysRevD.91.122002 [arXiv:1506.00013 [astro-ph.HE]].
- [114] S. Adrian-Martinez *et al.* [KM3Net], J. Phys. G **43** (2016) no.8, 084001 doi:10.1088/0954-3899/43/8/084001 [arXiv:1601.07459 [astro-ph.IM]].
- [115] K. Abe *et al.* [Hyper-Kamiokande], [arXiv:1805.04163 [physics.ins-det]].
- [116] S. Adrian-Martinez *et al.* [ANTARES], JCAP **10** (2015), 068 doi:10.1088/1475-7516/2015/10/068 [arXiv:1505.04866 [astro-ph.HE]].
- [117] M. G. Aartsen *et al.* [IceCube], Eur. Phys. J. C **76** (2016) no.10, 531 doi:10.1140/epjc/s10052-016-4375-3 [arXiv:1606.00209 [astro-ph.HE]].
- [118] C. El Aisati, C. Garcia-Cely, T. Hambye and L. Vanderheyden, JCAP **10** (2017), 021 doi:10.1088/1475-7516/2017/10/021 [arXiv:1706.06600 [hep-ph]].
- [119] M. Cirelli, G. Corcella, A. Hektor, G. Hutsi, M. Kadastik, P. Panci, M. Raidal, F. Sala and A. Strumia, JCAP **03** (2011), 051 [erratum: JCAP **10** (2012), E01] doi:10.1088/1475-7516/2012/10/E01 [arXiv:1012.4515 [hep-ph]].
- [120] A. De Simone, G. F. Giudice and A. Strumia, JHEP **06** (2014), 081 doi:10.1007/JHEP06(2014)081 [arXiv:1402.6287 [hep-ph]].
- [121] L. J. Hall, K. Jedamzik, J. March-Russell and S. M. West, JHEP **03** (2010), 080 doi:10.1007/JHEP03(2010)080 [arXiv:0911.1120 [hep-ph]].

- [122] J. McDonald, Phys. Rev. Lett. **88** (2002), 091304 doi:10.1103/PhysRevLett.88.091304 [arXiv:hep-ph/0106249 [hep-ph]].
- [123] R. T. D’Agnolo and J. T. Ruderman, Phys. Rev. Lett. **115** (2015) no.6, 061301 doi:10.1103/PhysRevLett.115.061301 [arXiv:1505.07107 [hep-ph]].
- [124] R. Allahverdi, B. Dutta and K. Sinha, Phys. Rev. D **86** (2012), 095016 doi:10.1103/PhysRevD.86.095016 [arXiv:1208.0115 [hep-ph]].
- [125] D. G. Cerdeño, A. Cheek, P. Martín-Ramiro and J. M. Moreno, Eur. Phys. J. C **79** (2019) no.6, 517 doi:10.1140/epjc/s10052-019-6979-x [arXiv:1902.01789 [hep-ph]].
- [126] A. Bouquet, P. Salati and J. Silk, Phys. Rev. D **40** (1989), 3168 doi:10.1103/PhysRevD.40.3168
- [127] L. Bergstrom, Phys. Lett. B **225** (1989), 372-380 doi:10.1016/0370-2693(89)90585-6
- [128] S. Rudaz, Phys. Rev. D **39** (1989), 3549 doi:10.1103/PhysRevD.39.3549
- [129] J. M. Gaskins, Contemp. Phys. **57** (2016) no.4, 496-525 doi:10.1080/00107514.2016.1175160 [arXiv:1604.00014 [astro-ph.HE]].
- [130] V. Lefranc, E. Moulin, P. Panci, F. Sala and J. Silk, JCAP **09** (2016), 043 doi:10.1088/1475-7516/2016/09/043 [arXiv:1608.00786 [astro-ph.HE]].
- [131] J. Einasto, [arXiv:0901.0632 [astro-ph.CO]].
- [132] J. F. Navarro, C. S. Frenk and S. D. M. White, Astrophys. J. **490** (1997), 493-508 doi:10.1086/304888 [arXiv:astro-ph/9611107 [astro-ph]].
- [133] J. F. Navarro, A. Ludlow, V. Springel, J. Wang, M. Vogelsberger, S. D. M. White, A. Jenkins, C. S. Frenk and A. Helmi, Mon. Not. Roy. Astron. Soc. **402** (2010), 21 doi:10.1111/j.1365-2966.2009.15878.x [arXiv:0810.1522 [astro-ph]].
- [134] A. M. Sirunyan *et al.* [CMS], Phys. Rev. D **97** (2018) no.9, 092005 doi:10.1103/PhysRevD.97.092005 [arXiv:1712.02345 [hep-ex]].
- [135] O. Buchmueller, M. J. Dolan and C. McCabe, JHEP **01** (2014), 025 doi:10.1007/JHEP01(2014)025 [arXiv:1308.6799 [hep-ph]].
- [136] J. Abdallah, H. Araujo, A. Arbey, A. Ashkenazi, A. Belyaev, J. Berger, C. Boehm, A. Boveia, A. Brennan and J. Brooke, *et al.* Phys. Dark Univ. **9-10** (2015), 8-23 doi:10.1016/j.dark.2015.08.001 [arXiv:1506.03116 [hep-ph]].
- [137] J. I. Read, J. Phys. G **41** (2014), 063101 doi:10.1088/0954-3899/41/6/063101 [arXiv:1404.1938 [astro-ph.GA]].
- [138] L. Roszkowski, E. M. Sessolo and S. Trojanowski, Rept. Prog. Phys. **81** (2018) no.6, 066201 doi:10.1088/1361-6633/aab913 [arXiv:1707.06277 [hep-ph]].

- [139] T. Bringmann, J. Edsjö, P. Gondolo, P. Ullio and L. Bergström, JCAP **07** (2018), 033 doi:10.1088/1475-7516/2018/07/033 [arXiv:1802.03399 [hep-ph]].
- [140] M. Gustafsson, E. Lundstrom, L. Bergstrom and J. Edsjo, Phys. Rev. Lett. **99** (2007), 041301 doi:10.1103/PhysRevLett.99.041301 [arXiv:astro-ph/0703512 [astro-ph]].
- [141] G. Bertone, C. B. Jackson, G. Shaughnessy, T. M. P. Tait and A. Vallinotto, JCAP **03** (2012), 020 doi:10.1088/1475-7516/2012/03/020 [arXiv:1009.5107 [astro-ph.HE]].
- [142] C. B. Jackson, G. Servant, G. Shaughnessy, T. M. P. Tait and M. Taoso, JCAP **07** (2013), 021 doi:10.1088/1475-7516/2013/07/021 [arXiv:1302.1802 [hep-ph]].
- [143] M. Cirelli, M. Kadastik, M. Raidal and A. Strumia, Nucl. Phys. B **813** (2009), 1-21 doi:10.1016/j.nuclphysb.2008.11.031 [arXiv:0809.2409 [hep-ph]].
- [144] M. Benito, N. Bernal, N. Bozorgnia, F. Calore and F. Iocco, JCAP **02** (2017), 007 [erratum: JCAP **06** (2018), E01] doi:10.1088/1475-7516/2017/02/007 [arXiv:1612.02010 [hep-ph]].
- [145] J. Zavala, Phys. Rev. D **89** (2014) no.12, 123516 doi:10.1103/PhysRevD.89.123516 [arXiv:1404.2932 [astro-ph.HE]].
- [146] E. Del Nobile, C. Kouvaris, P. Panci, F. Sannino and J. Virkajarvi, JCAP **08** (2012), 010 doi:10.1088/1475-7516/2012/08/010 [arXiv:1203.6652 [hep-ph]].
- [147] A. Belyaev, E. Bertuzzo, C. Caniu Barros, O. Eboli, G. Grilli Di Cortona, F. Iocco and A. Pukhov, Phys. Rev. D **99** (2019) no.1, 015006 doi:10.1103/PhysRevD.99.015006 [arXiv:1807.03817 [hep-ph]].
- [148] A. Belyaev, L. Panizzi, A. Pukhov and M. Thomas, JHEP **04** (2017), 110 doi:10.1007/JHEP04(2017)110 [arXiv:1610.07545 [hep-ph]].
- [149] K. Mimasu and V. Sanz, JHEP **06** (2015), 173 doi:10.1007/JHEP06(2015)173 [arXiv:1409.4792 [hep-ph]].
- [150] N. Zhou, D. Berge and D. Whiteson, Phys. Rev. D **87** (2013) no.9, 095013 doi:10.1103/PhysRevD.87.095013 [arXiv:1302.3619 [hep-ex]].
- [151] A. H. Abdelhameed *et al.* [CRESST], [arXiv:1905.07335 [astro-ph.CO]].
- [152] A. H. Abdelhameed *et al.* [CRESST], Phys. Rev. D **100** (2019) no.10, 102002 doi:10.1103/PhysRevD.100.102002 [arXiv:1904.00498 [astro-ph.CO]].
- [153] P. Agnes *et al.* [DarkSide], Phys. Rev. Lett. **121** (2018) no.8, 081307 doi:10.1103/PhysRevLett.121.081307 [arXiv:1802.06994 [astro-ph.HE]].
- [154] R. Catena, T. Emken, N. A. Spaldin and W. Tarantino, Phys. Rev. Res. **2** (2020) no.3, 033195 doi:10.1103/PhysRevResearch.2.033195 [arXiv:1912.08204 [hep-ph]].

- [155] A. Ibarra, B. J. Kavanagh and A. Rappelt, *JCAP* **12** (2018), 018 doi:10.1088/1475-7516/2018/12/018 [arXiv:1806.08714 [hep-ph]].
- [156] N. P. Pitjev and E. V. Pitjeva, *Astron. Lett.* **39** (2013), 141-149 doi:10.1134/S1063773713020060 [arXiv:1306.5534 [astro-ph.EP]].
- [157] C. M. Bidin, G. Carraro, R. A. Mendez and R. Smith, *Astrophys. J.* **751** (2012), 30 doi:10.1088/0004-637X/751/1/30 [arXiv:1204.3924 [astro-ph.GA]].
- [158] X. Chu, J. Pradler and L. Semmelrock, *Phys. Rev. D* **99** (2019) no.1, 015040 doi:10.1103/PhysRevD.99.015040 [arXiv:1811.04095 [hep-ph]].
- [159] X. Chu, J. L. Kuo and J. Pradler, *Phys. Rev. D* **101** (2020) no.7, 075035 doi:10.1103/PhysRevD.101.075035 [arXiv:2001.06042 [hep-ph]].
- [160] R. Primulando, E. Salvioni and Y. Tsai, *JHEP* **07** (2015), 031 doi:10.1007/JHEP07(2015)031 [arXiv:1503.04204 [hep-ph]].
- [161] R. Catena, T. Emken and J. Ravanis, *JCAP* **06** (2020), 056 doi:10.1088/1475-7516/2020/06/056 [arXiv:2003.04039 [hep-ph]].
- [162] S. Fichet, *JHEP* **04** (2017), 088 doi:10.1007/JHEP04(2017)088 [arXiv:1609.01762 [hep-ph]].
- [163] G. Magill, R. Plestid, M. Pospelov and Y. D. Tsai, *Phys. Rev. D* **98** (2018) no.11, 115015 doi:10.1103/PhysRevD.98.115015 [arXiv:1803.03262 [hep-ph]].
- [164] I. M. Shoemaker and J. Wyenberg, *Phys. Rev. D* **99** (2019) no.7, 075010 doi:10.1103/PhysRevD.99.075010 [arXiv:1811.12435 [hep-ph]].
- [165] N. Weiner and I. Yavin, *Phys. Rev. D* **86** (2012), 075021 doi:10.1103/PhysRevD.86.075021 [arXiv:1206.2910 [hep-ph]].
- [166] N. Weiner and I. Yavin, *Phys. Rev. D* **87** (2013) no.2, 023523 doi:10.1103/PhysRevD.87.023523 [arXiv:1209.1093 [hep-ph]].
- [167] A. Crivellin and U. Haisch, *Phys. Rev. D* **90** (2014), 115011 doi:10.1103/PhysRevD.90.115011 [arXiv:1408.5046 [hep-ph]].
- [168] D. C. Latimer, *Phys. Rev. D* **95** (2017) no.9, 095023 doi:10.1103/PhysRevD.95.095023 [arXiv:1706.08029 [hep-ph]].
- [169] L. G. Cabral-Rosetti, M. Mondragón and E. Reyes-Pérez, *Nucl. Phys. B* **907** (2016), 1-17 doi:10.1016/j.nuclphysb.2016.03.025 [arXiv:1504.01213 [hep-ph]].
- [170] F. Kahlhoefer, K. Schmidt-Hoberg, T. Schwetz and S. Vogl, *JHEP* **02** (2016), 016 doi:10.1007/JHEP02(2016)016 [arXiv:1510.02110 [hep-ph]].
- [171] A. De Simone and T. Jacques, *Eur. Phys. J. C* **76** (2016) no.7, 367 doi:10.1140/epjc/s10052-016-4208-4 [arXiv:1603.08002 [hep-ph]].
- [172] P. J. Fox, R. Harnik, R. Primulando and C. T. Yu, *Phys. Rev. D* **86** (2012), 015010 doi:10.1103/PhysRevD.86.015010 [arXiv:1203.1662 [hep-ph]].



- [173] Y. Bai, P. J. Fox and R. Harnik, *JHEP* **12** (2010), 048 doi:10.1007/JHEP12(2010)048 [arXiv:1005.3797 [hep-ph]].
- [174] I. M. Shoemaker and L. Vecchi, *Phys. Rev. D* **86** (2012), 015023 doi:10.1103/PhysRevD.86.015023 [arXiv:1112.5457 [hep-ph]].
- [175] M. Endo and Y. Yamamoto, *JHEP* **06** (2014), 126 doi:10.1007/JHEP06(2014)126 [arXiv:1403.6610 [hep-ph]].
- [176] F. Kahlhoefer, *Int. J. Mod. Phys. A* **32** (2017) no.13, 1730006 doi:10.1142/S0217751X1730006X [arXiv:1702.02430 [hep-ph]].
- [177] J. Goodman, M. Ibe, A. Rajaraman, W. Shepherd, T. M. P. Tait and H. B. Yu, *Phys. Lett. B* **695** (2011), 185-188 doi:10.1016/j.physletb.2010.11.009 [arXiv:1005.1286 [hep-ph]].
- [178] J. Goodman, M. Ibe, A. Rajaraman, W. Shepherd, T. M. P. Tait and H. B. Yu, *Phys. Rev. D* **82** (2010), 116010 doi:10.1103/PhysRevD.82.116010 [arXiv:1008.1783 [hep-ph]].
- [179] P. J. Fox, R. Harnik, J. Kopp and Y. Tsai, *Phys. Rev. D* **84** (2011), 014028 doi:10.1103/PhysRevD.84.014028 [arXiv:1103.0240 [hep-ph]].
- [180] A. Rajaraman, W. Shepherd, T. M. P. Tait and A. M. Wijangco, *Phys. Rev. D* **84** (2011), 095013 doi:10.1103/PhysRevD.84.095013 [arXiv:1108.1196 [hep-ph]].
- [181] A. L. Fitzpatrick and K. M. Zurek, *Phys. Rev. D* **82** (2010), 075004 doi:10.1103/PhysRevD.82.075004 [arXiv:1007.5325 [hep-ph]].
- [182] S. Kang, S. Scopel, G. Tomar, J. H. Yoon and P. Gondolo, *JCAP* **11** (2018), 040 doi:10.1088/1475-7516/2018/11/040 [arXiv:1808.04112 [hep-ph]].
- [183] A. Ibarra and S. Wild, *JCAP* **05** (2015), 047 doi:10.1088/1475-7516/2015/05/047 [arXiv:1503.03382 [hep-ph]].
- [184] R. Foot and S. Vagnozzi, *Phys. Rev. D* **91** (2015), 023512 doi:10.1103/PhysRevD.91.023512 [arXiv:1409.7174 [hep-ph]].
- [185] F. Bishara, J. Brod, B. Grinstein and J. Zupan, *JHEP* **11** (2017), 059 doi:10.1007/JHEP11(2017)059 [arXiv:1707.06998 [hep-ph]].
- [186] T. Piff, C. Scannapieco, J. Binney, M. Steinmetz, R. D. Scholz, M. E. K. Williams, R. S. de Jong, G. Kordopatis, G. Matijević and O. Bienaymé, *et al. Astron. Astrophys.* **562** (2014), A91 doi:10.1051/0004-6361/201322531 [arXiv:1309.4293 [astro-ph.GA]].
- [187] N. Bozorgnia, F. Calore, M. Schaller, M. Lovell, G. Bertone, C. S. Frenk, R. A. Crain, J. F. Navarro, J. Schaye and T. Theuns, *JCAP* **05** (2016), 024 doi:10.1088/1475-7516/2016/05/024 [arXiv:1601.04707 [astro-ph.CO]].
- [188] S. Vandoren and P. van Nieuwenhuizen, [arXiv:0802.1862 [hep-th]].
- [189] A. Hook, *PoS TASI2018* (2019), 004 [arXiv:1812.02669 [hep-ph]].

- [190] P.A. Zyla *et al.* [Particle Data Group], Prog. Theor. Exp. Phys. 2020, 083C01 (2020)
- [191] G. 't Hooft, Phys. Rev. Lett. **37** (1976), 8-11 doi:10.1103/PhysRevLett.37.8
- [192] S. M. Barr, Phys. Rev. Lett. **53** (1984), 329 doi:10.1103/PhysRevLett.53.329
- [193] M. Yoshimura, Phys. Rev. Lett. **41** (1978), 281-284 [erratum: Phys. Rev. Lett. **42** (1979), 746] doi:10.1103/PhysRevLett.41.281
- [194] R. D. Peccei and H. R. Quinn, Phys. Rev. Lett. **38** (1977), 1440-1443 doi:10.1103/PhysRevLett.38.1440
- [195] M. Srednicki, Nucl. Phys. B **260** (1985), 689-700 doi:10.1016/0550-3213(85)90054-9
- [196] H. Georgi, D. B. Kaplan and L. Randall, Phys. Lett. B **169** (1986), 73-78 doi:10.1016/0370-2693(86)90688-X
- [197] M. Bauer, M. Neubert, S. Renner, M. Schnubel and A. Thamm, JHEP **04** (2021), 063 doi:10.1007/JHEP04(2021)063 [arXiv:2012.12272 [hep-ph]].
- [198] K. Fujikawa, Phys. Rev. Lett. **42** (1979), 1195-1198 doi:10.1103/PhysRevLett.42.1195
- [199] G. Aad *et al.* [ATLAS], Eur. Phys. J. C **81** (2021) no.2, 178 doi:10.1140/epjc/s10052-020-08677-2 [arXiv:2007.02873 [hep-ex]].
- [200] A. M. Sirunyan *et al.* [CMS], Phys. Rev. D **100** (2019) no.7, 072002 doi:10.1103/PhysRevD.100.072002 [arXiv:1907.03729 [hep-ex]].
- [201] <https://twiki.cern.ch/twiki/bin/view/Main/WebHome>
- [202] M. S. Turner, Phys. Rept. **197** (1990), 67-97 doi:10.1016/0370-1573(90)90172-X
- [203] V. Brdar, S. Jana, J. Kubo and M. Lindner, Phys. Lett. B **820** (2021), 136529 doi:10.1016/j.physletb.2021.136529 [arXiv:2104.03282 [hep-ph]].
- [204] M. Bauer, M. Neubert, S. Renner, M. Schnubel and A. Thamm, Phys. Rev. Lett. **124** (2020) no.21, 211803 doi:10.1103/PhysRevLett.124.211803 [arXiv:1908.00008 [hep-ph]].
- [205] P. deNiverville, H. S. Lee and M. S. Seo, Phys. Rev. D **98** (2018) no.11, 115011 doi:10.1103/PhysRevD.98.115011 [arXiv:1806.00757 [hep-ph]].
- [206] N. Abe, T. Moroi and M. Yamaguchi, JHEP **01** (2002), 010 doi:10.1088/1126-6708/2002/01/010 [arXiv:hep-ph/0111155 [hep-ph]].
- [207] J. G. Korner, D. Kreimer and K. Schilcher, Z. Phys. C **54** (1992), 503-512 doi:10.1007/BF01559471
- [208] H. Nicolai and P. K. Townsend, Phys. Lett. B **93** (1980), 111-115 doi:10.1016/0370-2693(80)90106-9

- [209] H. C. Ohanian, Am. J. Phys. **54** (1986), 501-505
- [210] P. B. Pal, Am. J. Phys. **79** (2011), 485-498 doi:10.1119/1.3549729 [arXiv:1006.1718 [hep-ph]].